UNIVERSITY OF SOUTHAMPTON

Investigation of Optimal Descent Trajectories Using Feedback Control for the Olympic Sport of Bob-Skeleton

by

Chen Gong

A thesis submitted for the degree of
Doctor of Philosophy

in the
Faculty of Engineering and the Environment
Fluid, Structure and Interaction

March 2019

UNIVERSITY OF SOUTHAMPTON

ABSTRACT

FACULTY OF ENGINEERING AND THE ENVIRONMENT
FLUID, STRUCTURE AND INTERACTION

Doctor of Philosophy

INVESTIGATION OF OPTIMAL DESCENT TRAJECTORIES USING FEEDBACK CONTROL FOR THE OLYMPIC SPORT OF BOB-SKELETON

by Chen Gong

In the Olympic sport of Bob-Skeleton, the athletes compete to achieve the fastest possible descent of an ice track lying prone on a sled in contact with the ice via two circular section steel runners. Their elapsed time of descent is influenced by their speed after the initial sprint phase, aerodynamics and ice friction and critically their skill as a slider in being able to steer down the 'best' trajectory. Minimising the number and magnitude of steering control interventions is seen as key to minimising energy loss and hence achieving a fast time. Tracks typically have 12 to 14 corners, descend about 150 m vertically over a track length of 1500 m or so.

A physics based simulation developed by the University of Southampton was used as a test environment to investigate the fastest route of descent for a three dimensionally accurate bob-skeleton track. This simulation captures the inertial, gravitational, centripetal, friction and aerodynamic forces and moment acting on the slider and their sled. As the descent time is so short, 50 - 60 seconds, sliders prepare for events by walking the track and 'learning' the best route under the guidance of their experienced coaches. The simulation analysis was limited to computing the descent time for the coach specified trajectory. The aim of this research was to investigate how the optimum trajectory down a track can be determined. In order to do this it was necessary to develop a suitable control method to evaluate whether a potential trajectory was feasible. A series of control algorithms were investigated and simulation times compared to those achieved in competitions to verify the approach. This thesis has established that control laws can be used to ensure path following during descent. The control law used, in the main, was of the proportional plus derivative form but promising initial results were also obtained for model based control laws, such as model predictive control.

Contents

List of Figures

List of Tables

Nomenclature

$\dot{\alpha}_{out}, \dot{\beta}_{out}$	New velocity after collision
$\alpha_{l,r}$	Longitudinal position of the left & right mass particle
$\beta_{l,r}$	Transverse position of the left & right mass particle
$\dot{\alpha}_{l,r}$	Longitudinal velocity of the left and right particles
$\dot{\beta}_{l,r}$	Transverse velocity of the left and right particles
$\ddot{\alpha}_{l,r}$	Longitudinal acceleration of the left and right particles
$\ddot{\beta}_{l,r}$	Transverse acceleration of the left and right particles
$A_{l,r}$, $B_{l,r}$	Generalised inertial forces acting on the both mass particles
a_z	Vertical acceleration to the sled reference frame
ang	Boolean variable defining slippage
C_dA, C_lA	Drag and lift areas
C_r	Coefficient of restitution of the ice wall
D	Aerodynamic drag of athlete and sled
$Damp_{a,b}$	Arbitrary damping coefficients
$e(k)_{l,r}$	Left and right error at sampling period k
ϵ_k	Slack variable at control interval k
ε	Adaptive controller threshold value
η	Lateral driving force
$F_{act} \cdot rl_{\alpha,\beta}$	Longitudinal & Transverse inertial forces for the left mass particle
$F_{act} \cdot rr_{\alpha,\beta}$	Longitudinal & Transverse inertial forces for the right mass particle
$F_{APD}(l,r)$	Left & right steering force from adaptive PD controller
$f_{interp_{xyz}}$	Interpolation function to map sled axis onto 3D world axis
$f_{L,R}$	Frictional force on the left and right runner generated from toe steering
$f_{lon_{l,r}}$	longitudinal friction forces on the left and right mass particle
$F_{MPC_\alpha}(l,r)$	Left & right actuation force in the α direction
$F_{MPC_\beta}(l,r)$	Left & right actuation force in the β direction
f_{lat}	Transverse runner friction force
f_{lon}	Longitudinal runner friction force
$f_{slip_{l,r}}$	lateral friction force caused by slipping
F_{toeL}, F_{toeR}	the steering forces detected on the respective load cells
F_l, F_r	Total actuation forces vectors for the left and right mass particle
Fol, For	Actuation force vectors on the left and right mass particles
$Fsteer(L,R)$	Left and right steering force from driver
g	Acceleration due to gravity
k	Current control interval

K	Common system gain at any sampling period
K_ϕ	Roll angle dependant adaptive gain
$K_{\Delta\beta_d}$	Scaling gain for derivative gain change w.r.t. $\Delta\beta_c$
$K_{\Delta\beta_p}$	Scaling gain for proportional gain change w.r.t. $\Delta\beta_c$
$K_{d_{Adaptive}}$	Adaptive derivative gain
K_{damp}	Arbitrary damping coefficients
$k_{nl,r}$	Local normal curvature of the left and right contact patch
$K_{p_{Adaptive}}$	Adaptive proportional gain
K_1, K_2, K_3	Arbitrary system gain at any sampling period
K_d	Derivative gain
K_i	Integral gain
K_p	Proportional gain
K_v	Velocity dependant adaptive gain
$knif(l,r)$	Contact surface length of the left and right knife
L	Aerodynamic lift of athlete and sled
m_l, m_r	Mass distributed to the left and right particle
μ	Friction coefficient of the ice wall
μ_t	Slip friction coefficient
$\mu_t oe$	Coefficient of friction between athlete's toe and the track surface
$N_{l,r}$	surface normal reaction forces
$n_{l,r}$	Unit normal for the left and right mass particle
n_{pred}	Predicted unit vector from left to right mass particle
N_p	Prediction Horizon
n_U	Number of manipulated variables
n_Y	Number of plant output variables
ϕ	Roll angle of the sled
$\phi(k)$	Roll angle of the sled at sampling period k
ϕ_{pred}	Predicted roll angle
ρ	Air density
ρ_ϵ	Constraint violation penalty weights. This is the set of ECR
R	3×1 Sled body stiffness
$R(k+i\|k)$	State Reference value
r	Radius of track curvature
$r_\alpha(l,r)$	Left & right spatial derivative in the α direction
$r_\beta(l,r)$	Left & right spatial derivative in the β direction
S_1	Unit vector parallel to the sled axial direction
S_2	Unit vector perpendicular to the sled axial direction
τ	Dead time delay, 0.1 for upwards actuation and 0.3 for downwards actuation
t_c	Unit tangent vector of sled velocity
θ	Yaw angle of sled
$U(k)_{Alg.II}$	Control inputs from adaptive PD algorithm II
$U(k)_{l,r}$	Left and right control inputs/steering forces at sampling period k
$U(k+i\|k)$	Calculated jth manipulated variable
$U(t)_{Alg.I}$	Control inputs from adaptive PD algorithm I
$U_{j,min}(i), U_{j,max}(i)$	Lower and upper bounds for jth manipulated variable

$\Delta U_{j,min}(i), \Delta U_{j,max}(i)$	Lower and upper bounds for jth manipulated variable rate
$v(k)$	Velocity of the sled at sampling period k
$v_{l,r}$	Velocity of the left and right mass particle
$V_{l,r}$, V_c	Velocity vector of the sled reference frame
v_{max}	Maximum recorded velocity for current testing track
ω_{so}	Desired distance between left & right mass particles
ω_s	Actual distance between left & right mass particles
$W_{i,j}^{\Delta U}$	Tuning weight for the $j$the manipulated
$W_{i,j}^{U}$	Tuning weight for the $j$the manipulated
$W_{i,j}^{Y}$	Tuning weight
W_l, W_r	longitudinal and translational friction forces due to wall hits
$Y(k+i\|k)$	Predicted plant output value
$Y_{j,min}(i), Y_{j,max}(i)$	Lower and upper bounds for jth plant output

Acronyms

3D	3 Dimensions
AMPC	Adaptive Model Predictive Control
APD	Adaptive Proportional Derivative
CSI	Cubic Spline Interpolation
DOF	Degree of Freedom
DTT	Driver Training Tool
EOM	Equations of Motion
FFT	Fast Fourier Transform
GB	Great Britain
GUI	Graphical User Interface
MPC	Model Predictive Control
PD	Proportional-Derivative
RTPE	Real-time Physics Engine
SC	Sled Characteristics
UDP	User Data Datagram Protocol

Declaration of Authorship

I, Chen Gong, declare that this thesis entitled Investigation of Optimal Descent Trajectories Using Feedback Control for the Olympic Sport of Bob-Skeleton and the work presented in it are my own and has been generated by me as the result of my own original research.

I confirm that:

1. This work was done wholly or mainly while in candidature for a research degree at this University;
2. Where any part of this thesis has previously been submitted for a degree or any other qualification at this University or any other institution, this has been clearly stated;
3. Where I have consulted the published work of others, this is always clearly attributed;
4. Where I have quoted from the work of others, the source is always given. With the exception of such quotations, this thesis is entirely my own work;
5. I have acknowledged all main sources of help;
6. Where the thesis is based on work done by myself jointly with others, I have made clear exactly what was done by others and what I have contributed myself;
7. Either none of this work has been published before submission, or parts of this work have been published as:
    - C. Gong, C. W. G. Phillips, E. Rogers, S. R. Turnock, "Analysis of Performance Indices for Simulated Skeleton Descents," *Procedia Engineering*, vol. 147, pp.712 - 717, 2016.

    .

Signed:

Date:

Acknowledgements

Firstly, I would like to give my sincerest gratitude to my supervisors, Professor Stephen R Turnock and Professor Eric Rogers. Whose invaluable advices and expertise made this work possible in the first place. Their continual support and encouragement was fundamental to the success of this research and will be forever appreciated.

Secondly, I would like to show my appreciation for the support from the EIS, without whom this work would not have been possible. I would also like to thank all the athletes ,coaches and supporting staff of GB Skeleton, whom I have thoroughly enjoyed working with. Their dedication and enthusiasm was not only inspiring but also ensured smooth development of this research. Thank you to Andreas Schmidt and Naomi Stenhouse for their expertise and professionalism and I would also like thank Dave Short in particular for his continual friendship, support and hard work.

Thirdly, a huge thank you goes to my fellow PhD friends, Joshua Taylor and Agata Tomaszewska, who not only provided me with much needed friendship and support throughout my time here, but also kept me entertained with sometimes questionable musical choices. I would like to thank the hard work of my Post Doc friend Christopher Phillips, who had put in a huge amount of time and effort helping me organising the relationship with the sport and chauffeuring me to and from Bath. Last but not least, I would to thank Dr. Calab Sawade, who have provided me with guidance and support since the very beginning of this PhD and helped me become a better engineer.

Finally, I reserve my deepest, most sincere gratitude to my best friend and my wife Xiaoqing Shi. Her unconditional love, encouragement and support filled me with inspiration and determination to work hard and succeed throughout the years. She made it possible for me to thrive in this PhD and in life, I owe everything to her and I cannot thank her enough.

Chapter 1

Introduction

1.1 The sports of Skeleton

The Bob-Skeleton (Skeleton) is named after the bony appearance of the sled and the Olympic sport of Skeleton is one in which the athlete lies prone on the sled to compete in a head first decent with the goal of achieving the quickest descent time. The sled consists of a steel frame and two circular runners with a machined knife edge on the back half. The athlete controls the sled by applying force in opposite shoulder and knee pairs simultaneously to contort the sled's frame, this action forces the knives into the ice and induces asymmetry in the friction between runners and ice, resulting in a steering moment. To steer left, the athlete would dig in their right shoulder and left knee, vice versa (see illustration in Figure 1.1). During a race, the athlete starts off by sprinting with the sled from the top of track. After approximately 50 m, the athlete will mount the sled at full running speed and proceed to steer through the track (1500 m, with around 14 to 16 corners), minimising their time of descent.

During a race, the sled will usually reach up to an average speed of 130 km/h; athlete can often experience sustained G-force of up to 6 G around high banking corners and constant high levels of vibration from bumpy ice surface, which often results in head impacts, contributing to dizziness. Executing accurate steering actions under these extreme conditions are very difficult. Due to these extremely limiting physical conditions, most athletes cannot rely on visual feedback to steer the sled. Instead, elite athletes are expected to memorise the desired descent trajectory, entry and exit positions/directions through the entire track and use steering cues such as g-force

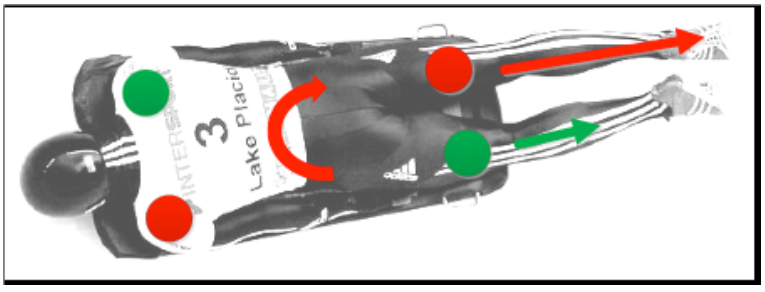

FIGURE 1.1: Illustration of steering in action by generating asymmetric friction

or roll motion to judge their relative position and make appropriate steering adjustments. The Olympic race consists of 4 separate runs down the same track and the time differences between the first 5 places can be as small as 0.46 seconds[49]. This puts immense amount of pressure on the athletes to perform their best consistently. It is clear to see that Skeleton is a sport that is both physically and cognitively demanding.

1.2 GB Skeleton and The University of Southampton

GB Skeleton is one of the most successful teams in the world. The profile of the sport has being significantly elevated following the consecutive gold medals obtained in the 2010 and 2014 Winter Olympics. These recent successes have largely been attributed to the research conducted by former University of Southampton PhD graduates Roche, (2010) and Blackburn, (2010) who had designed the sled and aerodynamic packages for the 2010 winner Amy Williams; and Sawade, (2014) who was responsible for designing and constructing the first virtual reality simulator for the GB Skeleton team to assist in pre-Olympic training for the 2014 gold medallist Elizabeth Yarnold. The simulator is currently being integrated into the sports regular training routines. Their work has provided the vital insights such as athlete/sled interaction, real time physical modelling of a Skeleton and the benefits of motion cuing training etc. These insights provided the foundation for this PhD to develop upon.

1.3 Motivation of Work

As previously stated, the goal of a Skeleton race is to achieve the quickest descent and each race can be separated into two distinct phases, the sprint phase and the sliding phase. To stay competitive, athletes must be trained to be both extremely skilled at sprinting and sliding. Training for the sprinting phase is relatively straight forward, the GB Skeleton team has access to some of the best training equipment, locations and research available for their athletes to condition their body physically. The sprinting phase make up approximately 5% of the race and the other 95% of race relies on predominantly the sliding skills of the athlete. It stands to reason that by optimising the descent process where most of the race takes place, the performance of the athlete could be improved. However, the sliding phase is much more difficult to train for as historically, the only way for athlete to become better at sliding is through experience gained whilst sliding on the track and there are no Ice tracks in Britain. GB Skeleton athletes must travel around the globe to train and compete, limiting their on ice practice time to roughly 120 minutes per year. With such restricted access, every second of on ice time becomes invaluable. Typically, athletes require at least 1 or 2 warm up runs to get into the racing mind set and start gaining benefits from on ice training, meanwhile the coaches are unable to give comprehensive feedback until after the training session when their filmed footage of the athlete could be analysed. Therefore, it would be of great benefit to be able to go into these limited training sessions with a pre-planned descent trajectory and sliding plan, as this would save valuable time that could be used to develop crucial steering skills.

The integration of the Mark II virtual reality simulator/driver training tool (DTT) proved to be successful in preparing the athlete's mental status before going on ice as well as in maintaining

athlete skill level by allowing them to 'slide' during the off season periods. Following this success, the principal stake holder, the English Institute of Sport has urged for the further research to be conducted to explore the full potential obtainable from using the DTT. It is believed that improving the functionality of the existing DTT will improve the quality of athletes' training and therefore having a positive impact on their performances.

After reviewing the Mark II DTT, it became apparent that although it was capable of asserting motion cues including roll and body/head G-force loading, the feedbacks from athletes and coaches who have being working with the DTT for an extended period of time suggest that there are still important motion cues missing. The most predominant missing cue was the pitching motion that athlete feels under their shoulder when sliding through a corner. There are also other missing minor cues such as leg G-force and yaw motion at the top of a turn.

The physics engine governing the simulation dynamics was also based on work from Bob-Sleigh [20] and later adapted to skeleton by Roche and Sawade [1, 2]. The model included numerous empirical formulas obtained from system identification of data gathered from instrumented sled. The lack of accuracy in modelling makes it inappropriate to implement human in the loop training with athletes. Instead during DTT training sessions, the athletes slide down a recorded trajectory, predetermined by the coaches. For the 2014 Winter Olympic cycle, the athlete trained on the Sochi ice track exclusively, and only used 1 descent trajectory. At that time, the only method of creating said trajectory was through manually steering the simulation, the process was laborious and inconsistent. The trajectories produced using this method are entirely based on the subjective knowledge of the coaches, thus there is no indication as to whether they are competitive/optimal as it was show in Bob-Sleigh research [33], that by optimising the descent trajectory, one can effectively reduce the descent time, sometimes by up to 0.5 seconds, which can potentially provide a huge advantage over their competition.

The DTT functions more than just a simple training tool, it offers unparalleled abilities to analyse athlete's performance by recording their actions whilst sliding on a simulated descent. This allows the coaches to rapidly identify the strength and weakness of each athlete and tailor personalised training routines for each individual athlete. However, no software interfaces existed that allowed for the coaches to easily analyse the athlete's performance.

1.4 Research Hypotheses

The aim of the research conducted in this PhD is to improve the quality of athlete training through tackling the challenges that GB Skeleton team faces as per described in section 1.3. The process of doing so can be concisely summarised by the two research hypotheses below:

1. The quality of athlete training using the DTT can be improved by augmenting the Mark II DTT's hardware infrastructure and operational software.
2. It is possible to compute optimised descent trajectories for any race track under the DTT's simulated environment.

The validation processes of these hypotheses can be further broken down into the following objectives:

Hypothesis 1:

- The Mark II DTT will be augmented to incorporate missing motions cue(e.g. shoulder pitching and leg G-force) and 5 motion cuing algorithms will be designed to work with said augmentations to improve training immersion.
- Motions stimuli experiments will be conducted to evaluate fidelity of new motion cuing system and to select the most effective motion cuing algorithm to use for learning and skills acquisition.
- DTT software in both Matlab(physics engine) and LabVIEW(hardware control) will be reprogrammed to incorporate new features, such as motion cuing, emergency safety, real-time feedback, session performance analysis etc. This is important to improve the quality of on simulator training sessions.

Hypothesis 2:

- Classical control(PD) algorithms will be implemented to investigate system dynamics and to develop an appropriate optimisation strategy for later MPC design. It is believed that optimal descent strategy will involve minimising the energy lost through over steering.
- More classical control(Adaptive PD) algorithm will be implemented to both confirm the findings from the PD controller and to get a good estimation for the best(fastest) baseline descent performance using an non-optimal control scheme.
- Optimal control algorithms (MPC & adaptive MPC) will be implemented to achieve optimal descent trajectory in an analytical, consistent manner. The performances of these optimal controllers will be compared against athletes' on-ice performances to check for data fidelity.

1.5 Thesis Structure

The rest of the thesis is separated into 7 chapters to address the different aspects of the research hypothesis, listed below is a quick summary of what each chapter details:

- Chapter 2 review the relevant literatures, including: the human perceptual systems, which is important in understanding the human body's response to motion cuing and help design the cuing system to ensure no negative impact on athlete's perception; Modelling of descent simulation done on similar sport such as Bob-Sleigh to both help refine the physics engine and design the trajectory prediction system. Although the basic control theories used throughout this research is important for accomplishing the research aim, by itself however, it offers no novelty value and is therefore placed in Appendix A.
- Chapter 3 begins by reviewing the existing features on the Mark II DTT as this provided a prospective to its functionality as a training tool. Following the review, the design and implementation of the key features that makes up the Mark III DTT will be described. Finally, the function of the DTT for training application will also be explained.

- Chapter 4 details the motion stimuli experiment to verify the effect incorporating the pitch motion cues have on athlete's learning and skills acquisition capabilities. Two motion stimuli experiments will be carried out. The first experiment was conducted using GB Skeleton coaches to subjectively assess the pitch motion cuing system and select the most appropriate pitching algorithm for the second experiment, which was conducted using GB Skeleton athletes to select the optimal pitching algorithm for training.

- Chapter 5 reviews the underlying physics engine governing the behaviour of the descent simulation. Key equations which are used later in the design of the classical and optimal control algorithms are listed here.

- Chapter 6 summarises the design, implementation and evaluation process of the classical control algorithms created to further understand the interactions between steering input and descent dynamics. Relationships between a number of simulation parameters, named performance indices will be investigated, and their concluding correlation will be used to design the cost function of the optimal control algorithms and ultimately predict the optimal descent trajectory.

- Chapter 7 summarises the design, implementation and evaluation process of the optimal control algorithm, more specifically, the model predictive control algorithm and the hybrid control algorithm. The performance of the each control algorithm on the PyeongChang Olympic track were recorded and compared to each other as well as pre-recorded descent data. Through this analysis, the fidelity and optimality of the predicted trajectories will be evaluated and an optimal descent trajectory for the track will be produced for training using the DTT.

- Chapter 8 provides a conclusion regarding the research conducted in this PhD and evaluates the research findings with respect to the original hypotheses. The author's objective and subjective opinion regarding the current state of the research will be given and possible future research direction will be discussed.

Chapter 2

Literature Review

2.1 Chapter Introduction

The literature review gives details on the background information that was crucial to the development of this PhD principle research aim previously mentioned. The literature review will include the following three sections:

- Fundamental cueing methods
- Dynamic modelling of the Skeleton descent
- Control algorithms developed thus far in other sports

In each section, related work completed by previous PhD's in the university of Southampton and their respective findings will be discussed.

2.2 Virtual Reality Simulator

Sawade [1] has detailed in his work the design philosophy behind the DTT. The earlier versions of the virtual reality simulator or Driver Training Tool (DTT) included both visual and motion cueing systems, the effect of both on athlete's skills acquisition and on-ice performance were comprehensively analysed. Each of the aforementioned sensory systems have their corresponding optimal working frequency domain, within which they will provide accurate details in response to the stimuli. When the brain is presented with motion stimulus from multiple sensory systems with different frequency responses, it mixes this multi-sensory information and switches between the cueing channels based on the most dominant signal from a particular frequency domain, this can be seen as a form of Kalman filter [31].

It is therefore easy to see that, in order to provide an authentic recreation of the sliding experience using the DTT, all sensory feedbacks must be taken into consideration. In accordance with the feedback from GB Skeleton team, their previous experience with the visual environment had

proven sufficient for their needs, however there lacks some distinct haptic feedback in the current build of the DTT. As part of the research object of this PhD, some of said missing haptic features will be added and the literature reviewed in this chapter will reflect on the theory behind these cueing methods:

- Motion perception
- Proprioception
- Haptic feedback

2.2.1 Motion Perception

Human body gather information regarding to its surroundings through the use of multiple sensory systems. Each sensory system takes 'incomplete' information and by combing these, the brain is able to acknowledge its current states such as where the body is, how it is moving and what position is it in [37, 36, 23]. There are five well known sensory systems: visual, aural, smell taste and touch. However there are other lesser known systems which controls balance and one's 'self - sense'. Angelaki & Cullen [10] stated in their work that balance is largely governed by the vestibular system, a complex set of organs within the inner ear. One's self sense is developed from a combination of many sensory systems, one of which is the proprioception system [15], which manages a more complex form of touch.

2.2.2 Proprioception

The proprioceptors inside a human body are muscles, joints, tendons and inner ear receptors. These proprioceptors send information to the brain relating to the body's position. Along with kinaesthesia, proprioception is responsible for one's relative sense of self [35], it governs one's feeling of movement, the strength of that movement and the effect on one's body. Proprioceptors provide constant feedbacks for the muscles and joints during motion, such as throwing a ball. This form of feedback is what enables precision control over one's muscles and joints, enabling the constant micro-adjustment of the body to keep one upright. Allerton [35] stated in his studies that the proprioceptors can be classed as exteroceptors (a sensory receptor that receives external stimuli) as well as interceptors (responsible for internal perceptions, such as pain, hunger etc.). When movement occurs in the body, resultant forces are received by these receptors. Nerves and sensory neurons detect stimuli and relays electro chemical signals to the brain. After the brain interprets the signal, motor signals are sent to the relevant muscles, forcing it to relax or contract. The proprioceptor relies on the body experiencing a force to create a signal. Once the acceleration experience by the body becomes zero the sensory network stops reacting and the body relies on the visual system for position until a change to the body state occurs. Research studies by Green and Angelaki [8] proposed a systematic study on human motion detection through the use of computational process to estimate body motion. In the study, separate sensory systems were isolated and cues were given to the primate subject to prompt a response. It was found that proprioception stimulation is critical to motion detection, therefore when implementing motion cueing algorithms in the simulator, proprioceptor simulation must be considered. Finally,

because the vestibular, proprioceptor and visual system are linked via the vestibular nuclei, it is therefore essential to ensure the motion cues and visual cues synchronize properly when using the simulator, otherwise motion sickness (simulator sickness) could occur [26]. To put in context of the DTT upgrades, shoulder pitching must be programmed to be in sync with visual and roll cueing.

2.2.3 Haptic Feedback

Haptic feedback is a form of touch stimulation, it can stimulate the proprioceptors. The application of haptic feedback requires force, vibration or motion feedback to the user. The operator could induce the feeling of three-dimensional touch stimulation onto the user by controlling the forces exerted. For example, if the user was to grab a ball shaped object, forces could be applied on the user's fingers/palm to make the object feel cubic instead. These type of haptic feedback have being available for medical and dental simulations since 1993. Defence industries have utilised haptic feedback in simulation training for many years. Motion platforms are incapable of producing sustained acceleration and as such pilots who use motion platforms to train for aerial manoeuvres were not subjected to g-force [47], this has significant impact on the immersion of the virtual environment. To compensate for the lack of fidelity, g-seats were introduced. The g-seat applies a force to the pilot and by exploiting human proprioception, induces the experience of g-force [47]. In the context of DTT, the torso and head g-force loading system adopted similar technology and has proven to be an effective method of improving fidelity without incurring large amount additional cost and system requirement. A similar approach is adopted for leg loading as part of the upgrade.

2.2.4 Work Completed by University of Southampton

Sawade [1] was successful in building the first single degree of freedom (DOF) DTT for the British Skeleton team. The simulator is capable of producing audio, motion, visual, vibration and proprioception cueing. The DTT was built within a constrained budget and time. As such it was not designed to try and replicate the real world with 100% fidelity. Instead the focus of his research is to incorporate perceptual learning paradigms into a low-cost training simulator and attempt to accelerate rate of learning new skills for Skeleton athletes.

His research reviewed that although visual is the primary sensory input for humans, it is inhibited during the sport of Skeleton for many athletes. Through his experiments it was shown that the inclusion of proprioceptor stimulation (i.e. force feedback), however presented, is required for the athlete to gain any benefits from using the simulator. His experiment also shows that in-simulator learning and performance was enhanced with the inclusion of motion cueing (vestibular system stimulation) for Skeleton steering tasks. He identified that both motion and proprioceptor and vestibular system stimulation were required within the virtual environment to make the virtual training effective. He presented compelling evidence that a low-cost DTT for Olympic Skeleton training could accelerate the rate of learning and increase an athlete's performance.

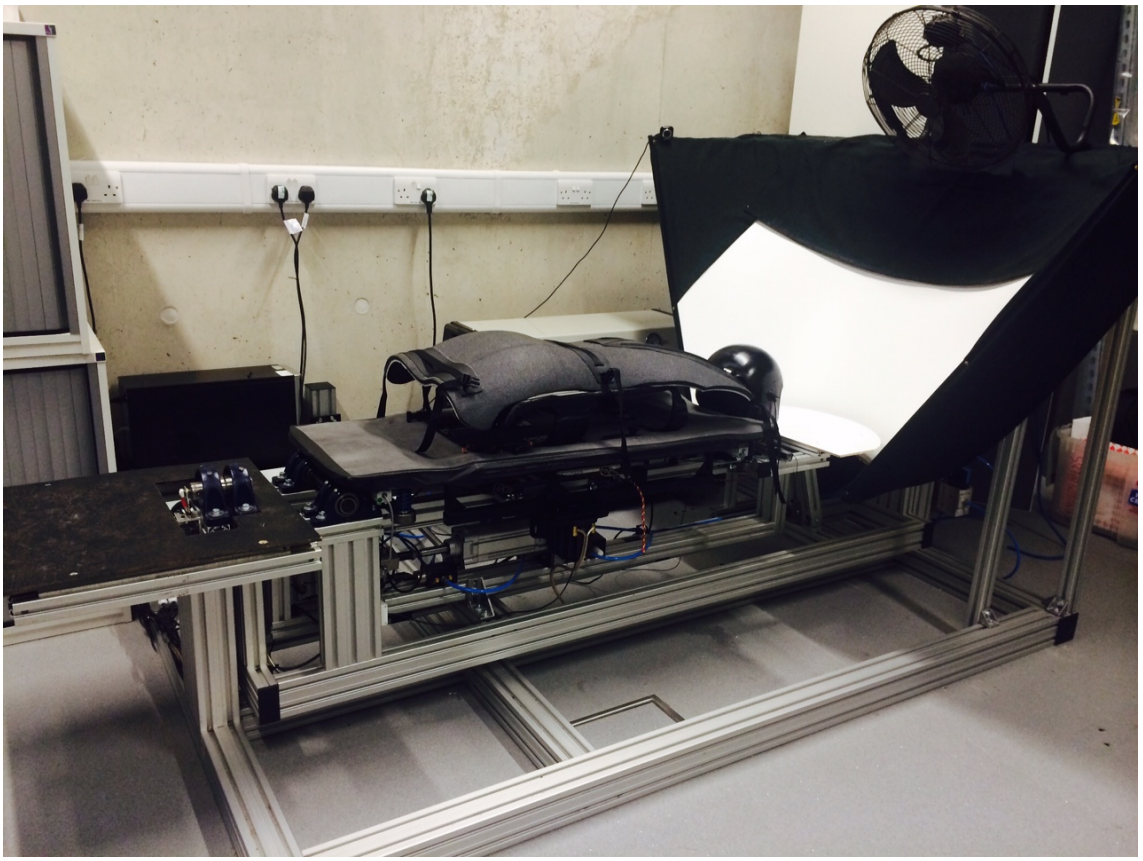

FIGURE 2.1: Fully assembled Skeleton DTT Mark II

2.3 Descent Simulation and Modelling

The principal aim of this PhD relies on the analysis of the physics model behaviour. A clear understanding of the physics model is therefore crucial. Before Roche [2], there were very few detailed studies regarding Skeleton simulations, however there have being various tools developed for bobsled and luge events. This section of the literature review will give a brief historical overview of the simulation and model development.

2.3.1 Single Degree of Freedom Particle Model

Baumann [30] developed a simple model of the descent of a luge down a track, which at the time was the nearest model to a Skeleton descent. He proposed a one degree of freedom equation of motion (Equation 2.1) for a sled travelling down a constructed model of the Konigsee track. The track is modelled in its original form by estimating corner radii and measuring lengths and heights of various points on the track.

$$\ddot{\alpha} = g(\sin\theta - \mu\cos\theta) - (\frac{\mu}{r} + \frac{C_d\rho A}{2m})\dot{\alpha}^2 \tag{2.1}$$

Baumann analysed the degree of accuracy of track modelling required to provide a realistic simulation of descent time. He used three different modelling techniques: 1) a straight line of

average gradient; 2) a straight line with varying gradient and 3) a series of straights and curves with variable gradients. The third approach was able to predict descent time within 1% of the track record for luge and therefore Baumann proposed that the model was a good tool for analysing where athletes lost time during the run. Balakin [28, 29] used the 1 DOF equation of motion to back calculate friction and aerodynamic drag data from a luge athlete at the Sigulda track. He gathered speed and time data at the entrance and exit between corner 14 and 15 and through corner 15. From the data he was able to estimate the athlete's drag area CdA and value of the ice friction coefficient in the straight and curved sections of the track. Bromley [3] designed two methods for analysing skeleton sled performance over a whole run as well as using the back calculation by Balakin to analyse the forces on a Skeleton athlete at the Altenberg track. The first model used a modified version of the 1 DOF equation of motion to include the effect of sled roll angle in the corners (Equation 2.3.1).

$$\ddot{\alpha} = g(\sin\theta - \mu\cos\theta\cos\phi) - (\frac{\mu}{r}\sin\phi + \frac{C_d\rho A}{2m})\dot{\alpha}^2$$

The equation allows for the calculation of descent time, once the start and finish velocity were known. The calculation is based on knowledges of gravitational potential energy at the start and the friction and drag coefficients of the sled. Bromley highlighted in his paper that this method uses many assumptions and ignores important factors such as track geometry.

2.3.2 Two Degrees of Freedom Particle Model

Models described so far do not take into account the 3 dimensional aspect of the simulation. They do not include across track speed or specify the transverse position of the sled. The interaction between the athlete and the sled is ignored, assuming the sled takes a fixed path down the approximated track without any steering force applied. Hubbard [20, 21] developed the first 2 DOF model on part of a bobsled track. Using a 3 dimensional model of corner 7 at Calgary, the track was presented as a network of point clouds. These points were parameterised in the along track α and across track β direction such that $r = (x, y, z) = r(\alpha, \beta)$. Figure 2.2 shows the sled represented as a point P on the track and its position falls between the point clouds and is derived through B-spline interpolating. Hubbard performed several simulations of this single particle bobsled model though Calgary corner 7 uncontrolled. He observed the oscillatory path taken by the sled through the corner and identified it as a path often seen when observing novice bobsled drivers and Skeleton drivers of all levels. Hubbard developed a crude steering model, simply a lateral force in the beta direction, to observe the damping of the oscillatory path by the steering forces in the early part of the corner. Huffman [25] used the same model as the basis for a driver training simulator used by the USA bobsled team before the 1992 Olympic Games. He expanded on the model to include wall collisions and a more representative steering model. The simulator was used by the elite athletes to learn tracks and perfect driving lines during the off season. However they questioned the value of its use close to major competitions. There were notable restrictions in the fidelity of the simulator, including the lack of g force and immersive visual environments. The biggest limitation of the model was the approximation of the sled as a single particle. This implies that sled heading angle is zero relative to the sled velocity and prohibits any form of skidding or sled rotation. Later Huffman [4] developed several iterations

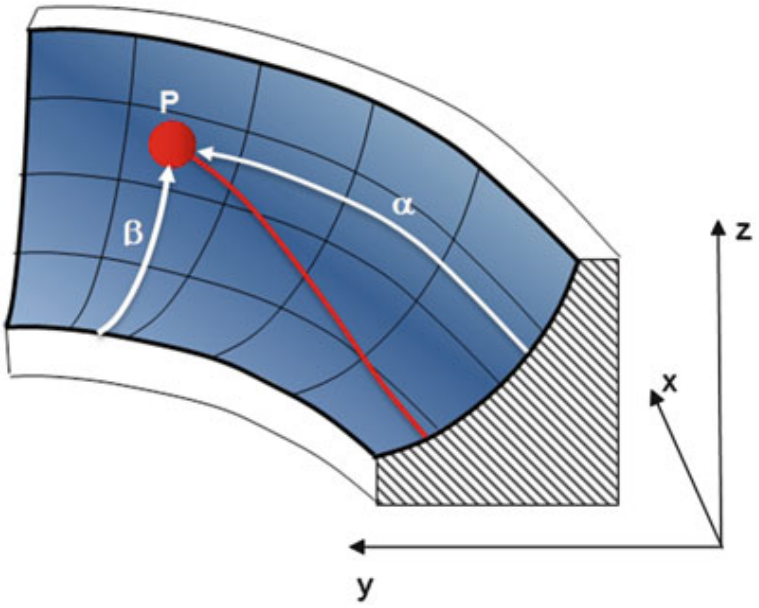

FIGURE 2.2: 3D representation of 2 DOF particle model on track surface [33]

of the sled model, investigating the possible methods of converting it to 3 DOF. He found that by modelling the sled body as a set of two particles connected with a spring mass damper was the best approximation to a real system.

2.3.3 Work Completed in University of Southampton

After reviewing the work done by Baumann [30] and Hubbard [9], Roche [2] successfully developed equivalent 1 DOF particle models for the Bob skeleton, incorporating force models by Bromley [3], to represent skeleton dynamics rather than bobsled. Using the 1 DOF model, he carried out comprehensive performance analysis on the Cesana and Whislter racing track. He evaluated simulation results that compares male and female athlete descent times and identified the cause for the principal discrepancy in the results to be push start times, total mass and body aero dynamics. From his findings, he found the optimum physique for a skeleton athlete using a weight equalised sled.

Later, Roche developed his 1 DOF model to include 2 DOF, adopting the basic architecture from the work of Huffman [4, 24, 25], and Hubbard [9, 20], who developed a similar model predicting bobsled descent dynamics and later built into a physical simulator. Principal findings using this new model include:

- The investigation of oscillatory nature of a cornering sled
- The convergence of practical descent lines
- A repetition of the athlete physique study which validated his conclusion from the 1 DOF model

Finally, Roche stated that the complex nature of the skeleton descent dynamic cannot be accurately represented using only 2 the DOF model. Therefore he expanded the model by modelling

each individual runner as separate bodies, thus introducing the third degree of freedom, yaw. A steering model was also included in his research to describe major friction mechanisms. He stated in the principal findings, that the 3 DOF model is a good initial structure for developing a comprehensive model of a skeleton descent, but requires more extensive testing and more comprehensive ice friction data before it can accurately reflect the dynamics of the skeleton sled. The 3 DOF model was used to develop the DTT by Sawade and will be used as the physical basis for this PhD.

2.4 Control Algorithms to Find Optimum Descent Route

The second research aim is to find the optimum descent route for Skeleton. There are currently no literatures regarding to finding the computed optimum descent route for a Skeleton simulation, however there are two pieces of literature solving a similar problems for bobsled. Literatures describe two different approaches for the implementation of a driver model, computation of optimal path and driver controls. The first approach applies optimal control theory to identify the steering action to minimize the travel time through either a single curve or the whole track. The second approach involves two tasks: identification of the optimal trajectory and implementing a controller to follow the trajectory as closely as possible.

2.4.1 Optimum Steering Control Approach

Zhang [33] utilised optimal control theory to develop smooth steering algorithms for the single particle 2 DOF bobsled model. Control actions were obtained for both one curve and the entire track (piecewise optimised) of Lillehammer. He also investigated the performance of minimum time control algorithms using hysteresis control strategy, which does not mimic the limitation of the human operator. Their results indicate that the sled's controllability decreases with speed and therefore the optimal control of the sled in the slower sections of the track is especially important. Zhang claims that the performance of his piece wise optimisation solution for the whole track is consistent with whole track optimisation. He argues that although one-curve optimisation solutions may not be the optimal solution of the whole tracking problem, it is still capable of reducing travel time of simulation for more than 0.5 s and increase the final speed by almost 2m/s compared to free-travelling models (see figure 2.3).

2.4.2 Trajectory Planning and Steering Control Approach

As previously mentioned, Braghin [12] describes an approach that designs the driver model in two separate tasks, the first task is to find the optimum descent trajectory. The trajectory is planned to reduce the run time of a simulation given the track geometry and initial condition. Braghin [12, 13] compared different strategies in achieving the optimum trajectory, and it was found that by minimizing the longitudinal energy dissipation, the target could be achieved. Braghin modelled the bob sled as a 3 DOF particle in space. He derived the relationship between the local and global sled reference system in 3D space. The optimum trajectory was determined by

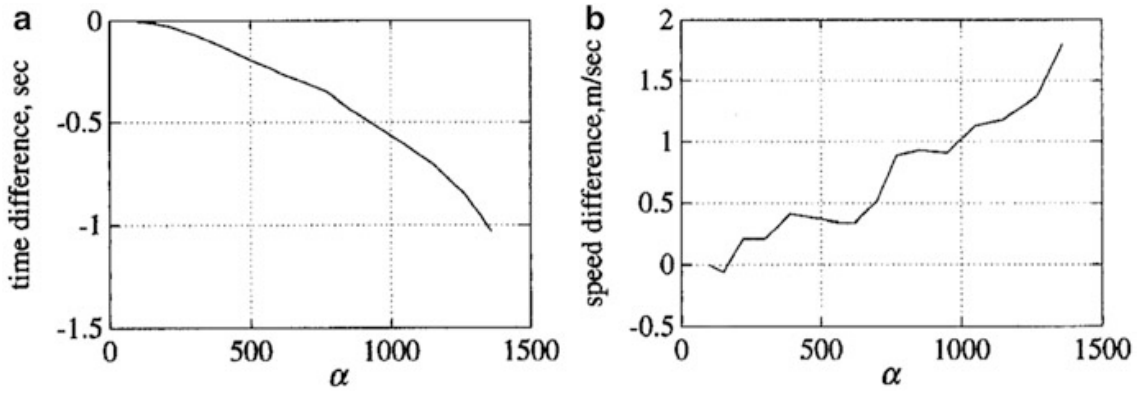

FIGURE 2.3: Time difference (a) and speed difference (b) of whole-track piecewise minimum time control for Lillehammer Olympic Track. [33]

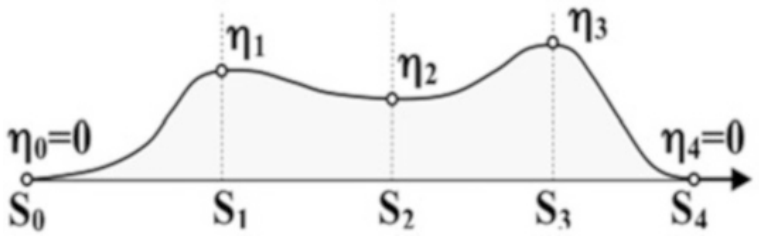

FIGURE 2.4: Variation of η inside a corner. [12]

solving a series of minimum time optimisation problems and integrating the resulting optimised lateral driving forces η (see Figure 2.4).

Once the trajectory has being identified, Braghin developed a PID controller to act on the steering axle. The controller was developed to mimic the behaviour of a professional bobsled driver and uses multi-body model of the sled. This allows for accurately representation of steering action on the sled trajectory. Figure 2.5 compares the steering angle demanded by the driver model and steering angle obtained from experimental data along the whole track. The result shows high similarities between the two sets of data.

2.4.3 Using MPC for Trajectory Planning and Tracking

Model predictive control (MPC) has a widely recognised shortfall in that it can only be used in applications with slow dynamics [34], the sampling time in these applications is usually in the range of seconds or even minutes. For this reason, MPC architectures have been popular within the chemical industry [19] for many decades, however, in recent years, extensive research have been conducted into utilizing MPC in trajectory optimisation of autonomous aero, terrestrial and submersible vehicles [18, 7, 17, 5]. The reason for moving towards MPC is it provides both constraint handling capability and a flexible degree of optimisation, depending on the required speed of the response dynamics [34], this combination of features proves to be very useful in autonomous trajectory planning to both conserve fuel and avoid hazadous scenarios [6, 27].

The challenge in trajectory planning is that it requires very fast response rate from the controller, usually within 5 ms range [34]. A well developed technique for increasing the response speed of MPC is to compute teh entire control law offline and uses the result as a look up table

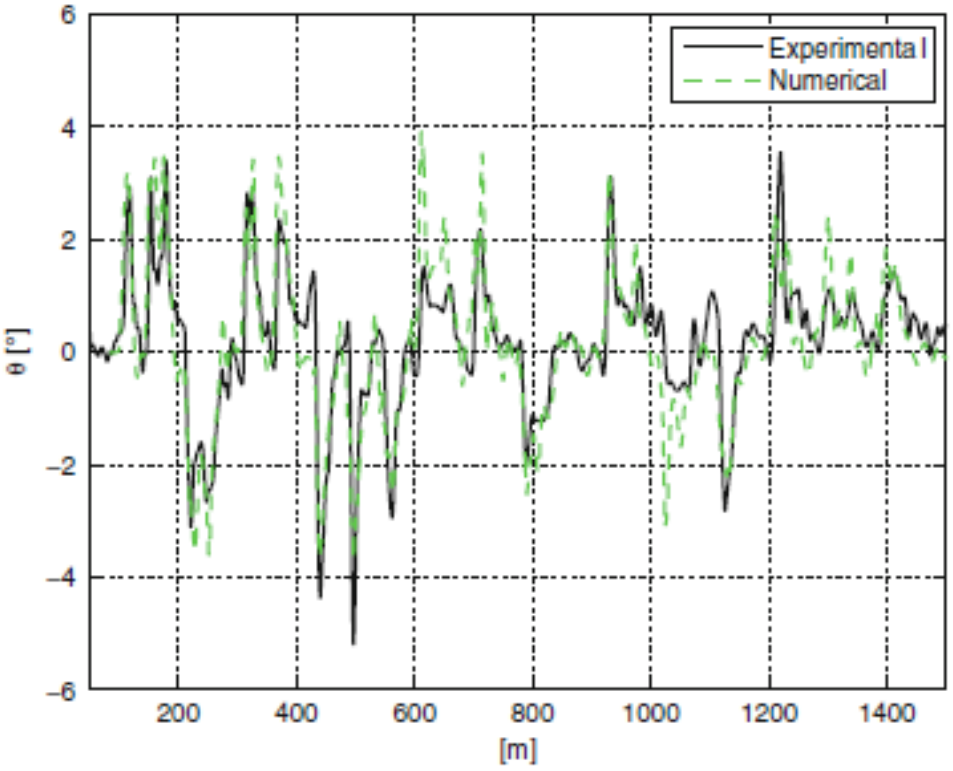

FIGURE 2.5: Steer angle vs travelled distance: comparison between numerical and experimental data from [12]

online depending on the plant environment. this method works well for systems with small number of states, few constraints and short time horizon. However, as the system becomes more complicated, the computational effort also increase exponentially, making this approach non-viable.

Other fast MPC frame works exist, one approach is to break down usually complex non-linear system model into smaller, linear sequential plants and iteratively optimising them using MPC [22]. This method can predict and optimise seconds worth of trajectories in just milliseconds and has being demonstrated to function on an AscTec Firefly hexacopter and Rezero, a ball balancing robot. Another method is to uses a hierarchical apparoach, combine two different layers of control strategies operating at different speed. In [32], flight path plans for quadcopters uses a slower MPC in the upper layer to generate optimised collision-free state reference, that will satisfy all relevant constraints, and a faster robust feedback linearisation controller in the bottom layer to track the optimised state reference and suppress any tracking errors during the fast control interval.

Although Skeleton's dynamic is fundamentally different from above mentioned autonomous vehicles, it is reasonable to believe that the MPC architectures can be transferred to control the simulation and provides a solid theoretical foundation for this PhD.

Chapter 3

Driver Training Tool

3.1 Chapter Introduction

The first research hypothesis involves augmenting the existing DTT and implement the key missing features previously mentioned in section 1.3. To assist the reader in understanding the full functionalities of the DTT, this chapter begins by presenting a brief overview of the Mark II DTT (refer to [1] for more details), followed by the augmentations carried out to construct the Mark III DTT. In particular, the hardware infrastructure of the Mark III DTT was designed to include the following features: pitch motions around the shoulders of the athlete; leg G-force loading; toe steering; Minor upgrades including quality of life features such as control penal and safety systems. The operational software of the DTT were also upgraded to include performance analysis and feedback graphical user interfaces. The final section of this chapter describes the different ways in which the Mark III DTT is being used by GB Skeleton as a training tool.

3.2 Mark II Virtual Reality Simulator

3.2.1 System architecture

The Mark II DTT is formed of an array of subsystems, ranging from physics model to graphics generation. All these subsystems need to be synchronised in real time, in order to achieve virtual control. To do so, a large amount of computational power and data processing is required and to achieve this, a system of three computers running in parallel was used. Figure 3.1 shows the basic interaction of the computers in block diagram format.

Computer A is the 'master' computer. All coordination process of the system architecture is performed here to ensure real-time synchronisation. The Simulink physics engine also resides in computer A, which governs the state of the simulation and provides the rest of the system with virtual parameters. The simulation executes at approximately 100 Hz, however the time step is synchronised with the internal clock of the computer to ensure real time operation. This is important as data is transmitted between computer via User Data Protocol (UDP) link, which

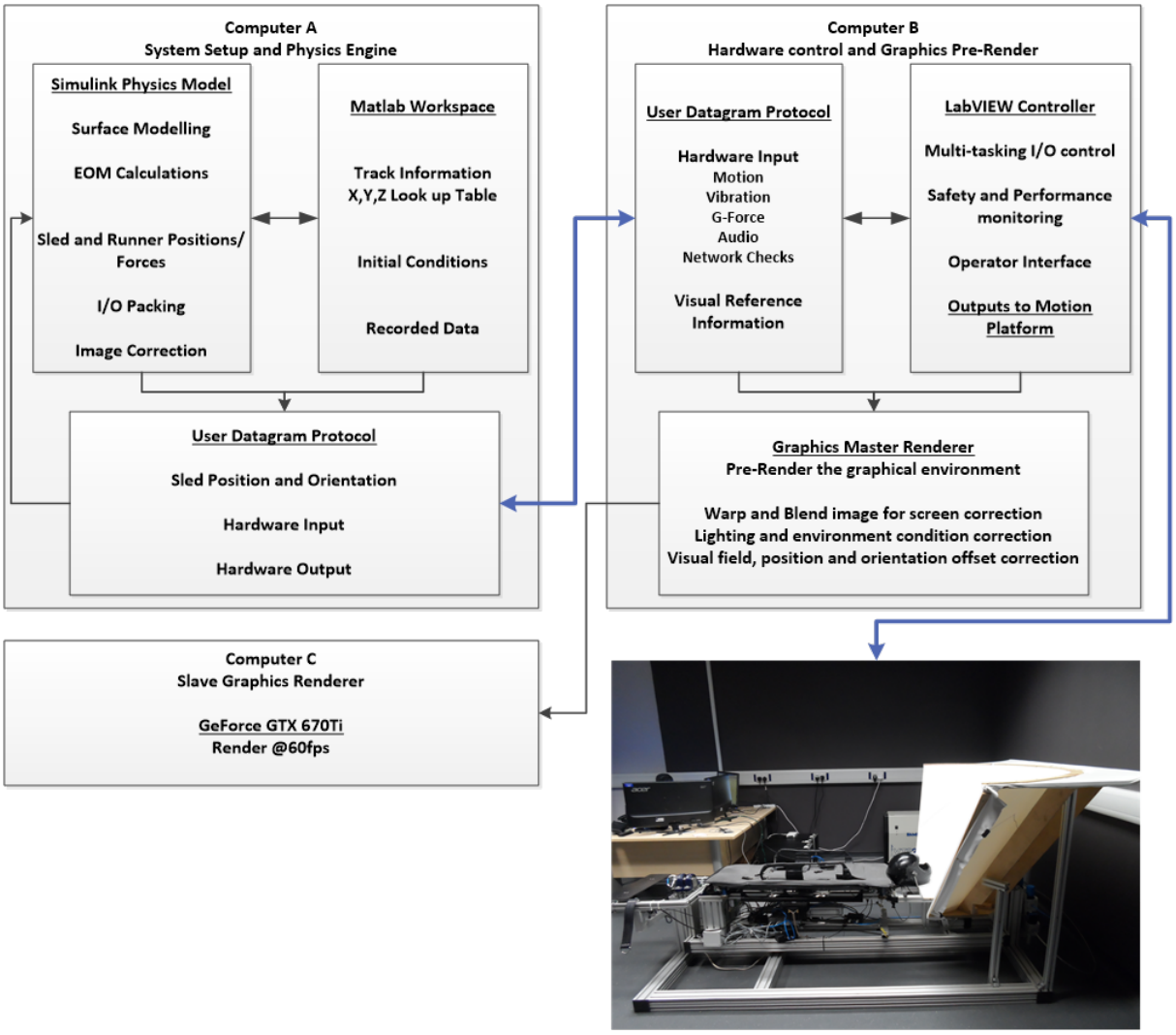

FIGURE 3.1: Top level system architecture

does not perform handshakes between sender and receiver or check for timing error, but requires less processing power and therefore enables faster communication [46].

Computer B (slave) is in charge of two primary functions:

1. Pre-render the graphics environment and broadcast instructions to the graphics renders in computer C.
2. Control the simulator hardware and measure system feedback and relay information back to computer A.

National Instruments LabVIEW was used to control the hardware. It sends and receives instructions via UPD from computer A and generates command signals to the motion platform through the NI Data Acquisition card. Commands generated this way include: Roll actuation, Proprioceptor actuation, Audio and Vibration signals. Operator can monitor any specific parameters through the graphical user interface in real time. The LabVIEW program is executed at approximately 1 kHz (subject to hardware speed), which is above the minimum Nyquist frequency

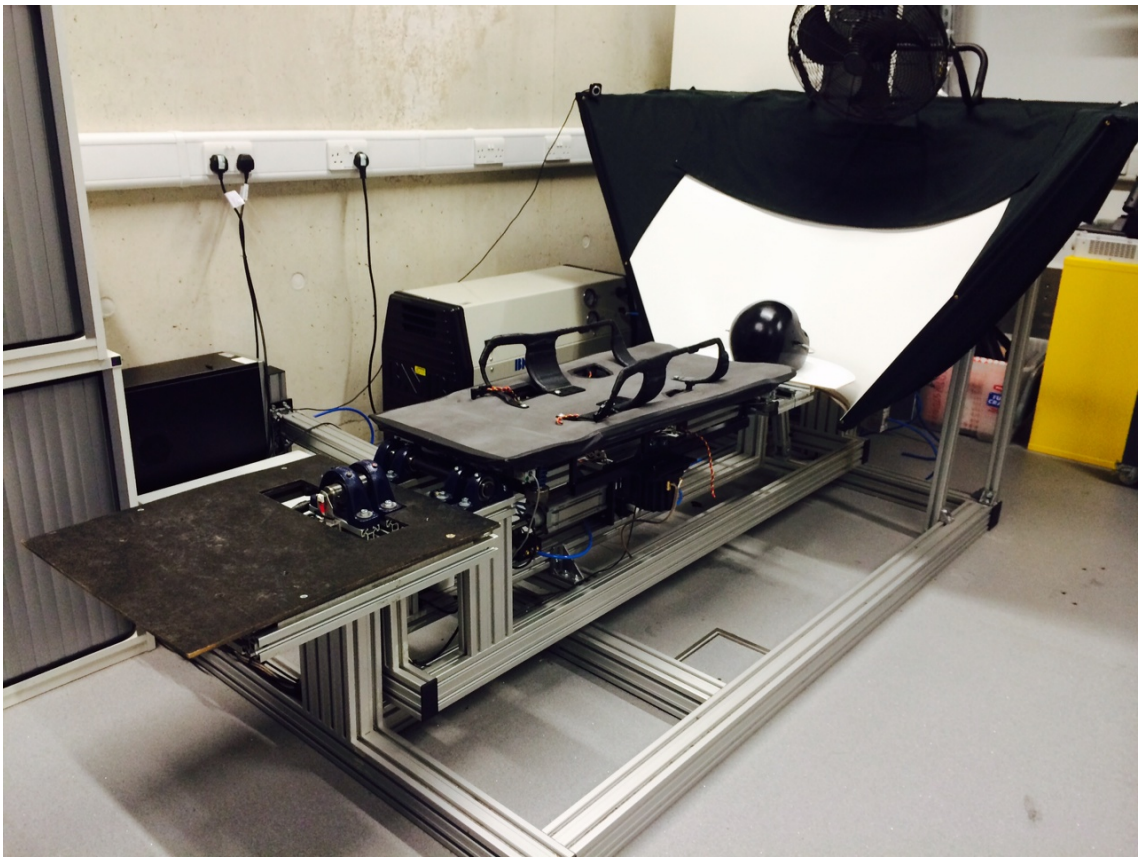

FIGURE 3.2: Fully assembled Mark II DTT

and can ensure command signals from computer A is not lost through sampling. Computer C (slave) is in charge real time rendering of the track during the simulation. It contains a GTX 670Ti graphics processing unit, capable of performing a final render of the virtual scene at 60 frames per second at a resolution of 1960 x 1080. The computer is linked to a Cannon WUX 4000 Full HD projector via DVI, which projects on a meter wide conical screen mounted on the simulator frame (see Figure 3.2).

3.2.2 Motion Platform

The platform was designed as a stacked system to minimise cost and maximise the movement range of the platform in particular DOF. The stacked design also allows for additional DOF to be added without affecting the rest of the system. From track testing, Sawade [1] has identified that roll and heave motions in the real sled system are dominant both in magnitude and frequency for their respective axis. There are motions with respect to other DOF, however due to constraints on cost, only roll and heave were included in platform. Heave motion was mostly the result of centripetal acceleration through the corners and would require far more amplitude than the platform could provide. Instead the heave cueing was produced using similar proprioceptor G-cueing system as the ones adopted for pilot training (refer to section 2.2), details of G-cueing system will be given in section 3.2.3.

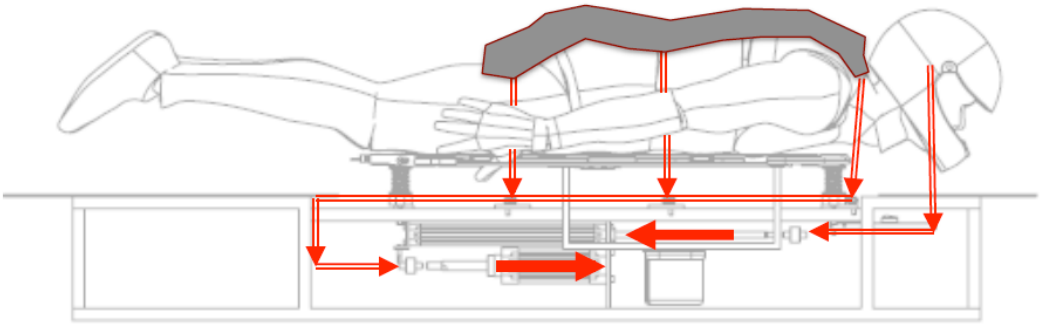

FIGURE 3.3: Mark II DTT G-cueing system setup [1]

The motion platform was built from aluminium extrusions, for weight and strength purposes. The structural design of the platform is modular, placing the athlete inside a rotating 'cradle' (moving section of the motion platform as shown in Figure 3.2), attached to the base frame via pillow block bearings. The cradle was designed to not obstruct athlete's field of view when moving. Roll motion is implemented using a dual action, Festo pneumatic actuator controlled by a high speed, Enfield positioning system (precision control valve with built in custom pseudo PID algorithms). The platform is capable of rotation up to +/- 47 degrees from neutral position, however much of this rotational freedom is for redundancy measures. In the real world, large angles of roll occur during the corners of a track, where the dominating gravitational pull experienced by the athletes is in the direction of the centripetal force, which is not available on the motion platform. Therefore, by holding athletes at large roll angles for a prolonged period of time, gravity can affects the vestibular system and cause motion ambiguity.

3.2.3 Proprioception G-cueing

A 'marionette puppet' style actuation system was used to introduce G-cueing. The system has two high speed pneumatic actuators which are attached to the frame underneath the athlete, allowing for maximum stroke length. The actuators are linked to the helmet and torso independently using dyneema ropes through a network of pulleys, this design allows for an even distribution of pulling force on the one piece torso harness, which is made from compressed foam and moulded to the shape of an adult male. The rope linking head actuator to the helmet feeds through a custom designed pivot that allows for freedom of movements in a 180 degree arc, enabling the athlete to move his/her head during the simulation. Figure 3.3 displays the routing of the ropes and the placement of the harness. The actuators are controlled by Enfield high speed valves which are controlled by external analogue PID controller. During the simulation, the controller is fed G-force as reference and uses force feedback to ensure a constant level of proprioception cueing and consequently improve the immersion of the simulation. The PID controllers are tuned to give underdamped step responses. According to the athletes, the small overshoot in the response induces a more 'natural' feeling.

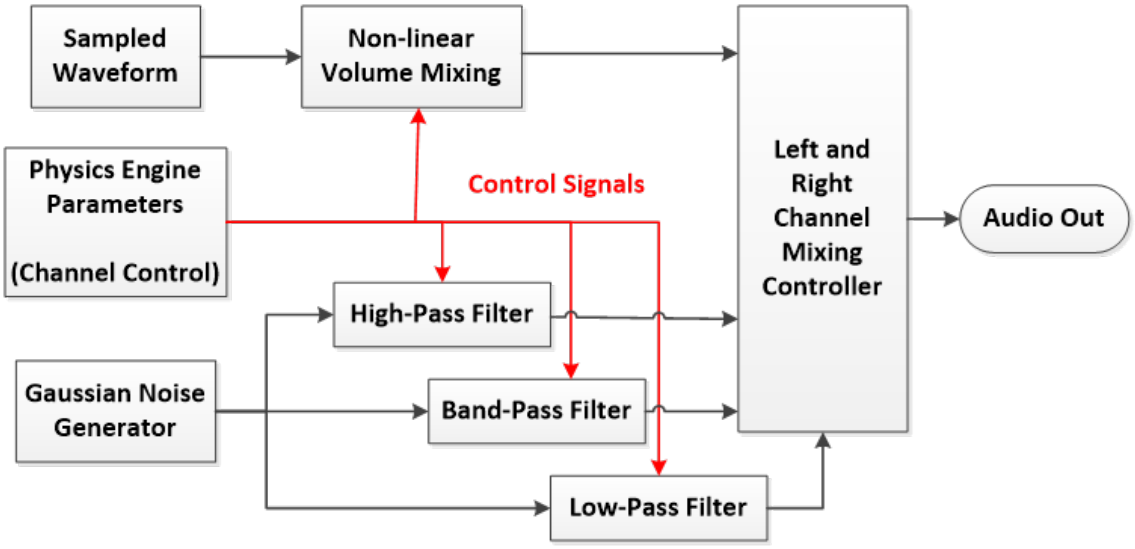

FIGURE 3.4: Audio algorithm schematics

3.2.4 Audio and Vibration Generation

For skeleton athletes, audio could be used to detect skidding, hitting a wall or roof and the vibration level of the sled. Although not often used as a steering cue, it is essential for realism as without audio, a distinct stimulus is missing from the virtual experience, causing a breakdown in immersion. Audio is fed to the athlete via in-ear headphone, which can provide stereo audio as well as cancel noise from the vibrating frame. The audio is generated on computer B in the LabVIEW hardware control program. The audio generation algorithm is shown in Figure 3.4. The algorithm can be broken down into three distinctive processes. Gaussian noise generator is used to generate the base sound which is fed to a group of filters. The cut off frequencies of the filters were obtained from performing FFT on the audio file from head-cam footages. The dominating harmonics are spread through lower frequencies, mostly caused by sled vibration on ice. There exist sparse harmonics in the higher frequency band, this is caused by the sled skidding and slipping on ice. The frequency which provides wall hitting sounds was found by empirically tuning the bandwidth of the band-pass filter. The amplitude of the filtered noises is controlled by scaled versions of the physics parameters (e.g. Wall hit controls band pass filter signals, Theta angle controls high pass filter signals etc.). Depending on the values of the parameters, audio is scale in either ear phones to create stereo effect. Finally, a sampled waveform representing 'ice chatter' was multiplied with a random number generator (to eliminate repetition of audio signals) and over laid on top of the generated audio signals for both ear phones.

Vibration is also a key contributing factor towards realism and a primary steering cue. Vibration is generated via electrodynamic shakers attached at bottom of the sled runner frames (see Figure 3.2), the signal controlling the vibration is spliced from the audio with its own independent level control. Vibration has negative impact on athlete fatigue level. For skeleton, a comparable level of vibration to real life is not ethically suitable for simulation training (see Appendix C). Therefore the level of vibration is capped in software to be 25% of the allowed real life at maximum as per ISVR standards (VDV $\approx 5.94\ m/s^{1.75}$; RMS $\approx 1.5\ ms^2$), for detailed audio noise and system vibration data, please refer to Appendix D.

3.3 Mark III DTT

The Mark II DTT has received mostly positive feedback from athletes and coaches regarding its function as a training tool, however comments were also made regarding to the missing motion cues, which lead to the occasional breakdown of immersion. As part of the continuous effort to improve athlete/coach experience using the simulator, Mark III DTT was designed with the following major upgrades:

- Pitch actuation
- Leg G-force cueing
- Toe steering control

3.3.1 Pitch Actuation System

Mark II DTT was built with limited motion cueing capabilities. After the athletes had time to practice on the Mark II, it was identified that some important steering cues were missing. One such cue is the pitching motion (that) athletes experience under their shoulders when the sled enters/exits a corner. The pitching motion is predominantly a proprioception cue, one which many elite athletes use to judge their steer timings. Therefore it is critical to produce an accurately timed motion cue.

Adding an extra motion cue onto the existing system could inadvertently affect the performance of other components on the DTT, such as the diminished response speed of the roll motion due to the distribution of flow rate. Therefore, it is important to select the appropriate components when designing the upgrades. In the DTT location, air is supplied by a Bambi VTS200 Silent Oil Free Compressor & Dryer unit, which have an average operating pressure of 8 bar during a typical simulated descent (less if consecutive simulations were performed). The existing system uses approximately 5 bars of pressure whilst in operation, in theory this implies only actuators with an operating pressure of 3 bars or less could be used. In practice, since the platform will only be actuated through corners, there exist margins of flexibility. However, to ensure performance and to comply with health and safety regulation when using the compressor, the actuator that requires the lowest operation pressure and fulfils the design specifications was used. Through physical experimentation, it was deemed that a pitching distance of at least 20mm is required for the participant to experience the motion cue.

Spring Guide Assembly

The real sled is free to move vertically from bouncing and vibrating on ice, it is also free to contort. This freedom of motion gives the feeling of the sled runner compressing and ultimately allow the athlete to perceive the texture of the ice surface. If the sled on the simulator is not permitted to move and contort, the steering motion will feel very unnatural. A spring guide system was developed to suspend the sled and athlete from the frame. Figure 3.5 displays an exploded view of the spring guide and Figure 3.6 shows the fully assembled spring guide as it is

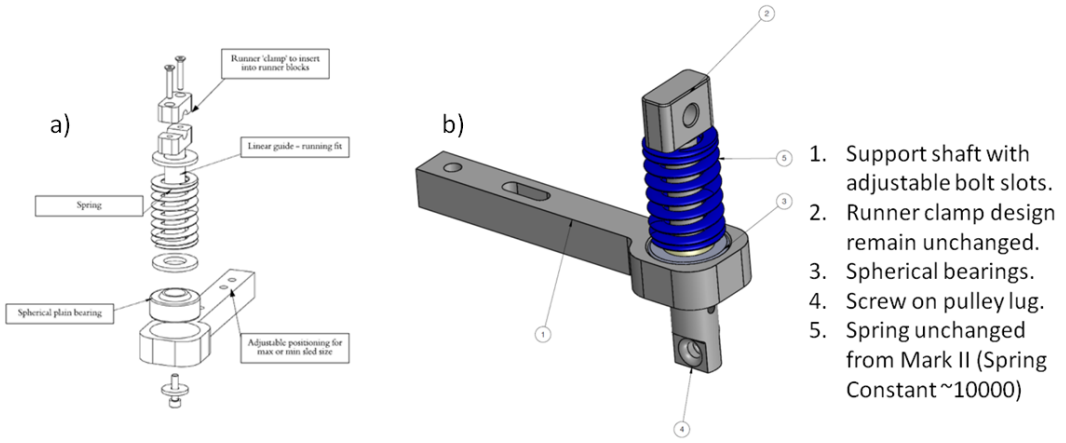

FIGURE 3.5: a)Spring guide system from Mark II, b)Spring guide system from Mark III

implemented in the Mark III DTT. The spring guide consists of a spring, a linear guide, a runner block and a spherical bearing which is housed on the custom base support shaft. The design ensures that the sled is free to pivot around its centre point to allow the athlete to feel contortion when steering. Stiffness of the spring was chosen to simulate the stiffness of the runners (2 springs equal 1 runner, each at approximately $10000 Nm^{-1}$). Due to budget constraints, Mark III DTT was designed to use as many parts from the Mark II as possible, therefore the springs and the support shaft were reused, but the linear guide and runner block had to be redesigned, refer to section 3.3.1 for detail.

Actuation System

Since minimum motion stroke required is 20mm and the spring stiffness is approximately 10000Nm-1, an estimation of the force required from the actuator can be calculated (200N). Athletes on the sled would also increase the frame stiffness. Therefore, even though there are flexibilities in the design, the actuators should still be selected base on the ability to generate at least 200N of force whilst operating on 3 - 4 bars of air pressure. The actuator selected for this task is the Festo standard cylinder DNCI-32 with integrated displacement encoder, which has maximum stroke length of 80mm and a piston diameter of 32mm. It has a minimum operating pressure of 0.6 bar and a theoretical force of 483 N at 6 bar of air. It is coincidentally the smallest pneumatic actuation unit Festo supplies suitable for this kind of application.

Early design concepts for the hardware layout consisted of vertical actuators mounted on pivots joints directly under the spring guide system to perform actuation through the linear guide. This design was deemed infeasible for the following reasons:

- Available space underneath the spring guide is limited, in order to install the actuator, considerable amount of additional frame works have to be installed underneath the current 'cradle'. This will weaken the structural integrity of the supporting framework and create a safety hazard. Installing additional framework also decreases the range of roll motion of the 'cradle', as the extra material will intercept with the base frame.

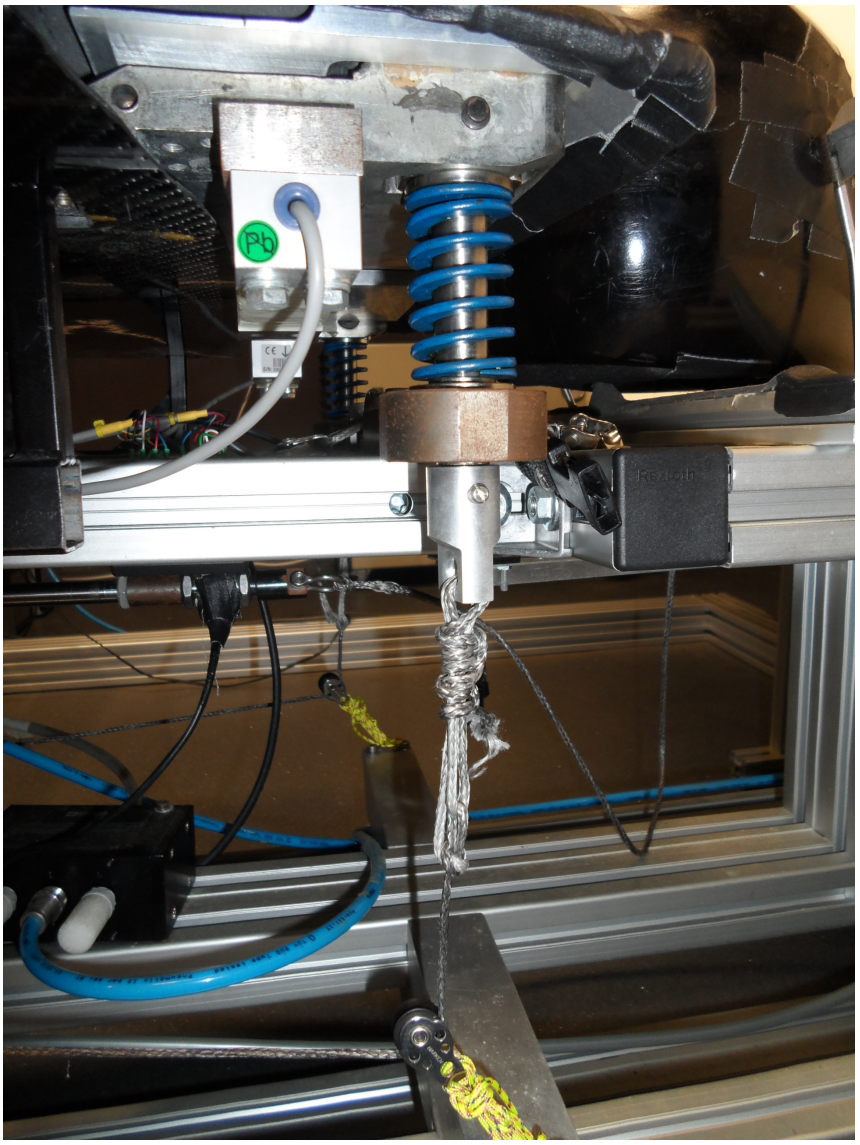

FIGURE 3.6: Fully assembled spring guide system

- In this proposed setup, the actuator has to be mounted on pivoting joint, to allow for rotation when the sled body is pitched. However this pitching motion creates a side force of up to 250 N on the piston rod, which is not designed to withstand any form of perpendicular force loading. This is especially true for the model with integrated displacement encoder. Any application of side forces will damage the sensors embedded in around the rim of the piston. Piston support could be added in the form of FEN-FENG. In order to apply adequate support at stroke length of 20 mm, the minimum rod diameter has to be 32mm. This implies each linear guide would weigh 1.57 kg and require an unreasonable amount of frame works to be added, which is simply not practical.

Figure 3.7 displays the final actuation system layout. The new layout adopts a pulley based design, removing the major disadvantages from the previous iteration. The new design requires the installation of only one v-shaped aluminium crossbar underneath the spring guides to act as the attachment points for the pulleys. The aluminium crossbar was attached within the

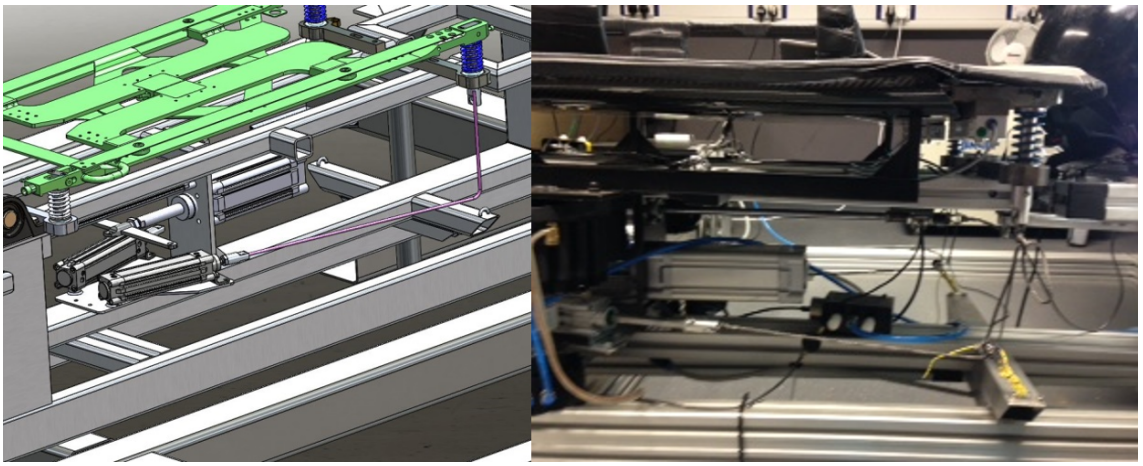

FIGURE 3.7: CAD design of shoulder actuation system(left), Implemented actuation system(right)

inner 'cradle' and will therefore not obstruct the movement range of roll. The actuators are installed on a horizontal planed, inclined at the angle that produces the least amount side forces (effectively none) on the piston rod. The placement of the actuators and the crossbar is designed for even weight distribution. The system uses two modes of actuation. Whilst pitching upwards, the spring guides provide all necessary force and the movement and the actuators are used to control the rate of pitch. Whilst pitching downwards, the actuators produce all the forces buy pulling on the spring guides. The original spring guides were modified, the linear guides have being elongated and threaded on one end for attaching to the pulley lug (refer to Figure 3.5). Actuators and spring guides are connected via tort steel cables to minimise loss of system response rate.

3.3.2 Leg G-Force Cueing

Athletes who have used the DTT for training would often comment on the lack of 'pressure' (the athlete and coaches refer to g-force loading as pressure) experienced on their legs through corners of the track. Some athlete stated that this sudden break away from realism have affected their steering decisions. This feature was therefore included as part of the upgrade. Leg G-force cueing is achieved through pulling down on the athlete's carves in sync with g force generated from the simulation. Leg straps are pulled by a length of bungee cord, attached to the torso actuator as illustrated in Figure 3.8. As a result of using bungees, the response rate of the leg g-force cueing is slower. It is used to not accidentally injure the athletes' knee when abrupt changes in g-force occur. The bungee is attached to the torso actuator through key ring lug, which allows it to move freely between the left and right legs and consequently ensuring a consistent application of g-force when the athlete moves. Human experiments will be conducted to determine the optimal thickness of the bungee that will produce the most realistic haptic feedback for athletes whilst complying with health and safety protocols.

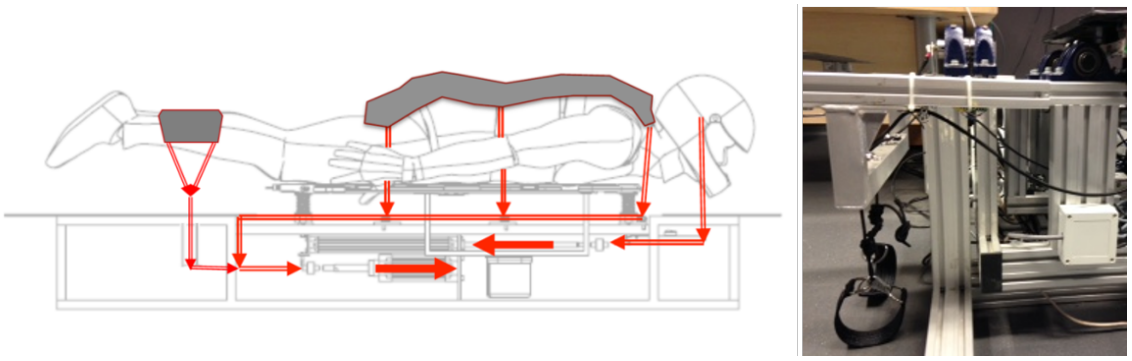

FIGURE 3.8: Leg strap actuation arrangement(left), Implemented leg g-force cueing system(right)

3.3.3 Toe Steer Control

In order to use the DTT as a driver training tool, the fidelity of the physics engine have to be improved substantially. As an effort towards achieving this, toe steering capabilities were added in the Mark III upgrades. Skeleton athletes may apply toe steering to create a larger than usual steering moment, usually as a last resort to correct their mistakes. These form of steering action is frequently short and aggressive, therefore it is crucial to design a sensor system which is able to detect such abrupt steering actions.

The foot steering system consists of a carbon fibre contact plate and two high speed single point load cells, the position of the system can be adjusted with respect to individual athlete's height (see Figure 3.12). Carbon fibre has as a very high stiffness to weight ratio. Its high stiffness minimises energy loss from the deformation of the plate and the low weight implies less energy is required to overcome the moment of inertia. Both features improve the system's sensitivity to the athlete's steering actions.

The HBM K-PW6C single point load cells are capable of producing approximate linear reading within their respective halves of the plate. This means the total steering force and direction of steer can be obtained with good accuracy across the entire plate. The dynamics behind toe steer is currently unknown. An estimation of the relationship between athlete's steering action and the resulting friction force is presented in Equation 3.1 and 3.2. The equation is arranged so that the direction of the steer is determined by the ratio between left and right toe steering forces.

$$f_L = a\mu_{toe}\frac{F_{toeL}}{2} \tag{3.1}$$

$$f_R = a\mu_{toe}\frac{F_{toeR}}{2} \tag{3.2}$$

- f_L and f_R – Frictional force on the left and right runner generated from toe steering
- a – empirical scaling factor to be determined from human experiments
- μ_toe – Coefficient of friction between athlete's toe and the track surface
- F_{toeL}, F_{toeR} – the steering forces detected on the respective load cells

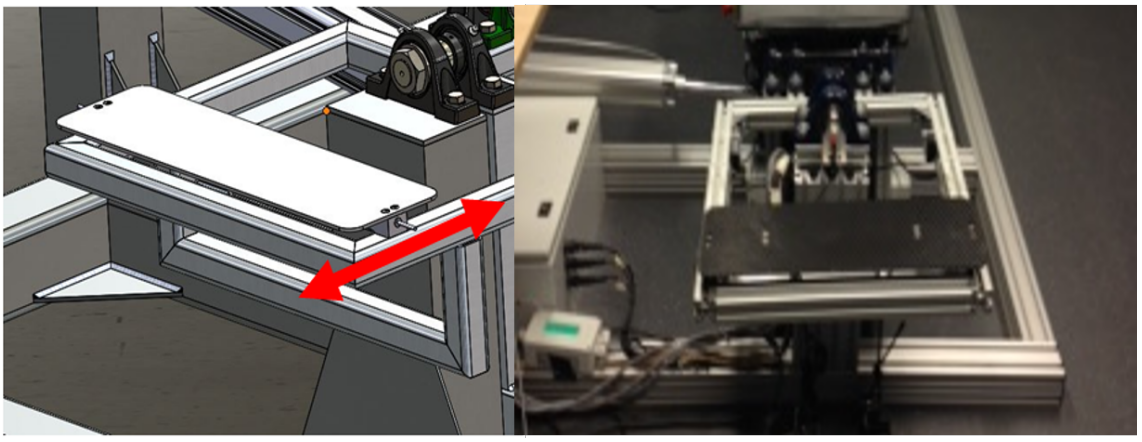

FIGURE 3.9: CAD design of toe steering system (left), Photograph of implemented toe steering system (right)

3.3.4 Commissioning of Mark III DTT

Unlike the Mark II DTT, which was primarily built as research tool, operated and maintained by members of the University of Southampton. The Mark III DTT was designed to be a training tool for the GB Skeleton team, implying it will be operated and maintained by the sport's own technical staff/coaches outside of the university. As such, not only does the Mark III DTT's hardware and software infrastructure must both to meet the industrial standard of safety, a simplified user control penal must also be installed before it can be commissioned. Although this work is important and has taken considerable amount effort and time, they are however not of any significant values academically and will therefore not be detailed in this thesis. Instead a list summarising the work carried out on the DTT is given below:

Hardware:

- Design and construction of external break circuits to deliver power and relay command and feedback between all additional components.
- Design and Installation of industrial standard safety systems including two independent emergency stop circuit and inlet safety dump valve (see Figure 3.10).
- Design and redistribution of the pneumatic piping system for more efficient air flow.
- Installation of user control penal (see Figure 3.11).
- Maintenance and replacement of rusty components Mark II DTT.

Software:

- LabVIEW control software updated to account for upgrades to Mark II DTT and eliminate redundant codes.
- LabVIEW control software reprogrammed to include emergency stops.
- LabVIEW graphical user interface reprogrammed to improve clarity.

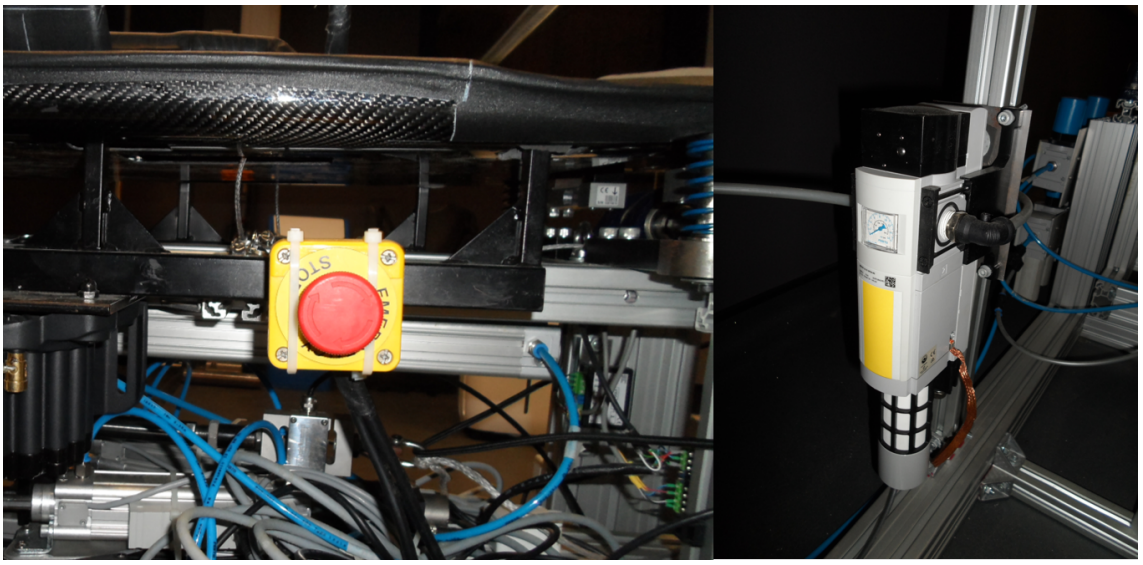

FIGURE 3.10: Emergency stop & industrial standard safety dump valve on DTT

FIGURE 3.11: User control penal with incorporated emergency stop

- LabVIEW graphical user interface and control software revised to give high level user more customisation abilities.
- Simulink physics model updated with steering wheel control, capabilities of accepting new track maps for trajectory generation.
- Simulink physics model updated to incorporate upgrades made to Mark II DTT.
- Simulink replay model updated to incorporate upgrades made to Mark II DTT.
- User manual written for typical operation procedure.
- Technical staff and coach training complete to use Mark III DTT.

3.4 Coaching Software

An important factor in improving an athlete's performance is the coaches' input. Traditionally, coaches would stand trackside in a particular corner of interest and film the athletes as they pass. The footages will later be analysed in slow motion using video capture software. This information along with subjective feedback from the athletes was all the coaches had to work with when giving instruction and support to the athletes. The introduction of the DTT enables coaches to analyse many aspects of the athletes' performance (e.g. left shoulder steering force in corner x) in detail, and provide much more comprehensive and personalised support. However, most coaches were ex-athletes or have always being involved with the sport and are unlikely to be able to interpret complex data from the DTT. It is therefore important to create simple and informative analytical interfaces for the coaches and athletes to use. By presenting performance data to the coaches both in real time and post training, they were able to understand the unique driving styles of each individual athlete and rapidly identify the areas which they needed to improve upon.

3.4.1 Post Training Analysis Graphical User Interface

The DTT records the athlete training performance and generates vast amount of raw data, it is important to develop software that interprets these raw data and present only the key information in the format useful to the coaches. The post training analysis graphical user interface (GUI) is a tool developed for rapid extraction and analysis of performance data. The GUI is an ongoing development tool, feature were added or taken away depending on the training objectives set by the coaches. However, the key philosophy behind the design process remains the same: automation. To elaborate on the automation process, an example analysis routine using the current version of the post training analysis GUI is given below:

1. Starting the GUI opens up the interface illustrate in Figure 3.13. There are a total of 8 buttons and 3 comment boxes.
2. By pressing the 'Load Run' data, the user will be prompted to load in the raw performance data file. Depending on the data received, the GUI will automatically load the appropriate tracks from which the data was obtained.
3. 'Plot Run' will plot the top-down view of the selected track and enable data cursor, which allows the user to select a specific section of the track to be analysed.
4. '3D Pot' opens up a second figure (see Figure 3.13) and plot a 3D mesh of the selected track segment as well as over laying the left and right runner traces on the map. Data cursor will be enabled at this point for figure 2, allowing the user to select the point of interest (usually a particular steer) to be analysed.
5. By pressing the 'Analysis' button, 6 subplots representing various virtual parameters from the performance data will be plotted, the 3 subplots on the right side are zoomed in versions of the plots on the left side. In the plot of athlete steering input, the GUI automatically identifies the starting and end time of the selected steer as well as the time taken to reach

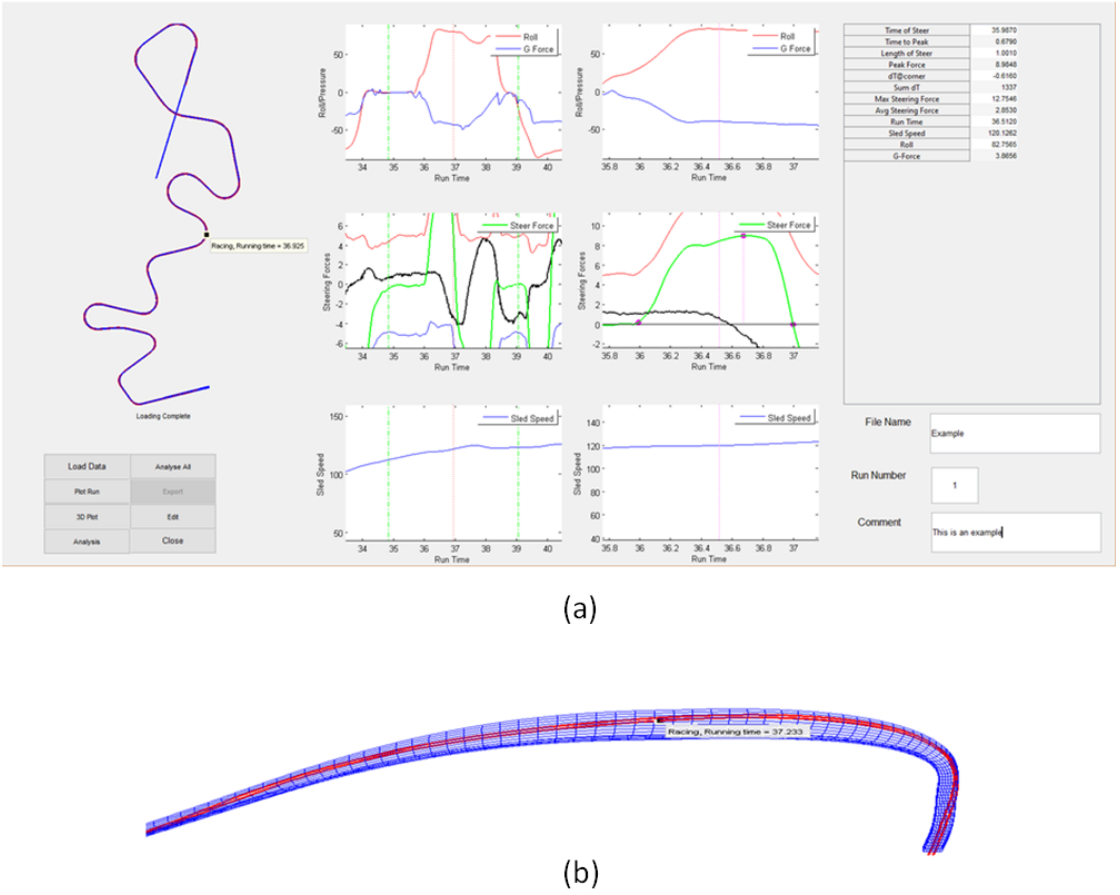

FIGURE 3.12: a) Post training analysis GUI main, b) 3D track model and runner traces of selected track segment.

maximum power within the steer (represented in Figure 3.13 as pink dots). A table of performance parameters requested by the coach will be automatically generated.

6. 'Analyse all' automatically performs the 'Analysis' function to all corners in the given track. Performance parameters are stored as temporary variables within the GUI.

7. The 'Export' button automatically formats and exports the temporary data generated by 'Analyse all' into a Microsoft Excel file with the name, tab number and comments defined by the user.

8. The 'Edit' button allows the user to reinvestigate any questionable point of interest on the 3D graph, recalculates the performance parameters and override the exported Excel file.

9. 'Close' closes the GUI and clears the data in the local workspace.

3.4.2 Real Time Performance Feedback Graphical User Interface

During training sessions, athletes will sometimes be asked to steer at a specific corner. Their time will then be compared with a predefined steering time by the coach. The difference between

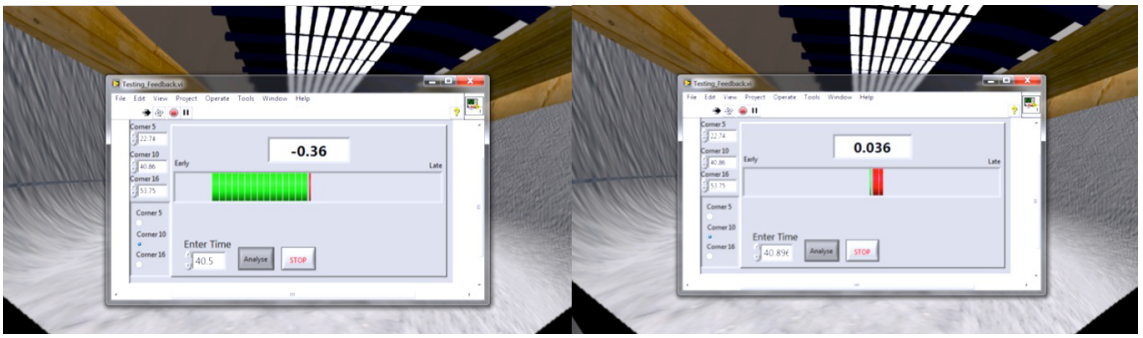

FIGURE 3.13: Performance feedback GUI

the two steering times will be fed back to the athlete in between runs in the form of a bar graph. Green indicates the athlete is early, red indicates the athlete is late as shown in Figure 3.13.

This GUI is designed in LabVIEW and uses simple combinatorial logics to calculate the time differences. The GUI design was based on request from the coaches, whose particular training session required the data from three specific corners to be processed. The GUI can be expanded to include all the corners for any given track.

3.5 DTT Training Application

The Mark III DTT was constructed with the capability for human in the loop controlled descent. However, due to the low fidelity of the physics engine (refer to section 5.5, this form of training is not advised. Instead, all the training carried out on the DTT uses pre-recorded descents and the athletes are simply strapped into the DTT and is exposed to the cues appropriate to the training they undergo. This format of training highlights the importance of being able to consistently and reliably produce simulated descent trajectories, optimal or otherwise. Hence develop methods for optimal trajectory generation is vital to the quality of athlete training. The GB Skeleton team mainly uses the DTT for two different training exercises:

- Steer timing, force and pattern training
- Pre-Match priming of the athletes

For the steer timing, force and pattern training exercise the athlete is given a pre-determined steer time, force and pattern to follow. These were decided by the coaches before the training begins and it trains the athlete's ability to steer at the correct time with the appropriate amount of force and the ability to adjust their steers with the help of feedback between each descent. This exercise is extremely useful in identifying and isolating which cue each individual athlete uses prominently and the using the result of the exercise, coaches could formulate personalised training plans accordingly.

The purpose of pre-match priming is just as the name suggests, it allows the athletes to carry out practice runs on the race track before a competition. This method of training helps the athlete to form a clear mental image of the track, minimises unexpected sled behaviours and enables them to formulate the optimal steering strategy.

3.6 Chapter Summary

The physical augmentation process to the infrastructure of Mark III DTT were summarised in this chapter. Critical hardware and software feature of the DTT were upgraded to complies with industrial safety regulation and the DTT can now be commissioned as a training tool. Arguably the most important upgrade carried out was the integration of the pitch motion cuing system, therefore, next step in the process will be the verification of the effectiveness of pitch as a motion cue. This is achieved through a series of motion stimuli experiments as will be detailed in the Chapter 4.

Chapter 4

Motion Stimuli Experiment Part III - Pitch

4.1 Chapter Introduction

After successfully integrating the pitch motion cueing system into the DTT. Its effectiveness on athletes' training need to be assessed. In particular, the improvement in simulation immersion and the the usefulness of the pitching motion cues as a stimulus for learning and skills acquisition when sliding. Through discussions made with coaches, it is apparent that pitch motions are most distinct during the transitions between curved and flat sections of the track (i.e. entrances and exits the corners). However, there exist a number of uncertainties that needs to be clarified, such as 'Is pitch distinguishable between left and right shoulder?' and 'How does pitch cue affect athlete's reaction within the corner?' To answer these, numerous pitch cuing algorithm have being developed and a series of preliminary motion stimuli experiments were conducted on the coaches to find two subjectively best performing cuing algorithms. Four Skeleton athletes were then experimented on using the selected algorithms to obtain both objective and subjective feedback in order to identify the most effective pitch motion cuing algorithm to be implement into the DTT as part of the training routine.

4.2 Statement of Ethics

The studies contained within this thesis were given ethical approval. The University of Southampton's Ethics and Research Governance granted approval (ID: 15398), in accordance with the documentation presented in Appendix C to H. All subjects gave informed consent prior to the start of the experiments.

4.3 Coach Experimental Goals

The goal of this experiment was to determine if the addition of pitch motion cues will accelerate athlete's learning and skills acquisition rate. The pitch actuation system was at its initial implementation stage, and was not ready for athlete testing. A number of pitch cuing algorithms needed to be tested to find the most appropriate one for training and the pneumatic system feedback needed to be examined to ensure the correct timing of pitch cues.

Subjective feedback from experts at Skeleton who has had previous exposure to the DTT was important at this stage. Four GB coaches were selected to take part in the experiment. The objective of the experiment was to obtain pitch actuator hardware feedback data with different body loads as well as coaches' subjective feedback on the fidelity of the pitch actuation system. Finally the coaches were asked to select two subjectively best performing algorithm to be tested on the athletes.

4.4 Pitch Motion Cuing Algorithm

The design of the pitch algorithms takes inspriation from the previous motion simulous experiment performed to verify the addition of roll to the DTT [1], where the 'Scaled Roll Algorithm' and the 'Scaled Roll with Washout Algorithm' delivered the best performance. For this experiment, 5 pitch actuation algorithms were used. All the algorithms uses roll angle as a base signal to generate pitch command since it is the variable most directly related to the curvature of the track. The command signal form the algorithm is capped at 15 degrees which represent 20 mm stroke lengths in the physical actuator. The pitch actuation signal is dependent on the direction of the corner, e.g. entering a right turning corner would pitch the left shoulder first followed by the right shoulder after a time delay which is related to the transverse speed of the sled.

Three different groups of pitch cuing algorithms have being designed:

- Group 1 uses a simple scaled version of the roll command as the pitch command.
- Group 2 uses the same principle as group one but the signal is fed through a classic washout filter, therefore at max pitch, the actuators will slowly return to home position. This is done because on the exit of any given corner, the corresponding shoulder is pitched up rather than down from and elevated position, e.g. exiting a left turning corner would pitch the left shoulder should pitch up instead of down as per Group 1 algorithms.
- Group 3 uses the start of the roll command as a signal to produce a single impulse as the pitch command. Table 4.1 presents a brief description of all the available algorithms so far, motion experiments with athletes are required to validate the effectiveness of these algorithms.

In the first two groups of pitch algorithms, there exist the double shoulder, alternating version of the command signal, this is done because entering and exiting the same corner will lead to pitch under different shoulders, e.g. entering right turning corner will pitch the left shoulder first, however exiting a right turning corner will pitch the right shoulder first instead. All algorithms

Algorithm	**Design Information**
Single shoulder scaled roll (Group 1)	Uses scaled roll angle controls actuation length, capped to 20 mm. Only pitch one shoulder with respect to the direction of the corner.
Alternating scaled roll (Group 1)	Uses scaled roll angle controls actuation length, capped to 20 mm. Pitches both shoulders with phase lag in between. The lead pitch signal depends on the direction of the corner.
Single shoulder washout roll (Group 2)	Uses scaled roll angle controls actuation length, capped to 20 mm. Only pitch one shoulder with respect to the direction of the corner. Filter out low frequency commands (i.e. when command capped at 20)
Alternating washout roll (Group 2)	Uses scaled roll angle controls actuation length, capped to 20 mm. Pitches both shoulders with phase lag in between. The lead pitch signal depends on the direction of the corner. Filter out low frequency commands (i.e. when command capped at 20)
Alternating impulse (Group 3)	Uses roll angle as cue to initiate impulse, maximum stroke applied when impulse is received. Pitches both shoulders with phase lag in between. The lead pitch signal depends on the direction of the corner.

Table 4.1: Pitch Algorithms

were written to take this into account and switch the pitch signals depending on the nature of the corner.

Figure 4.1 displays the command signals of alternating scaled roll algorithm during a typical descent on the Igls track as an example. The X axis represents command signal in degrees and the Y axis represents simulation time. In the graph, the red dotted line is the calculated platform roll angle, the blue line is the pitch command for the left actuator and the black line is the pitch command for the right actuator.

High speed Enfield pneumatic valves with integrated digital proportional-derivative-integral controller are used to control the pitch actuators. After tuning the controller to produce critically damped step response, dead time delays of approximately 0.3 seconds when actuating down and 0.1 seconds when actuating up were identified. This delay was most likely caused by the mechanical lag within pneumatic system. To mitigate these delays, a predictive compensator was used with the pitch algorithm for producing actuation commands. The compensator uses knowledge the current speed and position of the left and right mass particle to predict the future unit vector between them and consequently the future roll angle. Depending on the nature of the actuation (up or down) the predictive compensator uses different parameters. Equation 4.1 and 4.2 is the governing equation behind the compensator.

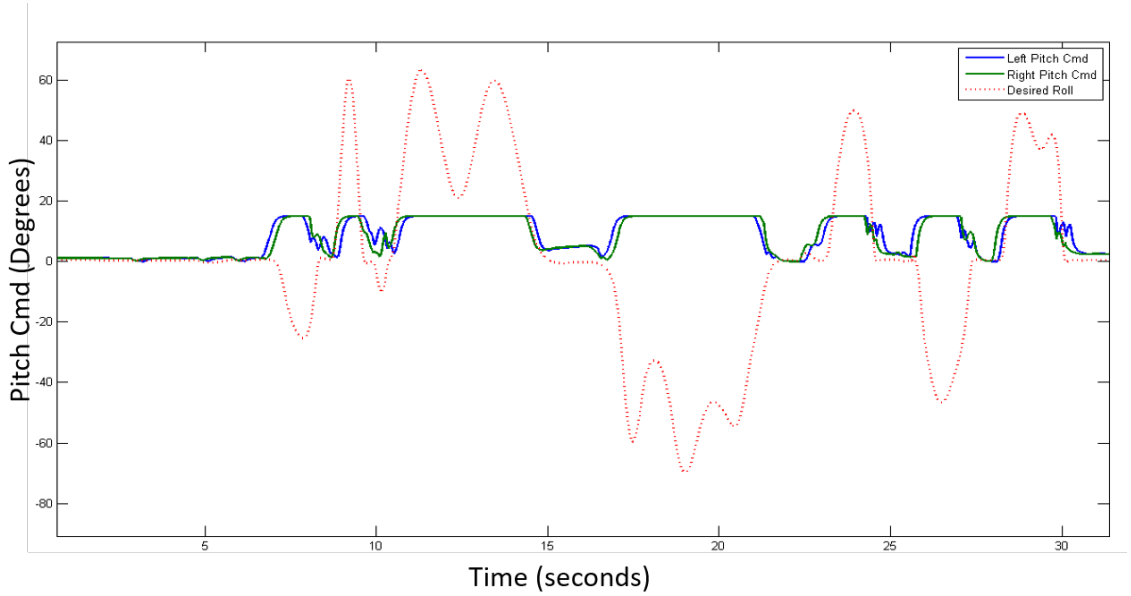

FIGURE 4.1: Alternating scaled roll algorithm command signal

$$n_{pred} = \frac{f_{interp_{xyz}}\left(\left(\left(\frac{|v_r|+|v_l|}{2}\right)\tau + \alpha_l\right), \beta_l\right) - f_{interp_{xyz}}\left(\left(\left(\frac{|v_r|+|v_l|}{2}\right)\tau + \alpha_r\right), \beta_r\right)}{\omega_s} \tag{4.1}$$

$$\phi_{pred} = \cos^{-1}(n_{pred} \cdot [0,0,1]^T) \tag{4.2}$$

where

- $f_{interp_{xyz}}$ – Interpolation function to map sled axis onto 3D world axis
- v_l and v_r – Velocity of the left and right mass particle.
- $\alpha_l, \beta_l, \alpha_r, \beta_r$ – Longitudinal and transverse positions for the left and right mass particles
- τ – Dead time delay, 0.1 for upwards actuation and 0.3 for downwards actuation
- n_{pred} – Predicted unit vector from left to right mass particle
- ϕ_{pred} – Predicted roll angle
- ω_s – Distance between left and right mass particle

4.5 Coaches Experiment Methodology

The basic principle of this experiment is straight forward. Each coach was instructed to steer the entire track so that they can be fully immersed. Each coach will slide 5 simulated descents with full motion cues consecutively with a small break of 1 minute in between. Before each simulated descent, they were told which pitch cuing algorithm was used for that particular descent and

after 5 descent were completed they were asked to fill out a questionnaire, rating the usefulness of pitch as a motion cue to help them steer out of a score between 0 and 10 (0 being not helpful at all and 10 being extremely helpful). They were also asked to rate the 5 pitch cuing algorithms in order of helpfulness and comment on the fidelity of the pitch motion.

The metrics from hardware feedback were collected and analysed at the end of the experiment, the pitch actuator's position feedback was compared against the sled's roll position feedback. The differences between the feedback signals were examined to ensure that the pitching motion occurred at the correct time.

4.6 Coach Experimental Feedback Analysis

4.6.1 Hardware Feedback

For the purpose of demonstration, the feedback signals from the pitch actuation is scaled to be plotted on the same figure as the roll feedback signal and provide a comparable display, this is done since the important factor is the pitch actuation time rather than magnitude. Only Coach A's hardware feedback metrics will be displayed here, however in all cases, the feedback metrics displayed similar patterns.

Figure 4.2 illustrates the pitch actuation feedback produced by Group 1 and 2's single shoulder pitch cuing algorithms. In each case the x axis represent time as a unit-less index and the y axis represent pitch and roll angle in radians. In the figure, the blue line represents the left pitch feedback and the orange line represents the right pitch feedback; the yellow dashed line represents roll feedback. It is clear from the figure that both left and right shoulder pitch motion occurs just before the roll motion and therefore confirming that the pitch cuing algorithm is functioning correctly.

Figure 4.3 illustrates the pitch actuation feedback from group 1, 2 and 3's double shoulder alternating pitch algorithm. In each case the x axis represent time as a unit-less index and the y axis represent pitch and roll angle in radians. In the figure, the blue line represents the left pitch feedback and the orange line represents the right pitch feedback; the yellow dashed line represents roll feedback. The figure shows that for all three groups, pitching occurs just before the roll motion and the left/right pitching mode has being switched correctly in accordance with the corresponding corner's nature. These pitch cuing algorithms are functioning as per designed.

There exist small amounts of error between left and right pitch actuator's feedback magnitude. These errors are most likely caused by the imperfections in the pneumatic actuator as well as the differences in rope length in the pulley set-up for the different shoulders (refer to section 3.3.1).

4.6.2 Coach Subjective Feedback

From the questionnaires feedback, all four coaches felt that the inclusion of pitch has made a difference to their steering. On average, the coaches felt that the inclusion of the pitch motion cue made steering easier, a score of 7.5/10 was given by three coaches and 10/10 by the other.

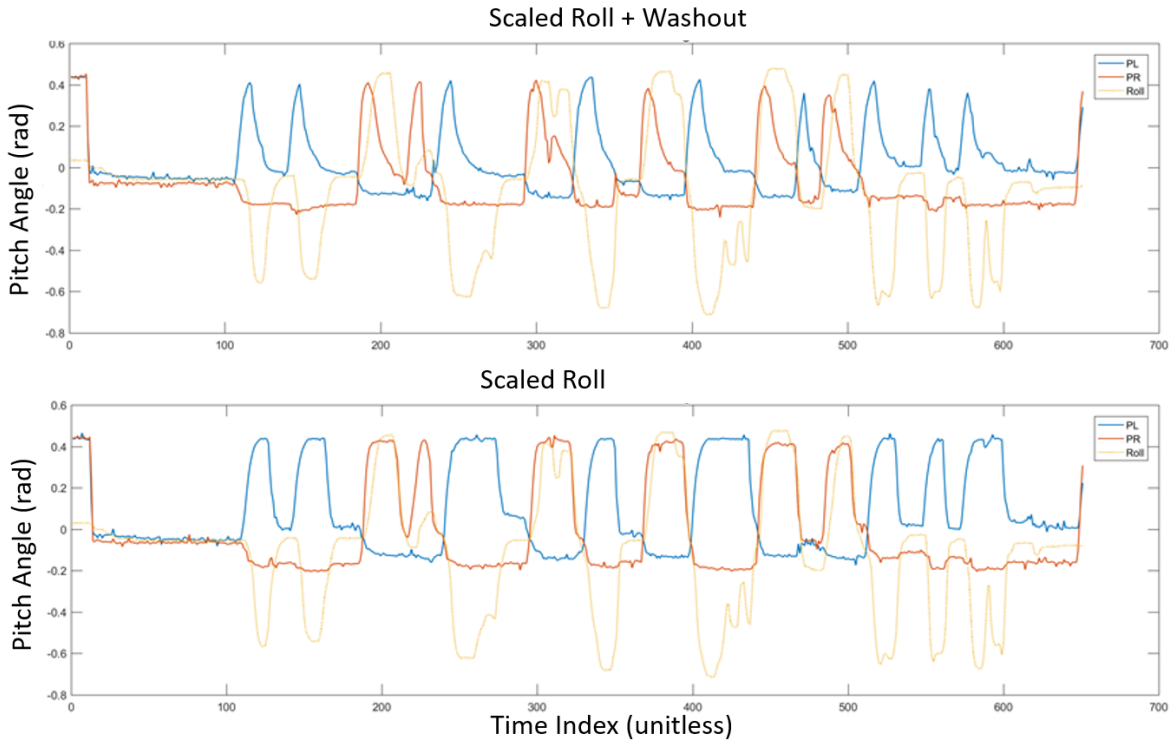

FIGURE 4.2: Group 1 Single shoulder scaled roll feedback (top), Group 2 Single shoulder washout roll feedback (bottom)

Out of the four coaches, three had voted Group 1 double shoulder scaled roll to be the most useful algorithm. The second most useful algorithm is the Group 3 double shoulder impulse. The general comment on these algorithms is that they are the most distinctive and easy to pick up. However, due to back injury, the last coach was not subjected to g-force loading and his verdict was that group 2 double shoulder washout roll was the best performing algorithm, this is most likely due to the fact that g-force loading on the shoulder section is too great under normal circumstances and the group 2 algorithms' washout behaviour causes the actuator to pull down on the spring before it could be fully extended to produce the pitch motion cue. In general the coaches find the inclusion of pitch actuation beneficial toward steering and approve the use of said motion cue as part of the regular training routine for their athletes.

For the purpose of the athlete motion stimuli experiment, Group 1 and Group 3 pitch algorithm will be used as one is the most distinct for training whilst the other is the most realistic for immersion purposes.

4.7 Athlete Experimental Goals

The goal for this experiment was to obtain both objective and subjective feedback from the athletes regarding which of two cuing algorithms selected by the coaches were most beneficial to them individually. With the feedback given by the athletes and objective analysis performed

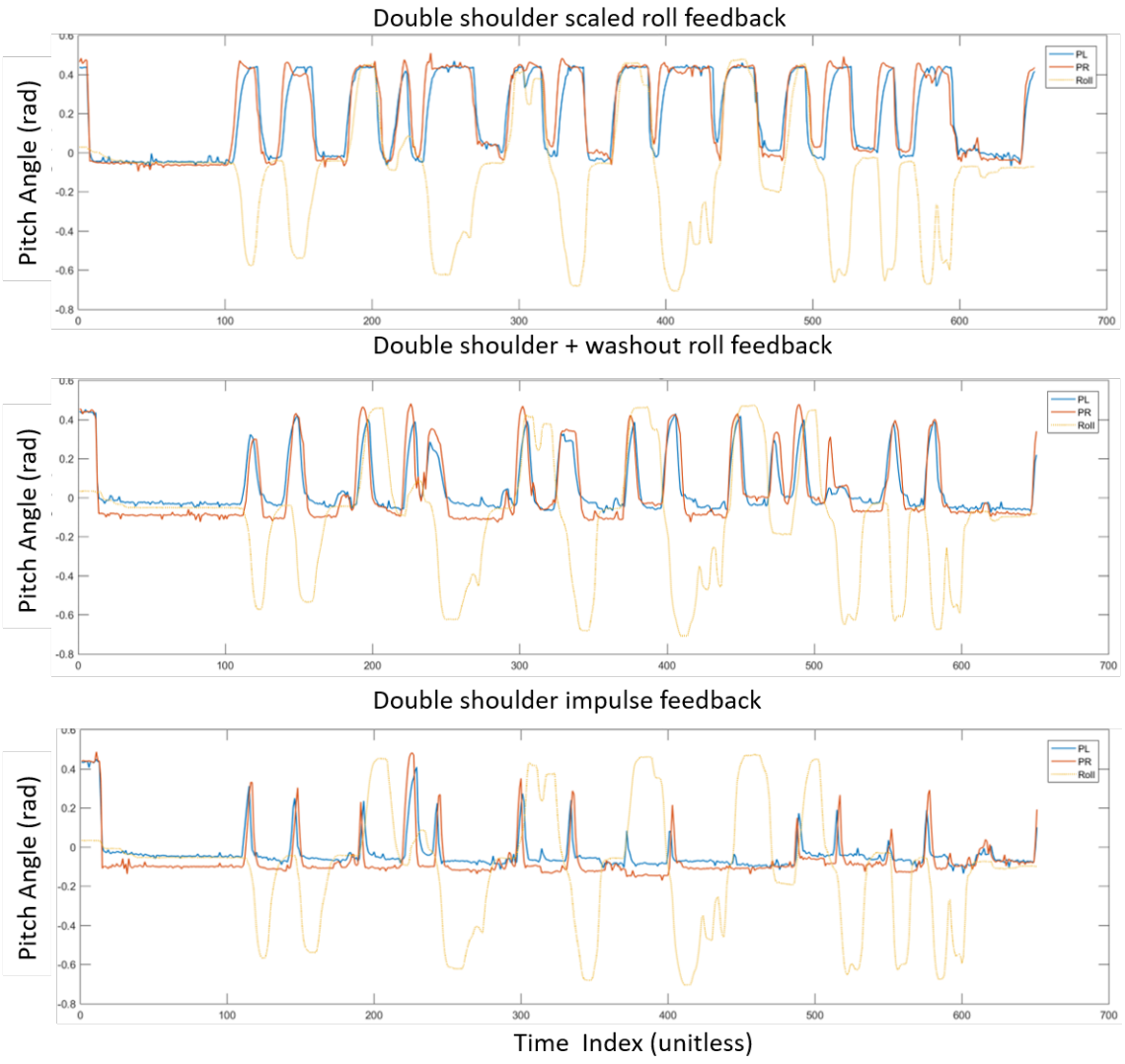

FIGURE 4.3: Group 1 Double shoulder scaled roll feedback (top), Group 2 Double shoulder washout roll feedback (middle), Group 3 Double shoulder impulse feedback (bottom)

based on their performance, a intuitive decision were made regarding which algorithm was implemented into the DTT for training purposes.

4.7.1 Athlete Experiment Methodology

The motion experiment involved the participation of 4 athletes, 1 at Olympic competition level, 2 at International Cup level and 1 at novice level to give the elements of variety to the experiment. Each athlete were asked to attend 2 sessions of experiments. During each session they were asked to perform 5 full descents on the the DTT following the Sochi Olympic race track, with a 2 minute break in between to gather their thoughts. The athletes were asked to steer every corner of the track with focus on the entrance of corner 5 for the first session, and the entrance of corner 10 for the second. For each session, the 1st descent used no motion cues in order to provide a baseline performance for data comparison, the 2nd and 3rd descent used Group 1 (Algorithm 1) pitch algorithm and the 4th and 5th descent used Group 2 (Algorithm 2) pitch

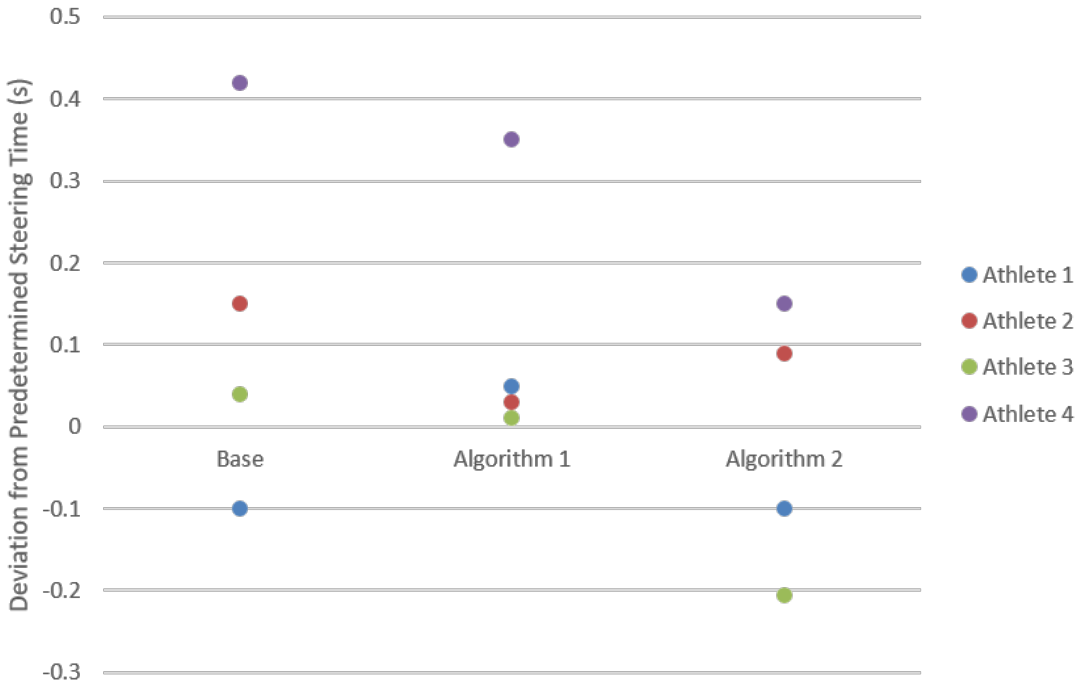

FIGURE 4.4: Corner 5 performance feedback

algorithm. After each descent their steer timing data were collected and and compared with pre-determined steer timing, the error between the two time were given to the athlete in the form of a GUI as per described in section 3.4.2, thus allowing them to adjust their steer timing using the pitch motion cues. At the end of each session they will be provided with a feedback form to fill in to provide subjective feedback regarding whether they felt the inclusion of pitch was useful for their steering and which algorithm did they feel was most useful. A scoring system of $X/10$ were used here for the athlete to give their feedback.

4.7.2 Athlete Feedback Analysis

Athlete Performance Feedback

To assess the effectiveness of each pitch motion cue on athlete's learning and skills acquisition, the previously stated differences between steer timings for the athletes were collected and analysed. The average error over the 5 descents for each algorithm were calculated and presented in Figure 4.4 and Figure 4.5.

Table 4.2 shows the average deviation of the athlete's steer times from pre-determined 'correct' times. It is important to note here that Athlete 4 stated in his/her feedback that he/she did not find pitch useful as a motion cue but would like to have it for immersion purposes. Therefore his/her results will be discarded from this objective analysis. when compared with base performance in corner 5, Algorithm 1 (scaled roll) improved athletes' steer timing by an average of 0.0675 s and Algorithm 2 (scaled roll with washout) improved athletes' steer timing by 0.04125 s. In corner 10, Algorithm 1 improved athletes' steer timing by an average of 0.0635 s and Algorithm 2 improved athletes' steer timing by 0.0885 s. There are no definitive patterns here to indicate

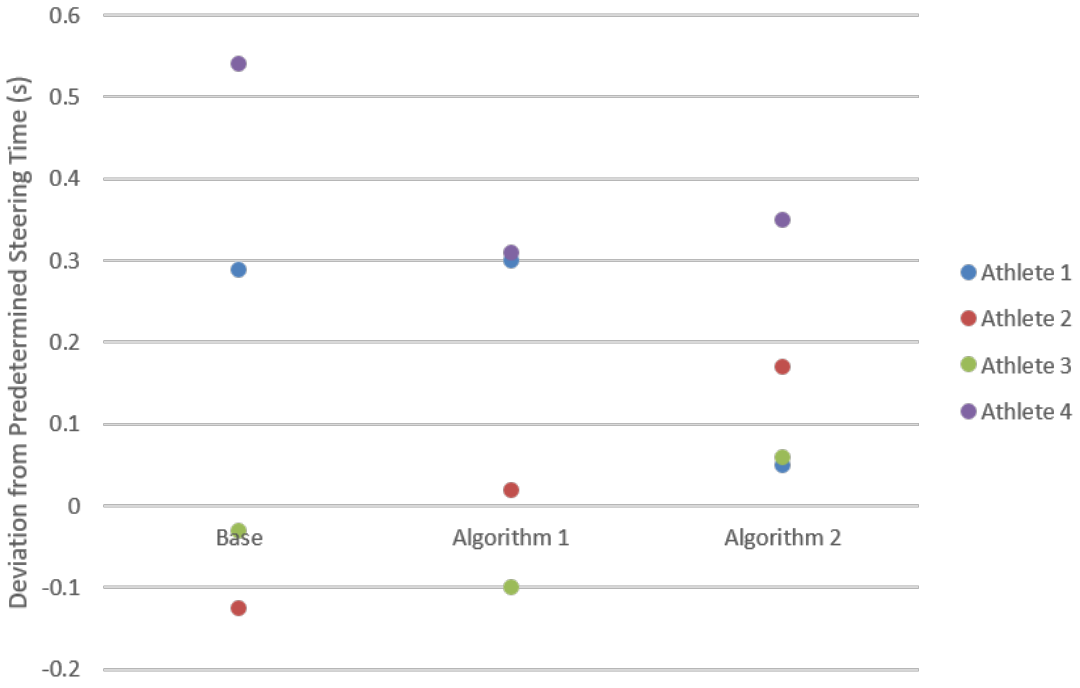

FIGURE 4.5: Corner 10 performance feedback

Athlete/Corner	**Base Performance**	**Algorithm 1**	**Algorithm 2**
Athlete 1/Corner 5	-0.1	0.05	-0.1
Athlete 2/Corner 5	0.15	0.03	0.09
Athlete 3/Corner 5	0.04	0.01	-0.21
Athlete 4/Corner 5	0.42	0.35	0.15
Athlete 1/Corner 10	0.289	0.3	0.05
Athlete 2/Corner 10	-0.125	0.02	0.06
Athlete 3/Corner 10	-0.03	-0.1	0.06
Athlete 4/Corner 10	0.54	0.31	0.35

TABLE 4.2: Deviation from Pre-determined Steering Time(s)

which pitch algorithm is objectively superior, but it does appear that both pitch algorithms have positive effects on athletes' steering for those who utilises it as a motion cue. However due to the limited sample size of this experiment, subjective feedbacks from participating athletes may be more critical.

Subjective Feedback

From the feed back given by the 4 athletes, a summary of the subjective reviews are given below:

- 3/4 athletes stated that they use pitch cuing algorithm for motion cuing purposes and gave an average score of 9.16/10 on their preference regarding including pitch cuing to

their DTT training. 1/4 athlete did not use the pitch motion cue, whom shall be dubbed as athlete X for result presentation purposes from this point onwards.

- Regarding the algorithm's usefulness to assist steering, 3/4 athletes gave an average score of 7.3 for Algorithm 1 and 5.5 for Algorithm 2. Athlete x gave a score of 1/10 for both algorithms.
- Regarding the realism of the cuing algorithms, 4/4 athletes gave an average score of 5.5 for Algorithm 1 and 7.5/10 for Algorithm 2.

4.8 Chapter Summary

Although the small sample size of this motion stimuli experiment made it difficult to analytically assess the performance of the pitch cuing algorithms, but both the coaches and athlete 100% agree that the pitch motion cuing system needs to be added to the current DTT for enhanced training experiences. Whilst not all athlete's uses the pitch cues for steering, they all appreciated the improvement in immersion it provided. To compensate for athletes' difference in preferences, both pitch algorithm were implemented into the DTT with the ability to select in between them prior to the training session depending on if the athlete requires them. This chapter concludes all the work related to the augmentation of the physical DTT. The rest of the thesis will report on the research conducted with regards to predicting the optimal descent trajectory on a given track, with the next chapter describing the underlying physics equations governing the descent dynamics.

Chapter 5

Real Time Physics Engine

5.1 Chapter Introduction

In order to predict the optimal descent trajectories for any given track, first a reliable method of controlling the descent simulation must be formulated. In the research conducted for this PhD, this was achieved through the implementation of numerous control algorithms in place of human steering input to control descent simulation. However, before one can begin designing the appropriate controllers, one must first have an in depth understanding of the principal physics equations governing the descent dynamics behind the simulation. This is especially true in the case of the optimal controller design (see Chapter 7 for detail), as its plant model will be based directly upon the existing physics.

This chapter provides a brief overview of the internal structure of the real time physics engine (RTPE) and their principle interactions. It is important to note here that the physics engine is very complicated and it would be unsuitable to list all the equations it contains within this chapter. Instead only the fundamental physics equations which either is directly used within or influences the design decisions of the control algorithms were listed here. In particular the Equations of Motion (EOM) and the Sled Characteristic (SC) steering model will be discussed in detail in this chapter.

5.2 Model Architecture Overview

The current RTPE is largely based on work inherited from Roche [2] and Sawade [1]. Who used similar underlying equations of motion, surface mapping techniques and characteristic calculation as Hubbard et al. [20], but implemented in Matlab Simulink to operate in real time with the DTT. Hubbard's original work used a single particle approach to make a 2 degree of freedom (DOF) model, which ignored some critical dynamics such as skidding. Roche adapted this model to provide 3 DOF by modelling the sled as a spring damper system, linking two mass particles that represent the left and right sled runners, therefore incorporating yaw into the system dynamics.

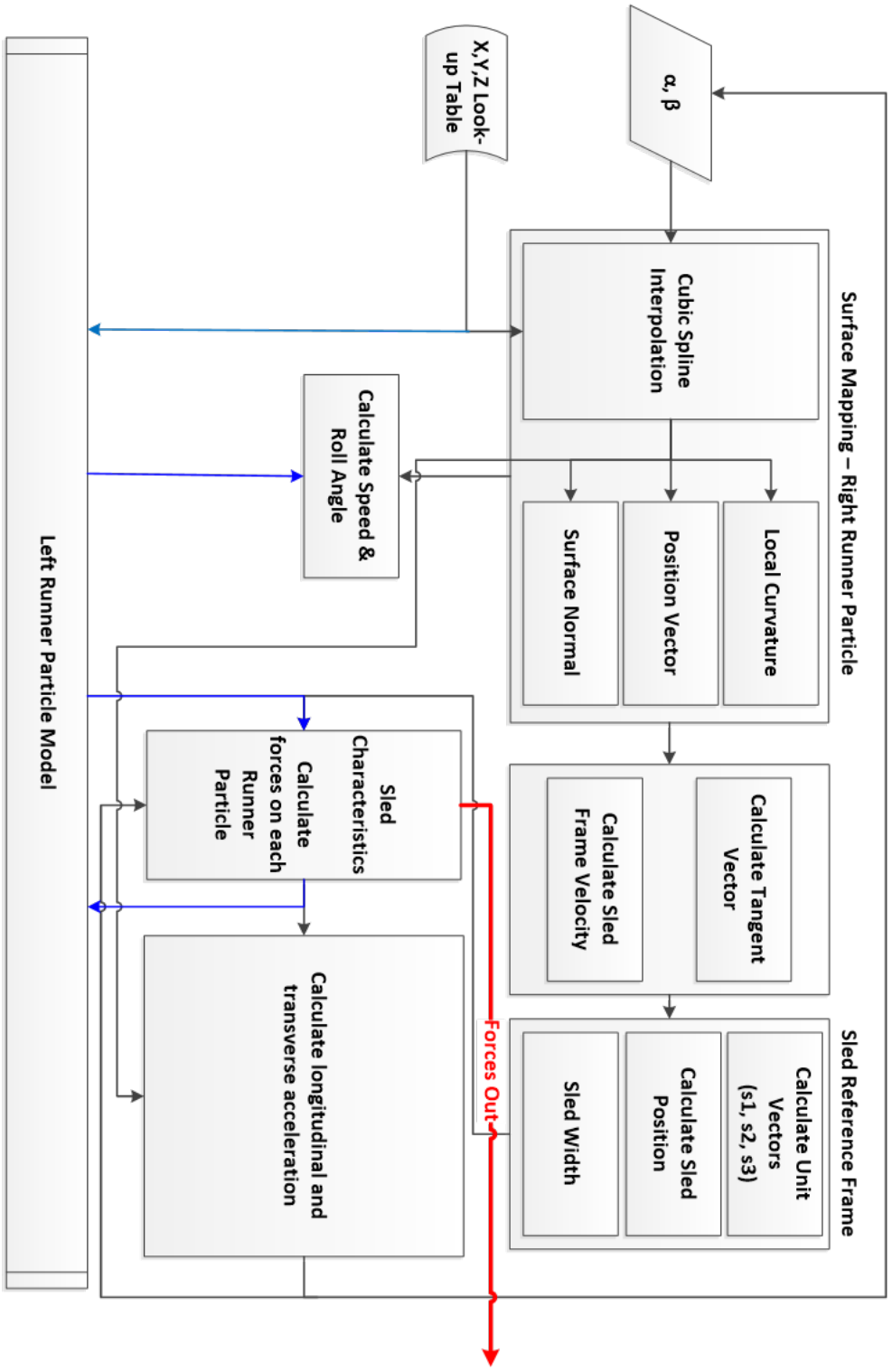

FIGURE 5.1: Block diagram of model interaction for the right mass particle

The RTPE can be separated into two mirrored sectors with respect to the left and right mass particle. Each sector can be further divided into three functional blocks, which are: 'Surface Mapping', 'Sled Characteristics' and 'Equations of Motion'. Figure 5.1 illustrates the top level model architecture in block diagram form.

Track geometry and initial conditions are uploaded into the physics engine at the start of a simulated descent. Thereafter during each time step, the following sequence (as seen in Figure 5.1) of calculations is executed by the RTPE:

- Firstly, the Surface Mapping functional block maps the current sled location onto the track geometry and calculates general inertial forces around the runner contact points. Calculated data are passed onto the Sled Characteristics and Equations of Motion functional blocks.
- Secondly, the Sled Characteristics functional block uses data from the Surface Mapping to calculate unit force vectors in the sled's reference frame and combines the results with human/computer inputs to compute the actuation forces vector on each individual mass particle. Results are fed to the Equations of Motion functional block. (note that sled characteristics also calculate roll and g force, however these are for hardware control and is therefore not include in this chapter)
- Finally, the Equations of Motion functional block uses inertial data from Surface mapping and actuation force from Sled Characteristics to calculate sled acceleration, velocity and position along and across the track to use as initial condition for the next time step.

5.3 Surface Mapping Functional Block

5.3.1 Track Geometry

The track surface is exported form the CAD software as three $N \times M$ matrices, representing the X, Y and Z co-ordinates in world frame. N is the across track dimension which is predefined. Currently N uses the value 14 for all processed tracks in the DTT. M is the longitudinal track dimension which has a fixed interval of $1.5m$ between each point and varies according to track length. This form of geometry definition divides any given track surface into $(N-1) \times (M-1)$ surface patches.

The position of the mass particle is described as a pair of dimensionless parameters α and β (See Figure 5.2), where α is the longitudinal track position and β is the across track position. α increases from 0 (start of track) to M (end of track); β increases from 0 (left most edge of the track) to N (right most edge of the track). The mass particle's position is mapped onto the track geometry through a cubic spline interpolation scheme (refer to section 5.3.2). This way, all positions on the track can be represented the function $r(X, Y, Z) = r(\alpha, \beta)$. Figure 5.2 demonstrates the basic principles of geometry definition and surface mapping.

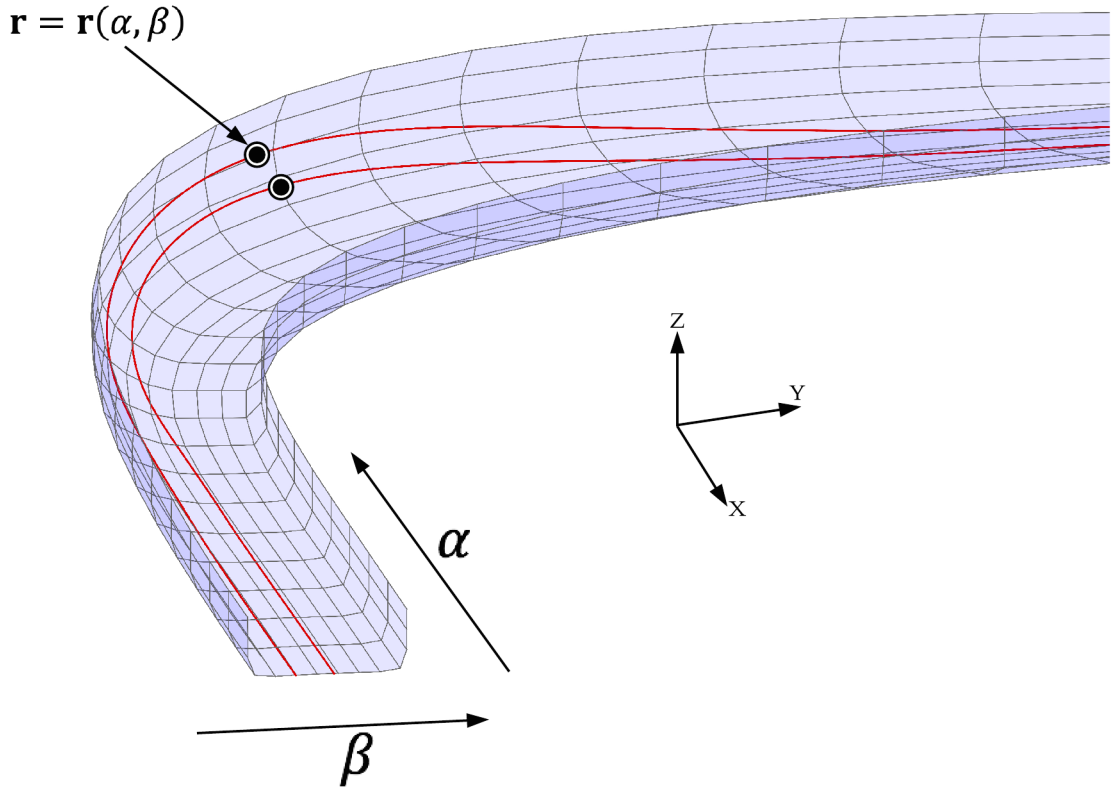

FIGURE 5.2: Section of track showing a mapping of α, β onto X, Y, Z co-ordinates

5.3.2 Cubic Spline Interpolation

Cubic spline interpolation (CSI) is important method that is used frequently within the RTPE. Both the surface mapping and spatial derivative calculations is dependent on CSI. For the reader's benefit, an example specific to the application of CSI within the RTPE will be used to explain the basic theories of spline interpolation.

Referring to Figure 5.3, a particle located at $r(\alpha, \beta)$ is within the surface patch denoted by the vertices $r(x1, y1, z1), r(x2, y2, z2), r(x3, y3, z3)$ and $r(x4, y4, z4)$. In order to map the particle onto the surface patch, the x, y, z coordinate of the particle must be represented as a function of the polynomial of the differences between the particle location its respective surface patch edges (i.e. $(\alpha - \alpha_i)$ and $(\beta - \beta_i)$). CSI uses cubic functions of differences to describe the shape of the surface patch between the patch edges and the particle location (denoted as the red dashed lines), as shown in Figure 5.3. The x, y, z coordinates of the particle is expressed as the sum of these polynomials. Boundary conditions for CSI are that the position and curvature at the corners of the surface patch must be continuous with respect to its immediate neighbours.

5.3.3 Contact Patch Analysis

In order to find the local surface characteristics beyond the point of contract around the particle, a set of quadratic equations were used over a predefined 'contact patch' $C_\alpha \times C_\beta$ (See Figure

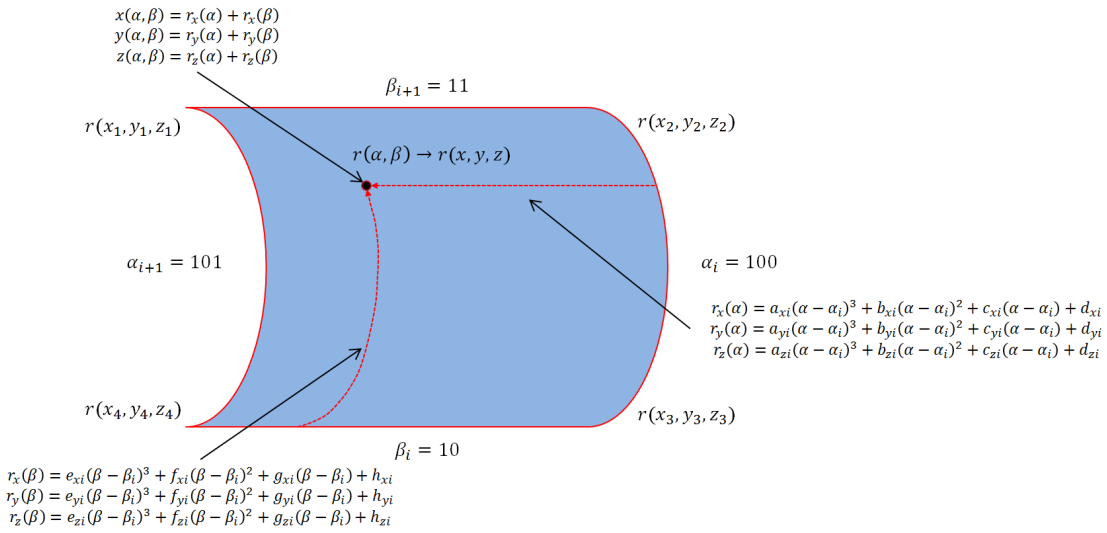

FIGURE 5.3: Basic principle of cubic spline interpolation

5.4), where C is the contact patch coefficient. By differentiating the quadratic equations with respect to α and β, the spatial derivatives can be obtained. For example:

$$r_{\alpha\beta} = \frac{\partial r}{\partial\alpha\partial\beta}$$

The contact patch is a one of the key elements affecting the accuracy of the simulation, the other being the fundamental sample time. In the original model by Roche, a contact patch coefficient of 0.1 was used for both C_α & C_β; this however is no long adequate for use with the modified physics model. C_α&C_β has being modified to be 0.0002. Corner and edge position of the contact patch is obtained through the following equations:

$$r_n = r(\alpha + \frac{C}{2}, \beta);\ r_s = r(\alpha - \frac{C}{2}, \beta);\ r_w = r(\alpha, \beta + \frac{C}{2});\ r_e = r(\alpha, \beta - \frac{C}{2});$$
$$r_{ne} = r(\alpha + \frac{C}{2}, \beta - \frac{C}{2});\ r_{nw} = r(r(\alpha + \frac{C}{2}, \beta + \frac{C}{2});$$
$$r_{se} = r(\alpha - \frac{C}{2}, \beta - \frac{C}{2});\ r_{sw} = r(r(\alpha - \frac{C}{2}, \beta + \frac{C}{2})$$

Where the position reference frame of the contact patch is based on the sled body rather than track surface (α lies on the longitude and β lies on the latitude) and n, s, w, e represent north, south west and east.

The spatial derivatives required for calculating local curvature (to compute sled reference) and solving equations of motion are $r_\alpha, r_{\alpha\alpha}, r_\alpha, r_{\beta\beta}$ and $r_{\alpha\beta}$. These are solved by differentiating r along the line $r_n - r - r_s$, similarly r_β and $r_{\beta\beta}$ are solved by differentiating r along the line $r_e - r - r_w$. r is solved by first differentiating along the edges $r_{ne} - r_e - r_{se}$ and then along the edge $r_{sw} - r_w - r_{nw}$. Local unit normal (n) and consequently the local curvature (k_n) are calculated with the following equations:

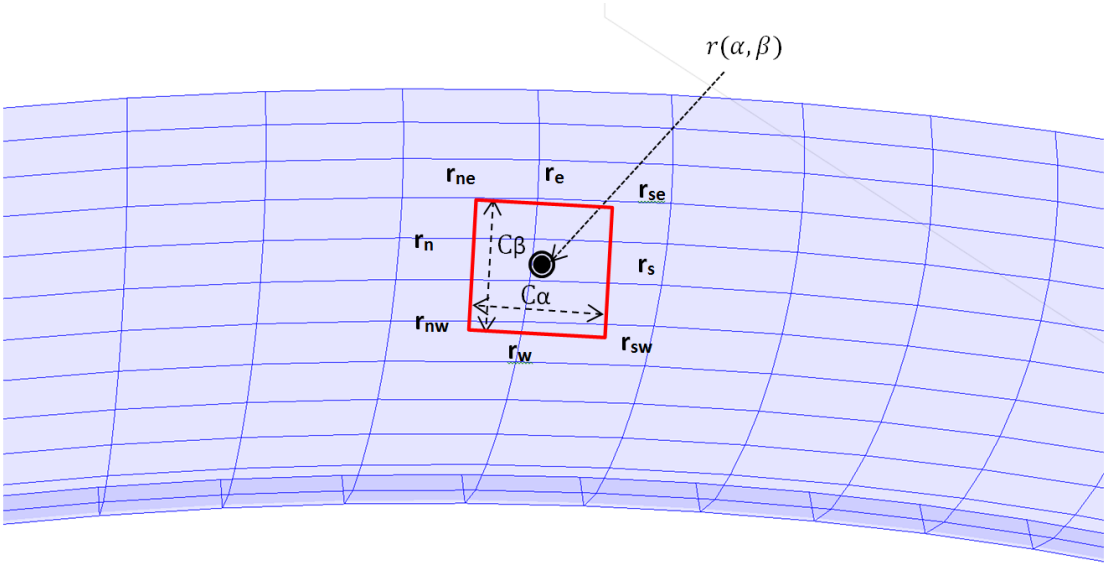

FIGURE 5.4: Contact Patch of particle at position r, with r_{ref} representing the position of the corners and edges

$$n_l = \frac{\dot{\alpha}_l \times \dot{\beta}_l}{|\dot{\alpha}_l \times \dot{\beta}_l|}$$
$$n_r = \frac{\dot{\alpha}_r \times \dot{\beta}_r}{|\dot{\alpha}_r \times \dot{\beta}_r|}$$

$$k_{nl} = \frac{(n_l \cdot r_{\alpha\alpha})\dot{\alpha}_l^2 + 2(n_l \cdot r_{\alpha\beta})\dot{\alpha}_l\dot{\beta}_l + (n_l \cdot r_{\beta\beta})\dot{\beta}_l^{\,2}}{(r_\alpha \cdot r_\alpha)\dot{\alpha}_l^{\,2} + 2(r_\alpha \cdot r_\beta)\dot{\beta}_l^{\,2} + (r_\beta \cdot r_\beta)\dot{\beta}_l^{\,2}}$$
$$k_{nr} = \frac{(n_r \cdot r_{\alpha\alpha})\dot{\alpha}_r^2 + 2(n_r \cdot r_{\alpha\beta})\dot{\alpha}_r\dot{\beta}_r + (n_r \cdot r_{\beta\beta})\dot{\beta}_r^{\,2}}{(r_\alpha \cdot r_\alpha)\dot{\alpha}_r^{\,2} + 2(r_\alpha \cdot r_\beta)\dot{\beta}_r^{\,2} + (r_\beta \cdot r_\beta)\dot{\beta}_r^{\,2}}$$

where:

- n_l and n_r –Unit normal for the left and right mass particle
- k_{nl} and k_{nr} – Local normal curvature of the left and right contact patch
- $\dot{\alpha}_l, \dot{\alpha}_r, \dot{\beta}_l, \dot{\beta}_r$ – Longitudinal and transverse track velocity of the left and right particles

5.4 Equations of Motion Functional Block

The current version of the physics model uses Kane's method [38] to balance out the forces acting on the left and right particles and calculates the Equations of Motion. Referring to

section 5.2, the longitudinal and transverse track acceleration of both mass particles via the following equations:

$$\ddot{\alpha}_l = \frac{(Fol \cdot r_\alpha + A_l) \cdot r_\beta^2 - (Fol \cdot r_\beta + B_l)(r_\alpha \cdot r_\beta)}{m_l((r_\alpha \cdot r_\beta)^2 - r_\alpha^2 r_\beta^2)} \tag{5.1}$$

$$\ddot{\beta}_l = \frac{(Fol \cdot r_\beta + B_l)(r_\alpha \cdot r_\beta) - (Fol \cdot r_\alpha + A_l) \cdot r_\alpha^2}{m_l((r_\alpha \cdot r_\beta)^2 - r_\alpha^2 r_\beta^2)} \tag{5.2}$$

$$\ddot{\alpha}_r = \frac{(For \cdot r_\alpha + A_r) \cdot r_\beta^2 - (For \cdot r_\beta + B_r)(r_\alpha \cdot r_\beta)}{m_r((r_\alpha \cdot r_\beta)^2 - r_\alpha^2 r_\beta^2)} \tag{5.3}$$

$$\ddot{\beta}_r = \frac{(For \cdot r_\beta + B_r)(r_\alpha \cdot r_\beta) - (For \cdot r_\alpha + A_r) \cdot r_\alpha^2}{m_r((r_\alpha \cdot r_\beta)^2 - r_\alpha^2 r_\beta^2)} \tag{5.4}$$

with

$$A_{l,r} = -\big((\dot{\alpha}_{l,r}^2 r_{\alpha\alpha} + \dot{\beta}_{l,r}^2 r_{\beta\beta} + 2\dot{\alpha}_{l,r}\dot{\beta}_{l,r} r_{\alpha\beta}) m_{l,r} \cdot r_\alpha\big)$$
$$B_{l,r} = -\big((\dot{\alpha}_{l,r}^2 r_{\alpha\alpha} + \dot{\beta}_{l,r}^2 r_{\beta\beta} + 2\dot{\alpha}_{l,r}\dot{\beta}_{l,r} r_{\alpha\beta}) m_{l,r} \cdot r_\beta\big)$$

where:

- Fol, For – Actuation force vectors on the left and right mass particles (see section 5.5)
- $A_{l,r}$, $B_{l,r}$ – Generalised inertial forces acting on the both mass particles
- m_l, m_r – Mass distributed to the left and right particle.

This method of modelling the sliding motion is common amongst the different sliding sports, in particular bob skeleton and bob sleigh. The equations of motions above were well established and shown to be accurate when investigating the descent dynamics of single body models.

5.5 Sled Characteristics Functional Block

The Sled Characteristics functional block contains the equations that calculate forces applied onto the athlete and sled as one body from both external and internal sources. The force equations with in the SC block are either directly or indirectly dependant on the steering force inputs, therefore the SC block can also be treated as the steering model of the sled. In this section, only the principle forces that affect the descent dynamics and is used in the design of the control algorithms are listed. These forces are as listed below:

- W –Frictional forces resulted from wall collision
- L – Aerodynamic lift of athlete and sled
- D – Aerodynamic drag of athlete and sled
- f_{lon} – Along track runner friction force

- f_{lat} – Across track runner friction force
- R – Sled body stiffness

In the current version of the physics engine, the equations in the SC functional block were mostly emperical estimationg obtained through curve fitting of data collected from an instrumented sled on the Lake Placid Olympic ice track [1]. As a results, the accuracy of the descent simulation is also limited. Although performance analysis conducted by Sawade [1] showed that the current model estimation has an adequate degree of accuracy, it could however be improved by replacing these empirical equations with their respective analytical counterparts. The process of replacing the physics model is outside the scope of this PhD and will not be investigated here, but the current state of each equation will be briefly discussed and suggestions for possible changes will be given.

5.5.1 Wall Collision Function

The current collision model employs a series of Boolean logics to decide whether wall hit has occurred. The resultant Boolean variable equals to 1 if a mass particle 'hits' the wall and equals to 0 otherwise. The frictional force generated from wall hits are calculated by Equation 5.5 and 5.6.

$$W_l = LWHit \cdot \sqrt{\dot{\alpha_l}^2 + \dot{\beta_l}^2} \cdot \frac{\dot{\beta}_l}{3000} \tag{5.5}$$

$$W_r = RWHit \cdot \sqrt{\dot{\alpha_r}^2 + \dot{\beta_r}^2} \cdot \frac{\dot{\beta}_r}{3000} \tag{5.6}$$

Where:

- W_l, W_r – longitudinal and translational friction forces due to wall hits
- $(L, R)WHit$ – Boolean variable determined by weather the sled's body has made contact with the wall

This collision model does not consider the energy lost in the longitudinal direction. Therefore as a suggestion for future research, a classical collision model that calculates longitudinal and transverse track speed could be used to provide a more accurate representation of wall hit.

$$\alpha_{out} = \frac{|r_\alpha|\alpha_{in} - |r_\beta|\mu(1 + C_r)|\beta_{in}|}{b}$$
$$\beta_{out} = C_r \cdot \beta_{in}$$

Where:

- α_{out} and β_{out} – New velocity after collision

- μ – Friction coefficient of the ice wall
- C_r – Coefficient of restitution of the ice wall

5.5.2 Coulomb Friction Forces

Coulomb friction function calculates the friction coefficient parallel to the longitudinal direction of the track for each runner particle. The equations are as listed:

$$\mu_{l,r} = \frac{15Fsteer(R,L)\cdot(\dot{\alpha}_{l,r}^2+\dot{\beta}_{l,r}^2)}{m_{l,r}(a_z-\frac{g}{2})} - \frac{Fsteer(L,R)\cdot(\dot{\alpha}_{l,r}^2+\dot{\beta}_{l,r}^2)}{10m_{l,r}(a_z-\frac{g}{2})} + knif(l,r) + fwall_{l,r} \quad (5.7)$$

Where:

- $Fsteer(L,R)$ – Left and right steering force from driver.
- m_l and m_r – Combined mass of the sled and the athlete distributed on each mass particle.
- g – Acceleration due to gravity.
- a_z – Vertical acceleration to the sled reference frame.
- $knif(l,r)$ – Contact surface length of the left and right knife, which currently have constant values. However, they should be functions of steering forces and will be revised for future iterations of the physics model.

The longitudinal friction forces were calculated using the respective coefficients from Equation 5.7, producing Equation 5.8:

$$N_l = N_r = \frac{1}{2}(-100a_z + mg) \quad (5.8)$$

$$f_{lon_{l,r}} = -mu\cdot|N_{l,r}|\cdot t_c \quad (5.9)$$

Where:

- $f_{lon_{l,r}}$ – longitudinal friction forces on the left and right mass particle
- $N_{l,r}$ – surface normal reaction forces
- t_c – Unit tangent vector of sled velocity

Currently, research on interaction between steel runners and ice are still at its early stage and there lacks a definitive mathematical model to accurately represent this relationship. The empirical nature of Equation 5.7 is shown by the fact that units do not add up appropriately. It is expected that the accuracy of the equations will improve when further research have being conducted regarding the interaction between runners and ice.

5.5.3 Aerodynamic Drag and Lift Function

The Aerodynamic drag $D_{l,r}$ and lift $L_{l,r}$ of the combined body from athlete and sled uses the following equations for each of the mass particles:

$$D_{l,r} = -\frac{1}{4}\rho \cdot C_d A \cdot |V_{l,r}|^2 \cdot S_1$$
$$L_{l,r} = \frac{1}{4}\rho \cdot C_l A \cdot |V_c|^2 \cdot N_{l,r}$$

Where:

- ρ – Air density
- $V_{l,r}$, V_c – Velocity vector of the left and right mass particles as well as the centre point of the sled reference frame
- S_1 – Unit vector parallel to the sled axial direction
- $C_d A$ and $C_l A$ – Drag and lift areas.

Here the drag and lift areas are constant, when in reality these should be a function of sled speed, implying the accuracy of the physics model can be improved by replacing these constant values by their appropriate equation representation.

5.5.4 Sled Stiffness Function

A spring damping model was implemented as linkage between the two mass particles, in order to prevent them from colliding into each other and give the sled a degree of stiffness.

$$R = (Damp_a(\omega_s - \omega_{so}) + Damp_b(V_r - V_l) \cdot S_2)S_2$$

Where:

- R – Sled stiffness
- $Damp_{a,b}$ – Arbitrary damping coefficients
- ω_{so} – Desired distance between the two particles
- ω_s – Actual distance between the two particles
- V_r, V_l – Velocity vector of the two particles
- S_2 – Unit vector perpendicular to the sled axial direction

A real sled's stiffness varies at different locations on the sled's body. The physics model uses two mass particles to represent the sled body and carries no information regards to this variation in stiffness. Roche has identified in his thesis that this form of spring damper model distributes the weight of the athlete's body solely on the runner contact points, consequently lowers the accuracy of the model and prohibits the possibility of modelling steering mechanics such as mass shifting.

5.5.5 Sled Slip Function

Slipping of the sled occurs when the angle of the sled's axial direction and sled's velocity direction differs beyond a predefined threshold. The resultant friction force affects both along track and across track translations of the sled and is represented by the following empirical formulae in the current physics engine. By its definition, the slip function introduces an element of discontinuity and this has major influences on the design of the optimal control algorithms, which will be discussed in Chapter 7.

$$f_{slip_{l,r}} = -\mu_t \cdot ang \cdot S_2 |N_{l,r}| \sin(V_c \cdot S_2) \tag{5.10}$$

$$f_{lat_{l,r}} = \frac{1}{2}(f_{slip_{l,r}} \cdot S_1)S_1 + \frac{1}{2}(f_{slip_{r,l}} \cdot S_1)S_1 \tag{5.11}$$

Where:

- $f_{slip_{l,r}}$ – cross track friction force caused by slipping.
- ang – Boolean variable which is defined as $1, 0$ or -1 depending on the thresh hold for slippage.
- μ_t – Slip friction coefficient.

As with the coulomb friction, the lack of knowledge regarding to runner and ice interaction results in above formulae being empirical by nature and will be improved when further research is done on said subject.

5.5.6 Actuation Forces

At the end of each time step, SC sums up the individual actuation forces on each mass particle to calculate two 3×1 force vectors representing the total actuation force on the respective mass particles, using equation 5.12.

$$F_l = (W_l + L_l + f_l + D_l + f_{slip_l} + f_{lon_l} - R) \tag{5.12}$$

$$F_r = (W_r + L_r + f_r + D_r + f_{slip_r} + f_{lon_r} + R) \tag{5.13}$$

Where:

- F_l, F_r – Total actuation forces vectors for the left and right mass particle
- W_l, W_r – longitudinal and translational friction forces due to wall hits

5.5.7 Chapter Summary

In this chapter, The physics equations which influences the design of the control algorithms used to predict the optimal descent trajectory have being briefly reviewed. It is clear that there is a distinct lack of accuracy in these empirical equations. However, it is also important to note that the primary goal of this PhD is to formulate a framework of computational methods to predict the optimal descent trajectory and should be designed to accommodate for any future changes to the physics engine. Therefore the current inaccuracy in the physics engine only superficially affects the outcome of this research. As a reference for future iterations of the physics engine, a summary of limitations in the current physics engine has been included in table 5.1. The next chapter will discuss the design, implementation and evaluation of the control algorithms used to study the dynamical relationship between steering input and descent performance.

Features	**Current status & Development proposal**
Aero-dynamic drag and lift model	Current drag and lift model uses a static drag area, a more appropriate approach should be using a drag area as a function of sled velocity. This can be further customised to take into account of athlete's frontal cross sectional areas.
Sled model	Current sled is modelled as 2 mass particles attached with a single stiff spring, this leads to numerous problems involving sled stability. A possible solution is to use a more complex multi-body model the runners as solid bodies rather than a particle. This will also provide stability to the sled body allowing the 'stiff spring' to be replaced by several bars, which are far more appropriate.
Toe steering model	This feature is missing from the current physics engine and needs to be implemented. More experimental data is required to formulate a relatively accurate equation correlating toe force and friction.
Wall collision model	Current wall collision model uses crude boolean equations to add/subtract unit force, this is incorrect. A more traditional collision model using coefficient of restitution and friction of sled against ice wall is recommended.
Yaw model	Current simulation allows the sled to yaw up to 15 degrees, beyond which, the sled will switch into 'slip' mode. This interaction is not fully understood at the time of writing and will need to be investigated further.

TABLE 5.1: Physics Engine Limitations

Chapter 6

Descent Trajectory Generation & Analysis using Classical Control Methods

6.1 Chapter Introduction

The second research hypothesis of this PhD requires the formulation of methods for predicting the optimal descent trajectory for any given Skeleton track. To achieve this goal, control methods from the optimal control sub-sector is required. The method adopted in this PhD is based on the concept of model predictive control, Chapter 7 will be discuss the design and evaluation process of said optimal controllers in detail. However, before designing any optimal controller, it is crucial have a clear understanding the dynamics of the system plant in order to design a profound optimisation strategy, or cost function.

This chapter is dedicated to understanding the dynamics of the descent system, its interaction with steering forces and to identify the key elements required in the design of the cost function. To achieve this goal, two versions of classical control algorithms, the 'Proportional-Derivative' (PD) and the 'Adaptive Proportional-Derivative' controllers, were used to steer the descent simulation. Results yielded from experiments conducted using these controller will be used in the next chapter to design the cost function for the optimal control algorithms. The rest of this chapter contains details regarding the design, application and evaluation process for both PD and adaptive PD control algorithms.

6.2 Descent Simulation Control Structure

Before designing the actual controller, one must first understand the structure of the descent simulation and where the controller will be integrated into said structure. Chapter 5 provided details regarding the underlying physics engine governing the behaviour of descent simulation

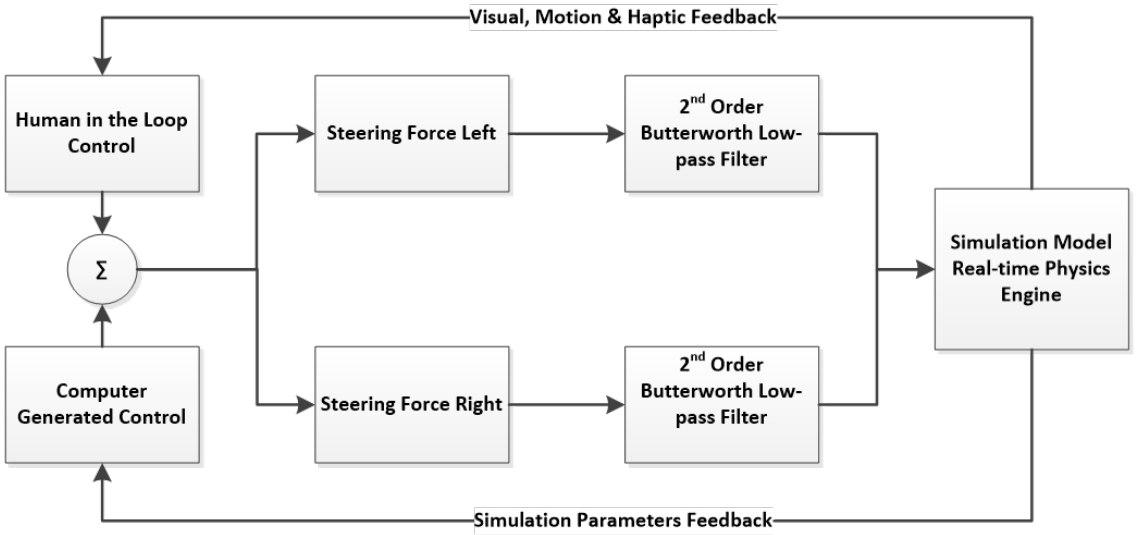

FIGURE 6.1: Integration structure of PD and adaptive PD controller

and in said chapter, the steering forces from athletes feeds directly into the 'Sled Characteristics' block, which contains the algorithms that uses these forces to calculate acceleration on the left and right mass particle that represent the sled. Both the PD and adaptive PD controller acts in the same manner as the human athletes and use the 'Black Box' approach when calculating their control inputs (manipulated variables). Where the controller does not take into account of the mathematical model of system but simply treat it as a black box and calculate control inputs based purely on the deviation between the reference given and the feedback they receive. Further more, both the PD and adaptive PD controller share the same integration structure as illustrated in Figure 6.1.

6.2.1 System Transfer Function

There are two reason that both PD and adaptive PD controllers use the black box approach instead of using the traditional transfer function to calculate control inputs. The first is that in the sled characteristic block, the algorithms used to calculate actuation forces on each mass particles contains non-linearity in the form of slip functions (refer to section 5.5.5). The second is that equations of motion governing the behaviour of the sled's descent are inherently non-linear as well. As both PD and adaptive PD controller are by nature linear control algorithms, the presence of these non-linearities makes it difficult to calculate the exact solutions required to meet the control demands. However, knowledge of a linearised version of the system transfer function proves to useful when choosing the correct combination between proportional, integral and derivative controllers. This section explores the reasons for selecting the proportional and derivative controller architecture.

Classical controllers used to steer the descent simulation functions by tracking a given reference and the only feasible reference for tracking is the transverse sled position β (more details regarding reference generation in section 6.3.3). Therefore, to investigate the effect of control actions on the descent simulation, an input-out transfer function with steering forces as the input and β as the output has to be constructed. The equations of motion from section 5.4 describes

the input/output relationship for the left and right mass particles separately, these are however identical bar their relative spatial derivatives and the steering forces applied to them. Therefore taking transfer function for either one of these mass particle should give a good representation of the system's response as a whole and for the rest of the section, all manipulations will be performed left mass particle. It is important to note that the relationship described in section 5.4 is non-linear and can not be transformed using standard Laplace methods, however if the instantaneous values of the non-linear elements in the relationship were taken as constants, the a reasonably accurate approximation of system dynamics can be made by performing the Lapace transform on the equations of motion of the left mass particle with the following boundary conditions:

$$\beta_l(0) = 7$$
$$\alpha_l(0) = 0$$

The following system transfer function can be obtained:

$$s^2\beta_l(s) - 7s - 7 = \frac{(F_l \cdot r_{\alpha_l} + \gamma \cdot r_{\alpha_l})(r_{\alpha_l} \cdot r_{\beta_l}) - (F_l \cdot r_{\beta_l} + \gamma \cdot r_{\beta_l})r_{\alpha_l}^2}{m\big((r_{\alpha_l} \cdot r_{\beta_l})^2\big) - r_{\alpha_l}^2 r_{\beta_l}^2} \tag{6.1}$$

where

$$\gamma = s^2\alpha_l(s)^2 r_{\alpha_l\alpha_l} + (s\beta_l(s) - 6)^2 r_{\beta_l\beta_l} + s^2\alpha_l(s)(\beta_l(s) - 6)r_{\alpha_l\beta_l}$$

In Equation 6.1, the spatial derivatives, $\alpha_l(s)$ and $\beta_l(s)$ are all functions of time and in order to produce the linear transfer function, approximation of all such parameters are required. This can be obtained exactly by reading the simulated values at any simulation instance. Rearranging said approximation will net the following open-loop transfer function:

$$\frac{\beta_l(s)}{F_l} = K\frac{\frac{K_1}{K}s + \frac{K_2}{K}}{\frac{K_3}{K}s^2} \tag{6.2}$$

where

- K_1, K_2, K_3 – Arbitrary system gain at any sampling period
- K – Common system gain at any sampling period

Here K is a simple scaling factor so that all three gains an be incremented simultaneously, it used as an indicator value for evaluating the stability of the system when combined with different controller architectures (More details will be given in section 6.2.2).

6.2.2 Controller Architecture Stability Evaluation

The controllers must be designed to remain stable for the entire simulated descent. The stability of different controller architectures will be investigated here through the use of the root locus method in Matlab. To calculate the root locus, one needs to first obtain the total open-loop transfer function (i.e. system transfer function from Equation 6.2 plus the transfer function of

the controller). Referring to Appendix A, the open-loop transfer function of a proportional-integral-derivative (PID) controller is:

$$TF_{PID} = K_p + \frac{K_i}{s} + K_d s$$

where

- K_p – Proportional gain
- K_i – Integral gain
- K_d – Derivative gain

To get to transfer function for different controller architectures, simply remove the terms with the appropriate gains. The total open-loop transfer function for a PID controller is therefore:

$$TF_{total} = TF_{PID} \times TF_{System} = K\frac{as^3 + bs^2 + cs + d}{\frac{K_3}{K}s^4} \tag{6.3}$$

where

$$\begin{aligned} a &= K_d K_1 \\ b &= K_p K_1 + K_d K_2 \\ c &= K_p K_2 + K_i K_1 \\ d &= K_i K_2 \end{aligned}$$

There are 7 possible combinations of control architectures, these are: P, I, D, PI, PD, ID and PID, Figure 6.2 presents the respective root locus plot for each of these controller architectures. Here the importance of common gain K is reflected in Equation 6.3. Since for the system to be stable, the root locus of the system's total open-loop transfer function has stay on the left half plane of the root locus plot for all values of K. To put this into perspective, the only controller architecture that would have kept the system stable at all times are the P, D, and PD controllers. The PID controller is partially stable, however when the common gain K is below a certain thresh hold (this threshold changes depending on the values of K_p, K_i *and* K_d) the system will become unstable. Figure 6.3 indicates the range of K over the period of a typical simulated descent, which varied from 0 to approximately 390, and because the value of K will drop to 0 at some point during the simulation, the PID controller architecture will be unstable. As per stated in Appendix A , pure derivative control has a feed forward control structure which can anticipate the system response by extrapolating the change in error. However, it does not guide the system to a steady state and need to be used in conjunction with proportional control. Therefore the PD controller architecture was selected to steer the descent simulation. This choice was later validated as neither pure P nor D controller could complete a full stable descent in simulation.

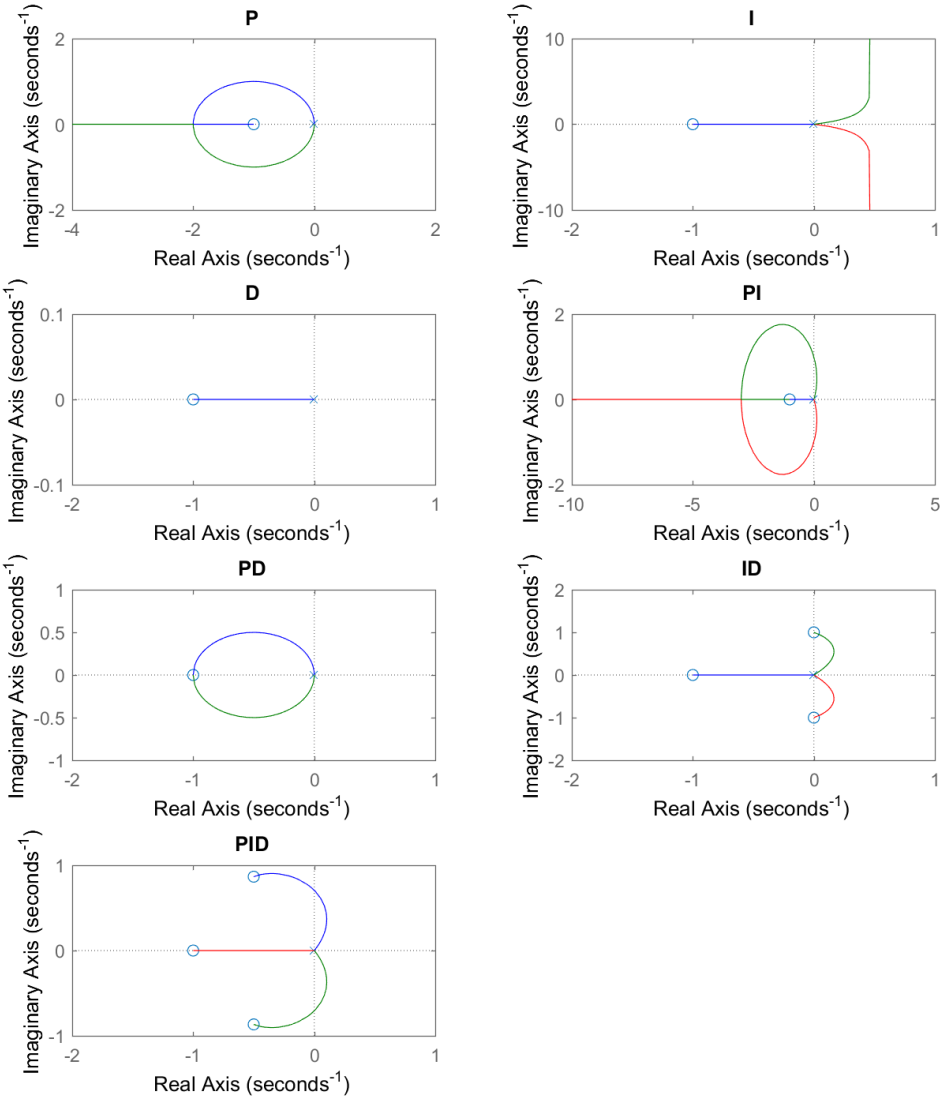

FIGURE 6.2: Root locus of 7 PID based controller designs

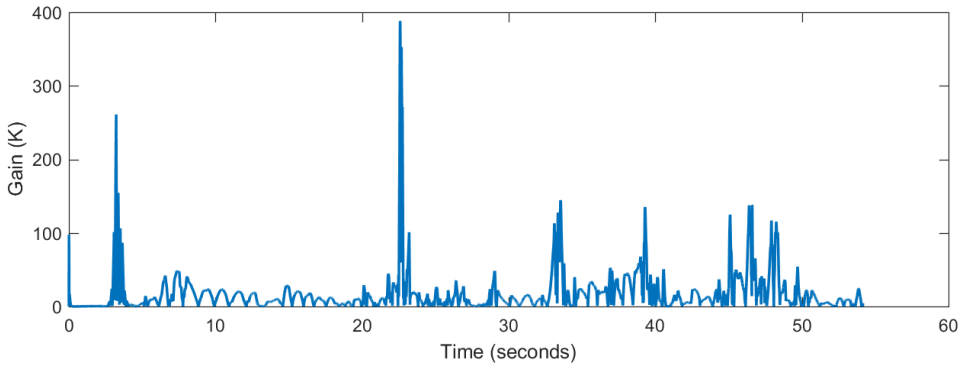

FIGURE 6.3: Common gain K over a typical simulated descent

6.3 Proportional-Derivative Control Algorithm

6.3.1 PD Controller Objectives

As previously stated, the classical control algorithms (PD & adaptive PD) uses the 'Black Box' approach to steer the sled, meaning the control actions they generates are entirely reactionary with no predictive components, this control/steering behaviour is akin to that of a novice athlete. However the performance of classical controllers are dependent on the accuracy of the physics engine, the track geometry and the referencing signal. Optimal performance is based entirely on *ad hoc* tuning for one specific combination of these factors. This lack of predictability and consistency in performance makes the classical controllers unsuitable for predicting the optimal descent trajectories. Therefore, the PD and adaptive PD controllers were not designed to accomplish this task, rather, they were designed to generate baseline performance for comparison with the optimal controller, and to identify key correlations between critical performance indices (e.g. energy dissipation, transverse distance travelled etc.) and how they affect the performance of the simulated descent. These correlations will then be used as guidelines for designing the cost functions and tuning the cost weights of the optimal control algorithms.

6.3.2 Controller Design Constraints

In order to mimic human athlete behaviour and yield realistic descent routes, constraints must be imposed to the control inputs. There are two sets constraints: The magnitude of the steering inputs and the slew rate of the steering inputs. By analysing simulation data from previous motion stimulus experiments on elite athletes, the following conclusion regarding input constraints were drawn:

- Steering forces were measured through flexible thin film force sensor located at the under the shoulder and knees of the athlete. The maximum steering force achieved within the current GB Skeleton team is $\approx$ 150 N. Since there is no inherent method to apply constraints in the PID based controls, the input amplitude were limited through the use of a input saturation block, which can occasionally lead to unnatural steering behaviours.
- The maximum slew rate of steering inputs from elite athlete can reach 2 Hz or 9 rad/s. In the PID based controller, this constraint was applied through the addition of a $2nd$ order Butterworth low-pass filter with a cut off frequency of 9 rad/s directly after the input, before the system model.

6.3.3 Reference Generation

PD controller generate control actions based on the deviation between the sled's current centre position, β_c, and the reference signal, β_{ref}, it was given. Choosing the correct reference will therefore have direct effect on the performance of the controller. Initially, the PD controller uses the centre line of the ice track as its reference trajectory(i.e. $\beta_ref = 7$). This kind of referencing system performed poorly as the centre line is in most cases are not the optimal descent route, and

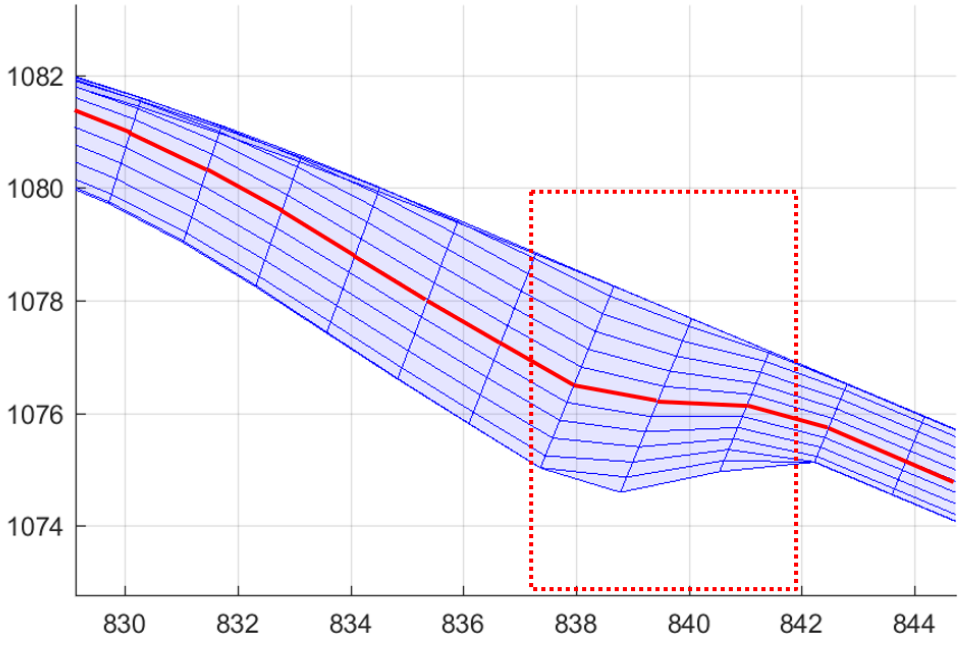

FIGURE 6.4: Surface geometry of the Igls track at entrance to corner 1 where the sudden change in β occurs

tracking this will cause the controller to generate undesirable control inputs. Another cause for the poor performance is due to the way track surface is defined in the physics engine. Referring to section 5.3.1, a track surface is divided into N segments evenly across, represented by distinct β values. This division method leaves β_{ref} vulnerable to sudden changes in the shape of the track. Figure 6.4 shows an example of sudden change in the value of β, represented by the red line inside the dashed box, this change was caused by the introduction of a 2nd entrance on the track. These undesirable changes in geometry will cause the centreline to warp abruptly and consequently causes the controller to produce undesirable harsh corrective control actions, therefore a new method for reference generation was necessary.

The method developed for reference generation is called 'On-line position orientated reference generation'(OPORG). This method requires a lookup table of paired longitudinal and transverse positions, obtained through recording a manually steered descent(either by a coach or an operator with steering instructions from a coach) on the selected track. The centre positions of the sled from this descent simulation is recorded and sorted into corresponding $\alpha_c(rec)$ & $\beta_c(rec)$ pairs to form an $M \times 2$ matrix, where M is the longitudinal descent trajectory dimension (total number of α_c recorded). During the simulation, at any sampling period k, an on-line search algorithm is performed, which compares the current $\alpha_c(k)$ value of the sled against the $\alpha_c(rec)$ values stored in the lookup table. Once the closest values of $\alpha_c(rec)$ is found, the corresponding $\beta_c(rec)$ values is then used as the transverse position reference, β_{ref}, for that sampling period. A new reference is generated for every simulation, the reference generated using this method eliminates the problem with sudden changes in β as previously discussed. Further more because this reference generated this way is not time orientated but rather dependant on the position of the sled, allowing it to handle external disturbances which may affect the longitudinal velocity of the sled. Figure 6.5

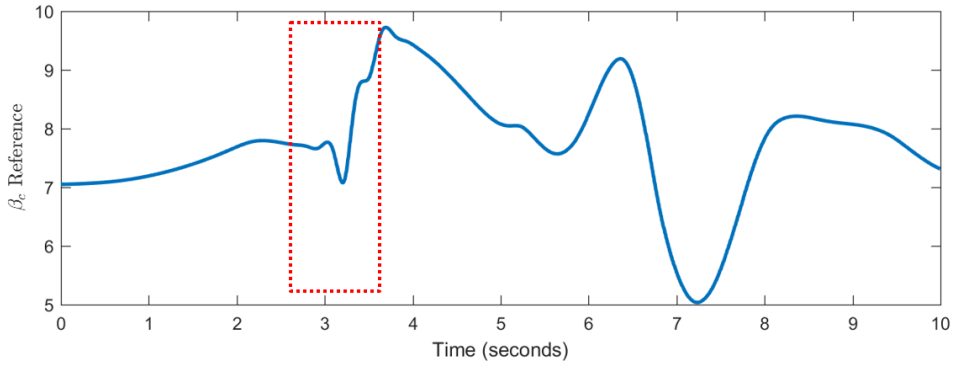

FIGURE 6.5: β_ref of Igls track for the first 10 seconds

shows the first 10 seconds of the reference signal generated via OPORG on the Igls track. The red dashed box in the figure highlights the issues regarding the entrance to corner 1, the dip in reference represent how the OPORG compensates for the change in β values.

References generated via OPORG yields much 'smoother' trajectories than the centre line reference, this also allows controller to produce more 'human like' steers. Further more, descent simulations using the OPORG is in general $\approx$ 16% quicker than those that uses the centre line referencing system. The reference signals used in rest of the section were generated using OPORG.

6.3.4 PD Controller Design

Two PD controller were designed to be used in conjunction to control both the left and right mass particles. Error between the reference signal and current transverse sled position is first separated into left and right hand errors, then it is fed into the appropriate PD controller as inputs and the outputs of the controllers get passed through a saturation block followed by a 2nd order Butter-worth low pass filter before passing on as left and right hand steering forces. The controller structure is illustrated in Figure 6.6. The individual PD controller uses standard discrete controller structure, and is shown in Equation 6.4.

(Note: by default, Matlab Simulink uses discrete controller designs, therefore, the format for all forthcoming controller designs used for this PhD is also discrete with a sampling frequency of $1/0.007 \approx 143$ Hz)

$$U(k)_{l,r} = e(k)_{l,r}K_p + \delta e(k)_{l,r}K_d \tag{6.4}$$

with

$$e(k)_l = \beta_c(k) - \beta_{ref} + 0.5$$
$$e(k)_r = \beta_c(k) - \beta_{ref} - 0.5$$
$$\Delta e(k)_{l,r} = e(k)_{l,r} - e(k-1)_{l,r}$$

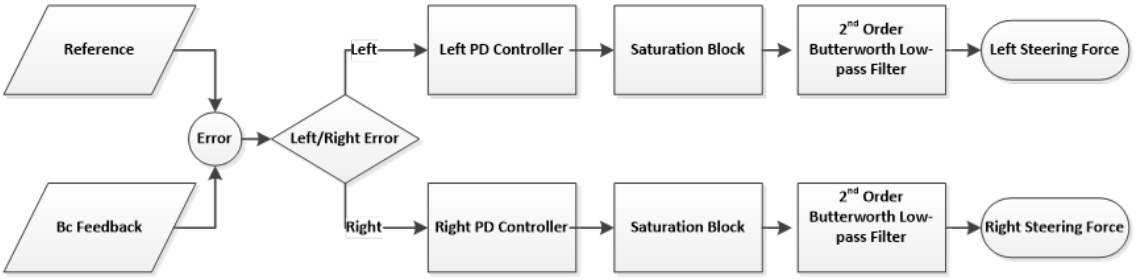

FIGURE 6.6: PD controller structure

where

- $U(k)_{l,r}$ – Left and right control inputs/steering forces at sampling period k
- $e(k)_{l,r}$ – Left and right error at sampling period k

6.3.5 PD Controller Performance Indices Analysis

Systematic analysis of simulated descents on a Sochi Olympic race track were carried out to identify correlations between the performance indices and assist in the design of the optimal control algorithm's cost function. The indices were chosen based on the factors that are typically associated with sliding, these include descent time, transverse distance travelled and energy dissipation. For fair analysis of correlation, the performance indices are to be compared with an independent variable. In this particular case, the independent variable is steering input force. The controller gains were tuned over a region ($Kp \in [0.015, 0.05], Kd \in [0.04, 0.07]$) where the physics model were able to complete the entire simulated descent, this region of controller gains was name the 'stable region' and the corresponding steering forces were recorded. It was shown that the steering forces were directly proportional to the magnitude of the controller gains. The rest of this section presents the data from the simulations as both surface plots to observe overall behaviour and contour plots to identify correlations between the performance indices.

Descent Time

Descent time is the most self-evident performance index to investigate as it ties in directly to the outcome of the race. Although the descent time is *ad hoc* to the dynamic model and track geometry, it can however adequately provide an understanding of general system behaviour and be utilised as a performance reference to gauge against other possible indices.

Figure6.7 indicates that the descent time exhibits a quadratic structure initially decreasing proportionally with the value of K_d and K_p. However, once K_d is sufficiently small, the descent time increases as K_p approaches its stable boundaries. This is not truly representative of the index behaviour for the following reason: When K_d is small, a large K_p will induce aggressive control actions and lead to instability in the system therefore leading to undesired oscillations, which causes a slower descent time. This is a defect caused by design of the controller and will skew the simulation data. In Figure 6.8, the x and y axes represent K_d and K_p respectively, the colour of the contour represent descent time. To avoid using data resulted from the aforementioned

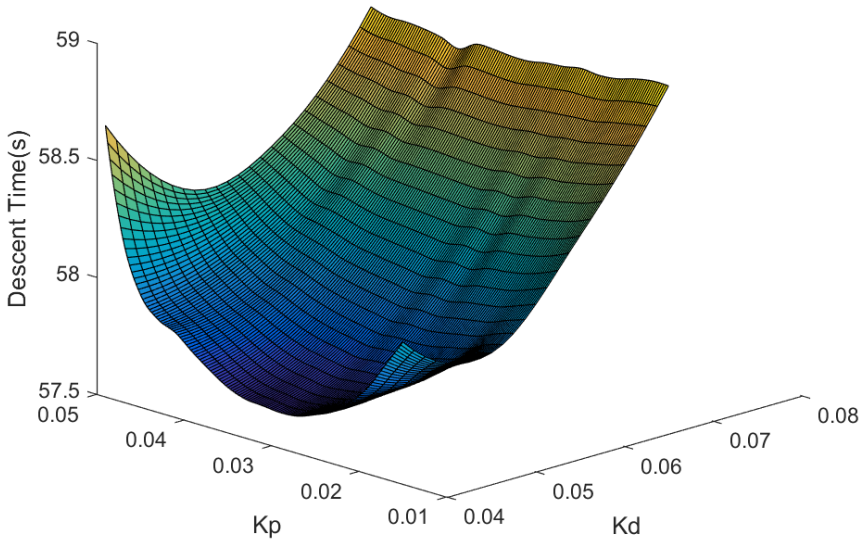

FIGURE 6.7: Descent time vs Steering force surface plot

defect, a 'Representative Region' was put in place, indicated by the dashed box. The region cuts off at $K_d = 0.004$, which is the minimum value of K_d. Therefore within the region, the PD controller remains D dominant and should provide useful data. The colour of the contour also represent the general trend of descent time with respect to steering forces:

Increments in steering force leads to increments in descent time.

To keep the analysis relevant, only data from the representative region will be used for the other two performance indices.

Transverse Distance Travelled

In the parametric surface representation, the centre longitudinal spline, although varying slightly and not actually representing a viable trajectory would represent a minimal distance. The cross track error (e.g. the distance away from the prescribed trajectory) is referred to as the transverse distance travelled and its total is calculated by integrating $|\beta_c|$ over the duration of the simulated descent. α was not included in the calculation since all simulated descent start and end are at the same α values.

Figure 6.9 presents the simulation data in different axes orientation to provide a better view for the overall system behaviour. It is clear that distance travelled is also skewed by the controller defect. In Figure 6.10, the x and y axes represent K_d and K_p respectively, the colour of the contour represent the trend of distance travelled with respect to steering force:

Increments in steering force leads to decrements in travel distance.

Energy Dissipation

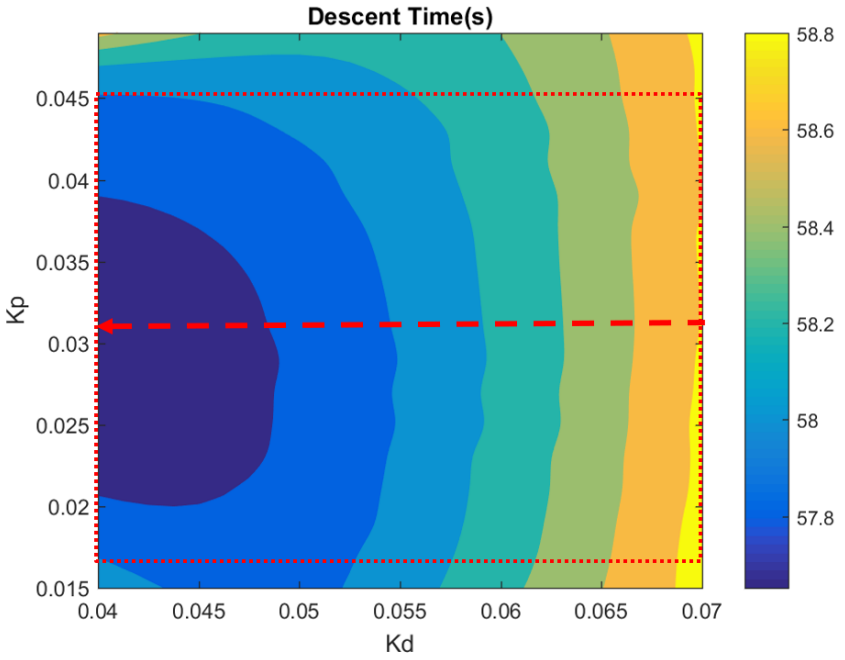

FIGURE 6.8: Descent time vs Steering force contour plot

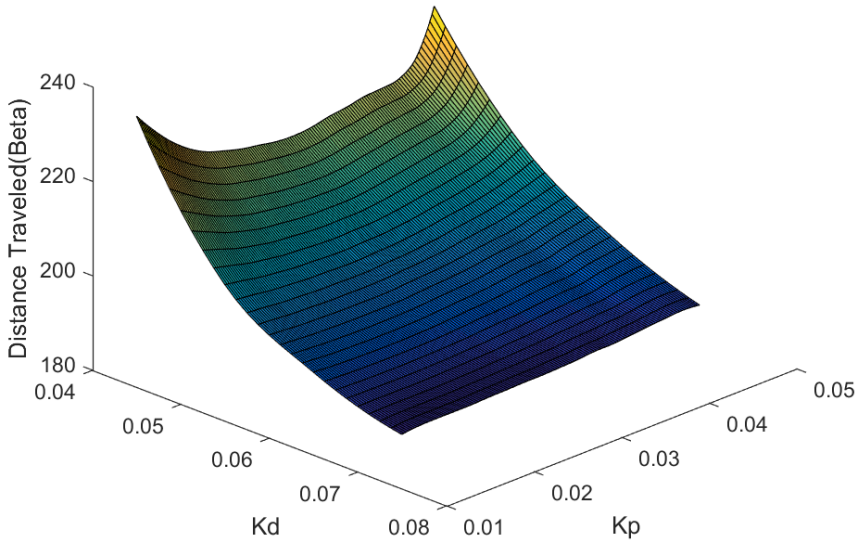

FIGURE 6.9: Transverse distance travelled vs Steering force surface plot

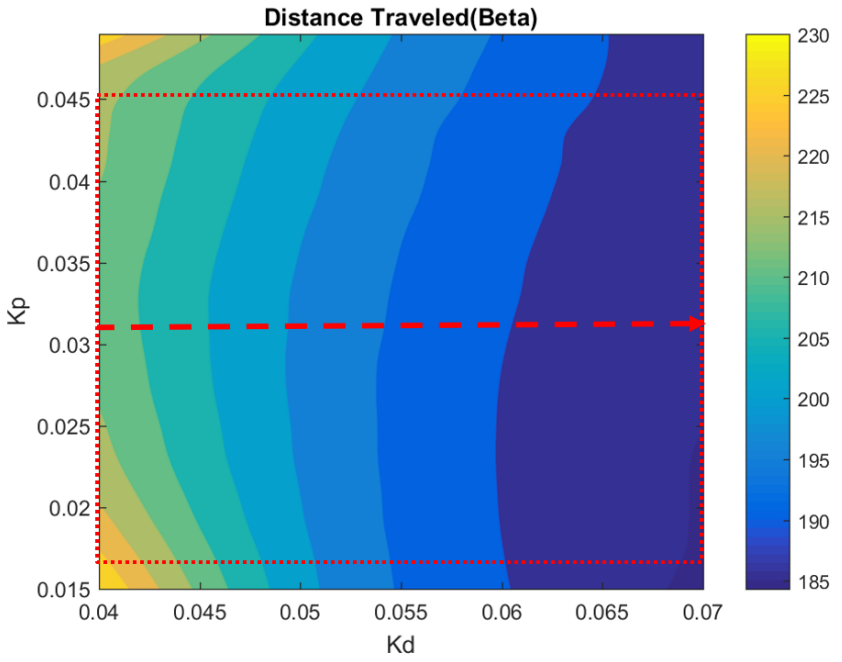

FIGURE 6.10: Transverse distance travelled vs Steering force contour plot

In this model, energy is lost through friction and drag ($E_{k_{lost}}$). The dissipation is calculated by subtracting kinetic energy gained from the potential energy lost through the simulation. Kinetic energy gained is calculated via $\frac{1}{2}m(v - v_0)^2$ where v_0 is the initial velocity after the sprint phase and v is the terminal velocity, (usually at the track finish). The complete equation is shown below in Equation 6.5.

$$E_{k_{lost}} = m\big(g(h_f - h_0) - \frac{1}{2}(v_f^2 - v_0^2)\big) \tag{6.5}$$

Figure 6.11 and 6.12 shows that energy dissipation is affected by the controller defect to a much lesser degree. The reason for this is that energy lost is only proportional to friction caused by steering force (i.e. a simulated descent could take longer to complete but still have low energy lost). Figure 6.12, the x and y axes represent K_d and K_p respectively, the colour of the contour represents the trend of energy lost with respect to steering force:

Increments in steering force leads to increments in energy lost.

Performance Indices Correlation

To obtain suitable correlations for use in the optimal control designs, the values of each performance index were averaged across all the K_p values within the representative region. Figure 6.13 presents the processed data compared against change in K_d, which can be perceived as steering forces at this point.

Characteristics identifications were carried out and the following correlations can be drawn from analysing the figures:

- Descent time exhibits a quadratically increasing characteristic with respect to the steering force.

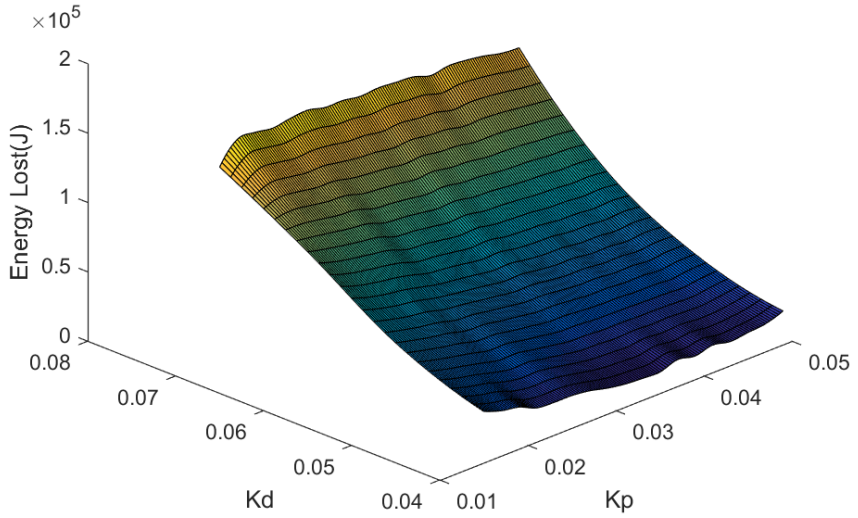

FIGURE 6.11: Energy lost vs Steering force surface plot

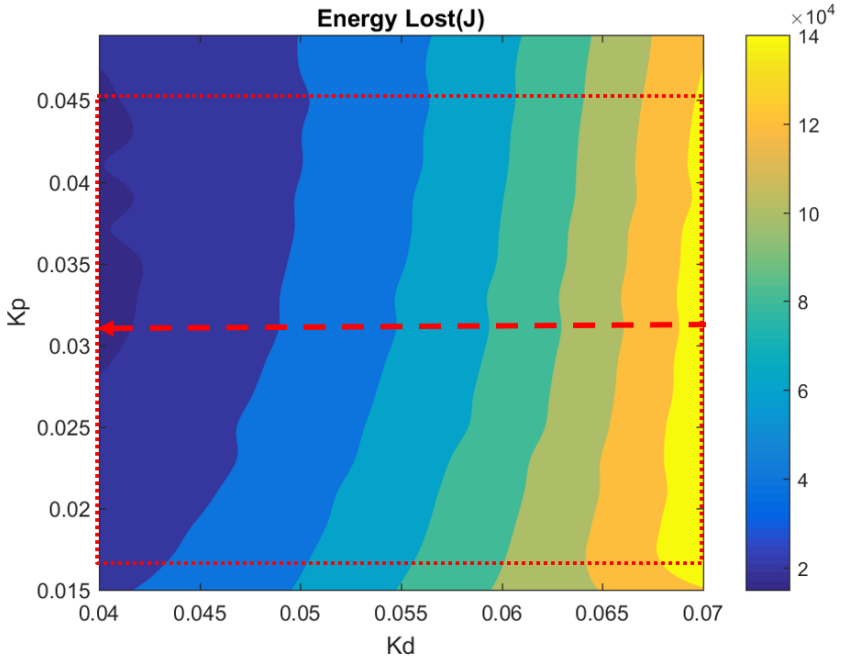

FIGURE 6.12: Energy lost vs Steering force contour plot

- Transverse distance travelled exhibits a quadratically decreasing characteristic with respect to the steering force.
- Energy dissipation exhibits a quadratically increasing characteristic with respect to the steering force.

A clear correlation between performance indices can be drawn from above characteristics:

Increments in energy dissipation
→ Decrements in transverse distance travelled
→ Increments in descent time.

However, using only this correlation would indicate that 'by maximising the transverse distance travelled, one would minimising descent time', which is logically absurd. Therefore, a second correlation needs to be investigated around the Kd value that yielded the minimum descent time (i.e. $Kd = 0.04$) for clarification. Figure 6.14 shows the correlations between performance indices within the stable range of Kp values. Figure shows that the all three performance indices matches closely and descent time increases with increasing distance travelled and energy lost(minimum descent time indicated by dashed red line). Analysing both sets of indices correlation indicates that transverse distance needs to both increase and decrease to minimise descent time, which leads to a contradiction. Therefore, the only plausible explanation is that transverse distance travelled is **uncorrelated** with descent time and should be ignored in the cost function. On the other hand **Minimising energy loss is the key strategy in minimising descent time.**

6.4 Adaptive Proportional-Derivative Control Algorithm

6.4.1 Controller Objectives

Whilst the PD controller provided acceptable base performance to give yield a relevant performance indices analysis. There are however numerous sections where its system performance is poor and displays steering behaviours uncharacteristic to human athletes. This inconsistency in performance reduces the credibility of the correlation analysis and need to be improved before any results from the correlation analysis can be applied to the design of the optimal cost function. The sections that displayed poor performance include: large, undesirable oscillatory motions around low speed corners; oscillatory motion on the straight sections of the track and wall collisions near the entrance and exists of high velocity corners. The main cause of these poor performances are the static nature of the control gains K_p and K_d, which were tuned to achieve both the quickest descent possible and to also maintain system stability. Therefore, it is inevitable to encounter difference in control performance as the sled traverse the entire track, the effectiveness of the control actions generated by the PD controller changes drastically between high and low velocity sections as well as between straight and corner sections of the track. To tackle this issue in performance, several adaptive PD control algorithm was developed. The adaptive PD controller shares the same controller objective as the PD controller, that is to not find the optimal descent trajectory but to investigate the correlations between key performance indices. Further more, the adaptive PD controller aims to adjust its control forces to assert

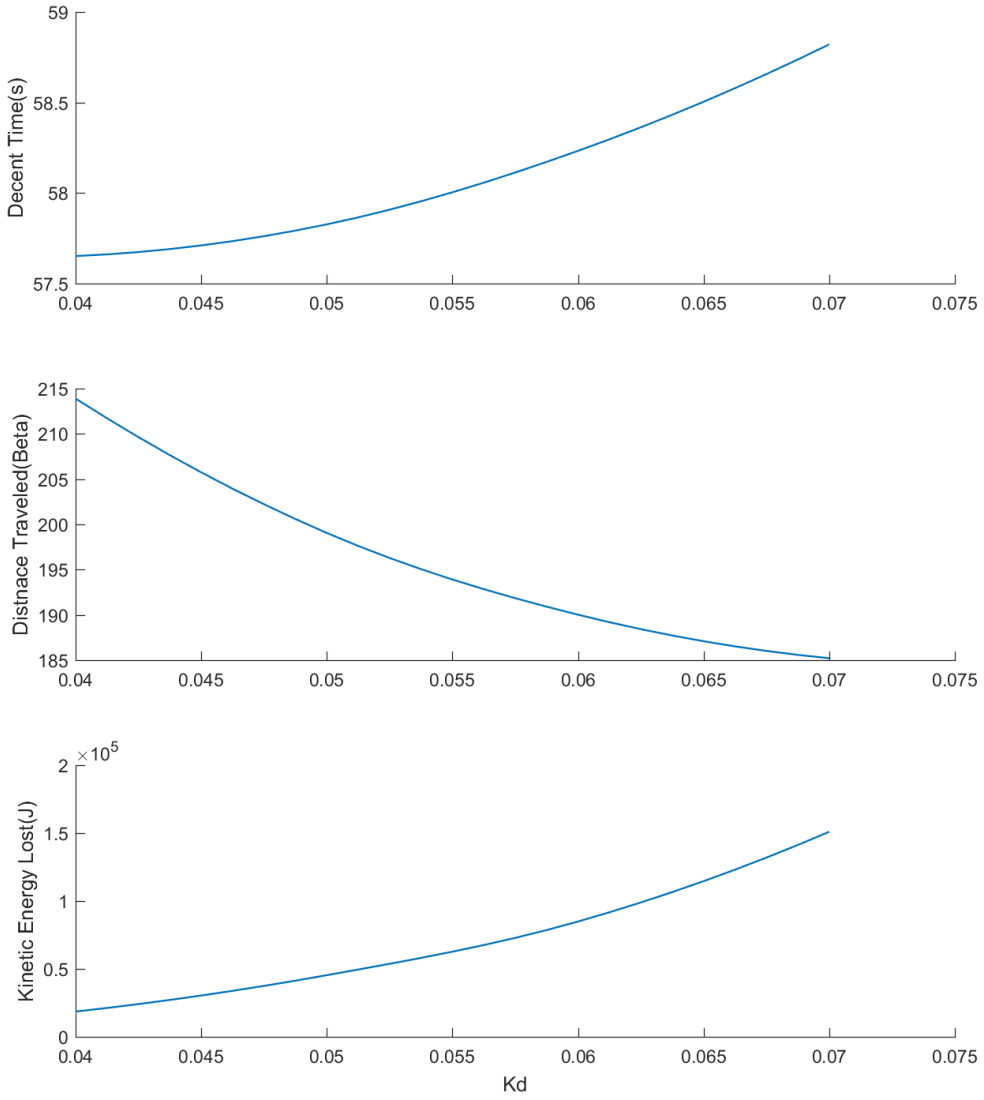

FIGURE 6.13: Correlation between performance indices

more human like steering actions. Details regarding the design and verification process of these adaptive PD controllers will be presented in the rest of this section.

6.4.2 Control Authorities

It is stated in the previous chapter that one of the main reason for the inconsistent performance standards during a simulation is the static nature of the control gains in the the PD controller design. A logical step towards improving controller performance is to first identify the sections on track where these inconsistencies occur and observe for common causes that are present in these sections.

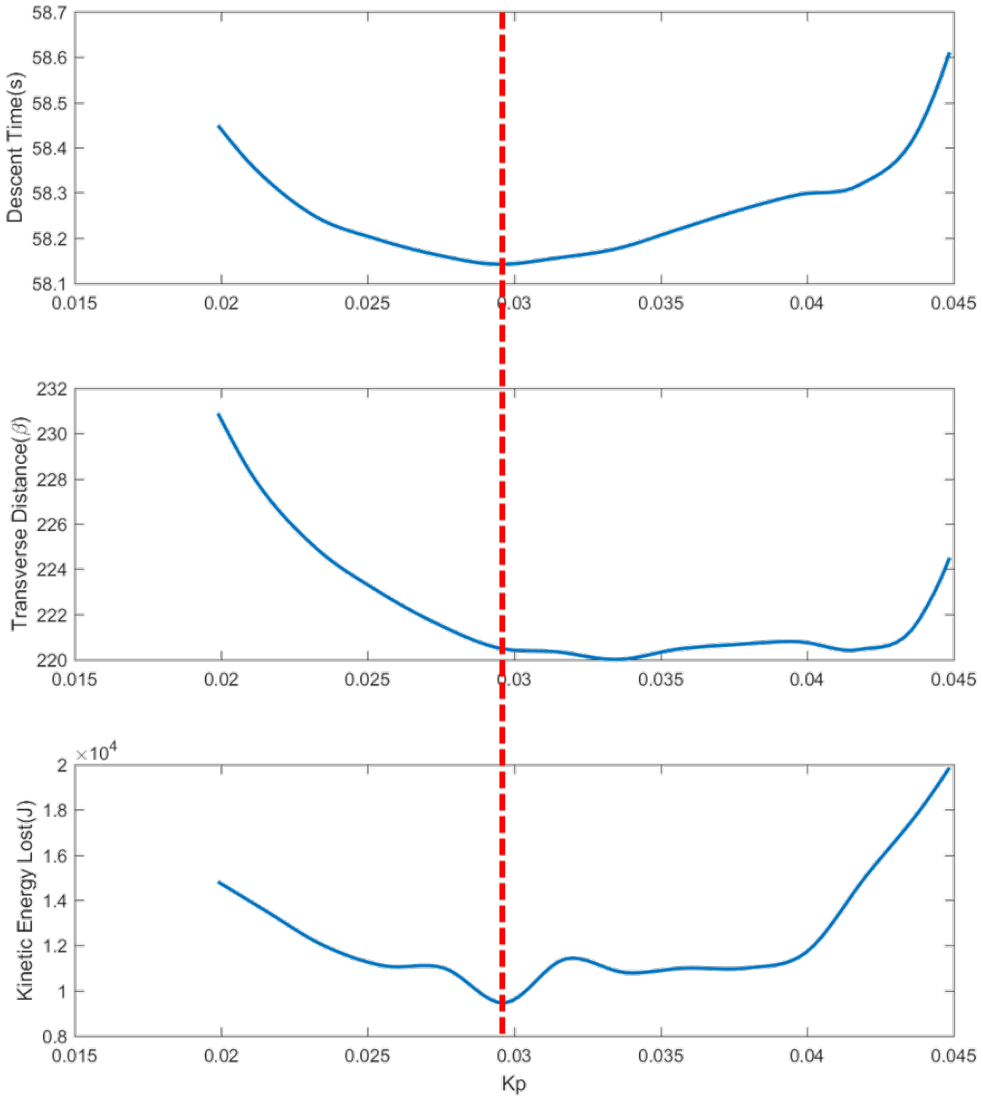

FIGURE 6.14: Correlation around minimum Kd

One possible hypothesis states that 'the control forces generated by the PD controller become too low to be relevant at certain points along the track and thus causing the poor system performance'. To verify said hypothesis, a descent simulation was conducted on the Sochi race track using the PD controller, tuned for the fastest descent and the its left/right control forces were recorded. The recorded forces were then divided by their respective total actuation forces to obtain a final ratio in terms of a percentile, known as the 'Control Authority' ratio. Figure 6.15 displays this control authority percentile and correlated it against a figure displaying the β_ref signals (orange dashed line) and feedback (solid blue line) trajectories. The sections where performance of the controller proved to be poor, as per demonstrated by the large tracking errors and frequent, high magnitude transverse motion of the sled, matched up exactly with the sections of the track that has the lowest control authority. These sections were highlighted by the red

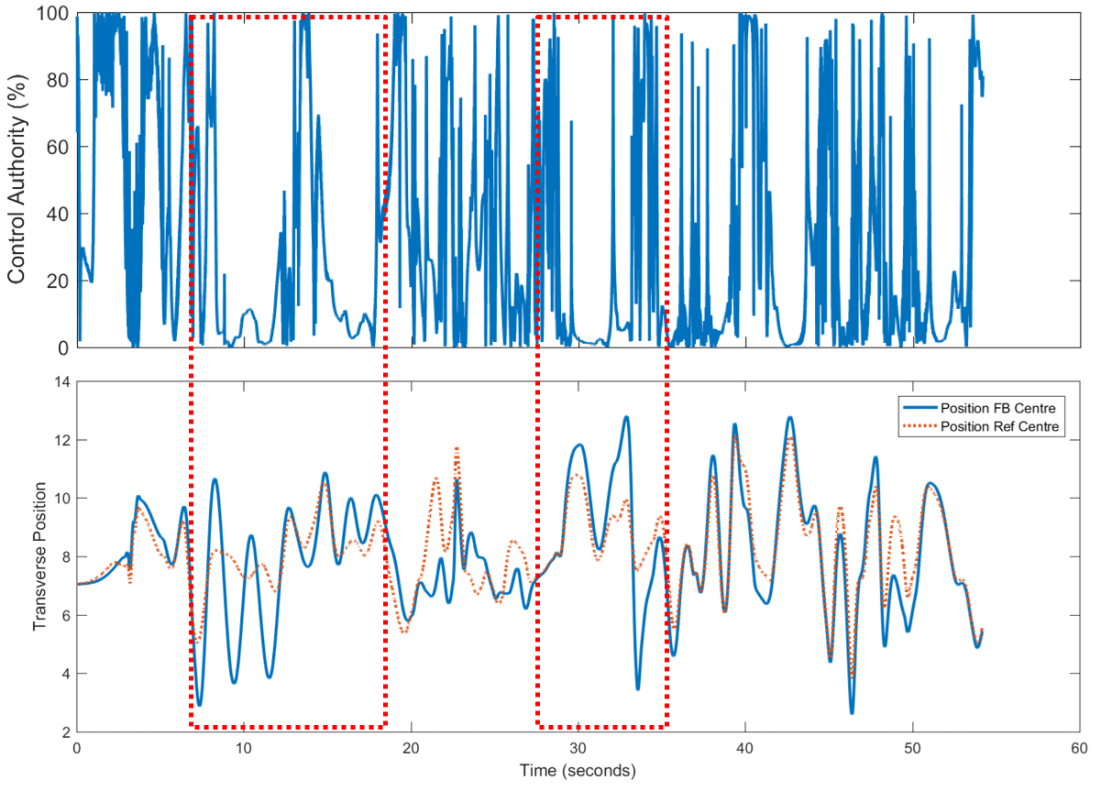

FIGURE 6.15: Control authorities during full descent on the Sochi race track

dashed boxes and validated the hypothesis. Therefore, it is reasonable to make the assumption that by increasing the control forces in the areas with low control authorities, the performance of the controller can be kept consistently at an adequate level throughout the entire descent.

6.4.3 Adaptive PD Controller Design

After verifying the hypothesis in section 6.4.1, it is clear that no amount of tuning using the current PD design structure will be able to compensate for the change in descent dynamics and yield consistency in performance standard. Therefore, two control algorithms were developed using the 'Adaptive PD' controller structure.

Adaptive Algorithm I - Rapid Transverse Motion Compensation

The first of the two adaptive PD controller was developed with the goal to resolve the issue regarding large, abrupt transverse motions that usually occurs at the exists of high velocity corners. An example of this can be found at the exit of corner 7 on the Igls track(although this can be seen in multiple places throughout the track, corner 7 on Igls is the most effected and is therefore used as the example here), where the sled typically exits with a transverse velocity above 70 km/h. This results in a rapid change in both the sled's centre position(β_c) and the sled's transverse velocity($\Delta\beta_c$). The PD controller's static gain is usually tuned to handle the slower changing dynamics in the rest of the track to avoid undesirable oscillations, and is therefore unable to control this adequately. Figure 6.16(a) displays the on track trajectory

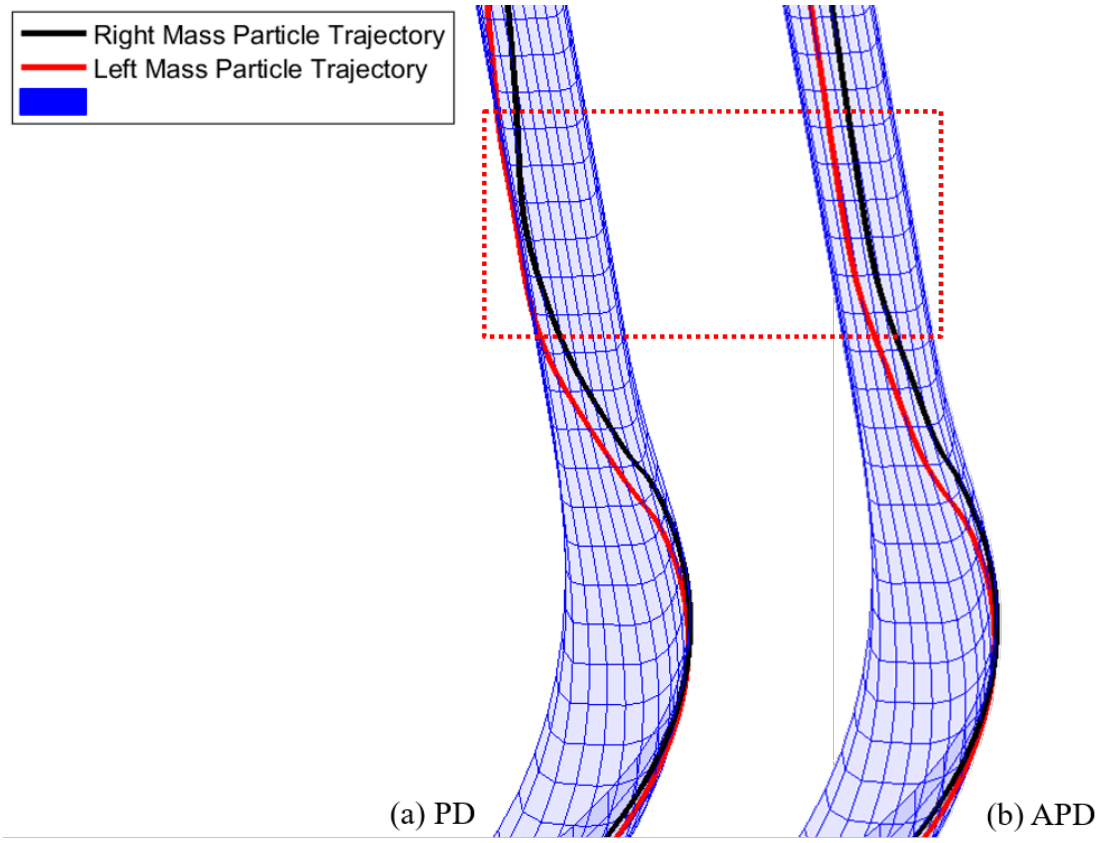

FIGURE 6.16: On track descent trajectory at exit of corner 7 on Igls

generated using the PD controller during a typical full descent of the Igls track where a failure in performance has occurred in the form of wall collision.

The adaptive PD controller resolves this issue by actively adjusting both proportional and derivative control gains with respect to transverse velocity, $\Delta\beta_c$, to assert more aggressive control actions (This is the same steering technique that elite athletes uses when cornering). This adjustment in control action only occurs when $|\Delta\beta_c|$ is above a pre-determined threshold, ε. This is done to ensure that this portion of the adaptive PD algorithm do not interfere with the performance of the sled at low velocity corners. Algorithm I is show below between Equation 6.6 and 6.7.

$$K_{p_{Adaptive}} = K_p - min\left[(|\Delta\beta_c| - \varepsilon) \times K_{\Delta\beta_{c_p}}, K_{p_{min}}\right] \tag{6.6}$$

$$K_{d_{Adaptive}} = K_d + min\left[(|\Delta\beta_c| - \varepsilon) \times K_{\Delta\beta_{c_d}}, K_{d_{min}}\right] \tag{6.7}$$

where

- $\Delta\beta_c$ – Transverse velocity of sled
- $K_{p_{Adaptive}}$ – Adaptive proportional gain
- $K_{d_{Adaptive}}$ – Adaptive derivative gain

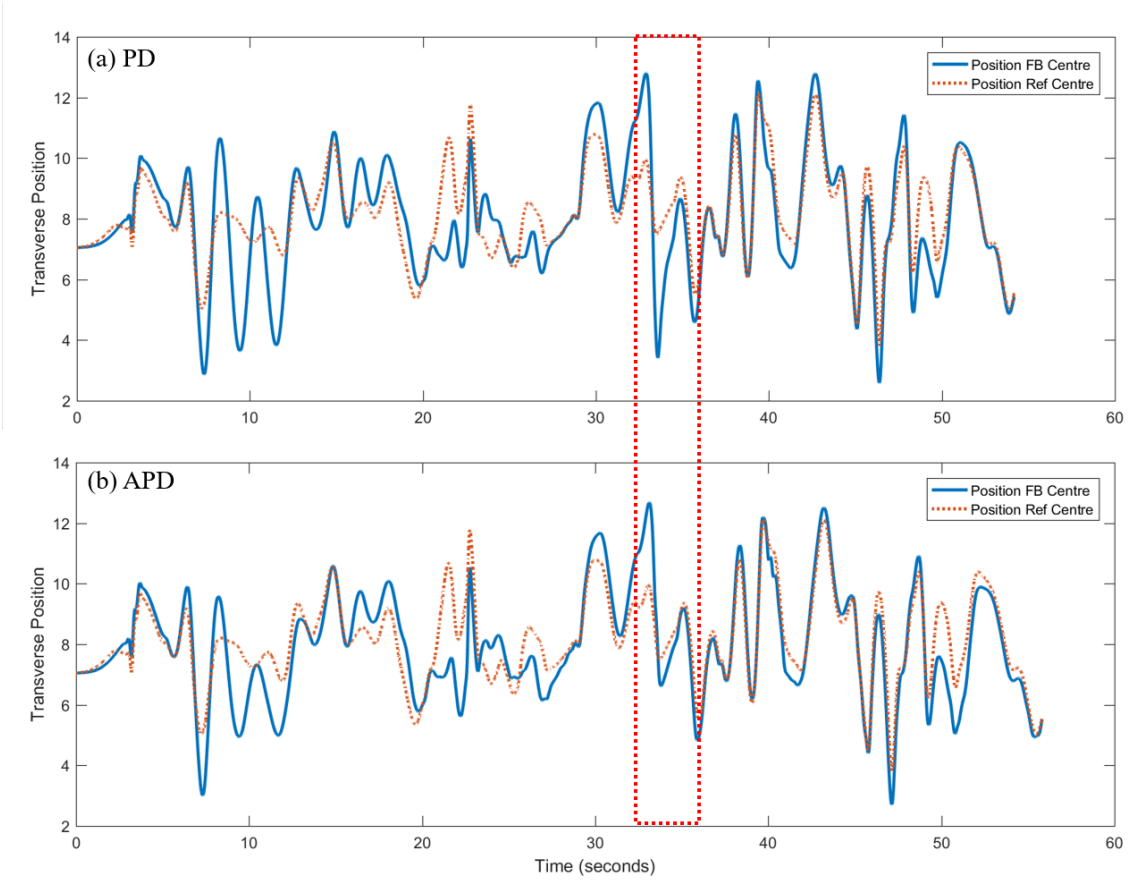

FIGURE 6.17: Trajectory comparison plot of PD and adaptive PD controllers on Igls, highlighting exit of corner 7

- $K_{\Delta\beta_p}$ – Scaling gain for proportional gain change w.r.t. $\Delta\beta_c$
- $K_{\Delta\beta_d}$ – Scaling gain for derivative gain change w.r.t. $\Delta\beta_c$
- ε – Adaptive controller threshold value

Figure 6.16 (b) displays the on track trajectory generated using the adaptive PD controller, and the red dashed box highlights the difference the adaptive algorithm has made to the performance in this particular corner. The figure shows that Algorithm I has successfully nullified the previous wall collision and is therefore functions as intended. Figure 6.17 illustrates the descent trajectories as a function of time, here the orange dashed lines represent the β_{ref} reference trajectories and the solid blue line represent the β_c feedback. The red dashed box in this figure shows the trajectory of corner 7's exit. More specifically it matches the red dashed box in Figure 6.16.

Adaptive Algorithm II - Control Authority & Slow Dynamic Shift Compensation

The second adaptive algorithm deals with the loss of control authority from cornering and slow dynamic shifts. The slow dynamic shift is term used for the loss of control authority caused by the increasing velocity of the sled. The equation of motion, which calculated the transverse acceleration $\ddot{\beta}$ for either the left or right mass particle is:

$$\ddot{\beta} = \frac{(F \cdot r_\alpha + A)(r_\alpha \cdot r_\beta) - (F \cdot r_\beta + B)r_\alpha}{m\big((r_\alpha \cdot r_\beta)^2 - r_\alpha^2 r_\beta^2\big)} \tag{6.8}$$

where

$$A = -\big((\dot{\alpha}^2 r_{\alpha\alpha} + \dot{\beta}^2 r_{\beta\beta} + 2\dot{\alpha}\dot{\beta} r_{\alpha\beta})m \cdot r_\alpha\big)$$
$$B = -\big((\dot{\alpha}^2 r_{\alpha\alpha} + \dot{\beta}^2 r_{\beta\beta} + 2\dot{\alpha}\dot{\beta} r_{\alpha\beta})m \cdot r_\beta\big)$$

Equation 6.8 indicates when the longitudinal and transverse velocities are low, the transverse acceleration is calculated mainly depending on the magnitude of the spatial derivatives and the actuation forces, F, which in turn is dependant on the steering forces. A and B in Equation 6.8 both include a number of quadratic terms involving the longitudinal and transverse velocities, and by the nature of quadratic formulas, as $\dot{\alpha}$ and $\dot{\beta}$ increases, they become increasingly dominant, therefore leading to the loss of control authority. To resolve this issue to second adaptive algorithm normalises and adjusts the total control output from the first algorithm with respect to velocity, both cancelling out undesired oscillatory motions in lower velocity sections of the track and increase control authority in higher velocity sections of the track. The second adaptive algorithm also increases the magnitude of the control inputs in correlation to roll angle ϕ of the sled, so that the adaptive PD controller asserts more control forces during the corners of the track than on the straights. Equation 6.9 illustrates the second adaptive PD control algorithm.

$$U(k)_{Alg.II} = U(k)\left(K_v\big(\frac{v(k)}{v_{max}}\big)\big(1 + K_\phi \phi(k)\big)\right) \tag{6.9}$$

where

- $U(k)$ – Control inputs from Equation 6.6 & 6.7
- $U(k)_{Alg.II}$ – Control inputs from adaptive PD algorithm II
- K_v – Velocity dependant adaptive gain
- K_ϕ – Roll angle dependant adaptive gain
- $v(k)$ – Velocity of the sled at sampling period k
- v_{max} – Maximum recorded velocity for current testing track
- $\phi(k)$ – Roll angle of the sled at sampling period k

Figure 6.18 and Figure 6.17 present descent simulations on the same track using different control algorithms. The red dashed box highlights corner 1 of the track, it is clear from the figure that without the adaptive control gains, the sled experienced large amounts of oscillation within the corner. With the adaptive controller however, the amount of oscillation was adequately suppressed, thus demonstrating the effectiveness of the adaptive PD algorithm. There exist a caveat to the adaptive control algorithm however, during the straight sections of the track, the adaptive component of the Algorithm II exerts unnecessary control forces to zero the lateral sled velocity and causes the sled to slow down through loss of kinetic energy. Therefore, in practice to achieve the best possible performance, Algorithm I(PD) and Algorithm II(adaptive PD) were

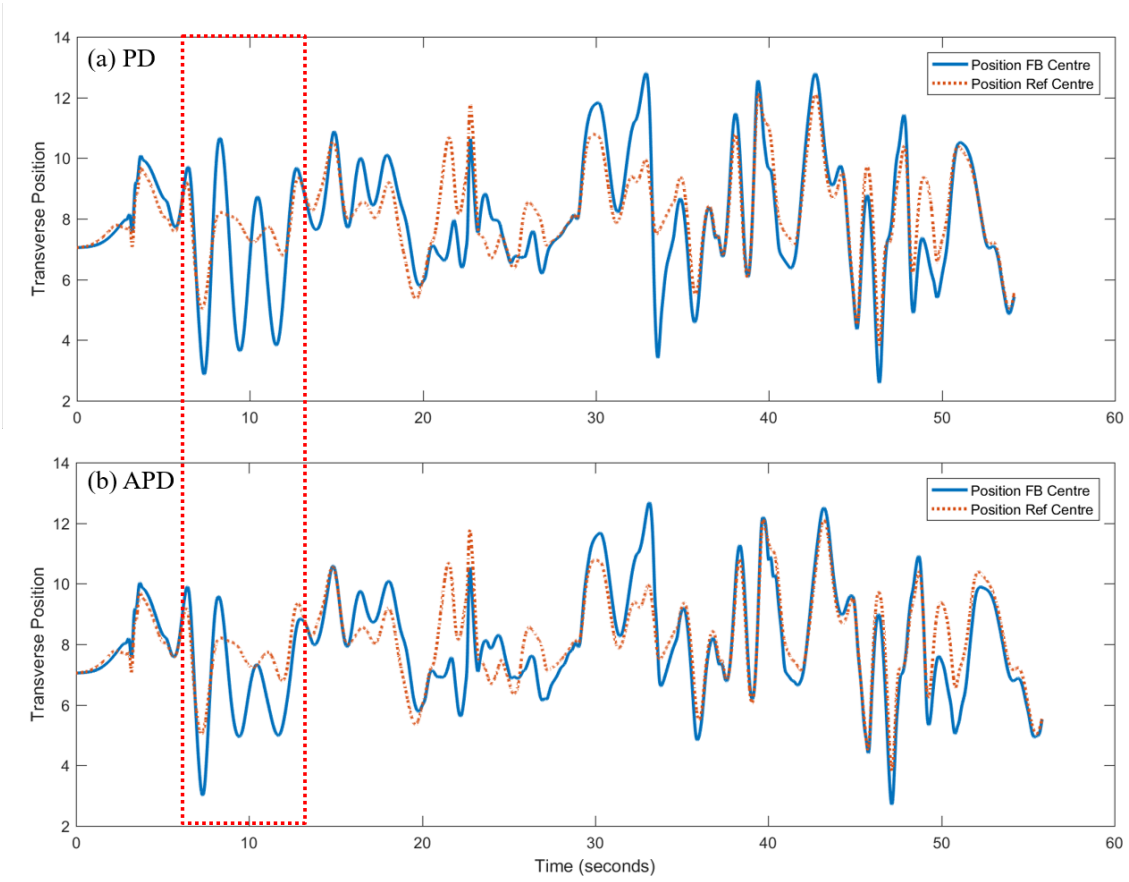

FIGURE 6.18: Trajectory comparison plot of PD and adaptive PD controllers on Igls, highlighting corner 1

Algorithm	**Descent Time**	**Energy Lost**	**Distance Travelled**
Proportional - Integral	58.120	9460	220.785
Adaptive Proportional - Integral	59.073	18833.69141	246.701
Adaptive Proportional - Integral + Proportional - Integral	56.314	11252.34375	226.493

TABLE 6.1: Performance Indices vs. Control Algorithms

used in conjuration, where Algorithm I was used to steering through the straights and Algorithm II was used for the corners. The results of applying said algorithms in this fashion is that the sled is able to achieve better tracking of the β_{ref} through both the corners without loosing energy through excessive steering during the straights, resulting in the descent becaming more stable and subjectively (according to subject matter experts) more 'realistic'. Table 6.1 presents a comparison of descent performance indices between the fastest descent using PD, adaptive PD and combined control algorithms.

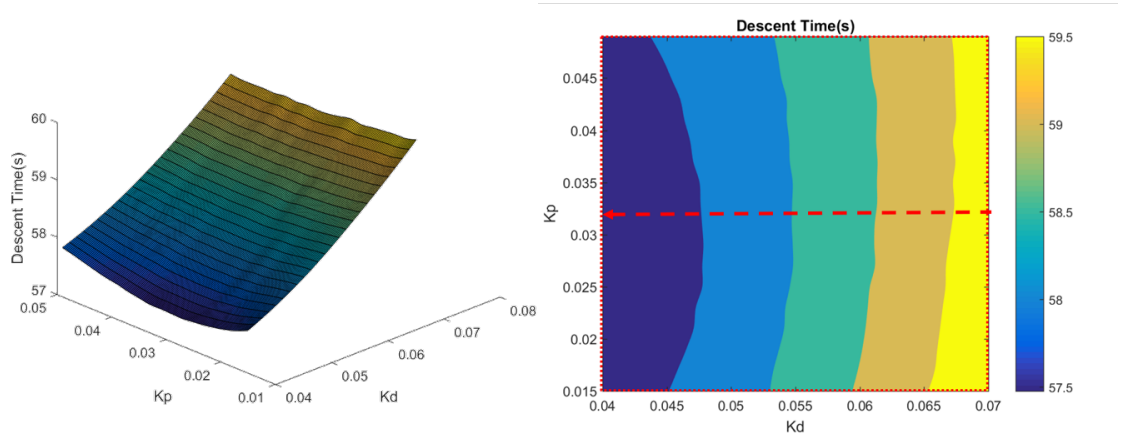

FIGURE 6.19: Adaptive PD controlled descent time mesh and contour plot

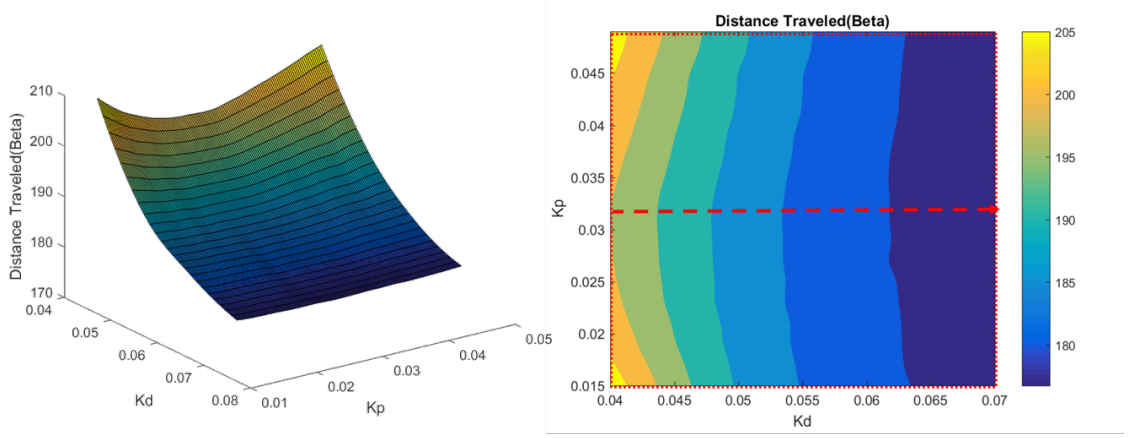

FIGURE 6.20: Adaptive PD controlled transverse distance travelled mesh and contour plot

6.4.4 Adaptive PD controller Performance Indices Analysis

The same performance indices analysis as section 6.3.5 was conducted using the adaptive algorithms to verify the correlation obtained from the previous analysis. To ensure a fair comparison, the exact simulation conditions were applied to the analysis this time as well (i.e. The same racing track and the same 'Stable Region'). Results obtained from the the second analysis is presented below between Figure 6.19 to 6.21. These figure shows that the descent controlled by the adaptive PD controller exerted very similar behaviours to those controlled by the PD controller, however the behaviour appears to be more linear, this may be due to the adaptive nature of the controller, thus confirming the results obtained by the previous performance indices analysis.

6.5 Chapter Summary

By analysing the correlation between performance indices using both PD and adaptive PD controllers, a feasible cost minimisation strategy could be determined. The relationship between energy dissipation and descent time is clear and logically sound. However, the effect of transverse distance travelled on the descent time is more complicated and further researches with different

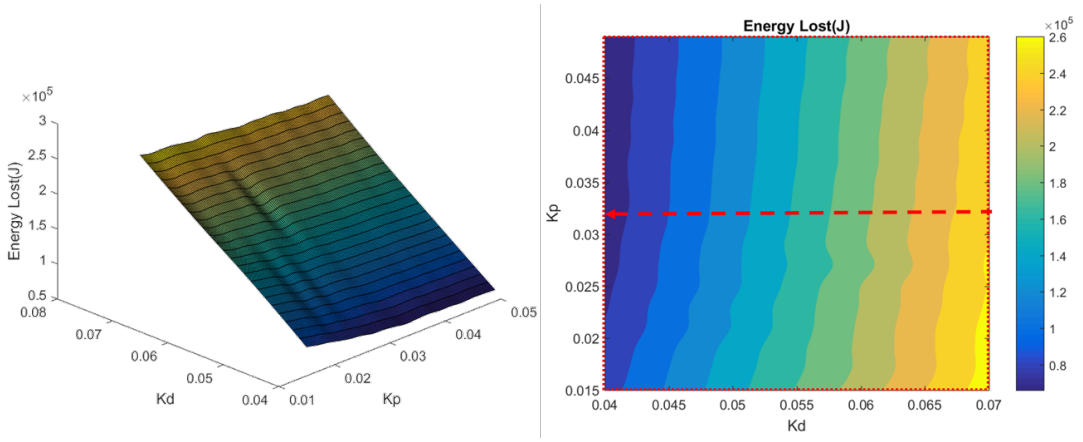

FIGURE 6.21: Adaptive PD controlled energy lost mesh and contour plot

steering strategies are required to clarify this. Currently, to achieve the best descent time, the optimal control algorithm should aim to minimise the energy lost through the race by limiting its steering actions. This is consistent with the strategy of the best sliders who aim to steer an optimum trajectory with a minimum of course keeping interventions. In the next chapter, the designs, implementation and evaluation of the optimal control algorithm used to predict the optimal descent trajectory will be described in detail.

Chapter 7

Prediction of Optimal Descent Trajectories Using Model Predictive Control Algorithms

7.1 Chapter Introduction

Fundamentally, there are two criteria that a computer controlled descent must fulfil, achieving a stable descent throughout the entire track and sliding down the given track on the most optimal trajectory (i.e. The trajectory which yields the quickest descent time). The adaptive PD controller offered stable and adequately human-like descent simulation on all three Olympic tracks. However, due to the nature of their designs and tuning methods, there are no clear quantifiable ways to determine whether the descent trajectories created are optimal. The only method for finding best descent trajectories using the current adaptive PD steering algorithm is to compare the descent time through trial and error, making this approach both time consuming and inaccurate. Thus, to tackle this problem, steering algorithms that uses model based optimal control in place of human steering should be used to provide qualitative methods for evaluating the optimal descent trajectory. There are numerous optimal control algorithms available for this kind of application, in prior studies, minimal time and linear quadratic control methods have being experimented with, the conclusions drawn of these studies were that the physical dynamics of a descent simulation is complicated and fast changing for open-loop control designs to predict and control accurately through the whole track and the presence of inequality constraints makes it extremely difficult to obtain an analytical solution to the optimal control problem. As such, the optimal control methods selected for this PhD is the Model Predictive Control(MPC). Unlike previously noted methods, MPC is a closed-loop control design, which is essential for ensuring stability and also provides good numerical approximation to the optimal solutions of the real time descent simulation.

This chapter explains in detail the design, implementation and experimental verification processes of a controller using the linear MPC algorithm, a controller using the adaptive MPC

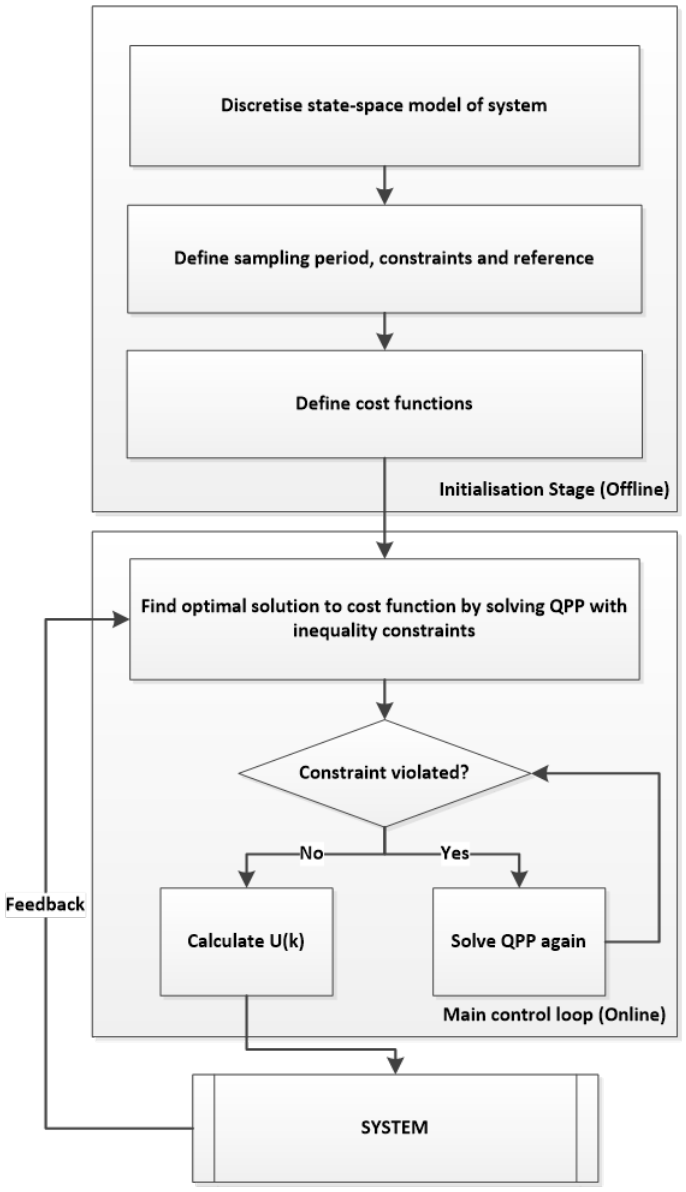

FIGURE 7.1: Overall MPC design structure

algorithm as well as a hybrid controller. The potential training applications of the hybrid controller will be discussed at the end of the chapter.

7.2 MPC Algorithm Design

7.2.1 MPC Design Structure

The design of the MPC algorithm can be described by two main stages; the 'Initialisation' stage and the 'Main Control Loop' stage. Here the content of each stage will be briefly discussed and a graphically illustration of the the whole design structure will be given in Figure 7.1.

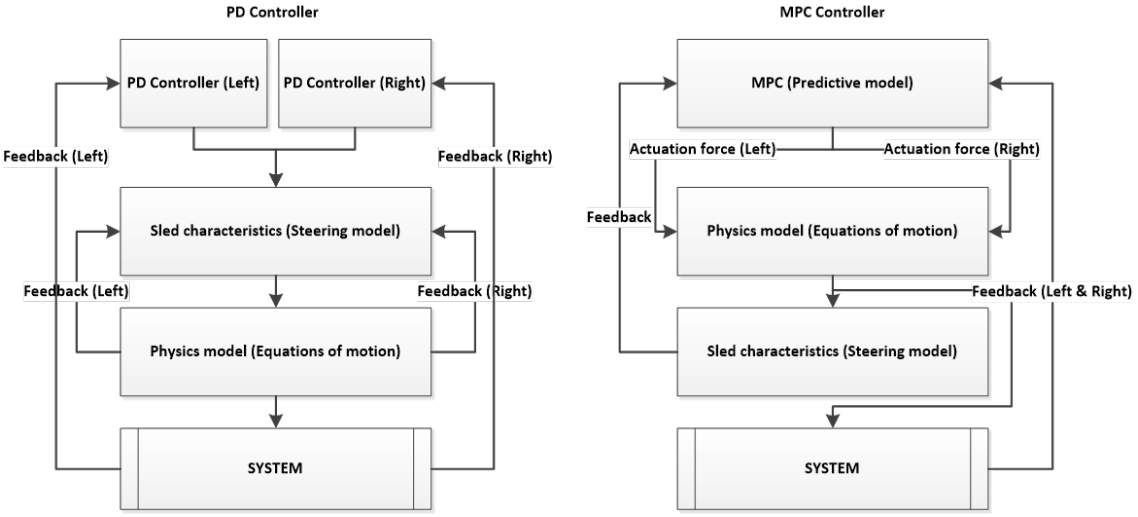

FIGURE 7.2: Controller integration structure comparison between Adaptive PD and MPC

Initialisation

The initialisation stage occurs prior to the on line simulation, where the fundamental information regarding the design of the MPC algorithm is defined. In this stage, a continuous state space model will be built, which will subsequently be discretised using a predefined sampling rate which the controller will operate at. This new discrete model will later be used in the Simulink model to predict the future plant output, Y, by using the current state-variable vector X and the future control values, U. Cost functions are defined in accordance to this discretised model and is a function of the deviation between system reference and feedback, the magnitude of control inputs and the magnitude of the rate of control inputs. The final initialisation process include defining constraints and checking system stability via a static simulation. All above processes will be discussed later in the chapter.

Main Control Loop

The purpose of the main control loop is to find the optimal descent trajectory. During this stage, a sequence of optimal future control inputs, U, will be calculated by minimising the cost function defined in the initialisation stage using quadratic programming methods. The optimisation process will be subjected to prediction horizon, control horizon and constraints defined in the initialisation stage. The first value of calculated control inputs will be applied to the system then the process will be repeated.

The rest of the 'MPC Algorithm Design' section will detail the 'Initialisation' stage. Information on the 'Main Control Loop' stage will be covered in implementation and analysis sections regarding the adaptive MPC controller.

7.2.2 MPC Integration Structure

The integration structure of the MPC controller is different from the other controller designs. Previously, the Adaptive PD controller replaces human inputs with computer generated control

forces, which were fed into the steering model within the 'Sled Characteristic' functional block. These control forces were combined with ice-sled coulomb frictions, sled stiffness force and wall collision forces to calculate the actuation forces on each of the mass particles. However, as previously stated in section 5.5.5, there exists a 'Slip Function' which determines which algorithm to use for calculating the ice-sled coulomb friction, dependant on the yaw angle of the sled. This causes in a discontinuity in the steering model, making it extremely difficult to form a state space between steering input and mass particle accelerations. To solve this problem, the sled characteristic block was bypassed entirely and the MPC controls longitudinal and transverse actuation forces directly on both mass particles. This procedure allows for a direct mathematical model to be made in accordance with the equations of motion listed in section 5.4. However, this bypass method raises a number of problems in regards to loosing the interactions between sled and track surface as well as interactions between individual mass particles. This may result in the loss of stability in control when the descent dynamic could not be accurately predicted as shown later in the chapter. Figure 7.2 shows a simplified illustration of control structure for both the adaptive PD and MPC controller, highlighting the difference discussed here.

7.2.3 State Space Model

One of the key aspect of an MPC algorithm is its capability to predict future plant outputs and produce predictive control forces accordingly. In order to do that, the MPC controller requires a mathematical model of the system plant in a state-space representation. To do this, it is essential to first clarify the system input-output structure. By using the equations of motion described in section 5.4, the physics model can be represented as a Multi-input, Multi-output (MIMO) plant that has 4 manipulated variables(inputs) and 8 controlled variables(outputs) as listed below.

Manipulated variables:

- $F_{act} \cdot rl_{\alpha}$ – Longitudinal inertial forces for the left mass particle
- $F_{act} \cdot rl_{\beta}$ – Transverse inertial forces for the left mass particle
- $F_{act} \cdot rr_{\alpha}$ – Longitudinal inertial forces for the right mass particle
- $F_{act} \cdot rr_{\beta}$ – Transverse inertial forces for the right mass particle

Controlled Variables:

- α_l – Longitudinal position of the left mass particle
- β_l – Transverse position of the left mass particle
- $\dot{\alpha_l}$ – Longitudinal velocity of the left mass particle
- $\dot{\beta_l}$ – Transverse velocity of the left mass particle
- α_r – Longitudinal position of the right mass particle
- β_r – Transverse velocity of the right mass particle
- $\dot{\alpha_r}$ – Longitudinal velocity of the right mass particle

- $\dot{\beta}_r$ – Transverse position of the right mass particle

To clarify, from the view point of the rest of the simulation model, the manipulated inputs to the MPC is the actual desired outputs, as these are the variables which would be taken and used in the physics engine to calculate the iterative longitudinal and transverse accelerations. The controlled outputs of the MPC on the other hand are used internally as the iterative predictions of the sled's physical states.

Once the system input-output structure has being confirmed, the state space model can then be created. By rearranging the equations of motion found in Chapter 4, to fit the above structure and separating the actuation forces, the spatial derivatives and particle velocities, a continuous-time state space model can be formed.

Here, the standard continuous input-output state space model structure applies:

$$\dot{x}(t) = A(t)x(t) + B(t)u(t)$$
$$y(t) = C(t)x(t) + D(t)u(t)$$

Here, the longitudinal and transverse positions and velocities of both particle make up the 8×1 state-variable vector $x(t)$. A combination of general spatial derivatives and particle velocities make up both the 8×8 state matrix $A(t)$ and the 8×4 input matrix $B(t)$. the actuation forces make up the 8×4 input matrix $B(t)$. Control vector $u(t)$ is made up from the longitudinal and transverse actuation forces and has a dimension of 4. The output matrix $C(t)$ is a 8×8 identity matrix and feed forward matrix $D(t)$ is empty and therefore not included here. Finally, the resulting state space model is given in equation 7.1 and 7.2.

$$\begin{bmatrix} \dot{\alpha_l} \\ \dot{\beta_l} \\ \ddot{\alpha_l} \\ \ddot{\beta_l} \\ \dot{\alpha_r} \\ \dot{\beta_r} \\ \ddot{\alpha_r} \\ \ddot{\beta_r} \end{bmatrix} = A(t) \begin{bmatrix} \alpha_l \\ \beta_l \\ \dot{\alpha_l} \\ \dot{\beta_l} \\ \alpha_r \\ \beta_r \\ \dot{\alpha_r} \\ \dot{\beta_r} \end{bmatrix} + B(t) \begin{bmatrix} F_{act} \cdot rl_\alpha \\ F_{act} \cdot rl_\beta \\ F_{act} \cdot rr_\alpha \\ F_{act} \cdot rr_\beta \end{bmatrix} \tag{7.1}$$

$$\begin{bmatrix} \alpha_l \\ \beta_l \\ \dot{\alpha_l} \\ \dot{\beta_l} \\ \alpha_r \\ \beta_r \\ \dot{\alpha_r} \\ \dot{\beta_r} \end{bmatrix} = \begin{bmatrix} 1 & 0 & 0 & 0 & 0 & 0 & 0 & 0 \\ 0 & 1 & 0 & 0 & 0 & 0 & 0 & 0 \\ 0 & 0 & 1 & 0 & 0 & 0 & 0 & 0 \\ 0 & 0 & 0 & 1 & 0 & 0 & 0 & 0 \\ 0 & 0 & 0 & 0 & 1 & 0 & 0 & 0 \\ 0 & 0 & 0 & 0 & 0 & 1 & 0 & 0 \\ 0 & 0 & 0 & 0 & 0 & 0 & 1 & 0 \\ 0 & 0 & 0 & 0 & 0 & 0 & 0 & 1 \end{bmatrix} \begin{bmatrix} \alpha_l \\ \beta_l \\ \dot{\alpha_l} \\ \dot{\beta_l} \\ \alpha_r \\ \beta_r \\ \dot{\alpha_r} \\ \dot{\beta_r} \end{bmatrix} \tag{7.2}$$

subject to

$$A(t) = \begin{bmatrix} 0 & 0 & 1 & 0 & 0 & 0 & 0 & 0 \\ 0 & 0 & 0 & 1 & 0 & 0 & 0 & 0 \\ 0 & 0 & a_{11} & a_{12} & 0 & 0 & 0 & 0 \\ 0 & 0 & a_{21} & a_{22} & 0 & 0 & 0 & 0 \\ 0 & 0 & 0 & 0 & 0 & 0 & 1 & 0 \\ 0 & 0 & 0 & 0 & 0 & 0 & 0 & 1 \\ 0 & 0 & 0 & 0 & 0 & 0 & a_{31} & a_{32} \\ 0 & 0 & 0 & 0 & 0 & 0 & a_{41} & a_{42} \end{bmatrix}$$

with

$$a_{11} = \frac{\hat{a}\hat{c}}{(lr_\alpha \cdot lr_\beta)^2 - (lr_\alpha \cdot lr_\alpha)(lr_\beta \cdot lr_\beta)}$$
$$a_{12} = \frac{\hat{a}\hat{d}}{(lr_\alpha \cdot lr_\beta)^2 - (lr_\alpha \cdot lr_\alpha)(lr_\beta \cdot lr_\beta)}$$
$$a_{21} = \frac{\hat{b}\hat{c}}{(lr_\alpha \cdot lr_\beta)^2 - (lr_\alpha \cdot lr_\alpha)(lr_\beta \cdot lr_\beta)}$$
$$a_{22} = \frac{\hat{b}\hat{d}}{(lr_\alpha \cdot lr_\beta)^2 - (lr_\alpha \cdot lr_\alpha)(lr_\beta \cdot lr_\beta)}$$
$$a_{31} = \frac{\hat{e}\hat{g}}{(rr_\alpha \cdot rr_\beta)^2 - (rr_\alpha \cdot rr_\alpha)(rr_\beta \cdot rr_\beta)}$$
$$a_{32} = \frac{\hat{e}\hat{h}}{(rr_\alpha \cdot rr_\beta)^2 - (rr_\alpha \cdot rr_\alpha)(rr_\beta \cdot rr_\beta)}$$
$$a_{41} = \frac{\hat{f}\hat{g}}{(rr_\alpha \cdot rr_\beta)^2 - (rr_\alpha \cdot rr_\alpha)(rr_\beta \cdot rr_\beta)}$$
$$a_{42} = \frac{\hat{f}\hat{h}}{(rr_\alpha \cdot rr_\beta)^2 - (rr_\alpha \cdot rr_\alpha)(rr_\beta \cdot rr_\beta)}$$

where

$$\hat{a} = (lr_\beta \cdot lr_\beta)lr_\alpha - (lr_\alpha \cdot lr_\beta)lr_\beta$$
$$\hat{b} = (lr_\alpha \cdot lr_\beta)lr_\beta - (lr_\alpha \cdot lr_\alpha)lr_\beta$$
$$\hat{c} = \dot{\alpha}lr_{\alpha\alpha} + \dot{\beta}lr_{\alpha\beta}$$
$$\hat{d} = \dot{\beta}lr_{\beta\beta} + \dot{\alpha}lr_{\alpha\beta}$$
$$\hat{e} = (rr_\beta \cdot rr_\beta)rr_\alpha - (rr_\alpha \cdot rr_\beta)rr_\beta$$
$$\hat{f} = (rr_\alpha \cdot rr_\beta)rr_\beta - (rr_\alpha \cdot rr_\alpha)rr_\beta$$
$$\hat{g} = \dot{\alpha}rr_{\alpha\alpha} + \dot{\beta}rr_{\alpha\beta}$$
$$\hat{h} = \dot{\beta}rr_{\beta\beta} + \dot{\alpha}rr_{\alpha\beta}$$

and

$$B(t) = \begin{bmatrix} 0 & 0 & 0 & 0 \\ 0 & 0 & 0 & 0 \\ b_{11} & b_{12} & 0 & 0 \\ b_{21} & b_{22} & 0 & 0 \\ 0 & 0 & 0 & 0 \\ 0 & 0 & 0 & 0 \\ 0 & 0 & b_{31} & b_{32} \\ 0 & 0 & b_{41} & b_{42} \end{bmatrix}$$

with

$$\begin{aligned}
b_{11} &= \frac{lr_\beta \cdot lr_\beta}{\frac{1}{2}m(lr_\alpha \cdot lr_\beta)^2 - (r_\alpha \cdot lr_\alpha)(lr_\beta \cdot lr_\beta))} \\
b_{12} &= \frac{-(lr_\alpha \cdot lr_\beta)}{\frac{1}{2}m((lr_\alpha \cdot r_\beta)^2 - (r_\alpha \cdot lr_\alpha)(lr_\beta \cdot lr_\beta))} \\
b_{21} &= \frac{lr_\alpha \cdot lr_\beta}{\frac{1}{2}m((lr_\alpha \cdot r_\beta)^2 - (r_\alpha \cdot lr_\alpha)(lr_\beta \cdot lr_\beta))} \\
b_{22} &= \frac{-(lr_\alpha \cdot lr_\alpha)}{m((lr_\alpha \cdot lr_\beta)^2 - (r_\alpha \cdot lr_\alpha)(lr_\beta \cdot lr_\beta))} \\
b_{31} &= \frac{rr_\beta \cdot rr_\beta}{\frac{1}{2}m(rr_\alpha \cdot r_\beta)^2 - (rr_\alpha \cdot rr_\alpha)(rr_\beta \cdot rr_\beta))} \\
b_{32} &= \frac{-(rr_\alpha \cdot rr_\beta)}{\frac{1}{2}m((rr_\alpha \cdot r_\beta)^2 - (rr_\alpha \cdot rr_\alpha)(rr_\beta \cdot rr_\beta))} \\
b_{41} &= \frac{rr_\alpha \cdot rr_\beta}{\frac{1}{2}m((rr_\alpha \cdot r_\beta)^2 - (rr_\alpha \cdot rr_\alpha)(rr_\beta \cdot rr_\beta))} \\
b_{42} &= \frac{-(rr_\alpha \cdot rr_\alpha)}{\frac{1}{2}m((rr_\alpha \cdot r_\beta)^2 - (rr_\alpha \cdot rr_\alpha)(rr_\beta \cdot rr_\beta))}
\end{aligned}$$

Please refer to nomenclature for unspecified variables.

The above state space model contain numerous non-linear elements within the state space model such as the velocities and the spatial derivatives terms in the state matrix $A(t)$. The assessment of the effects of these non-linearities and methods to handle them will be discussed later in the chapter.

7.2.4 Plant Non-Linearity Assessment

Thus far, it is only established that the state space representation of the physics model is non-linear, however, a single linear MPC is often capable of controlling a non-linear plant near its nominal operating point as long as the plant non-linearity is not strong[51]. Therefore, here one must first assess the degree of non-linearity of the state space model by comparing linear plant characteristics around different operating points.

The typical assessment method for stability of a single input single output(SISO) system is to take the frequency responses of the plant at several given operating points and compare the changes in gain and phase. However, as the state space plant is an MIMO system. In MIMO systems, the gain and phase can change in all channels at once, and by a different amount each channel.

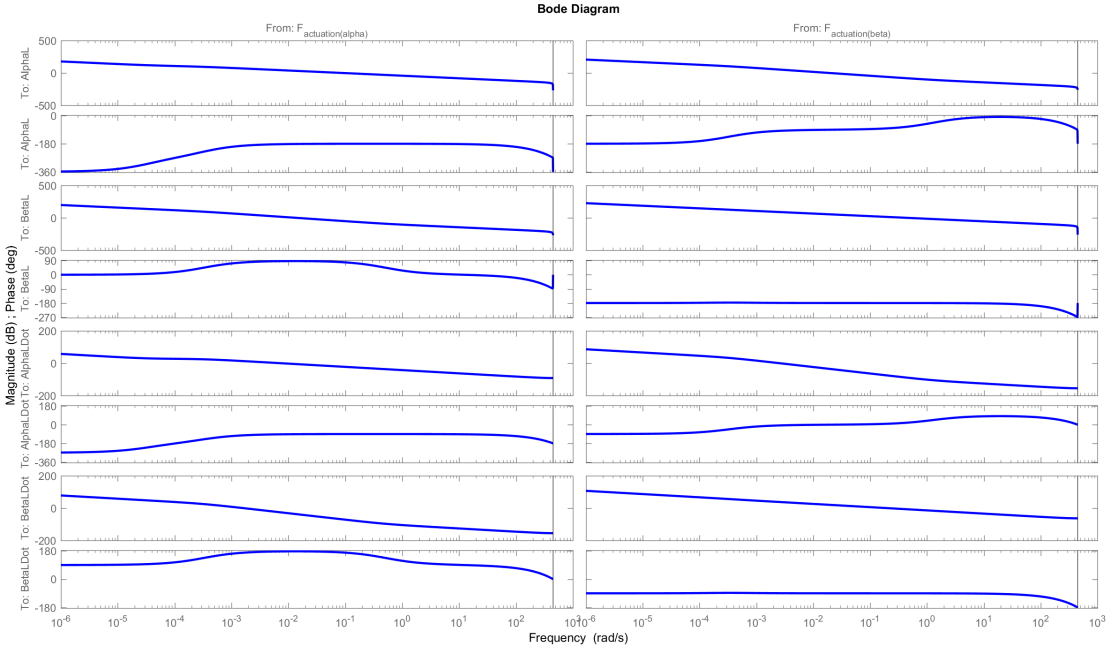

FIGURE 7.3: Frequency analysis at low operating point

At the same time, the gain and phase in MIMO systems also vary across frequencies like SISO systems. The standard frequency response analysis is inadequate under normal circumstances as there are potential multi channel cross-couplings which it can not account for. However, when the cross-coupling between channels are not strong, or if one can separate out the system into individual channels by linear approximation, then the frequency response analysis could be performed on each individual channels, this method is called the 'Individual Channel Analysis and Design' or ICAD for short[11]. Here for the descent model, similar procedures to the ICAD can be carried out, and linear transfer functions corresponding every element in the state-variable vector to every element of the input vector could be approximated. The assumption taken here is that since this is only to investigate the non-linearity effect of the plant and not to be used for design, an approximation of the system is therefore adequate.

To assess the non-linearity, the frequency response of the plant was obtained at two extreme operating points. Here, the two operating points were selected at the start of the track and at the highest velocity point within the corners of the track as this would represent the greatest difference between both velocity and the partial derivative vectors, which governs the majority of the descent dynamics. The PyeongChang Olympic track was be used for this analysis. The data for the low operating point Pt_{low} is taken at the a simulation time of 0 seconds with a velocity of 45 km/h and data from the high operating point Pt_{high} is taken at the simulation time of 43.2 seconds with a velocity of 134.89 km/h. The plant was then linearised and bode diagrams were plotted for the left mass particle(The right mass particle is the mirror of the left). as shown in Figure 7.3 and 7.4

The comparison of each individual channel shows that there are significant differences in both gain and phase. As an example, Figure 7.5 demonstrates the changes in gain and phase for the transverse velocity of the left mass particle in relation to the transverse actuation force. The DC

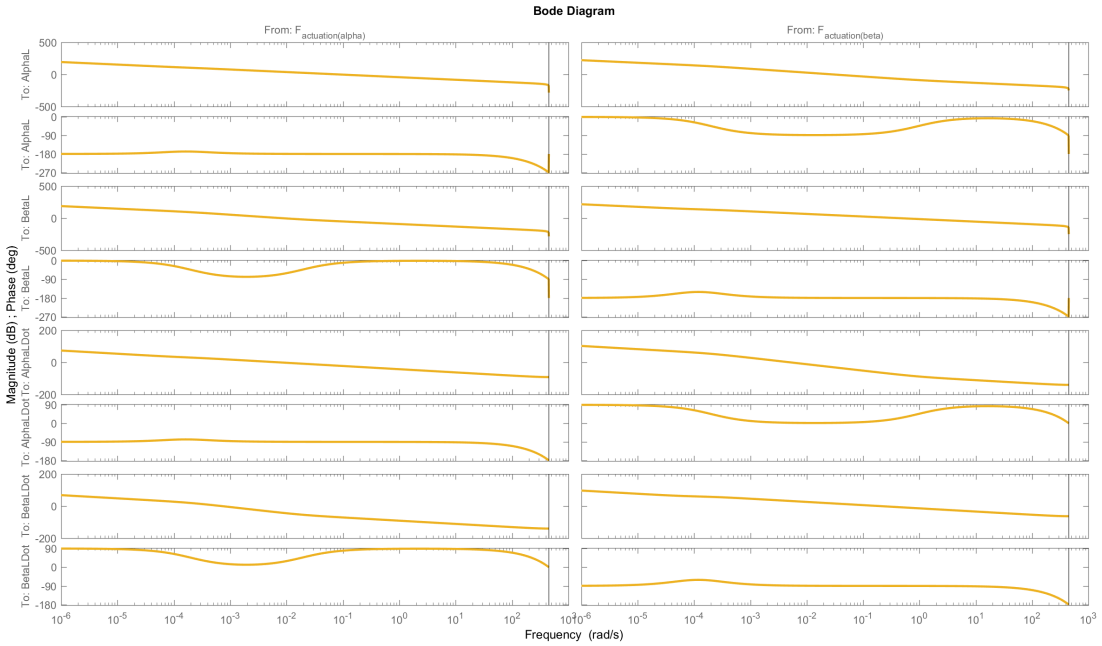

FIGURE 7.4: Frequency analysis at high operating point

gain of the plant at its high operating point is roughly half the DC gain of the plant at its low operating point and there is a significant phase change as well.

After establishing the degree of plant non-linearity, it is clear that a simple linear MPC will not be adequate to solve the control problem posed by the descent simulation. To tackle this in Matlab, there are generally two methods. The first is to design a robust linear MPC that can control the whole range of non-linear system dynamics throughout the entire range of operation the second is to use controller designs which are specifically built to target non-linear systems. The decision of which method to use is based on the degree of non-linearity of the system plant. The first approach is more suitable for models with lower degrees of non-linearity as it is more prone to comprises on optimisation performance and stability when dealing with models that has high degrees of non-linearity. As such, the second design method was adopted in this PhD. When using the non-linear MPC design method, there are again, two different approaches towards controller designs in Matlab. One is to generate multiple MPC models for each different operating point of the plant, the adaptive MPC design and gain-scheduled MPC design falls within this category. the other approach would be to use a non-linear plant model alongside a non-linear optimiser to solve the control problem. During the controller development phase, there was no readily available non-linear MPC blocks for Simulink and as this is a application and experiment orientated PhD, developing a custom optimiser is outside the scope and time constraints available. Therefore the approach of constructing an adaptive MPC was adopted for the purpose of this PhD, details regarding the design and implementation will follow in section 7.3.

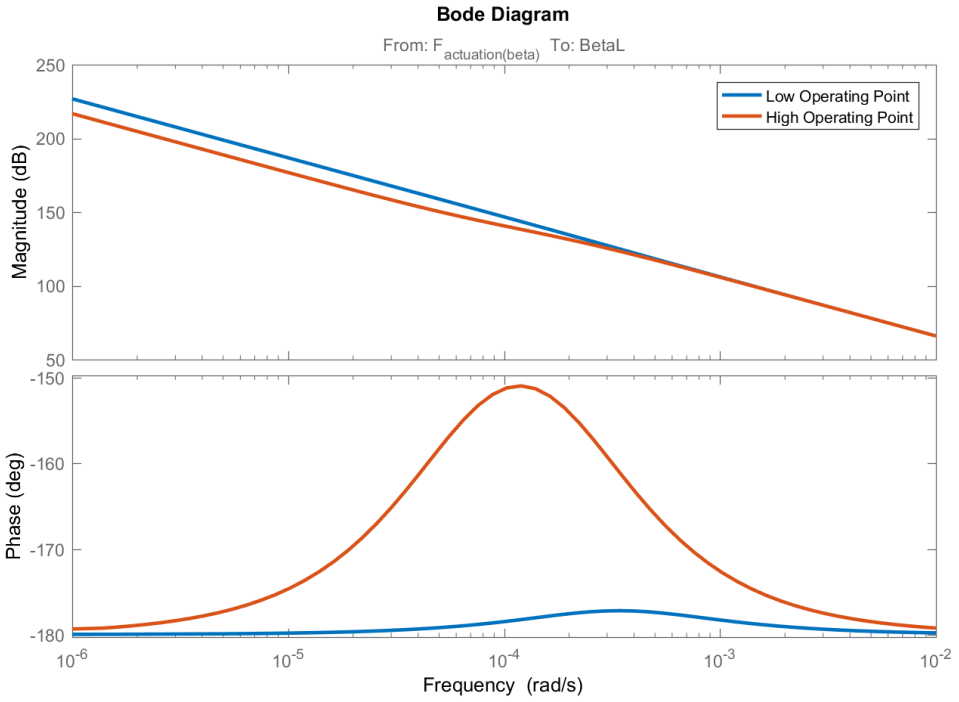

FIGURE 7.5: Gain and Phase difference of transverse velocity of left mass particle

7.2.5 Plant Discretisation

The MPC controller was built in the Matlab Simulink environment, which by default is a discrete environment, meaning all models used with in the MPC design which includes the state space model has to be discrete as well.

Sampling Rate

To convert the continuous time state space model to its discrete counterpart, the first task is to define a sampling rate at which the MPC controller will operate. This MPC sampling rate has to be a multiple of the inherent sampling rate which the whole simulation is operating at in order to maintain simulation stability. Simulink defines its sampling rate by specifying sampling time, which is the time difference between any two control intervals of the simulation, k_i and k_{i+1}. In the case of the descent simulation, the sampling time ΔT is 0.007 s, therefore, the sampling time of the MPC controller, Δt, is $n \times \Delta T$, where n is a rational scale factor.

The sampling rate of the MPC defines the accuracy of model stability transfer during the discretisation process, which in turn also defines the accuracy of the predicted future outputs from the state space model. The recommended practice for choosing sampling rate is to define a sampling time that is small enough to ensure the full capture of system dynamics but large enough to not compromise computational performance.

The sampling rate for this MPC design was selected through a number of trial and error experiments, the range of sampling time tested was between 0.007 s (inherent sampling time)and 0.7 s. Through this experiment, it was found that a sampling time of 0.07 s was best suited

for the MPC design as it yields acceptable accuracy at capturing the continuous time system's dynamics whilst allowed the simulation to run in real time, which is required for the process of trajectory generation.

Discretisation Algorithm

Once the sampling rate is defined, the state space model can be discretised using a number of different tranformation algorithms. The default transformation algorithm adopted by Simulink is the Zero-Order Hold method, which is simple and effective. However, this method does not guarantee the full transfer between pole stabilities, which has resulted in inaccurate output predictions and erratic control actions. As a result, the Tustin or bilinear transformation method was selected instead for the dicretistaion process. The bilinear transformation/approximation yields the best frequency domain match between the continuous time and discrete systems, ensuring pole stability, but causes warping of the zero and pole positions. This effect can be reverted using a process called pre-warping to ensure exact match between continuous time and discrete time responses at the pre-warped frequency. This method is not adopted here as maintaining system stability is the main concern.

To obtain the discrete state space model in the standard form of:

$$\begin{aligned} X(k+1) &= A(k)X(k) + B(k)U(k) \\ Y(k) &= C(k)X(k) + D(k)U(k) \end{aligned}$$

The following transformations is applied:

$$\begin{aligned} A(k) &= (I - \frac{A(t)}{2f_s})^{-1}(I + \frac{A(t)}{2f_s}) \\ B(k) &= \frac{1}{\sqrt{f_s}}(1 - \frac{A(t)}{2f_s})^{-1}B(t) \\ C(k) &= \frac{C(t)}{\sqrt{f_s}}(1 - \frac{A(t)}{2f_s})^{-1} \\ D(k) &= \frac{C(t)}{2f_s}(1 - \frac{A(t)}{2f_s})^{-1}B(t) + D(t) \end{aligned}$$

where

$$f_s = \frac{1}{\Delta t}$$

7.2.6 State Reference

Unlike the reference trajectory used for the adaptive PD controller, which were sets of longitudinal, α, and transverse, β, coordinates for the centre position of the sled, the MPC controller requires full state references to function properly. These are sets of predefined state-variable vectors, which include the positions and velocities of both the left and the right mass particle, making it very difficult to define. The pseudo equation below shows an example of the state

reference for an arbitrary control interval $t(k)$:

$$Ref(k) = [\alpha_l(k), \beta_l(k), \Delta\alpha_l(k), \Delta\beta_l(k), \alpha_r(k), \beta_r(k), \Delta\alpha_r(k), \Delta\beta_r(k)]^T$$

The position elements of state reference is relatively straight forward to dictate, this can be defined in similar fashion to the linear controller reference trajectory, by matching corresponding transverse position with the sled's current longitudinal position. The velocity elements of the state reference however, are much harder to define as each velocity element at control interval $t(k)$ is directly dependant on the position and velocity of the sled at control interval $t(k-1)$, which is extremely hard to predict prior to the actual simulation and is extremely prone to any form of disturbance. These design problems combined with the control objective of the MPC (not to achieve perfect tracking of any given reference, but to attain optimal descent whilst maintaining stability) suggests that the state reference should be designed to fulfil a different purpose than that of the references used by the linear controllers. The referencing system is therefore designed to obey the following criteria:

- The longitudinal position reference, α_l and α_r, can be set as either:
  1. The maximum length of the track to encourage the sled to move along the track in the correct direction.
  2. A series of longitudinal position coordinates to be paired with its corresponding transverse coordinates in similar fashion to that of the linear references.
- The longitudinal velocity reference, $\Delta\alpha_l$ and $\Delta\alpha_r$, should be set to the maximum velocity achievable on the given track to encourage the sled to travel faster and result in a quicker descent time.
- The transverse position reference, β_l and β_r, can be set as either:
  1. The mid position of the track to force the sled to move away from the track sides and promote stability.
  2. A series of transverse position coordinates to be paired with its corresponding longitudinal coordinates in similar fashion to that of the linear references.
- The transverse velocity reference, $\Delta\beta_l$ and $\Delta\beta_r$, should be set to 0 to induce stability in the sled's lateral movement and reduce the amount of undesired oscillation.

This referencing system require the proper use of cost penalty distribution to function. This will be discussed further in the section 7.2.7 and the exact references used for experimental analysis will be detailed in their respective experimental set-ups.

7.2.7 Tuning Parameters

As previously stated, the performance of the MPC is defined by the accuracy of its predictive model. However, another important factor that determines performance is the tuning process of the MPC. Generally speaking there are three tunable parameters in any MPC design, these are the 'Cost Function Weights', the 'Prediction Horizon' and the 'Control Horizon'. Choosing

these parameters correctly are usually the key difference between a turely optimal system and a seemingly optimal system [14].

Prediction & Control Horizon The basic concept of an MPC algorithm is that a mathematical model of the system is used by the controller to solve an optimisation problem at the current control interval $t(k)$ to produce a set of manipulated variables. The 'Prediction Horizon', N_p, is the number of control intervals over which the optimisation problem is solved and the 'Control Horizon', N_c, is the number of control intervals over which the manipulated variables must be optimised to solve said optimisation problem, hence both the prediction and control horizon are integer multiples of the sampling period. Selecting the correct prediction and control horizon is key to ensure optimal MPC performance, which includes model stability, model predictability as well as the aggression of the calculated manipulated variables. Below is a list of the common recommendations for selecting and tuning the horizon lengths:

- Prediction Horizon
  - The value of N_p should be defined such that the controller is internally stable and anticipates any constraints violation early enough to allow for corrective control actions. Larger values of N_p promotes less aggressive control actions and vice versa.
  - If the desired close loop response time is τ, and the controller interval is ΔT, then N_p should be defined such that $\tau \approx N_p \times \Delta T$
  - The recommended practice is to choose N_p early on in the controller design and hold it constant whilst tuning other parameters, such as cost function weights.
  - Small N_p combined with unfavourable plant dynamics can generate internally unstable controller. If this occurs, the value of N_p has to be increased. This should be done until any further increases in the value of N_p has negligible impact on controller performance.
- Control Horizon
  - The value of N_c should be defined such that $N_c \ll N_p$.
  - Smaller values of N_c means fewer variables to computer in the optimisation programming at each control interval, this promotes faster computation speed.
  - Larger values of N_c also promotes more aggressive control actions, which may lead to internally unstable controller designs.
  - Regardless of the values of N_c, when the controller operates, only the first calculated manipulated variable is used others are discarded.

Through repeated experimentations, the values of N_p and N_c, which yielded the fastest stable descent in the simulations across all three Olympic track were selected empirically and are listed below:

- Sochi – $N_p = 125; \quad N_c = 20$
- Igls – $N_p = 85; \quad N_c = 8$

- PyeongChang – $N_p = 100; \quad N_c = 10$

These will be the N_p and N_c values used for all simulation experiments conducted hence forth.

Cost Function

MPC solves an optimisation problem, more specifically a quadratic programming (QP) problem at each control interval. The solution to the QP determines the manipulated variables to be used in the plant until the next control interval. To solve the QP problem, the MPC design requires two things: an objective, or cost function and a set of constraints. The following section will detail the design of the 'Cost Function' for the simulated descent.

The 'Cost Function' is arguably the most important tuning parameter out of the three and its design needs to include all the necessary physical parameters which will affect the controller performance. Specifically in the case of the descent simulation, the cost function needs to take into account of the sled's position, velocity and the input forces asserted by the controller. The information regarding the exact tuning method is provided by the study done in section 6.3.5.

The standard cost function structure is the sum of four terms, each focusing on a particular aspect of the controller performance. These are: Reference Tracking; Manipulated Variable Suppression; Manipulated Variable Rate Suppression and Constraint Violation. Equation 7.3 shows the full structure of the cost function used for the MPC design of the descent simulation.

$$J(\zeta_k) = J_Y(\zeta_k) + J_U(\zeta_k) + J_{\Delta U}(\zeta_k) + J_\epsilon(\zeta_k) \tag{7.3}$$

where ζ_k is the solution of the QP problem, given by:

$$\zeta_k^T = \left[U(k|k)^T \; U(k+1|k)^T \cdots \; U(k+N_p-1|k)^T \; \epsilon_k \right]$$

Other terms of the cost function will be broken down and discussed in detail below:

Reference Tracking

$$J_Y(\zeta_k) = \sum_{j=1}^{n_Y} \sum_{i=1}^{N_p} \left\{ W_{i,j}^Y [R_j(k+i|k) - Y_j(k+i|k)] \right\}^2 \tag{7.4}$$

where

- k – Current control interval
- N_p – Prediction Horizon
- n_Y – Number of plant output variables
- $Y(k+i|k)$ – Predicted jth plant output value at the ith prediction horizon
- $R(k+i|k)$ – State Reference value for the jth plant output value at the ith prediction horizon

- $W_{i,j}^{Y}$ – Tuning weight for the jth plant output value at the ith prediction horizon (dimensionless)

The first term of the cost function is represented by Equation 7.4. The output $Y(k)$ in the equation contains information on both position and velocity of the sled, meaning this term of the cost function is capable of both tracking sled deviation and the energy lost in motion, where $R(k)$ is the predefined reference points. More specifically, the position difference, $\Delta\alpha(k)$, is used to encourage the sled to travel in the correct descending direction. The position difference, $\Delta\beta(k)$, is to track position deviation of the mass particles. The velocity difference, $\Delta\dot{\alpha}(k)$, is used to maximise descent velocity by setting the reference velocity to an arbitrary reference value. Finally, the velocity difference, $\Delta\dot{\beta}(k)$, is used to cancel undesirable lateral movements and promote system stability by setting the reference velocity to 0. In practice, W^Y is implemented as a 1×8 weight vector arranged in the same order to match the output vector, $Y(k)$, and reference vector, $R(k)$. The entries in W^Y are selected based on the results in section 6.3.5, which does not emphasises on achieving perfect tracking but stable descents. This implies that the weight distribution will bias heavily towards the velocity errors rather than the position errors (e.g. 10 for velocity error and 1 for positions errors).

Manipulated Variable Suppression

$$J_U(\zeta_k) = \sum_{j=1}^{n_U} \sum_{i=1}^{N_p-1} \left\{ W_{i,j}^{U}[U_j(k+i|k)] \right\}^2 \tag{7.5}$$

where

- k – Current control interval
- N_p – Prediction Horizon
- n_U – Number of manipulated variables
- $U(k+i|k)$ – Calculated jth manipulated variable at the ith prediction horizon
- $W_{i,j}^{U}$ – Tuning weight for the $j$the manipulated at the ith prediction horizon (dimensionless)

The second term of the cost function is represented by Equation 7.5. The purpose of this term is to assigns penalties to the size of the manipulated variables generated by the MPC controller, thus promoting the minimal steering effort strategy indicated by section 6.3.5 and minimise total energy lost. In practice, W^U is implemented as a 1×4 weight vector arranged in the same order to match the input vector, $U(k)$.

Manipulated Variable Rate Suppression

$$J_{\Delta U}(\zeta_k) = \sum_{j=1}^{n_U} \sum_{i=1}^{N_p-1} \left\{ W_{i,j}^{\Delta U}[U_j(k+i|k) - U_j(k+i-1|k)] \right\}^2 \tag{7.6}$$

where

- k – Current control interval
- N_p – Prediction Horizon
- n_U – Number of manipulated variables
- $U(k+i|k)$ – Calculated jth manipulated variable at the ith prediction horizon
- $W_{i,j}^{\Delta U}$ – Tuning weight for the $j$the manipulated at the ith prediction horizon (dimensionless)

The third term of the cost function is represented by Equation 7.6, where $U_j(k+i|k) - U_j(k+i-1|k)$ represent the rate of change in manipulated variables. This term penalises the change in manipulated variables, which, in physical terms is equivalent to applying soft constraints to the steering rate and promoting a smoother, more human like steering action. In practice, $W^{\Delta U}$ is implemented as a 1×4 weight vector arranged in the same order to match the input vector. Its value is selected empirically from DTT's experimental data to match the maximum steering rate of an average Olympic Skeleton athlete.

Constraint Violation

$$J_\epsilon(\zeta_k) = \rho_\epsilon \epsilon_k^2 \tag{7.7}$$

where

- ϵ_k – Slack variable at control interval k (dimensionless)
- ρ_ϵ – Constraint violation penalty weights. This is the set of ECR values used by Matlab, more details regarding this will be given in section 7.2.8 (dimensionless)

The final term of the cost function is represtend by Equation 7.7 and provides constraint softening for the input and output of the MPC. Due to state space model being a linear approximation of the non-linear plant, there will inevitably be situations where potential model misprediction will lead to infeasible QP solution if all hard constraints were to be obeyed. The MPC uses this dimensionless, non-negative slack variable, ϵ_k to qualify as the worst-case constraint violation in order to ensure feasibility of the QP solution. Note here, this slack variable used by Matlab for constraint softening is different from the traditional slack variable used for optimisation, which is used to transform non-equality constraints to equality constraints. In practice, ϵ_k is the maximum state difference between system feedback and system constraints, it is multiplied together with a corresponding ECR value and their product is added to the lower and upper bounds of input or the output to soften the constraint for the MPC design. A heavy weight penalty is usually associated with this term to discourage the violation of constraints. More details will be given in section 7.2.8.

7.2.8 Constraints

Constraints in the MPC design represent the physical limits that would usually be associated with system dynamics. Below is the standard structure for defining constraints during a typical

MPC design:

$$Y_{j,min}(i) - \epsilon_k V^Y_{j,min}(i) \leqslant Y_j(k+i|k) \leqslant Y_{j,max}(i) + \epsilon_k V^Y_{j,max}(i), \quad i = 1 : N_p, \quad j = 1 : n_Y$$
$$U_{j,min}(i) - \epsilon_k V^U_{j,min}(i) \leqslant U_j(k+i-1|k) \leqslant U_{j,max}(i) + \epsilon_k V^U_{j,max}(i), \quad i = 1 : N_p, \quad j = 1 : n_U$$
$$\Delta U_{j,min}(i) - \epsilon_k V^{\Delta U}_{j,min}(i) \leqslant \Delta U_j(k+i-1|k) \leqslant \Delta U_{j,max}(i) + \epsilon_k V^{\Delta U}_{j,max}(i), \quad i = 1 : N_p, \quad j = 1 : n_U$$

where

- $Y_{j,min}(i), Y_{j,max}(i)$ – Lower and upper bounds for jth plant output at ith prediction horizon
- $U_{j,min}(i), U_{j,max}(i)$ – Lower and upper bounds for jth manipulated variable at ith prediction horizon
- $\Delta U_{j,min}(i), \Delta U_{j,max}(i)$ – Lower and upper bounds for jth manipulated variable rate at ith prediction horizon

The parameter V, also known as the ECR value is a dimensionless scale factor adopted by Matlab for the purpose of constraint softening. V are dimensionless controller constants analogous to the cost function weights with a typical value ranging from 0 (hard constraint) to 20 (extremely soft constraint), where 1 is the normalised value representing average constraint softness. The larger the ECR value, the more likely the controller will deem it optimal to violate the constraint in order to satisfy your other performance goals.

There are a number of recommended design practices to follow when defining the constraint, below is a list summarising these recommendations:

- Manipulated Variable Constraints
  - Any known physical limits of the plant input should be included as hard manipulated variable constraints.
  - Any known physical limit on the rate of change of the plant input should be included as hard manipulated variable rate constraints.
  - Including both input and input rate constraints could lead to infeasibility when trying to solve the QP problem. If both constraints are important, soften one.
- Controlled Variable Constraints
  - Do not include controlled variable constraints unless they are critical for the application as this often leads to infeasible QP solutions. Alternatively, define output references and set cost function weights to keep controlled variable close to the reference.
  - If controlled variable constraints are critical, then all said constraints should be softened.
  - Do not include controlled variable constraints that are impossible to satisfy, even if softened.

Following the standard structure and design recommendation listed above, constraints specifically used with in the design of the MPC are illustrated between Equation 7.8 and 7.16. These represents the physical limits associated with sliding on ice.

$$Y_{j,min}(i) = 2, \quad i = 1 : N_p, \quad j = [2, 6] \tag{7.8}$$

$$Y_{j,max}(i) = 12, \quad i = 1 : N_p, \quad j = [2, 6] \tag{7.9}$$

$$U_{j,min}(i) = 0, \quad i = 1 : N_p, \quad j = [1, 3] \tag{7.10}$$

$$U_{j,max}(i) = 1000, \quad i = 1 : N_p, \quad j = [1, 3] \tag{7.11}$$

$$U_{j,max}(i) = -U_{j,min}(i) = 150, \quad i = 1 : N_p, \quad j = [2, 4] \tag{7.12}$$

$$\Delta U_{j,max}(i) = -\Delta U_{j,min}(i) = 40, \quad i = 1 : N_p, \quad j = [1, 3] \tag{7.13}$$

$$\Delta U_{j,max}(i) = -\Delta U_{j,min}(i) = 20, \quad i = 1 : N_p, \quad j = [2, 4] \tag{7.14}$$

$$V^Y_{j,min,max}(i) = 0.1, \quad i = 1 : N_p, \quad j = [2, 6] \tag{7.15}$$

$$V^U_{j,min,max}(i) = 1, \quad i = 1 : N_p, \quad j = [2, 4] \tag{7.16}$$

Equation 7.8 and 7.9 show the physical constraints of the transverse position of the sled and is determined by the geometric mapping method of the track. If at any point, $\beta \leqslant 2$ or $\beta \geqslant 11$, then the sled would have hit the track walls. Equation 7.15 shows that very little softening was placed on these constraints as hitting the wall will be detrimental to a Skeleton descent's time and therefore should be avoided whenever possible.

Equation 7.10, 7.11 and 7.13 show the physical constraints on the magnitude and rate of the longitudinal steering forces applicable in a typical descent. Most of the constraints here are the results of athlete's sprint speed and gravity. The numerical values were obtained through analysing descent data from previous simulations conducted on the Sochi, Igls and PyeongChang tracks. There are no constraints softening as the limits were selected with built-in redundancy causes constraint violations to be improbable.

Equation 7.12 and 7.14 show the maximum absolute magnitude and maximum absolute rate of the transverse steering forces achievable by an Olympic athletes (both male and female). These data were acquired from analysing previous motion stimulus experiments results. The numerical values used in Equation 7.12 represent the total transverse actuation force, which would normally be generated by the 'Sled Characteristic' functional block and is equivalent to approximately ± 55 N of force. The numerical values used in Equation 7.14 are obtained by analysing athlete steering patterns to identify the steering actions with the highest frequency and is calculate using $\frac{\Delta F_{actuation}}{\Delta T}$. The values approximate steering actions at 9 rad/s or 2 Hz. Since constraints are applied to both the input and input rate, following the design recommendation stated previously, one should be softened. In this case the constraint softening is applied to the input(see Equation 7.16) as this the more flexible constraints out of the two(i.e. athlete could be trained to deliver more steering power) and could be influenced by other forces such as coulomb friction and sled stiffness more easily.

Above constraints are implemented in the initialisation stage of the MPC controller design and the value of the constraints will be held constant throughout the simulation and the value of the constraints will be the same for all experiments conducted hence forth.

7.2.9 MPC Design Verification

Before implementing the MPC controller into the real-time descent simulation, the controller's internal stability and the feasibility its tuning parameters selected previously in this section will need to be verified. These can be determined by performing an off-line, static descent simulation using a linear MPC controller under the system's nominal operating conditions.

The simulation will be conducted on a 150 m long testing track constructed by modifying the mesh model of the straight track section after the final corner on the Sochi Olympic Track. The track is rotated to have 0% grade in the β direction to eliminate unintended transverse motion and a 20% grade in the α direction, which is approximately the average slope gradient of the Sochi track. The system nominal operating condition will be represented here by running the simulation from the start of this testing track at an initial longitudinal velocity of 50 km/h, which is approximately the average velocity of the sled passing through the first timing gate of an Olympic track.

Details regarding the experimental set-up such as simulation time, initial conditions system reference and tuning parameters are given below:

Simulation Time: The simulation time, t, used for this experiment will be 7 seconds or 100 iterations at $\Delta T = 0.07s$ per iteration. The simulation time is selected loosely based on typical descent times from the start of the track to the first corner on an Olympic track. The main criteria here is to create a simulation of sufficient length for controller performance assessment.

Initial Conditions: The initial state, $X(0)$, as shown in Equation 7.17, represents the longitudinal and transverse position and velocity of the sled and athlete (shown as the states of the left and right mass particles) immediately after the athlete mounts the sled and begins sliding. For this experiment the sled will start on the left side of the track with 0 transverse velocity and a longitudinal velocity of 50 km/h or 13.9 m/s. The rest of the initial conditions consists of the partial spatial derivatives used by the equations of motions and are obtained by running an uncontrolled simulation for 1 sampling period and taking the resulting values for these partial derivatives.

$$X(0) = \begin{bmatrix} 0 & 2 & 13.9 & 0 & 0 & 3.1 & 13.9 & 0 \end{bmatrix}^T \tag{7.17}$$

System Reference:

$$R(k) = \begin{bmatrix} 100 & 11 & 36.1 & 0 & 100 & 12.1 & 36.1 & 0 \end{bmatrix}^T \tag{7.18}$$

The reference used for this simulation is a static state reference that applies at all sampling instances, illustrated by Equation 7.18. To assess controller stability, a step input was given as the reference prompting the sled to travel from the left to the right side of the track. The longitudinal position reference is set as the maximum track length (100 is dimensionless index length, equivalent to 150 m) to ensure the sled is travelling in the right direction down the

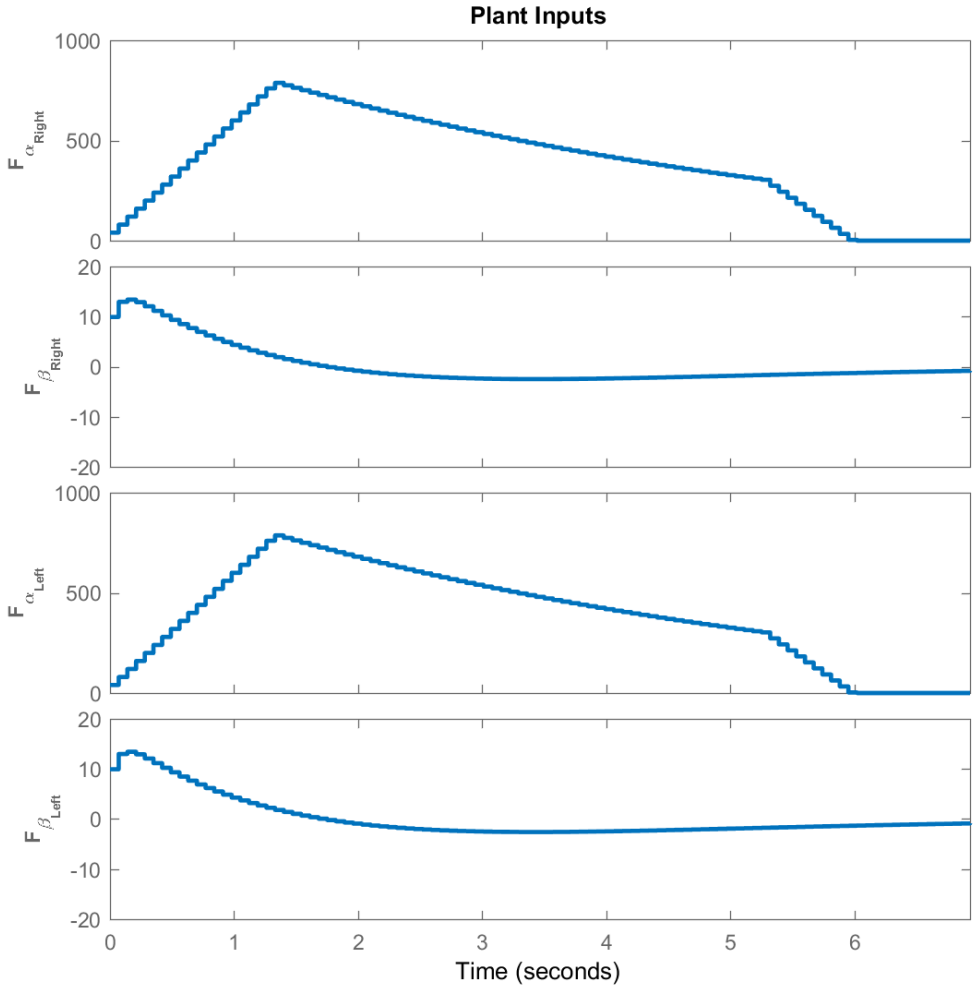

FIGURE 7.6: Actuation forces/Plant inputs

track and the longitudinal velocity reference is set to the typical reference velocity achievable on an Olympic track, in order to motivate the sled to travel as fast as possible. The reference transverse velocity is set to 0 to improve the stability of the descent by cancelling undesired lateral movements.

Cost Function Weight Vectors: The cost function for this experiment is tuned following the guidelines provided by section 6.3.5, thus it is tuned to achieve adequate reference tracking but prioritise energy loss minimisation and descent stability. The weight vectors displayed between Equation 7.19 and 7.21 are the tuned weights that yielded the best descent performance.

$$W^Y = \begin{bmatrix} 1 & 5 & 10 & 1 & 1 & 5 & 10 & 1 \end{bmatrix}^T \tag{7.19}$$

$$W^U = \begin{bmatrix} 0 & 1 & 0 & 1 \end{bmatrix}^T \tag{7.20}$$

$$W^{\Delta U} = \begin{bmatrix} 0 & 1 & 0 & 1 \end{bmatrix}^T \tag{7.21}$$

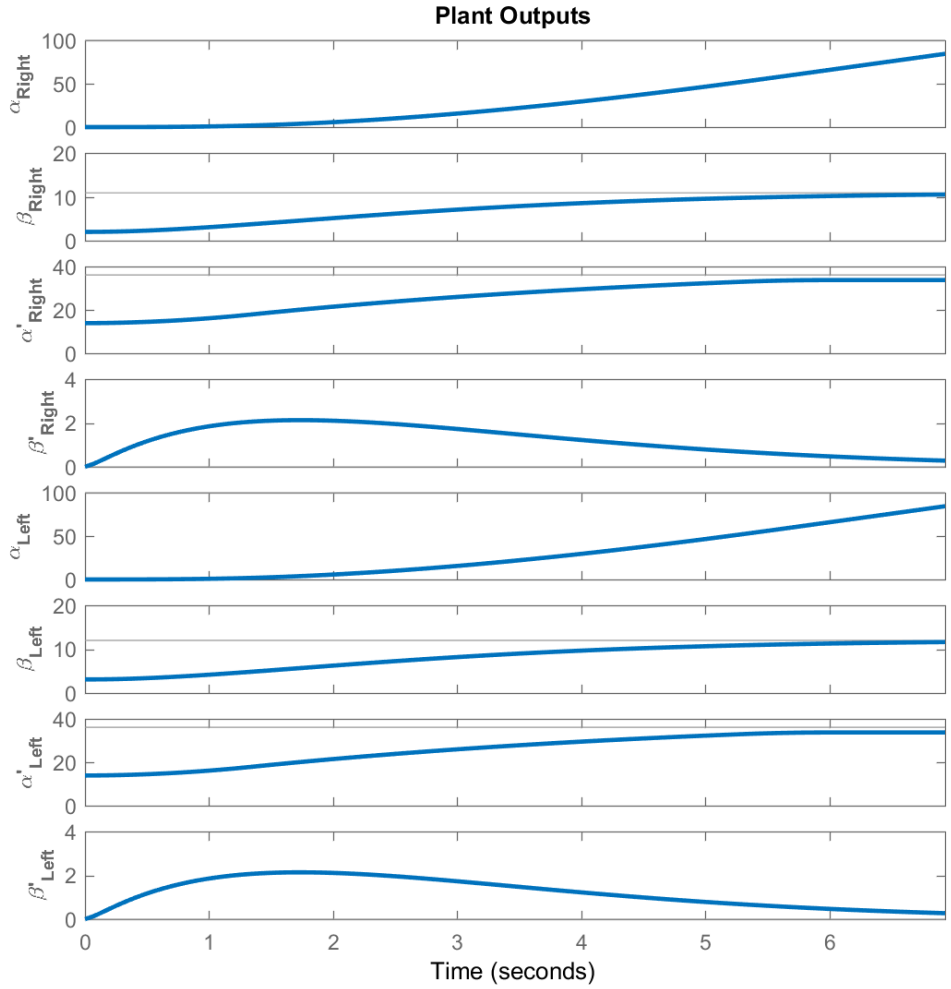

FIGURE 7.7: Plant outputs

Figure 7.6 and 7.7 shows the inputs and outputs of the physics model for both the left and right mass particles. Figure 7.6 demonstrates that the actuation forces (plant inputs) did not violate their respective constraints and Figure 7.7 shows that the sled was able reach the reference target with no overshoot right before completing the descent. It is important to note here that these weight vectors also resulted in the fastest descent velocity and travelled the furthest on the testing track, which can be equated to the quickest descent time when the track length is fixed instead of simulation time. Matlab's control object review function indicates that the linear MPC controller is internally stable and the results demonstrated here show that the tuning parameter selected are feasible for off-line application. The next stage of the PhD is to modify this control algorithm and apply it to the real time simulation.

7.3 Adaptive MPC Algorithm Design & Implementation

The rest of this section will focus on the 'Main Control Loop' stage of the MPC design, the implementation and experimental verification process of the adaptive MPC algorithm and the Hybrid control algorithm will be discussed here.

Section 7.2.4 demonstrated that the descent simulation can not be adequately controlled by a linear MPC algorithm, therefore an adaptive MPC algorithm must be used instead. A controller using adaptive MPC algorithm can adjust its prediction model at run time to compensate for non-linear plant characteristics. To do so, the controller must linearise its plant model at each control interval. This is achieved in the Simulink model through the implementation of a 'Successive Lineariser', detailed in the following section. Figure 7.8 shows the structural block diagram of the adaptive MPC controller and maps its interaction with the rest of descent simulation. Due to the nature of a simulation, all requisite feedback data can be acquired easily at any given sampling period and therefore no observer is required. At each sampling instance of the simulation, the following process will be carried out:

1. The MPC block reads in the sled's current state feedback, compare this with the reference given to produce state errors.
2. The MPC block generates longitudinal and transverse control actions for both left and right mass particles.
3. The control actions generated are fed to the respective equations of motion as well as the successive lineariser after being held in memory for 1 control interval.
4. Spatial derivatives of the current sampling instance and the estimated states by the MPC block from the previous control interval are fed to the successive lineariser.
5. The successive lineariser creates a new state space model for the MPC block to use.

7.3.1 Successive Linearisation

As illustrated in Figure 7.8, the 'Successive Lineariser' acquires values of the spatial derivatives at the current sampling instance. These data are then combined with the estimated state output from the MPC and the predicted control actions of the previous control interval to form a new continuous-time linear state space model following the format stated in section 7.2.3. This state space model is then manually discretised at a sampling rate of $\approx 14.29Hz$ (MPC sampling frequency). This process is repeated at every sampling instance of the simulation to create linearised discrete-time state-space models used for predicting future plant dynamics.

7.4 Adaptive MPC Algorithm Performance Analysis

In this section, a series of experimental analysis will be conducted to evaluate the stability and performance of the adaptive MPC algorithm. For each experiment, the details regarding the experimental set-up will be given before discussing the results, these include:

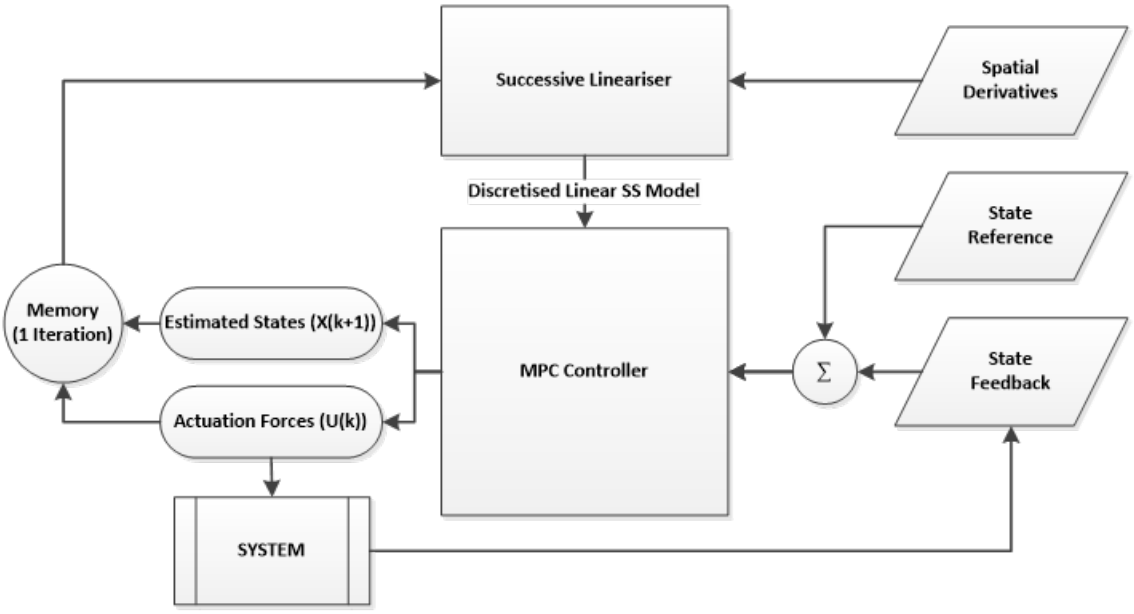

FIGURE 7.8: Structural block diagram of Adaptive MPC

- The objective of the experiment
- The track used for the experiment
- The initial state of the sled
- The state reference for the sled
- The tuned cost function weights that resulted in optimum performance

7.4.1 Experiment I - Straight Track Adaptive MPC Stability Evaluation

Experimental Objective

Experiment I contains of two sets of simulations, designed with the purpose to test the adaptive MPC algorithm's stability on a straight track during common maneuvers performed by the athlete when sliding. The experiment will have the sled to traverse from the either side of the track to the other to simulate typical positional transitions between the exist of one corner and the entrance of the next.

Experimental Set-up

- **Track:** Sim 1 & 2: The $150m$ Straight test track used for linear MPC analysis to represent the connection between two track corners was used here.
- **Initial State:** The two initial states represent the starting position and velocity of the sled for simulation 1 & 2. Specifically, simulation 1 have the sled starting at the left of the track heading to the right and vice versa for simulation 2.

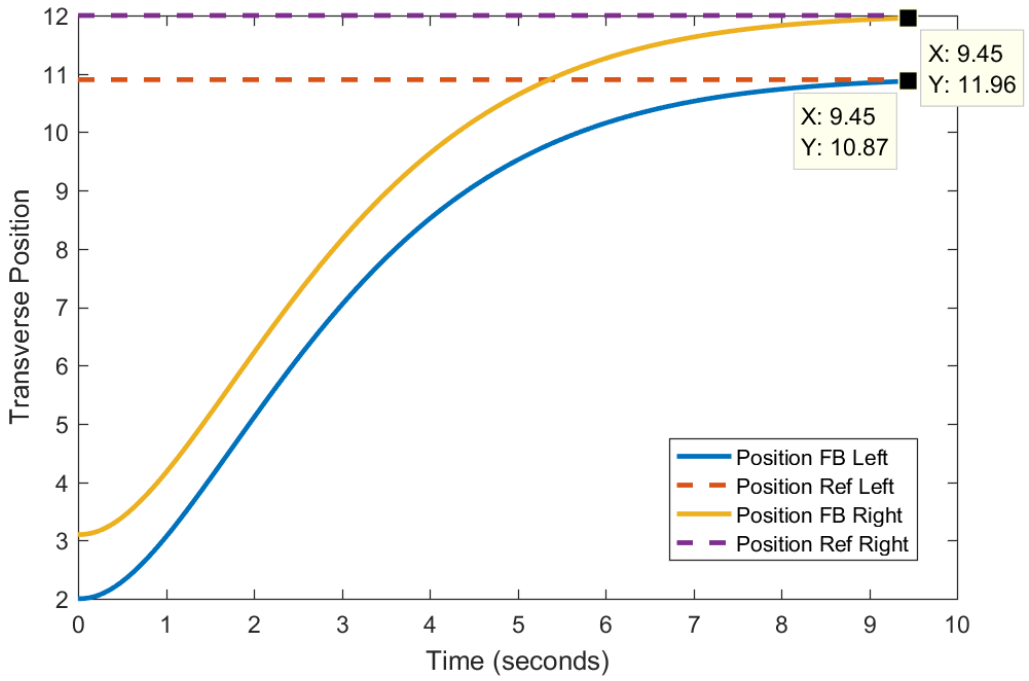

FIGURE 7.9: Simulation 1 transverse trajectories

- Sim 1: $X(0) = \begin{bmatrix} 0 & 2 & 13.9 & 0 & 0 & 3.1 & 13.9 & 0 \end{bmatrix}^T$
- Sim 2: $X(0) = \begin{bmatrix} 0 & 10.9 & 13.9 & 0 & 0 & 12 & 13.9 & 0 \end{bmatrix}^T$

- **State Reference:** Static References were used for both simulation. The final transverse position reference are given as a step reference at $k = 0$ and the longitudinal velocity reference is set as an arbitrary reference to maximise descent velocity. Therefore $\forall k \in \mathbb{N}$
  - Sim 1: $R(k) = \begin{bmatrix} 100 & 10.9 & 36.1 & 0 & 100 & 12 & 36.1 & 0 \end{bmatrix}^T$
  - Sim 2: $R(k) = \begin{bmatrix} 100 & 2 & 36.1 & 0 & 100 & 3.1 & 36.1 & 0 \end{bmatrix}^T$
- **Cost Function Weights:** The cost weights presented here were tuned empirically following the tuning guideline. These yielded the quickest descent whilst maintained stability. Adequate reference tracking (i.e The sled made its way to the other side of the track successfully) was achieved with minimal overshoot/undershoot using these cost weights. The cost function weight is identical for both simulation 1 & 2.

$$W^Y = \begin{bmatrix} 1 & 1.5 & 10 & 1 & 1 & 1.5 & 10 & 1 \end{bmatrix}^T$$
$$W^U = \begin{bmatrix} 0 & 1 & 0 & 1 \end{bmatrix}^T$$
$$W^{\Delta U} = \begin{bmatrix} 0 & 1 & 0 & 1 \end{bmatrix}^T$$

Experimental Result Evaluation

Figure 7.9 and 7.10 shows the transverse descent trajectory of both the left and right mass particles. In both simulations, the mass particles successful reached the target reference with

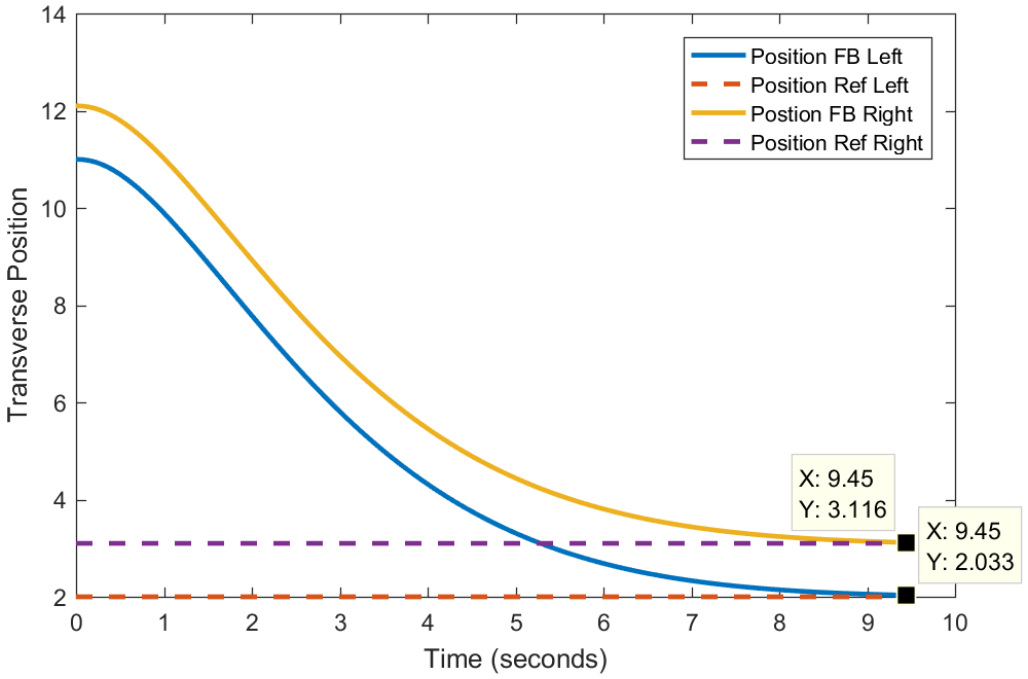

FIGURE 7.10: Simulation 2 transverse trajectories

0% overshoot. The final descent time for both simulation are identical and is 9.45 seconds. The descent trajectories of both simulation are reflections of each other about the centre line of the track. Stability of descent on straight track sections is clearly demonstrated by this experiment and as it is conducted under the scenario where maximum transition of transverse positions have occurred, it is therefore reasonable to assume that all other transverse positional transitions will be stable as well using the current controller set-up.

Changing the other tuning parameters, N_p and N_c generated results that matches with previous predictions made in the 'Initialisation' stage of the controller design. Specifically, increasing N_p and/or decreasing N_c lead to less aggressive control actions, causing the sled to go faster however also resulted in a lack of adequate tracking of the reference given. Similarly, increasing N_c and/or decreasing N_p leads to more aggressive control actions, which increased the descent time and lead to overshoots in reference tracking. Figure 7.11 demonstrates above effect on the left mass particle in simulation 2.

The other simulation parameter that may be subject to change is the initial longitudinal velocity of the sled, which is currently set to $50k$ m/h. Changing the initial velocity between 30 km/h and $130km/h$ have minimal effects on the shape of the descent trajectory, however it does have profound effects on the descent time. The general pattern is: faster initial velocity equates to faster descent, vice versa.

7.4.2 Experiment II - Straight Track Adaptive MPC, Adaptive PD Performance Comparison

Experimental Objective

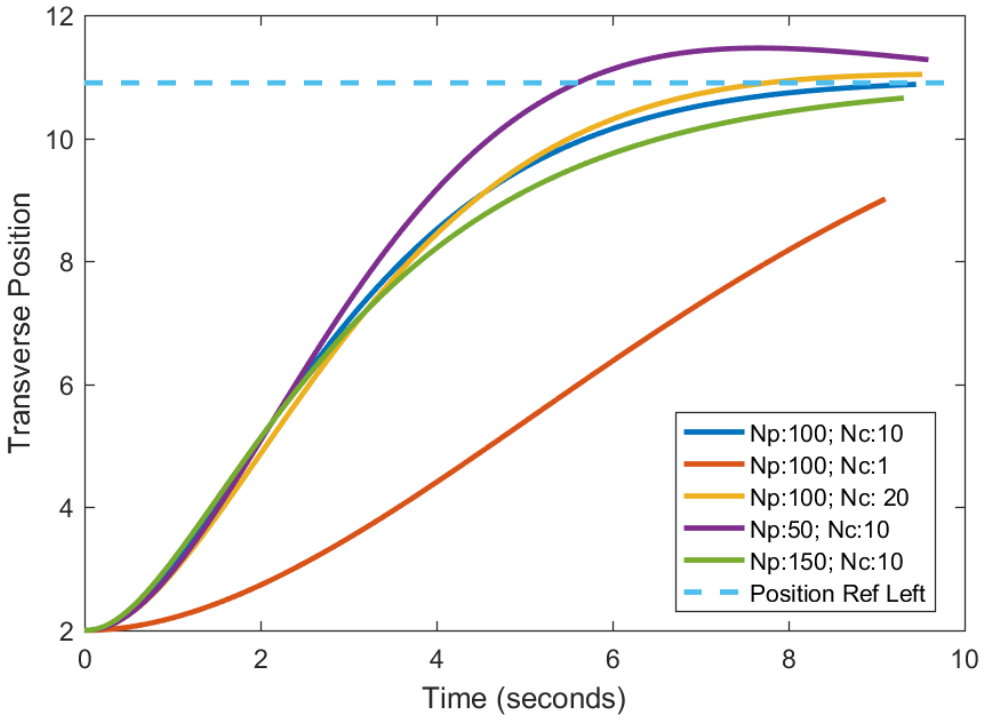

FIGURE 7.11: Effect of altering N_c & N_p

Experiment II was designed to compare the performance of the adaptive MPC controller with the performance of the adaptive PD controller from section 6.4. The purpose of this this experiment is to show that on the straight sections of an Olympic track, the adaptive MPC controller have superior performance in both reference tracking and descent time. Therefore, verifying that the descent trajectory obtained using the adaptive MPC is indeed optimal. The experiment contains of two sets of descent simulation steered by the adaptive PD controller and the results were compared with those generated from Experiment I.

Experimental Set-up

- **Track:** Sim 1 & 2: The $150m$ straight test track used in Experiment I.
- **Initial State:** To maintain consistency in comparison, the initial conditions used for Experiment II were the same as those used in Experiment I.
  - Sim 1: $X(0) = \begin{bmatrix} 0 & 2 & 13.9 & 0 & 0 & 3.1 & 13.9 & 0 \end{bmatrix}^T$
  - Sim 2: $X(0) = \begin{bmatrix} 0 & 10.9 & 13.9 & 0 & 0 & 12 & 13.9 & 0 \end{bmatrix}^T$
- **Position Reference:** Experiment II uses the adaptive PD controller which only requires transverse position references. The controller treats the sled as one body instead of separate mass particles, therefore only one reference for the centre position of the sled was required for each simulation.

  $\forall k \in \mathbb{N}$

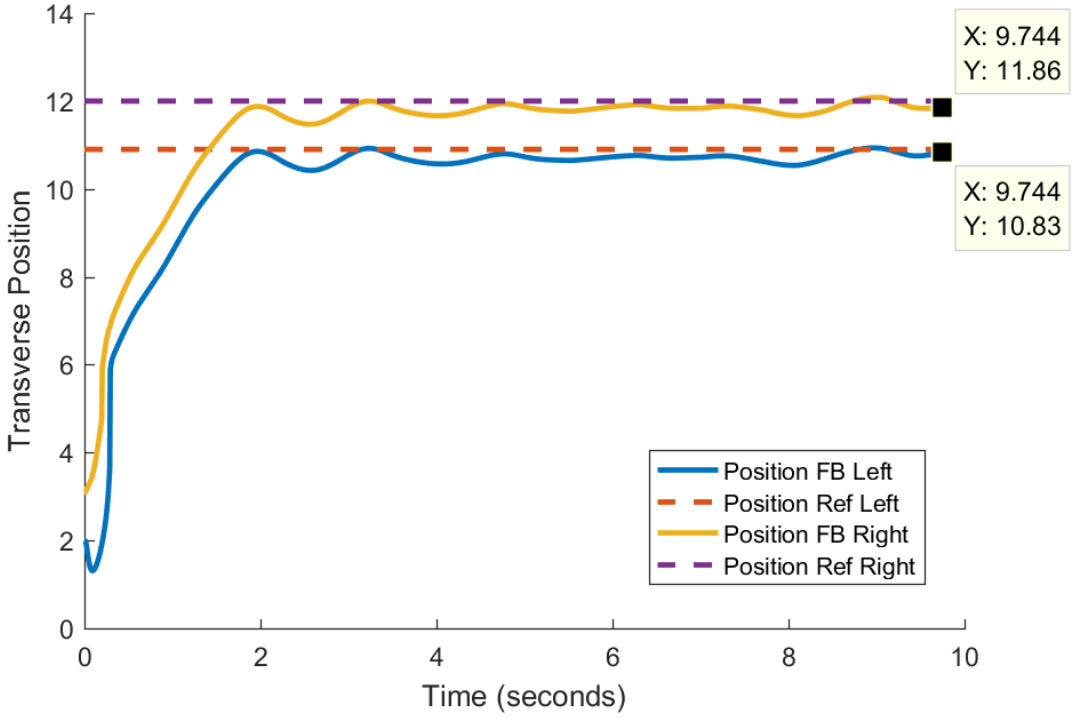

FIGURE 7.12: Simulation 1 transverse trajectories

- Sim 1: $Ref = 11.5$
- Sim 2: $Ref = 2.5$

- **Controller Gains:** Instead of cost functions, the adaptive PD uses a set of controller gains, which are optimal tuned to deliver the best descent performance on the straight test track. The optimal gains were obtained empirically through analysing simulation results across the stable region (as described section 6.3.5). The controller gains that needs to be selected were highlighted in Equation 6.6. The values of the controller gains are identical for Sim 1 & 2 and are listed below:

$$K_p = 0.027;\ K_{\Delta\beta_p} = 0.15;\ K_{p_{min}} = 0.01$$
$$K_d = 0.025;\ K_{\Delta\beta_d} = 0.005;\ K_{d_{min}} = 1.5$$

Experimental Result Evaluation

Figure 7.12 and 7.13 shows the transverse trajectory of the left and right mass particles. Simulation 1 took a total of 9.744 seconds to complete, whilst simulation 2 took 9.765 seconds to complete. Compared to experiment I, the rise time of the descent trajectory are much shorter, indicating more aggressive control actions have being used. There are also numerous undesirable oscillations and significant tracking errors in the descent trajectories created from both simulations, which are caused by the curvature of the track as the sled is approaching either side of the wall, where as the adaptive MPC controller can takes into account of these curvatures and generates the appropriate control forces accordingly to compensate. By comparing both tracking performance and descent time, it is clear to see that adaptive MPC algorithm should

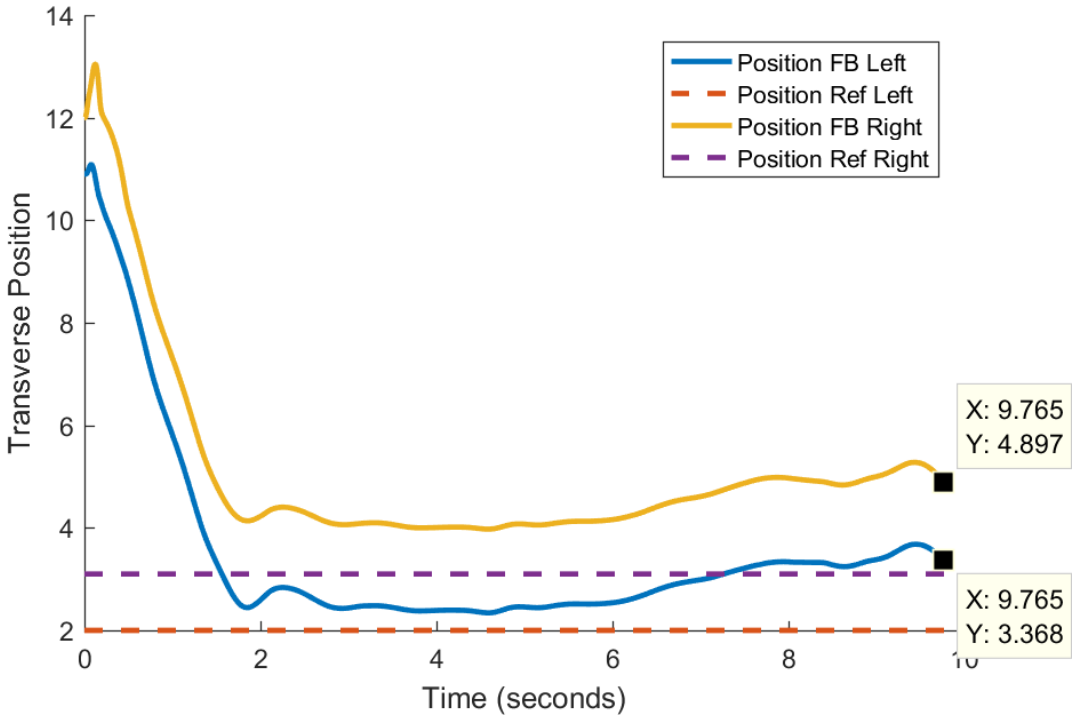

FIGURE 7.13: Simulation 2 transverse trajectories

be the superior choice for creating the optimal trajectory during straight sections of an Olympic track.

7.4.3 Experiment III - Corner Track Adaptive MPC Stability Evaluation

Experimental Objective

After establishing adaptive MPC algorithm's capability for stability and optimality, the next stage of the design process will be to evaluate its stability around the corner sections of the track. In this experiment, one simulation was conducted and the results, which will be discussed in detail later shows that with the current controller design, it is not possible to achieve stable descent around the track corners.

Experimental Set-up

- **Track:** For Experiment III, the testing track used was a cropped track section from the PyeongChang Olympic track. More specifically, from the entrance to the exit of corner 5 of the PyeongChang track. The reason for selecting the PyeongChang track is that this will be the track used in the the 2018 winter Olympics and would therefore be most beneficial to the sport to conduct analysis on this track. The reason for selecting corner 5 is that it is the longest corner with the highest curvature out of the entire track. Therefore, if

the controller could achieve a stable descent through this corner then in theory it should achieve stable descents through all other corners of the track as well.

- **Simulation Time:** The typical descent time through corner 5 is approximately 4.5 seconds, however it is unclear how the adaptive MPC controller will perform. Therefore a set simulation time of 5 seconds was used in order to introduce a portion of redundancy.

- **Initial State:** For the initial state of this experiment, the sled was placed in the middle of the track at the entrance to corner 5, which was reflected by the longitudinal positional index 215. The initial velocity was set to 95 km/h or 26.39 m/s, which is the desired entry speed specified by the track designer. The numerical representation of the initial velocity is therefore:

$$X(0) = \begin{bmatrix} 215 & 6 & 26.39 & 0 & 215 & 8 & 26.39 & 0 \end{bmatrix}^T$$

- **State Reference:** A static Reference were used for this simulation. The final longitudinal position were set to an arbitrary value greater than the index representing the exist point of the corner to ensure the sled is travelling in the correct direction. Like Experiment I, the longitudinal velocity reference is set as an arbitrary reference to maximise descent velocity. The transverse position reference is selected so that the sled would follow the centre line of the track. The reason for this is because centre line tracking is the least demanding operation for the adaptive MPC controller in terms of keeping track of changes to the system dynamics. This should be the simplest operation to maintain stability, if stability could not be achieved in this operation, there is no reason to assume stability will be achieved in an other operation either. The complete reference trajectory is:

$$R(k) = \begin{bmatrix} 500 & 6 & 36.1 & 0 & 500 & 8 & 36.1 & 0 \end{bmatrix}^T$$
$$\forall k \in \mathbb{N}$$

- **Tuning Parameters:** The initial cost function weights, prediction & control horizons and the sampling period used in this experiment are identical to those in Experiment I, these did not yield a stable descent. Therefore these parameters were tuned empirically in an attempt to stabilise the descent. However, none of the changes improved the stability sufficiently enough for a full descent through the corners. In the next section, the comparatively most stable simulation results (one that made it furthest into the corner) will be presented and below are the tuning parameters used for said simulation.

  - $N_p = 125$
  - $N_c = 10$
  - $\Delta t = 0.007$
  - Cost function:

$$W^Y = \begin{bmatrix} 3 & 5.5 & 5 & 4 & 3 & 5.5 & 5 & 4 \end{bmatrix}^T$$
$$W^U = \begin{bmatrix} 0.2 & 1.3 & 0.2 & 1.3 \end{bmatrix}^T$$
$$W^{\Delta U} = \begin{bmatrix} 0 & 2 & 0 & 2 \end{bmatrix}^T$$

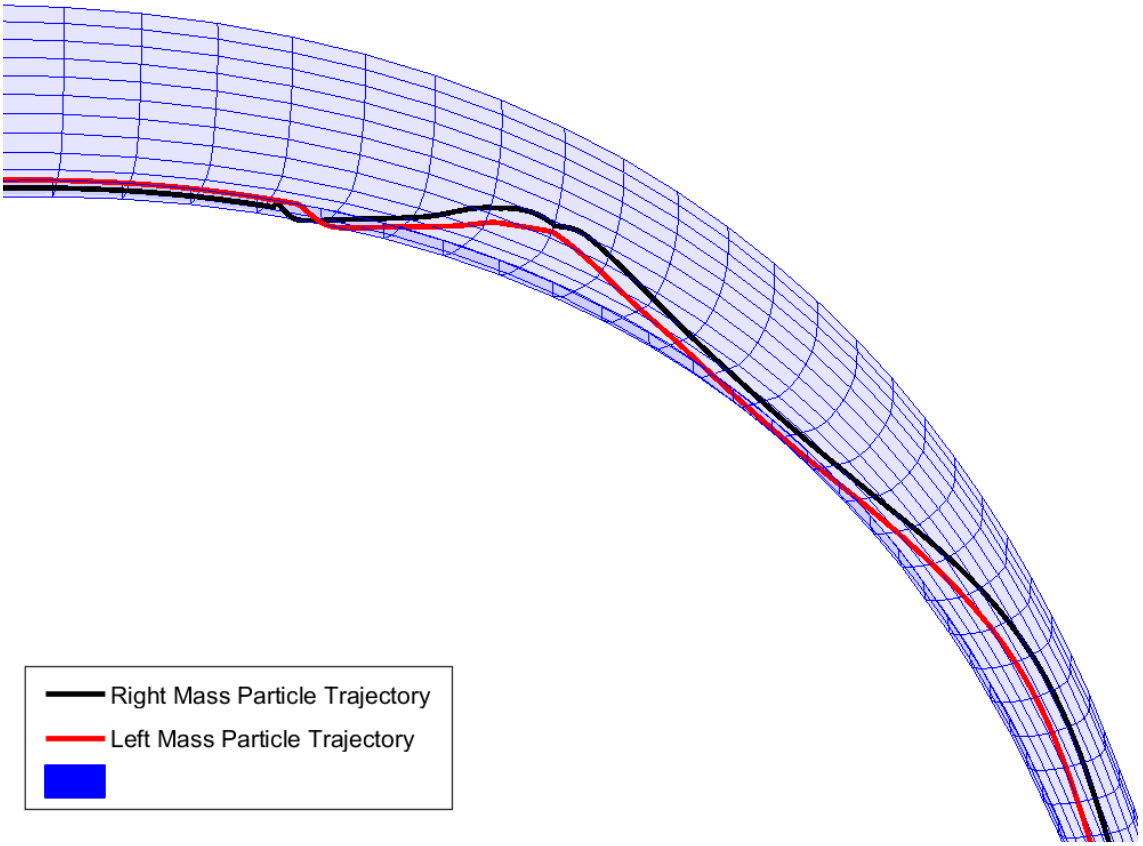

FIGURE 7.14: Sled trajectory in corner 5, PyeongChang

Experimental Result Evaluation

Figure 7.14 shows the descent trajectories of the left and right mass particle on the physical track surface and Figure 7.15 shows the corresponding transverse positions against simulation time. It is clear from the figure that the sled's stability is maintained at the entrance of the corner where the curvature is small and the adaptive MPC controller is performing at an acceptable level predicting the control actions, reflected by 'down-steer' at approximately 1.5 seconds. This is a typical steering decision made by athlete at the entrance of corners to counteract the centripetal force, which will drive the sled toward the outer edge of the track. However, as the sled enters the corner, the performance deteriorates and at 3.9 seconds into the simulation, the right mass particle went completely unstable and the descent went into failure mode from this point onwards. There could be a number of reasons for this loss of stability:

1. The sampling period could be too long and not able to encompass all the changes occurring during the simulation.
2. The prediction horizon could be of the wrong length and did not predict far enough ahead to take into account of the constantly changing curvature of the corner.
3. The cost function weights of the original MPC design was tuned to generate as smooth and minimal amount of control action as possible whilst maintaining stability. This kind of control strategy may not be be feasible under the track corner senarios and different tuning strategies needs to be explored.

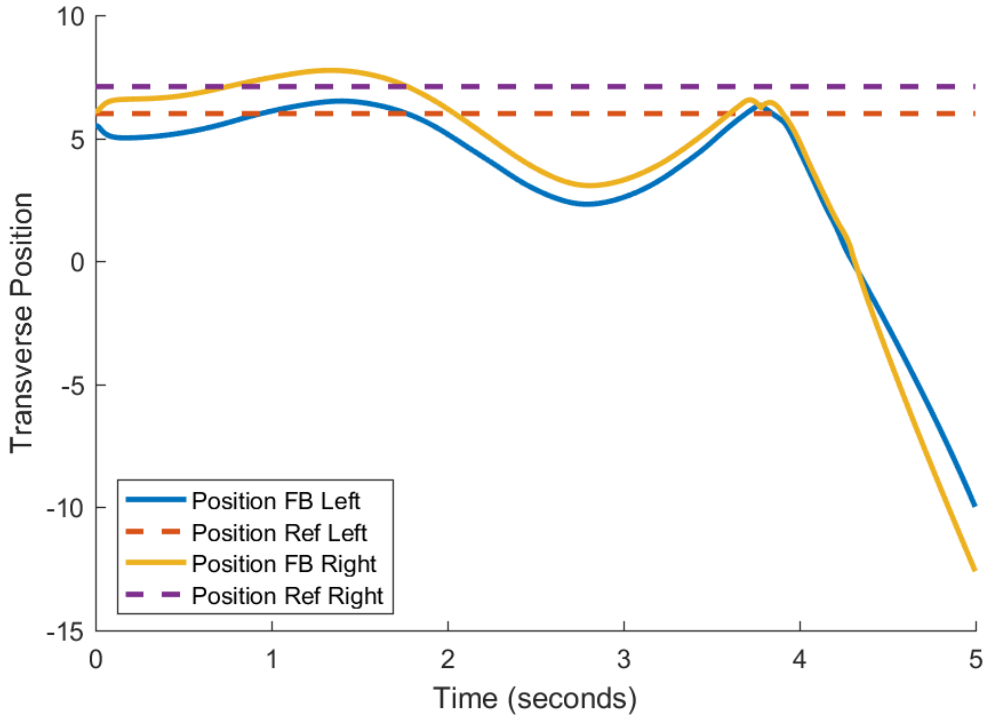

FIGURE 7.15: Trajectory references & feedbacks

4. At each control interval, the successive lineariser produces a discrete state-space model using the instantaneous values of the partial derivatives and mass particle velocity. The linear state-space model formed this way is an approximation of the plant state and can contain errors, these errors may move the poles of the plant to the right half plane and result in unstable plant dynamics.

5. The mathematical model used by the MPC to predict future plant behaviour is calculated at the start each control interval and held constant throughout. As previously stated, this is an approximation of the plant dynamics and the error in plant dynamics prediction could be a major contributing factor to the loss of stability.

Each of these possible reasons were explored and the corresponding results are presented below:

1. Decreasing the sampling period of the MPC controller from 0.07 s to 0.007 s, which is also the inherent sampling period of the descent simulation, allows for 'loss-less' data sampling and should in theory yield more accurate predictions of the plant dynamics. In practice, whilst decreasing the sampling period did improve the prediction accuracy, its effect on descent stability is not significant enough to be noticeable. The increase in computational demand is simply too great (approximately 13 times slower) for this to be a worthwhile compromise.

2. Increasing the prediction horizon allows the MPC controller to look further ahead in the track and take into account possible changes in the system dynamic that may affect the control actions calculated, but at the same time this also cause the controller to generate less aggressive controls which can lead to more instability. On the other hand, decreasing

the prediction horizon will result in more aggressive control actions, which may improve the stability of the descent but looses out on optimality. In practice neither of these changes had noticeable effects on the simulation output.

3. The original cost weights generated low magnitude and smooth control actions, which in turn yielded very unstable descents. By tuning the cost weights to more aggressively track the transverse position reference, the controller managed to assert control actions, the simulation results showed moderate improvement in performance, however this improvement is not enough to yield stable descent through corner 5. The results illustrated in Figure 7.14 was the best performing simulation amongst all the weight combination experimented. Further experiment was conducted where the system constraints were entirely removed to see if the limitation on control forces was the problem. However, these experiment resulted in much more aggressive control actions that caused the sled to crash earlier on in the track, which suggests that the main cause of instability is not to do with the style of control action but rather the mathematical models used to calculate the control actions.

4. Whilst the linear approximation of the state-space model gave acceptable adequate simulation performance during track sections with slow changing dynamics (i.e. straight sections of the track), this is not the case for simulation carried out on corner 5. The approximation error may be the cause of numerous pole instability during the simulation, as illustrated in Figure 7.16, the poles s to s^4 remained stable through the simulation and was therefore not displayed here. As the figure shows, the higher order poles of the system started to go into instability at approximately 1.8 seconds, which could be caused by the sled moving to close proximity of the wall and throwing off the prediction due to sudden changes in plant dynamics. This error cascaded from this point onwards, eventually lead to total system instability at 4.25 seconds. The default QP solver used by MatLab does not appear to be able to deal with these pole instabilities and therefore were not able to yield feasible optimal solutions, with or without constraints.

5. Problem 5 is the compounded result from Problem 2 & 4. The invariable nature of the state-space model during a control interval combined with the inaccuracy of the linear approximation resulted in inaccuracies in the prediction process of the MPC controller. This is a major cause of system instability, since if the controller can not predict future plant behaviour with relative accuracy, then the subsequent control actions calculated would be all incorrect which in turn will lead to yet more instability in the simulation. Figure 7.17 clearly demonstrates this issue. In the figure, the dotted lines represent the predicted future trajectories for the left and right mass particle and these predictions are oscillatory and unstable, nothing like what the position feedback is showing.

In conclusion, the results presented by Experiment III established that the adaptive MPC algorithm was unable to achieve a stable descent through the corner 5 of the PyeongChang track and is therefore inadequate to use as a controller design for obtaining the optimal descent trajectory for said track. A new controller design is required to perform this task, this will be discussed in section 7.5.

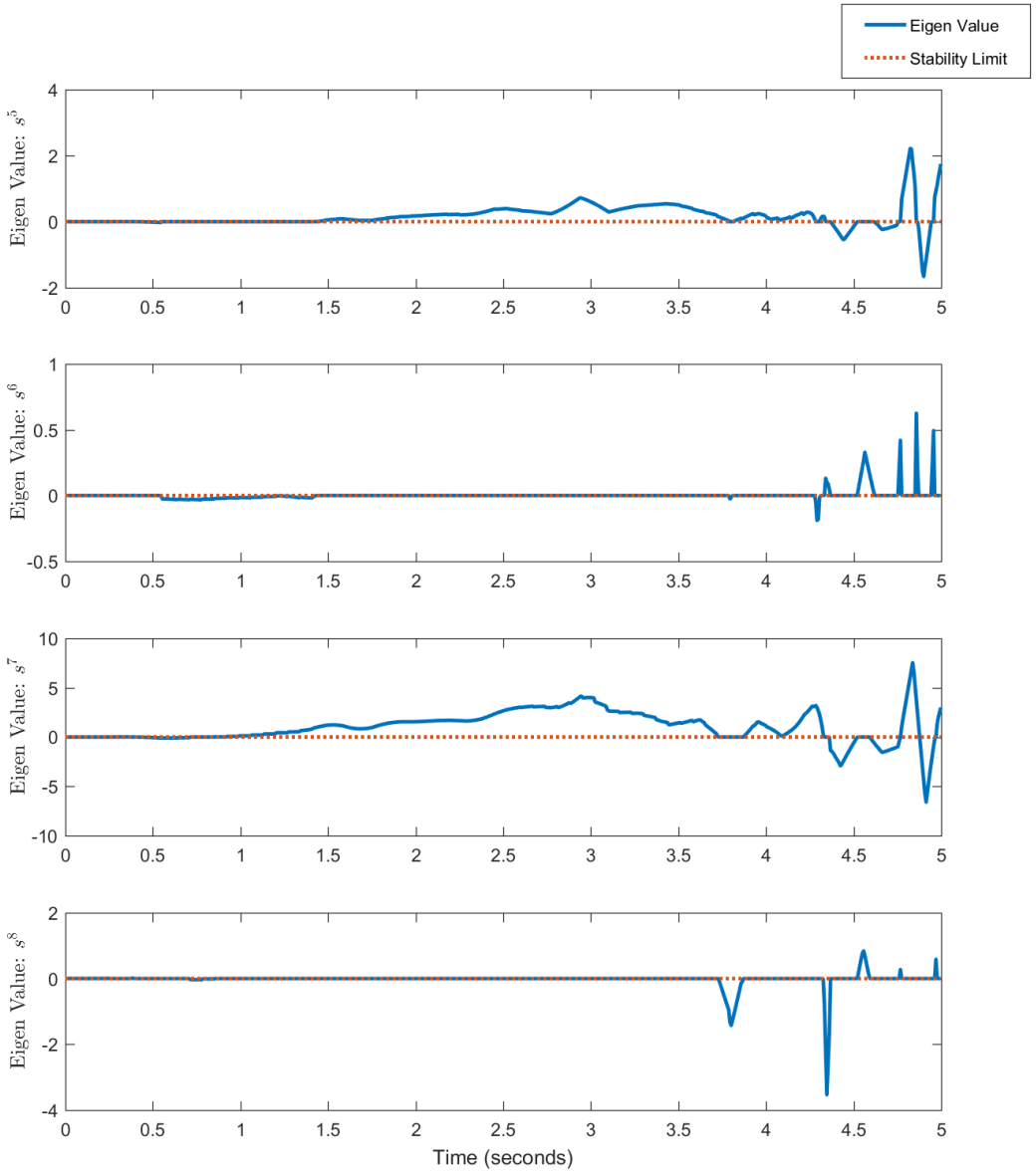

FIGURE 7.16: System eigen values 5th order pole - 8th order pole

7.5 Hybrid Controller

Even though the adaptive MPC controller was unable to achieve stable descent through corner sections of a track, is shows promising performance during the straight sections, superior to those yielded by the adaptive PD controller. The adaptive PD controller on the other hand displayed great stability through the corner sections of the track. Therefore a 'Hybrid Controller' was designed with the purpose to combine the strength of both adaptive PD and adaptive MPC controllers.

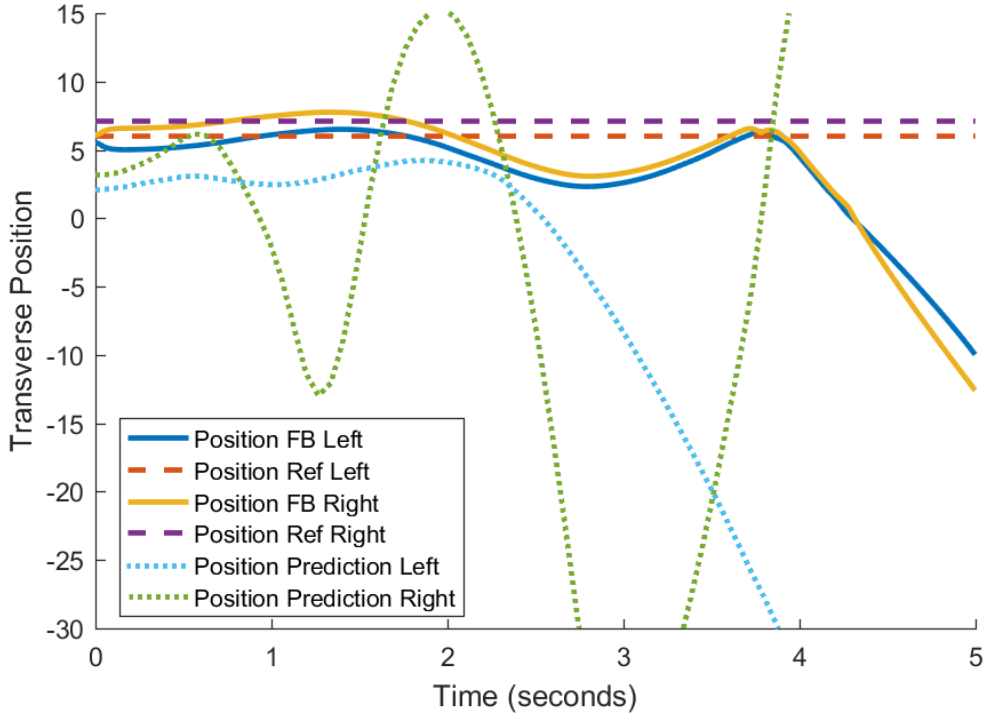

FIGURE 7.17: Transverse position prediction

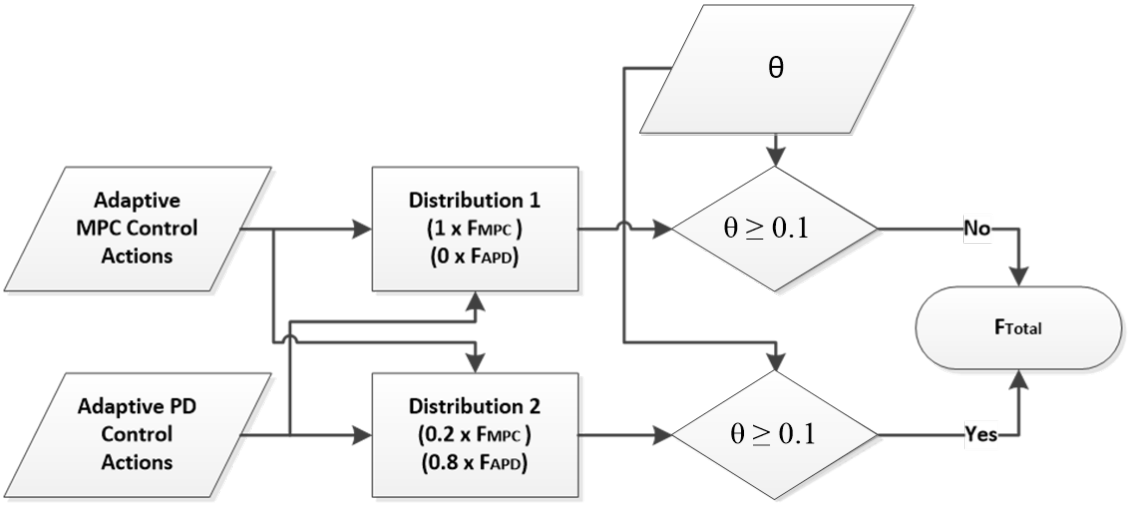

FIGURE 7.18: Hybrid controller design structure

7.5.1 Controller Design

The Hybrid controller uses sled orientation based decision algorithm to assign a proportion of the total control force to either controllers. Displayed in Figure 7.18 is the block diagram showing the design structure of the Hybrid controller. During each sampling period, the hybrid controller reads in the current roll(θ) value of the sled and chooses either one of the distribution algorithms to calculate the final actuation forces in both the longitudinal and transverse direction. A low pass filter is required at the output of the control signal to handle control signal transition and prevent sudden jerky control actions from being applied.

The equations used in distribution algorithm 1 and 2 to calculate the final actuation forces are listed in Equation 7.22 and 7.23. As the equations suggest, whilst the sled is not rolling (i.e. the sled is travelling on the straight sections of the track), all of the actuation forces are generated by the adaptive MPC controller. Here the value of 0.1 is used to mitigate the error in roll feedback resulted from vibrational noise of the sled. When the sled is rolling (i.e. the sled is travelling inside the corners of the track), 80% of the actuation force generated is by the adaptive PD controller, through the normal means of the 'Sled Characteristic' block and the rest 20% is generated by the adaptive MPC. This way, the adaptive PD controller is able to maintain stability and cancel out the effect of incorrect prediction from the MPC whilst still allowing a small degree of predictive control to take place. 80%/20% is currently the optimal amount of control force distribution for the hybrid controller on the PeyongChang track, any more force given to the adaptive MPC would result in unstable descents and any less would lead more aggressive control actions being generated by the Adaptive PD controller in some corner sections and result in slower descents.

$$F_{act_\alpha}(l,r) = f(\theta)F_{MPC_\alpha}(l,r) + g(\theta)F_{APD}(l,r)\cdot r_\alpha(l,r) \tag{7.22}$$

$$F_{act_\beta} = f(\theta)F_{MPC_\beta}(l,r) + g(\theta)F_{APD}(l,r)\cdot r_\beta(l,r) \tag{7.23}$$

with

$$f(\theta) = \begin{cases} 1, & \text{if } \theta \geqslant 0.1 \\ 0.2, & \text{otherwise} \end{cases}$$

$$g(\theta) = \begin{cases} 0, & \text{if } \theta \geqslant 0.1 \\ 0.8, & \text{otherwise} \end{cases}$$

where

- $F_{MPC_\alpha}(l,r)$ – Left & right actuation force from adaptive MPC controller in the α direction
- $F_{MPC_\beta}(l,r)$ – Left & right actuation force from adaptive MPC controller in the β direction
- $F_{APD}(l,r)$ – Left & right steering force from adaptive PD controller
- $r_\alpha(l,r)$ – Left & right spatial derivative in the α direction
- $r_\beta(l,r)$ – Left & right spatial derivative in the β direction

7.5.2 Hybrid Controller Stability Evaluation

The stability of the hybrid controller was evaluated under the same condition and using the same set-up as Experiment III from section 7.4.3. This was done to demonstrate the difference in stability between the hybrid controller and the adaptive MPC controller. No further tuning were conducted for this evaluation as both the adaptive PD and adaptive MPC has already being tuned to perform optimally in their respective operating regions. Figure 7.19 shows the both mass particles trajectory on corner 5's mesh model for visual presentation purposes and Figure

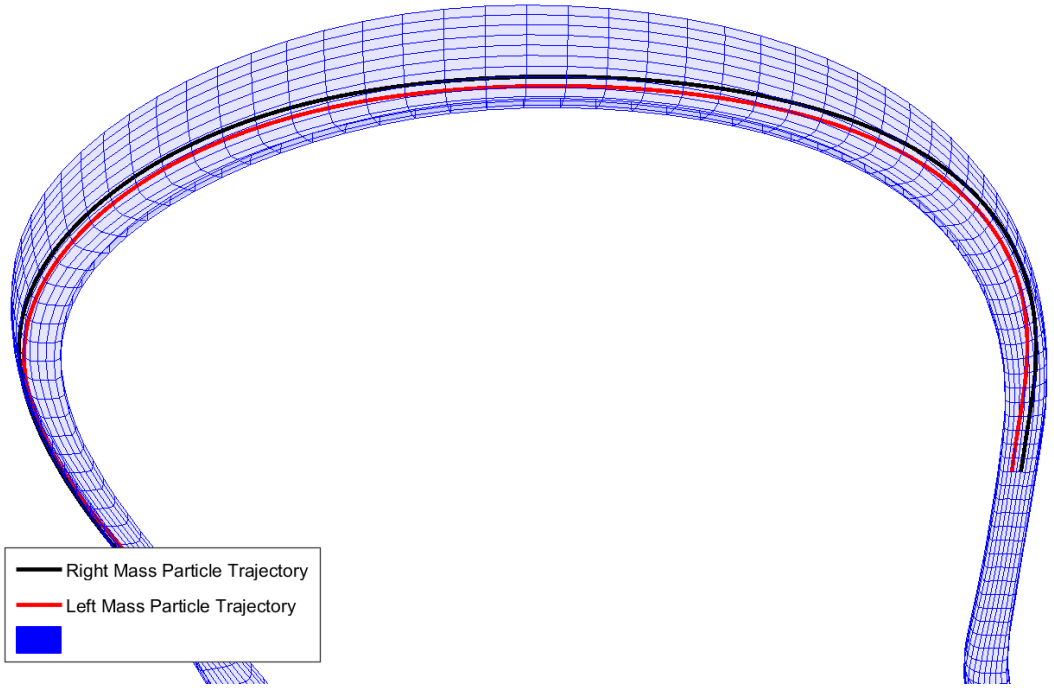

FIGURE 7.19: Sled trajectory in corner 5, PyeongChang

7.20 shows the corresponding position references, predictions and feedbacks. The simulation results shown here displayed fully stable descent through corner 5 with good reference tracking performance. The prediction of the plant dynamic was still erroneous, this was however expected and second distribution algorithm has dealt with inaccuracy in prediction adequately.

One further experiment was conducted to verify the stability of the hybrid controller on the whole track. This experiment was necessary because although stability was demonstrated for corner 5 and both adaptive MPC and adaptive PD controllers were stable in their own operating, the introduction of the low pass filter on the output means the stability of the hybrid controller can not be simply be assumed, especially around high velocity entrances and exists of corners since this is where the fast shift in plant dynamic occurs. This experiment was conducted on the entire PyeongChang track with an initial velocity of 26 km/h or 45 km/h at the first timing block. The result of this experiment, as presented in Figure 7.21 shows the position feedback against its prediction for both mass particles. It is clear from the figure that the entire descent was stable, implying that the introduction of the low pass filter did not compromise the stability of the simulation. The root mean square(RMS) value of tracking error (i.e. $\beta_{l.r} - \beta_{ref}$ is 0.899 units), indicating the signal to noise ratio is less than 10% and therefore a good level of position prediction tracking. This further proves the effectiveness of the controller design(at least on the PyeongChang track).

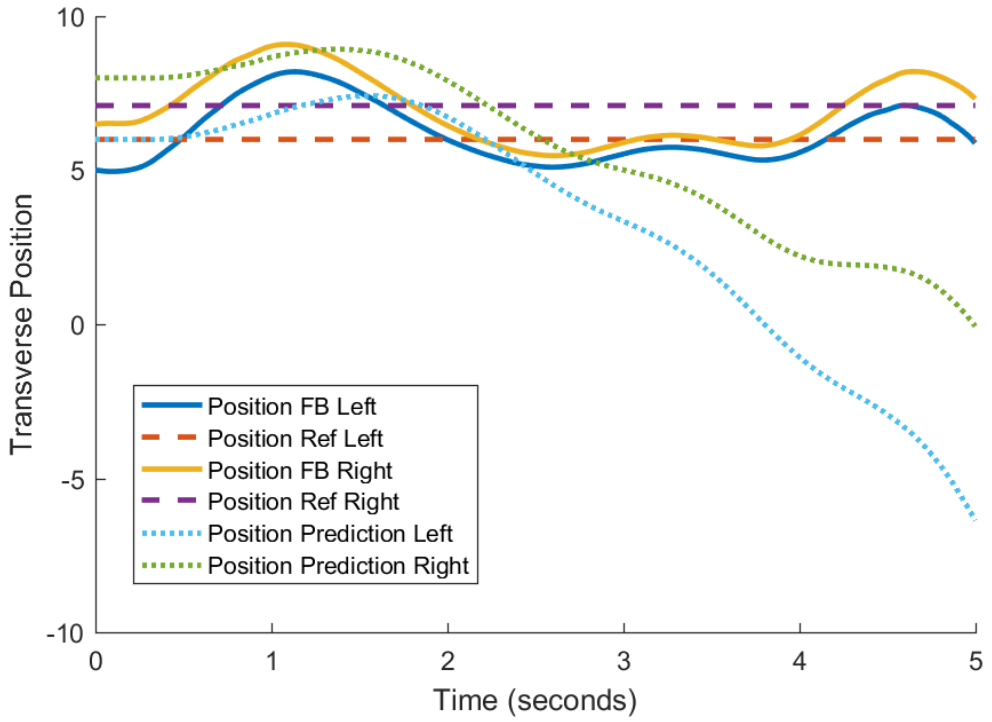

FIGURE 7.20: Transverse position prediction

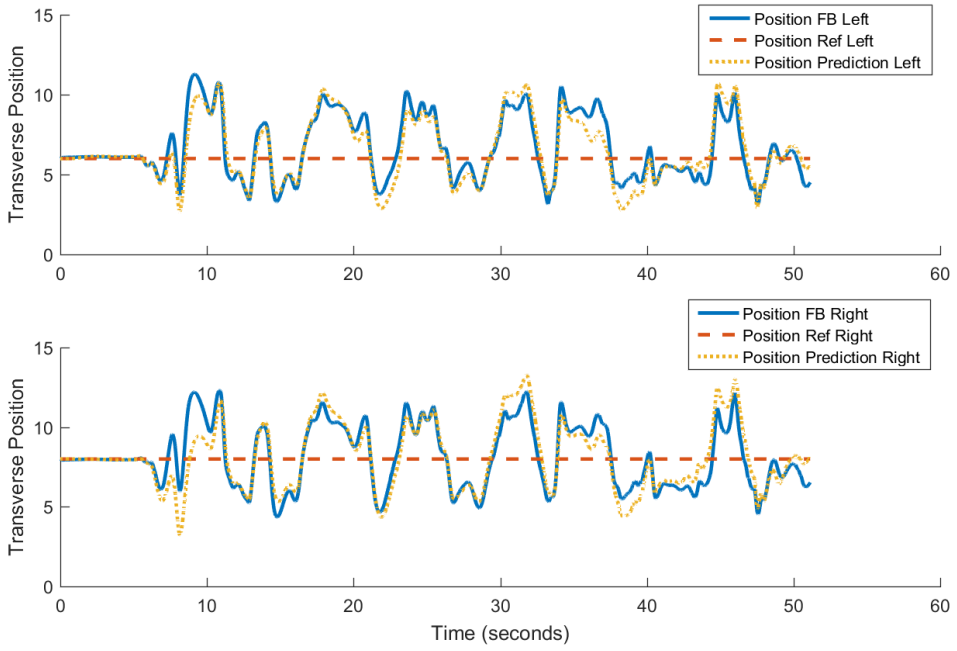

FIGURE 7.21: Full track trajectory prediction & feedback

7.5.3 Hybrid Controller & Adaptive PD Controller Performance Comparison

Experimental Objective After establishing stability of the hybrid controller, it was important to compare its performance against the adaptive PD controller, which was previously the best performing controller. This was done to show the hybrid controller was indeed yielding the optimal descent trajectories within the all the controller designs currently available. In order to get comprehensive review of the comparison between performances, a range of different initial sled velocities were used for each of the controller designs. 6 simulations were conducted per controller design, with different initial velocities encompassing the whole range of possible starting velocity by Skeleton athletes. This approach of the experiment also allowed for the verification of hypothesis, 'Faster sprint speed leads to quicker descent', which were traditionally agreed upon by the subject matter experts.

Experimental Set-up

- **Track:** The track used for this experiment was the PyeongChang Olympic track, since this will be the track for the 2018 winter Olympic and analysis on this track will have the most impact on enhancing athlete training.
- **Initial State:** The adaptive PD and adapitve MPC controller share the same initial condition. The initial condition have the sled start the simulation $50m$ from the beginning and at the centre of the track, this is where the athlete would normally mount their sled after sprinting with it. For the 6 sets of simulations, the initial longitudinal velocities vary from 25 km/h to 50 km/h in 5 km/h increments. The numerical values for the first set of simulation is listed below, other simulation will share all aspects of this initial condition bar the longitudinal velocity:

$$X(0) = \begin{bmatrix} 33 & 6 & 6.94 & 0 & 33 & 8 & 6.94 & 0 \end{bmatrix}^T$$

- **Reference Trajectory:** The reference trajectory used for the simulation was simply the centreline of the track, this means for the adaptive PD controller, the reference was set to a static 7 for the sled centre to track. For any controller including the adaptive MPC algorithm, the state reference is listed as below:

$$R(k) = \begin{bmatrix} 978 & 6 & 37.5 & 0 & 978 & 8 & 37.5 & 0 \end{bmatrix}^T$$
$$\forall k \in \mathbb{N}$$

- **Tuning Parameters:** The controller gains for the adaptive PD and cost function weights for the adaptive MPC used in this experiment were identical to those in Experiment I and II, since these yielded the optimal performance in their respective operating regions.

– Adaptive PD

$$W^Y = \begin{bmatrix} 1 & 1.5 & 10 & 1 & 1 & 1.5 & 10 & 1 \end{bmatrix}^T$$
$$W^U = \begin{bmatrix} 0 & 1 & 0 & 1 \end{bmatrix}^T$$
$$W^{\Delta U} = \begin{bmatrix} 0 & 1 & 0 & 1 \end{bmatrix}^T$$

– Adaptive MPC

$$K_p = 0.027;\ K_{\dot{\beta}_p} = 0.15;\ K_{p_{min}} = 0.01$$
$$K_d = 0.025;\ K_{\dot{\beta}_d} = 0.005;\ K_{d_{min}} = 1.5$$

Experimental Result Evaluation

The simulation results were evaluated via two methods. The first is to observe the change in velocity pattern of the sled with respect to time for the different initial velocities, this evaluation demonstrates the consistency in hybrid controller's performance and provides correlation between initial velocity and descent time. Figure 7.22 shows that the velocity patterns of all 6 descents are very similar. However, the maximum sled velocity achieved throughout all the simulations are exactly the same (134.89 km/h), indicating that the velocity decay rate of each simulation is different. By plotting the sled velocity against its longitudinal position instead of time, the difference in decay rate becomes instantly clear. Figure 7.23 shows that the sleds with higher initial velocity also decays more rapidly through the first 11 corners ($\alpha \in [0, 600]$), after which the velocity becomes piratically identical. This pattern behaviour is due that higher velocity sleds also requires higher control forces to maintain stability thus loosing more energy and speed during the descent. Figure 7.22 also shows that there's an almost linear relationship between the initial velocity and the descent time, specifically, for every increment of 5 km/h in the initial velocity the descent time decreases by ≈ 1 seconds.

The key result from this experiment was the comparison between descent time by the adaptive PD controller and the hybrid controller. Figure 7.24 shows a bar chart representing paired descent time from the 6 sets of descent simulation where the blue bars are the descent times of the simulations controlled by the hybrid controller and the yellow bar represent the simulations controlled by the adaptive PD controller. It is clear from the figure that the hybrid controller yielded the quicker descent for all of the initial velocities (≈ 0.299 seconds faster on average, see Table 7.1), therefore proves that under the current simulation conditions, it is the superior control algorithm to use for predicting the optimal descent trajectories.

7.6 Descent Trajectory Fidelity Validation

Due to the inaccuracy in the physics engine and steering model, the results generated from all previous experiments cannot be treated as credible or be utilised in athlete training without first validating their fidelities. Currently, this can be achieved empirically through data matching

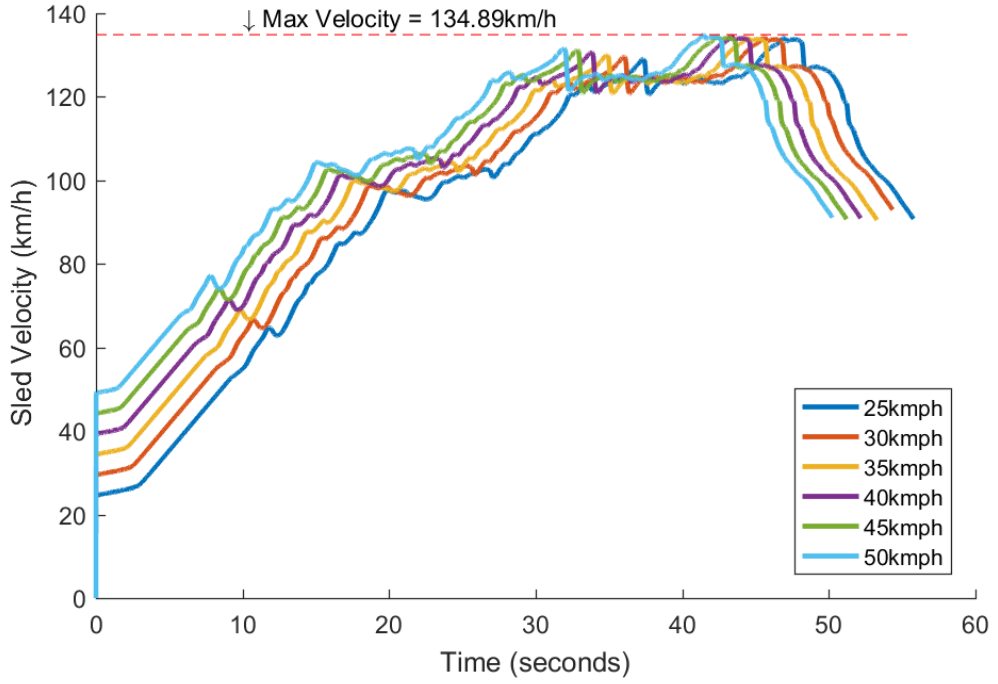

FIGURE 7.22: Sled velocity w.r.t Time

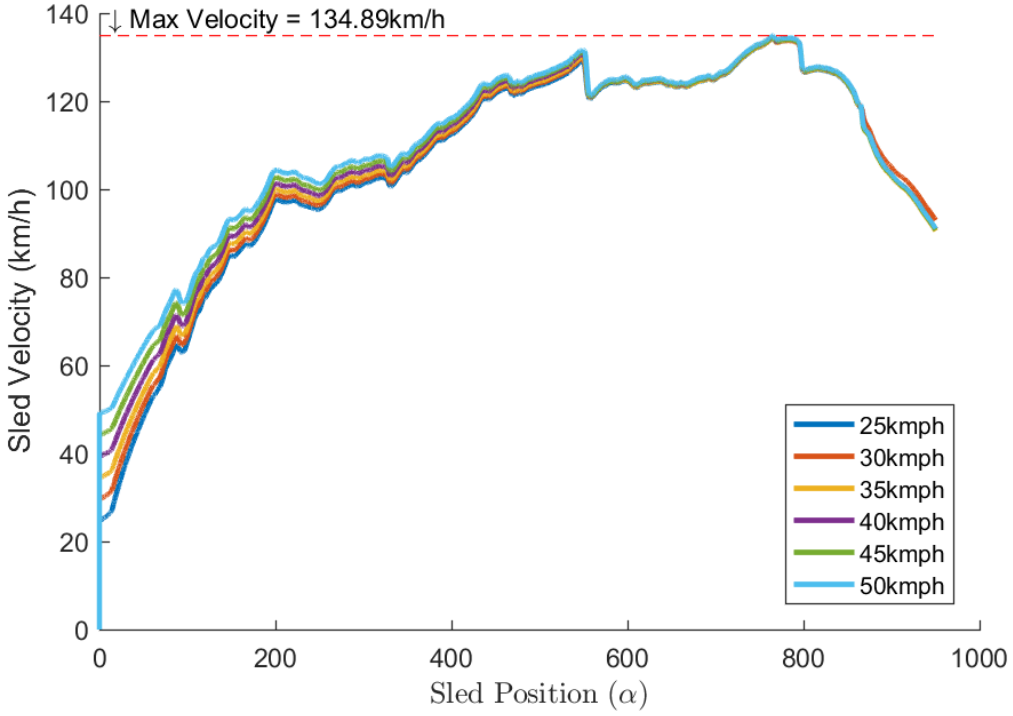

FIGURE 7.23: Sled velocity w.r.t. Sled position

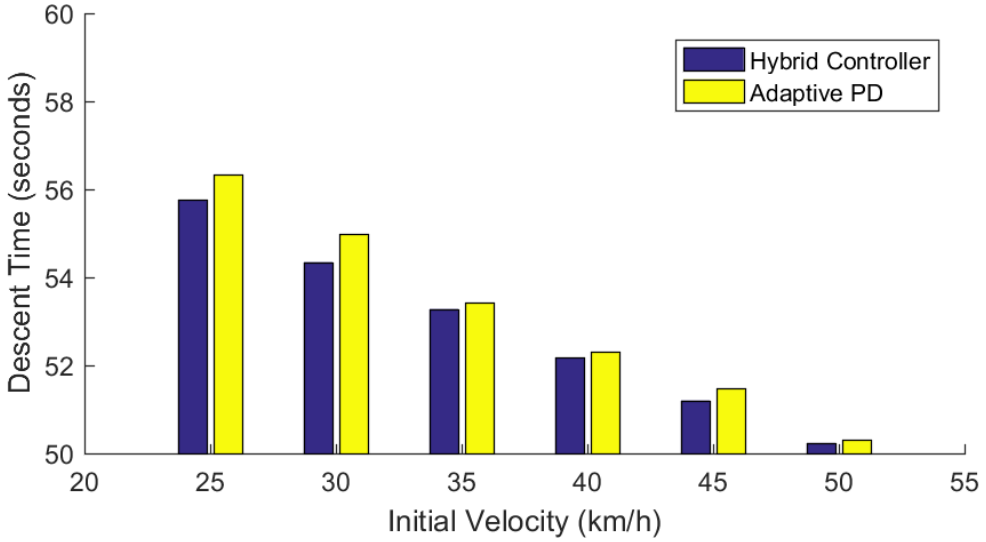

FIGURE 7.24: Descent time comparison with different initial velocities

Algorithm / Initial Velocity	**25**	**30**	**35**	**40**	**45**	**50**
Adaptive PD	56.314	55.170	53.607	52.455	51.700	50.198
MPC Hybrid	55.780	54.451	53.474	52.339	51.425	50.180

TABLE 7.1: Descent Time vs Initial Velocity vs Control Algorithm

between the results generated by the simulations and those recorded in the real world. In this subsection, two different verification methods will be used to scrutinise the fidelity of the 'optimal trajectories' generated by the hybrid controller. The first method compares the simulation data with recorded data obtained from the track designer of the PyeongChang Olympic track. The second method involves comparing the descent performance of the simulation against real athlete on the PyeongChang track.

7.6.1 Simulation vs Recorded Descent Data

The first method of fidelity validation compares the recorded data from an instrumented sled by the PeyongChang track designers to the data generated from the descent simulation controlled by the hybrid controller. The data available for comparison are the sled's velocities and the g-force experienced by the slider. Figure 7.25 shows the recorded data provided by the PyeongChang track design team, where the red line represent the sled's velocity throughout the track and the blue line represent the g-force. Both data were plotted against the sled's longitudinal position on the track.

In the recorded data, the sled had an initial velocity of 40 km/h at the 50 m block, where the athlete mounts the sled. A simulation using this initial condition were carried out and the results yielded were overlaid on top of the original graphics to produce Figure 7.26. Here, the orange dashed lines represent the simulated sled's velocity and the red dashed lines represent the

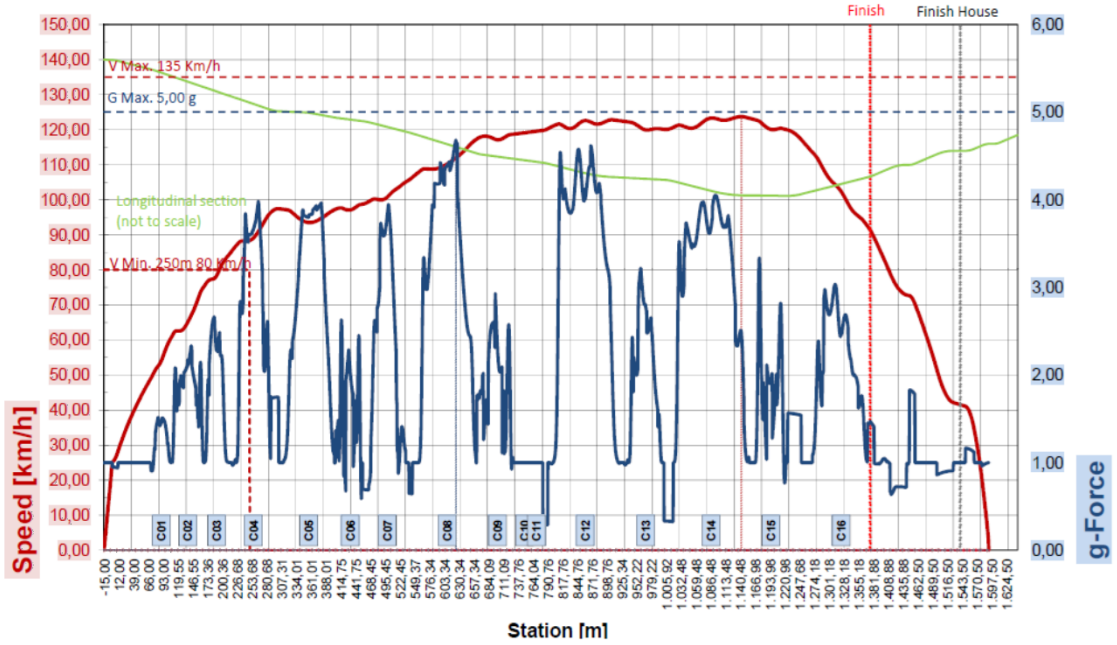

FIGURE 7.25: Recorded descent data of PyeongChang

	Max Velocity(km/h)	Max G-force(g)	RMS ΔVelocity	RMS ΔG-force
Recorded	124.8	4.6	n/a	n/a
Simulated	134.9	5.5	n/a	n/a
Recorded - Simulated	10.1	0.9	5.336	0.381

TABLE 7.2: Recorded and Simulated Metric Comparison

simulated g-force. The new figure shows great correlation(see Table 7.2) between simulated and recorded data during both high and low frequency (fast and slow changing dynamics) sections of the track. Comparing measured and simulated results demonstrates that, the current descent simulation possess a reasonably high levels of fidelity ($< 10\%$ difference for both velocity and G-force). It is worth noting here that the simulated run did not start with the same initial velocity as the recorded run. This is because the descent simulation does not include the sprinting phase and therefore can not account for the rapid acceleration at the start of the race. To compensate for this, a higher initial velocity was used to ensure a matching sled velocity as the first timing gate.

7.6.2 Simulation vs Athlete Performance

The International Bobsleigh & Skeleton Federation's official website (www.IBSF.org) stores the performance data of athletes for various training sessions and competitions. The data used for this analysis was from the most recent ITP (International Training Program) for Bobsleigh & Skeleton on 27/10/2017 ([49]). The performance data from 4 British athletes (2 females and 2 males) were selected for comparison: Dominic Parsons, Jeremy Rice, Laura Deas and Lizzy Yarnold. Each of their performance will be broken down into 2 seperate categories. The first

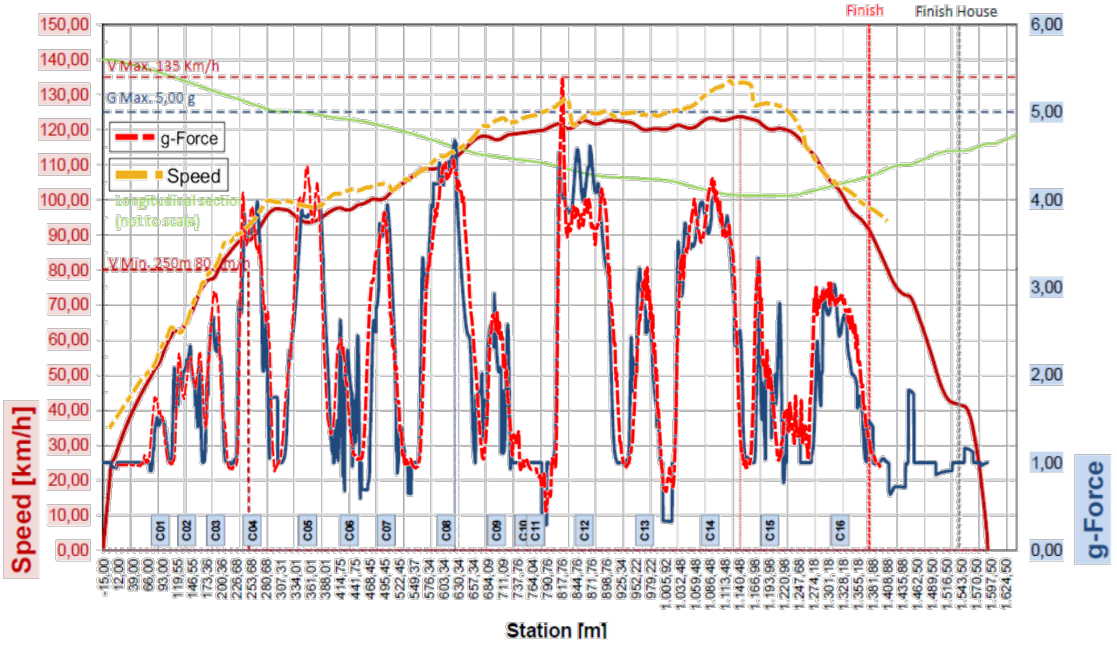

FIGURE 7.26: Recorded data with Simulation result overlay

being their intermediate times, that is the time at which they cross any of the 6 timing gates (at known longitudinal position) along the track. The second is their split speed at 4 out of the 6 timing gates, these were used here to both set the initial conditions of the simulation and to compare performance. Each athlete performed 3 descent on the training day and to take into account of human performance error, the average results across their 3 descent were used instead. Since the male and female athlete have different performance brackets due to physical differences between the genders, two simulation using different initial conditions were required for each of the validation comparisons.

Figure 7.27 shows that both male and female simulations' descent time match accurately to the athlete's actual descent time(i.e. on average, error is $<$ 0.2 seconds or $<$ 5 km/h) at each time gates. Both simulation yielded slightly faster descent than the athletes. Figure 7.28 verified the prior comparison through accurate matching the athlete's descent velocity as well. This second validation method also indicate a high level of fidelity in hybrid controlled descent simulation results. These validations allows the simulation results to be applied to athlete training with relative confidence.

7.7 Training Applications

The nature of elite sports makes it difficult to apply the research finding from virtual simulations, as the risk of transferring inaccurate and undesirable sliding techniques are high and would have hugely negative impact on athletes' performance. Therefore at the current time, athlete are not given access to steer the descent simulation in real-time, even though the capability is there all along. However, this did not stop the sports from incorporating the DTT as part of their training routine. Currently, the Skeleton athletes uses the DTT primarily as a priming tool for familiarisation of race tracks as well as a subjective assessment tool for athletes' steering style.

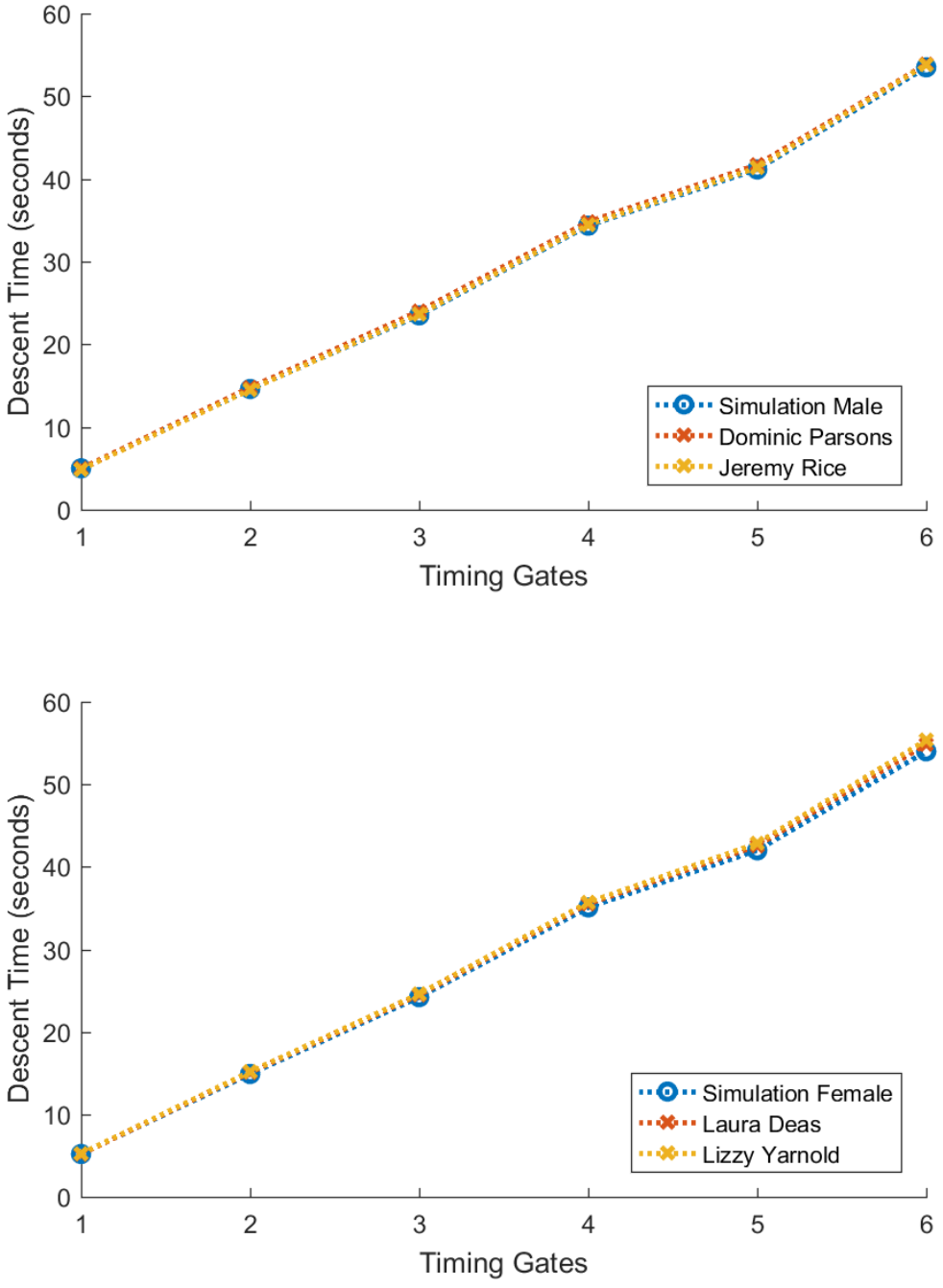

FIGURE 7.27: Simulated vs Athlete descent time comparison

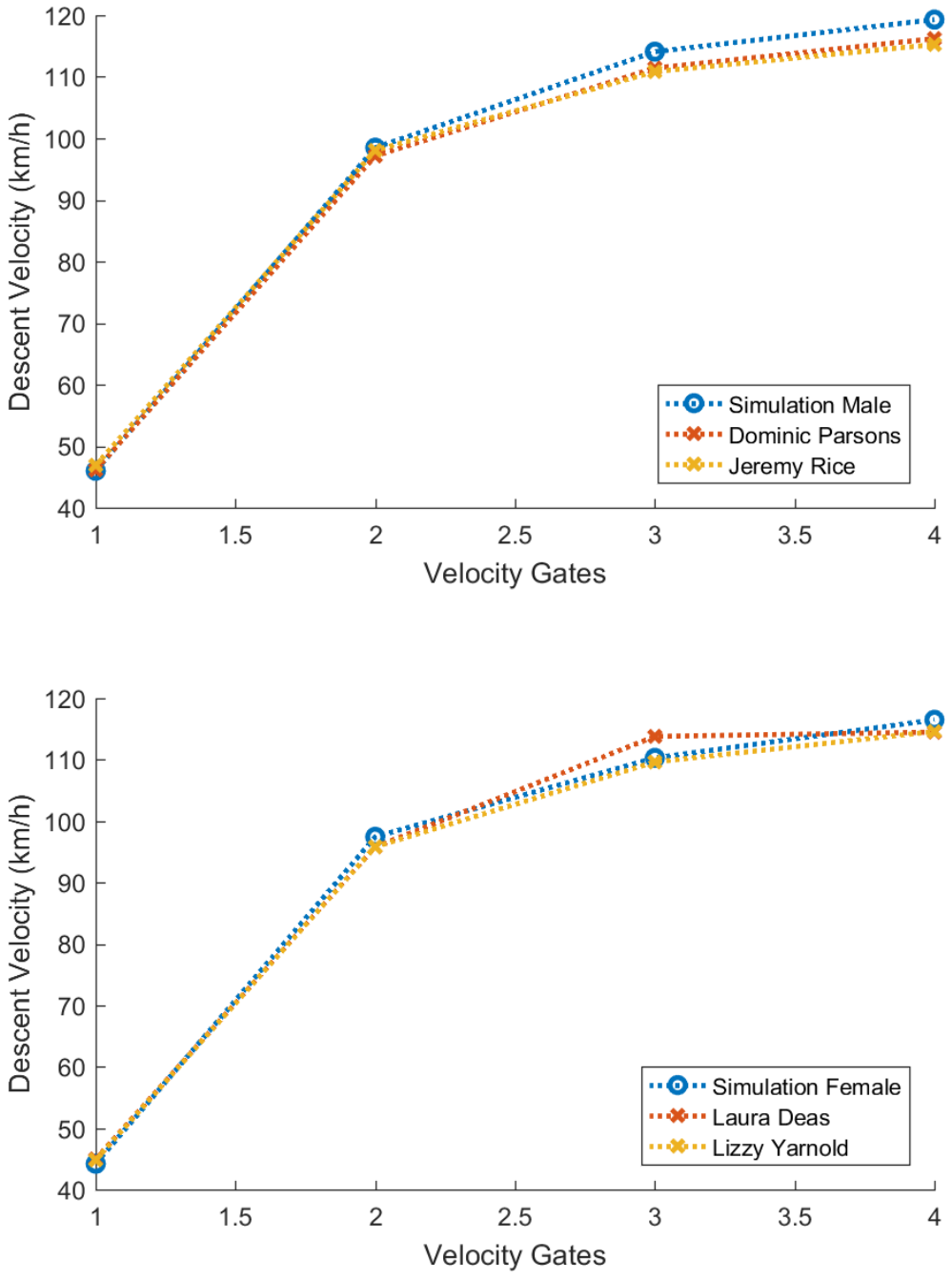

FIGURE 7.28: Simulated vs Athlete descent velocity comparison

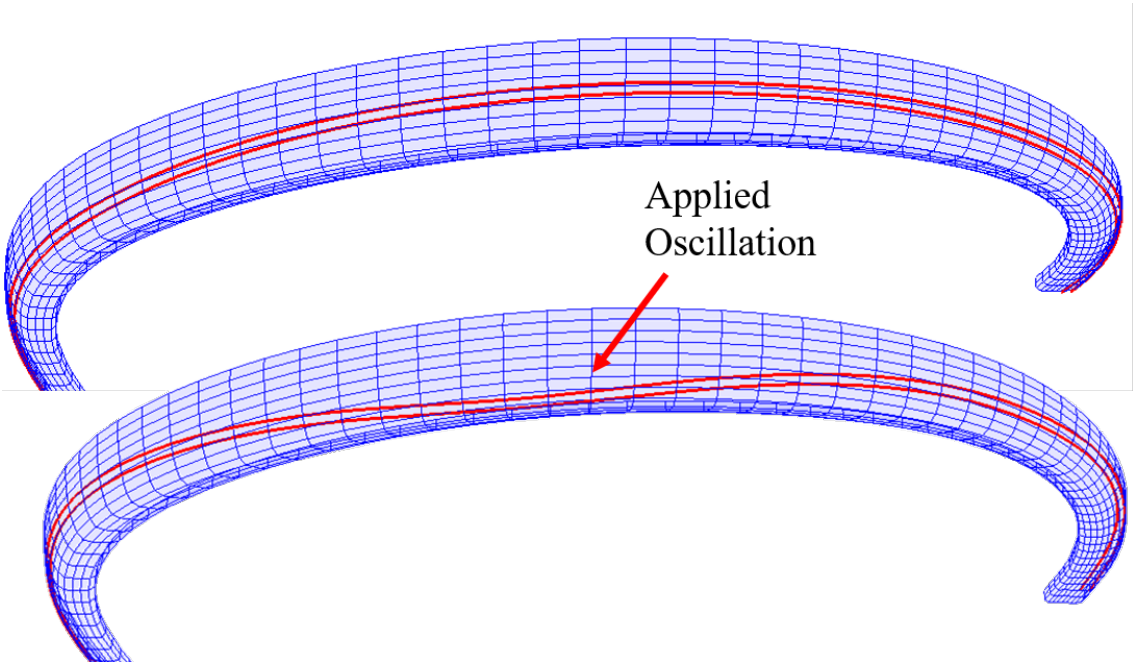

FIGURE 7.29: Trajectories comparison prior and after insertion of oscillation

Both of these applications uses the 'SimReplay' Simulink model, which plays a pre-recorded descent trajectories. The control designs developed in this section enables rapid productions of consistent, optimal descent trajectories to be used in these applications.

Since the athlete does not physically steer the simulation, therefore training-wise, only the accuracy of the descent trajectory matters but not the steering forces used to obtain said trajectory (The steering force are still important for simulation fidelity purposes). In the previous section, the fidelity of the optimally controlled trajectory was empirically validated. However, the according to the athletes' and coaches' subjective feedback, the trajectories generated this way is far too smooth (not enough oscillations around corners of a track) to be considered realistic in their opinion. This effect was the result of computer's ability to manage 'micro steering', which are the fine steering actions to maintain a smooth trajectory over the corners of any given track. These micro steers are performed within well within the limits of human athletes' steering abilities, both in terms of steering power and rate of steer. However the computer is far superior at detecting trajectory deviations and the forces acting upon the sled at any given moment, these allows the computer to react to sudden changes in descent faster and more accurately than its human counterpart. The difference between human and computer steering patterns can be further minimised by developing more human like control algorithms, this is a potential research area in the future.

For now, the most important contribution of the hybrid controller is its ability to produce consistent, repeatable and optimal baseline trajectories to use within the Simulink model. From this point, the coaches can manually apply steering actions at certain point during the descent and induce oscillations where they see fit. Figure 7.29 shows a comparison of descent trajectories in corner 5 of the PyeongChang track prior and after the insertion of oscillations.

7.8 Chapter Summary

This chapter concludes the research conducted thus far towards finding the optimal descent trajectory and its applications in athlete training. Although no 'true optimal descent' were achieved in the duration of this PhD, a framework of controller designs and model structures have being established. A validated attempt using comparatively simple control methods was made and generated the most optimal descent trajectories to use in the DTT for day to day training of the athletes. More sophisticated control methods such as non-linear MPC can be explored in the future to possibly yield better results.

Chapter 8

Conclusion

8.1 Research Summary

The research carried out throughout this PhD revolved around enhancing the training quality of GB Skeleton athletes using the DTT, and this was done through addressing the two research hypotheses as per section 1.4:

1. The quality of athlete training using the DTT can be improved by augmenting the Mark II DTT's hardware infrastructure and operational software.
2. It is possible to compute optimised descent trajectories for any race track under the DTT's simulated environment.

8.1.1 Hypothesis 1

Chapter 3 and 4 summarises the work performed with regards to the first hypothesis, which primarily concerns the augmentation process of the physical simulator and its associated software. Throughout the duration of this PhD, the Mark II DTT has been successfully augmented to include critical missing features. Some of the major new features include toe steering, leg G-force loading and most importantly, should pitch motion cuing. Minor features such as system overall safety infrastructure, easy to use operating user interface and an assortment of analysis software were also added to make up the Mark III DTT system. To date, the DTT has being commissioned for use at the Bath Sports Training Village to provide routine training sessions for the athletes.

The pitch actuation system was the major feature of this upgrade and its functionality to provide the vital motion cue were verified through 'Motion Stimuli Experiment III'. Initial experiment with the coaches received positive subjective feedback. Two pitching algorithms (scaled roll and scaled roll with washout) were then selected to be experimented with on the Skeleton athletes. Subsequent experiment with athletes concluded that not all athletes uses pitch as a motion cue, but the inclusion of said cue is important for immersion purposes in both cases. After

analysing the performance data on the athletes who uses pitch as a motion cue, it was shown that there was moderate improvement in steer timing. However, due to the small sample size, the result from this experiment cannot be conclusive. Instead, the subjective feedback of the athletes becomes much more important in selecting the optimal pitching algorithm for training. After reviewing the subjective feedback from both athletes and coaches, it was decided that the scaled roll pitching algorithm was best for cue identification whilst the scaled roll with washout algorithm was best for realism.

Overall, the feedback regarding the augmentation process of the DTT is extremely positive, all athletes and coaches agree that the additional cues helped with improving the quality of DTT training.

8.1.2 Hypothesis 2

Chapter 5, 6 and 7 presents the investigation of the second hypothesis. Previous researches [24, 33] concluded that it is possible to use minimum time control strategies to optimised descent trajectory for a single particle model of the Bob-Sleigh. However, applying above method in this PhD, which uses a real time non-linear model, proved to be difficult and a more intuitive and arguably more suitable method, MPC, was selected to control the descent simulation instead. As the first step of designing the MPC control system, a series of PD and adaptive PID controller were designed and implemented into the descent model to study the principle dynamics between the interaction of control forces and system response. Simulations performed using a PD controller yielded sets of performance data defined as 'Performance Indices', and by analysing the correlation between these performance indices the effects of system dynamics such as transverse distance travelled, and energy dissipated on descent time was collected. The resulting correlation enabled the design of the cost function for the MPC controller.

A Linear MPC was initially designed to control the descent but was quickly rejected due to its inability to produce stable control inputs for the dynamic non-linear descent model. An adaptive MPC controller has designed in its place and its performance was proven to be adequate on the straight sections of the track. The adaptive MPC however, did not provide adequate control on corner sections of the track, and therefore a hybrid controller using both adaptive MPC and adaptive PD was designed to control the whole descent on a given race track. The performance stability of the hybrid controller was validated, and its superior performance compared to other control algorithms designed thus far was shown through comparison experiments.

Finally, the fidelity of the trajectories generate by the hybrid controller was verified by cross matching against real life recorded data. The trajectories generated this way has now being implemented to work within the DTT, subjected to alteration from coaches and aid in enhancing the training quality of British Skeleton athletes.

8.2 Research Outcome Discussions & Future Research Recommendation

8.2.1 Driver Training Tool

Since the inclusion of the pitch motion cue proved to be successful, naturally, the next step would be to investigate the impact of other motion cues on athletes' training. One such cue would be yaw, or the feeling of turning at the top of an oscillation. However, the DTT was initially designed with only two motion cues in mind, roll and pitch. There are two different approaches to add yaw. The first is to start from scratch and design a new motion platform capable of movement in other degrees of freedom. The second is to place the existing motion platform onto a rotating surface. As an experimental equipment, the current DTT favoured flexibility in assembly over light weight and performance. The current pneumatic actuation system was also the result of budgetary constraints (Deny the use of electric actuation system)and University health and safety policies (Deny the use of hydraulic actuation system). These constraints imply that it would be inappropriate to use the second design approach for adding extra motion cues. It is therefore recommended that a new motion platform should be built with multiple degrees of motion in its design.

The physics engine at its current state is not of an adequate degree of accuracy for the athletes to practice steering on as it would be both dangerous (in terms of hardware system response) and irresponsible (in terms of developing bad sliding habits). Modifying the physics engine to include more up to date analytical models representing the act of sliding would be beneficial in moving the DTT towards being steerable by the athletes. Research regarding runner-ice interaction is currently under way in the University of Southampton. Once a satisfactory friction model has being developed, the process of placing said model into the current simulation would be easy due to the modular nature of the physics engine. However, from speaking with athletes and coaches, it would appear the steering of the sled is more complicated than the standard shoulder-knee model and it is therefore recommended that this be investigated thoroughly before attempting any form of human in the loop controlled descent.

8.2.2 Prediction of Optimal Descent Trajectory

In many ways, the research conducted in this PhD is about providing a framework of methods for approximating empirical solutions to the task. The quality of the solutions ties directly with the accuracy of the physics engine. Therefore although the hybrid controller currently in use can provide competitive descent trajectories for the descent simulation, it is still only an approximation to the true optimal descent trajectory. As possible future research, more complicated, non-linear optimal control methods (e.g. non-linear MPC) could be experimented with to obtain more analytical solutions that have the potential to both be faster and more stable.

Thus far in the thesis, the term 'optimal' has being used loosely, as there is not one universal optimal descent trajectory for a track due to the ever changing ice profile on it. Each different ice profile would in theory lead to a different optimal descent trajectory. All the simulation

performed in the DTT assumes a constant ice track surface which is not the case in real sliding environment and it is recommended to investigate into how the track surface changes with time, temperature, pressure and other varying parameters. If attaining such a model is possible, it would be of great benefit towards formulating sliding strategies tailored towards each athlete individually.

8.3 Impact on GB Skeleton

The research surrounding the Mark III DTT has being a success, at the time of writing up this thesis, the DTT system has being fully incorporated into GB Skeleton athletes' training routine and is getting utilised on a weekly basis. Although it is still incapable of simulating fully athlete steered descent with adequate accuracy, the current formats of training do not require it to do so. The DTT in its current state is fully capable of preparing the athletes for major and minor competitions alike.

Since 2015, the new DTT system has assisted the GB Skeleton team to obtain numerous gold to bronze medals in the World Championships and the European Championships [48]. It also contributed to many of the GB athletes achieving their personal best in world rankings. It is apparent that the DTT has become an invaluable piece of training equipment for the GB Skeleton Team.

References

[1] C. Sawade, "Learning Interventions in Olympic Skeleton through the use of Physical Simulation," Ph.D. thesis, Dept. Eng. Env., Univ. Southampton, Southampton, 2014.

[2] J. Roche, "Minimising Athlete Descent Time in Skeleton Using Race Simulation and Wind Tunnel Testing," Ph.D. thesis, Dept. Eng. Env., Univ. Southampton, Southampton, 2010.

[3] K. Bromley,"Factors Affecting Performance of Skeleton Bobsled", Ph.D. thesis, Dept. Mech. Eng., Univ. Nottingham, Nottingham, 1998.

[4] R. K. Huffman, "Design and Construction of an Interactive Virtual Reality Bobsled Simulator," Ph.D. thesis, Dept. Mech. Eng., University of California, California, 1995.

[5] T. Schouwenaars, "Safe trajectory planning of autonomous vehicles," Ph.D thesis, Dept. Aero. Astro., Massachusetts Institute of Technology, USA, 2006.

[6] A. Brooks, T. Kaupp, A. Makarenko, "Randomised MPC-based motion-planning for mobile robot obstacle avoidance," *2009 IEEE International Conference on Robotics and Automation*, 2009.

[7] A. Grancharova, E. I. Grotli, D. Ho, T. A. Johansen, "UAVs Trajectory Planning by Distributed MPC under Radio Communication Path Loss Constraints," *Journal of Intelligent & Robotic Systems*, vol. 79, pp.115 - 134, 2015.

[8] A. M. Green, D. E. Angelaki, "Internal Models and Neural Computation in Vestibular System," *Experiment Brain Research*, vol. 200, pp.197 - 222, 2010.

[9] A. Kelly, M. Hubbard, "Design and Construction of a Bobsled Driver Training Simulator," *Sports Engineering*, vol. 3, pp.13 - 24, 2000.

[10] D. E. Angelaki, K. E. Cullen, "Vestibular System: The many facets to a multimodal sense," *Annual review of Neuroscience*, vol. 31, pp.125 - 150, 2010.

[11] D. J. Murray-Smith, "An Application of the Individual Channel Analysis and Design Approach to Control of a Two-input Two-output Coupled-tanks System", *Acta Polytechnica*, vol. 52, 2012.

[12] F. Braghin, E. Sabbioni, "A Driver Model of a Two-man Bobsleigh," *Engineering of Sports*, vol. 13, pp.181 - 193, 2011.

[13] F. Braghin, F. Cheli, S. Melzi, E. Sabbioni, "Development of a Numerical Model of a Bobsled Driver: Trajectory Planning," *Proceedings of 12th Mini Conference on Vehicle System Dynamics, Identification and Anomalies*, pp.501 - 510, 2010.

[14] H. Rosenbrock, P. McMorran, "Good, Bad, or Optimal?," *IEEE Transactions on Automatic Control*, vol. 16, pp.552 - 554, 1971.

[15] J. Borah, L. R. Young, R. E. Curry, "Optimal Estimator Model for Human Spatial Orientation," in *Representation of Three-Dimensional Space in the Vestibular, Oculomotor, and Visual Systems* New York: The New York Academic of Sciences, 1988, pp.51 - 73.

[16] J. Roche, S. Turnock, S. Wright, "An Analysis of the Interaction Between Slider Physique and Descent Time for the Bob Skeleton," *Engineering of Sports*, vol. 7, pp.101 - 109, 2008.

[17] L. V. Steenson, S. R. Turnock, A. B. Phillips, C. Harris, M. E. Furlong, E. Rogers, L. Wang, "Model Predictive Control of a Hybrid Autonomous Underwater Vehicle with Experimental Verification," *Proceedings of the Institution of Mechanical Engineers, Part M: Journal of Engineering for the Maritime Environment*, vol. 228, pp.166 - 179, 2014.

[18] L. Singh, J. Fuller, "Trajectory generation for a UAV in urban terrain, using nonlinear MPC," *Proceedings of the 2001 American Control Conference*, 2001.

[19] M. G. Forbes, R. S. Patwardhan, H. Hamadah, R. Gopaluni, "Model Predictive Control in Industry: Challenges and Opportunities," *9th International Symposium on Advanced Control of Chemical Processes*, pp.532 - 539, 2015.

[20] M. Hubbard, M. Kallay, P. Rowhani, "Three Dimensional Bobsled Turning Dynamics," *International Journal of Sports Biomechanics*, vol. 5, pp.222 - 237, 1989.

[21] M. Hubbard, M. Kallay, K. Joy, J. Reus & P. Rowhani, "Simulation of Vehicle and Track Performance in the Bobsled," in Third Joint ASCE/ASME Mechanics Conference, San Diego, California, 1989.

[22] M. Neunert, C. Crousaz, F. Furrer, M. Kamel, "Fast nonlinear Model Predictive Control for unified trajectory optimization and tracking," *2016 IEEE International Conference on Robotics and Automation (ICRA)*, 2016.

[23] N. W. Heimstra, V. S. Ellingstad, *Human Behaviour - A Systems Appraoch*, Belmont: Wadsworth Publishing Company, 1972.

[24] R. K. Huffman, "A Three Degree of Freedom Model for Bobsled Dynamics Including Rotation," Masters thesis, Dept. Mech. Eng., University of California, California, 1991.

[25] R. K. Huffman, M. Hubbard, J. Reus, "Use of an Interactive Bobsled Simulator in Driver Training," in ASME Winter Annual Meeting, New Orleans, 1993.

[26] R. S. Kennedy, J. Drexler, "Research in Visually Induced Motion Sickness," *Applied Ergonomics* vol. 41, pp. 494 - 503, 2010.

[27] S. J. Anderson, S. C. Peters, K. Iagnemma, "Design and Development of an Optimal-Control-Based Framework for Trajectory Planning, Threat Assessment, and Semi-autonomous Control of Passenger Vehicles in Hazard Avoidance Scenarios," *Robotics Research - The 14th International Symposium*, 2009.

[28] V. A. Balakin, "Friction Performance of Sports Luges and Bobsleds Sliding Along Ice Track," *Journal of Friction and Wear*, vol. 17, pp.29, 1996.

[29] V . A. Balakin, V. N. Smirnov, O. V. Pereverzeva, "Sliding of a Sled Runner over Ice," *Soviet Journal of Friction and Wear*, vol. 9, pp.57 - 62, 1988.

[30] W. Baumann, "The Influence of Mechanical Factors on Speed in Tobogganing," *Medicine and Sport*, vol. 8, pp.453 - 459, 1973.

[31] W. T . Ang, P. K. Khosla, C. N. Riviere, "Kalman filtering for real-time orientation tracking of handheld microsurgical instrument," *International Conference on Intelligent Robots and Systsms*, 2004.

[32] W. Zhao, T. H. Go, "Quadcopter formation flight control combining MPC and robust feedback linearization," *Journal of the Franklin Institute*, vol. 351, pp.1335 - 1355, 2014.

[33] Y. L . Zhang, "Optimum Control of Bobsled Steering," *Journal of Optimization Theory and Applications*, vol. 85, pp.1 - 19, 1995.

[34] Y. Wang, S. Boyd, "Fast Model Predictive Control Using Online Optimization," *IEEE Transactions on Control Systems Technology* , vol. 18, pp.267 - 278, 2010.

[35] D. Allerton, *Principles of Flight Simulation*, Illustrated ed. John Wiley & Sons, 2009.

[36] J. J. Gibsen, *The Senses Considered as Perceptual Systems*, Boston: Houghton Mifflin, 1966.

[37] O. Houde, *Dictionary of Cognitive Science: Neuroscience, Psychology, Artificial Intelligence, Linguistics, and Philosophy*, New York: Psychology Press LTD, 2004.

[38] T. R. Kane, D. A. Levinson, *Dynamics: Theory and Application*, New York: McGraw-Hills, 1985.

[39] A. Boghossian, J. Brown, S. Zak, "PID Introduction," in *The Michigan Chemical Process Dynamics and Controls Open Text Book*, Michigan, 2006.

[40] Halvorsen, *Model Predictive Control in LabVIEW, Department of Electrical Engineering*, Information Technology and Cybernetics, Telemark University College, 2011.

[41] J. Bennet, A. Bhasin, J, Grant, "PID Tuning via Classical Methods," in *The Michigan Chemical Process Dynamics and Controls Open Text Book*, Michigan, 2006.

[42] J. A. Rossiter, *Model Predictive Control 2 - Main Components*, Dept. of Automatic Control and System Eng., Univ. Sheffield, 2014.

[43] M. Cannon, *Chapter 21: Model Predictive Control*, Dept. of Eng. Sci., Univ. Oxford, 2015.

[44] *Lecture 7, Root Locus Method - Introduction*, Dept. Mech. & Aero. Eng., HongKong Univ. Sci. & Tech., 2005.

[45] *Lecture 18, Root Locus Sketching Rules, Systems Modelling and Control*, Dept. Eng., MIT Open Courseware, 2007.

[46] J. Postel, "DOD Standard - Internet Protocol", *Protocol Document*, Information Science Inst., Univ. Southern California, California, 1980.

[47] P. Denne, "Motion Platform or Motion Seats", *Technical Report*, Transforce Development Ltd, 2000.

[48] IBSF.org: *Race and Results* [Online]. Available:
http://www.ibsf.org/en/races-results

[49] IBSF.org: *Training ITP Bobsleigh & Skeleton - PyeongChang 27/10/2017 03:00BST* [Online]. Available:
http://www.ibsf.org/en/component/events/event/169764

[50] Mathwork: *Nonlinear MPC Control of an Ethylene Oxidation Plant* [Online]. Available:
https://www.mathworks.com/examples/mpc/mw/mpc-featured-ex37361661-nonlinear-mpc-control-of-an-ethylene-oxidation-plant.html

[51] Mathwork: *Stability Margins in Control System Tuning* [Online]. Available:
https://uk.mathworks.com/help/control/ug/interpreting-stability-margin-plots.html

Appendix A: Background Control Theory

.1 Introduction

There are vast amounts of research published regarding to the theories and applications of control techniques applicable to this PhD thesis and it would be unrealistic to describe them all in detail. Instead, this chapter cover the basic principal theories regarding to the control techniques used within the thesis. These include introductions to basic root locus technique and background theories for both PID and MPC control designs.

.2 Root Locus

An open loop control system is a non-feedback system, where the control input is not affected by the output of the system. On the other hand, a closed loop control system is one where the output is feedback into the controller and used as part of the function that calculates the new control inputs. Closed loop systems are designed to automatically achieve and maintain a desired output level. Figure 5.1 illustrates a typical closed loop proportional control system, where K is system gain and H(s) is the open loop system transfer function.

The roots of the closed loop characteristic equation are the locations of the closed loop poles. For the configuration in figure 5.1, the closed loop transfer function is shown in equations 1 and the characteristic equation is the denominator of the transfer function.

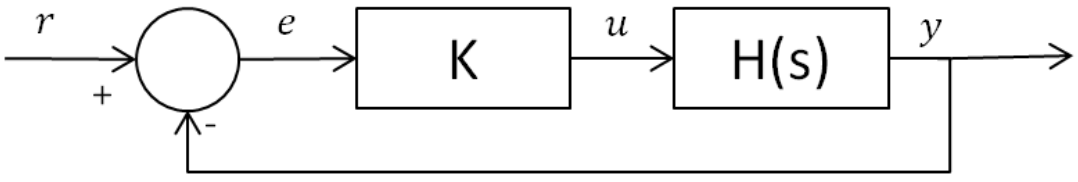

Figure 1: Example closed loop control system: P controller with unity feedback

Root Locus Plotting Rule	Description
Rule 1: Number of branches = Number of Poles	The number of root locus is determined by the number of poles in the closed loop characteristic equations.
Rule 2: Symmetrical about the real axis	Complex roots of the characteristic equation always come in conjugate pairs.
Rule 3: Root locus on the real axis always plot to the left after an odd number poles/zeros	Root locus only exist between the 1-2, 3-4, 4-5 pairs of poles or zeros.
Rule 4: Root locus begins at poles ends at zeros	Root locus only travel from Pole to zeros, or if no zeros are available between two poles, the root locus will meet and break away into infinity at a breakaway angle depending on the number of poles heading to infinity.
Rule 5: Imaginary axis crossing	Whilst the roots on the root locus are on the left hand side of the imaginary axis, the system is stable and exhibits damped system responses. If any of the roots land on the right hand side of the imaginary axis, the system is unstable and exhibits undamped system responses.

Table 1: Root Locus Plotting Rules [45]

$$TF_{cl} = \frac{KH(s)}{H(s)} \tag{1}$$

The relative stability of a closed loop system and its transient performance can be defined by the location of its closed loop poles. However, these locations will move when the control parameter (K) varies. Analysing the stability of a closed loop system can be difficult as the complexity of the system increases. The root locus is a graphical analysis method that uses knowledge of the open loop transfer function to determine the loci of closed loop poles in the s-plane as K varies, consequently describing the systems behaviour [44]. The root locus provides measure of sensitivity for the system and can be used for designing controllers to achieve specific responses (e.g. damping ratio). The root locus used in this particular thesis was drawn with Matlab. However, in order to interpret the root locus graphs, a basic understanding of the sketching method is necessary. Table 5.1 presents 5 basic rules for plotting the root locus used within the thesis. Figure 2 shows an example root locus plot following the plotting rules.

.3 Proportional, Integral, Derivative Control

Proportional, Integral, Derivative (PID) control is one of the most commonly used control algorithms in industrial control. The popularity of PID controller is related to its simplicity in design and application as well as its robust performance under a wide range of operating conditions. As the name suggests, PID control is comprised of three separate control algorithms: proportional,

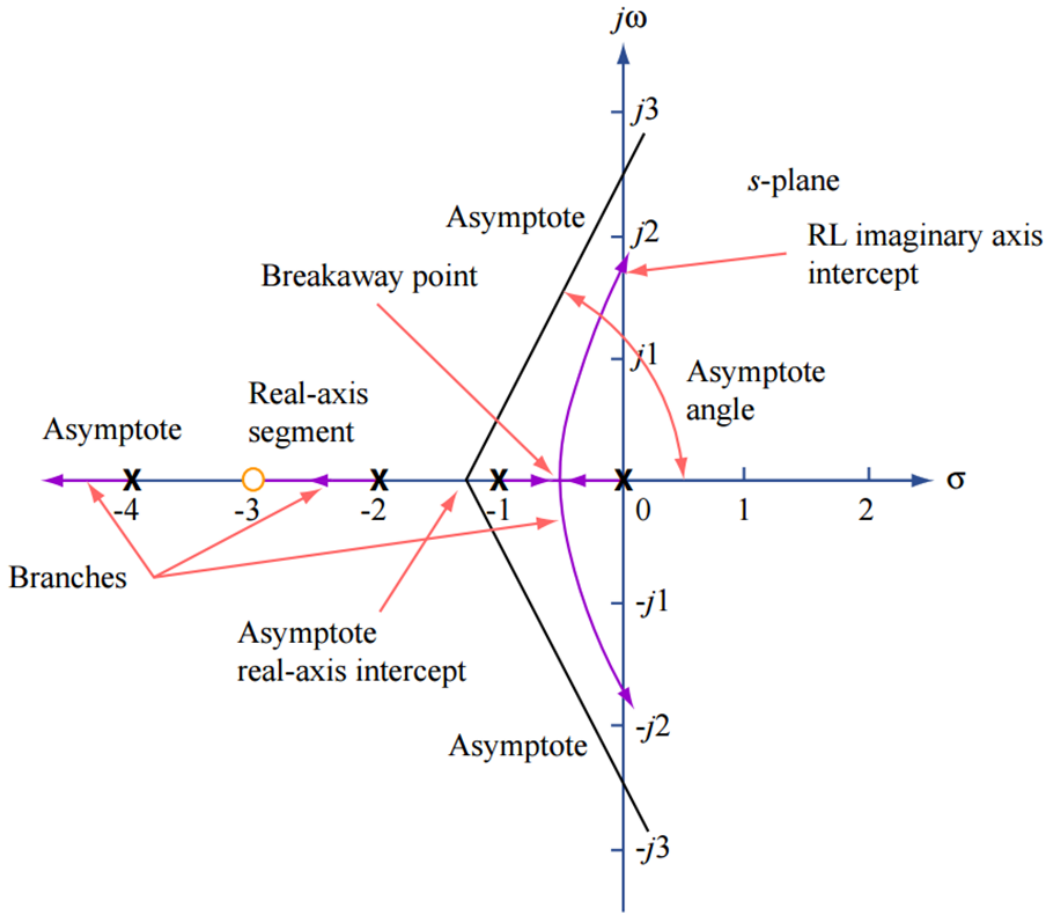

FIGURE 2: Example root locus plot demonstrating the plotting rules [45]

integral and derivative. These control algorithms operate on the basis of the error between desired output signal and the actual output signal from the plant to produce individual controlled variables (i.e. control input). The sum of these control variables are then used to actuate the plant, thus completing the closed loop system. Equation 2 governs the behaviour of the PID controller and Figure 3 illustrates the structural architecture of a typical PID controller.

$$u(t) = K_p e(t) + K_i \int_0^t e(\tau)d\tau + \frac{K_d de(t)}{dt} \tag{2}$$

Where:

- K_p, K_i and K_d are the proportional, integral and derivative gains respectively
- $u(t)$ is the controlled variable
- $e(t)$ is the error between the output and reference

Proportional (P) control is one of the simplest forms of feedback control which can be applied to a closed loop system. P control produces control inputs as scaled value of the instantaneous error signal (i.e. $K_p e(t)$) and provides faster responses than the other control designs. However

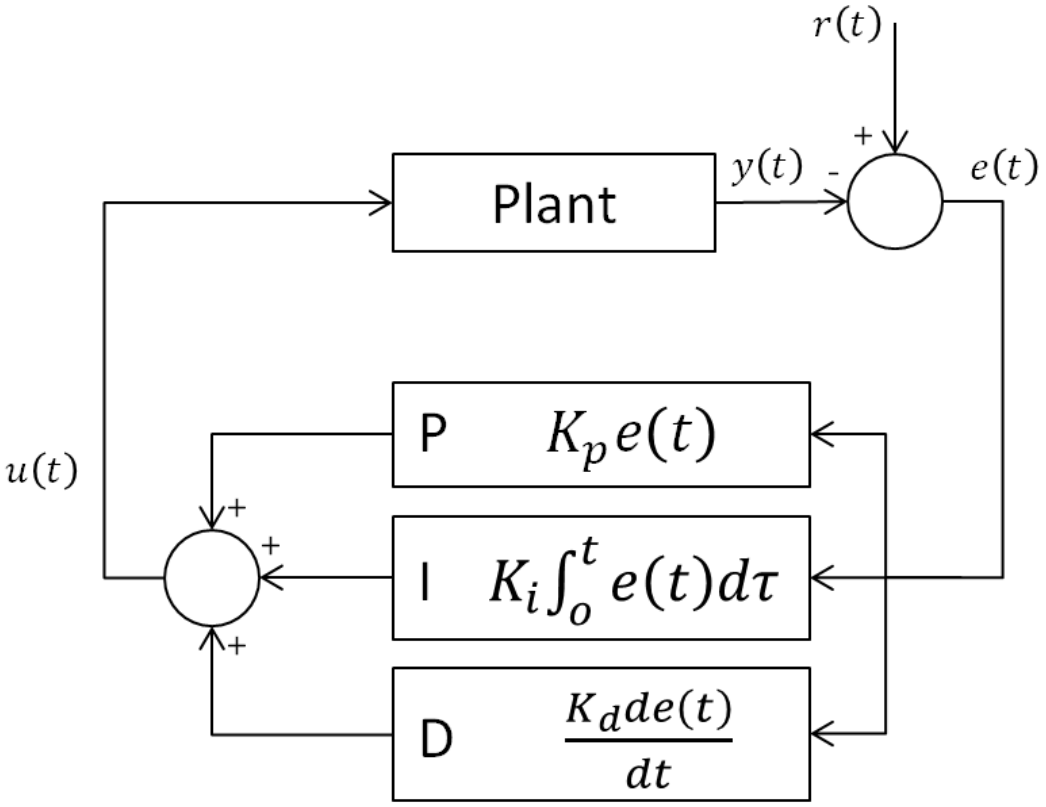

FIGURE 3: Block diagram of basic PID architecture

it is prone to produce undesirable offset, which implies that the system could not be kept at a desired output level in steady state. Although it is usually impossible to eliminate, the offset can be minimised by combining P control with another form of control such as I or D control [39]. Integral (I) control is another form of feedback control. It is often used in conjunction with P control to remove the offset. The I control produces control inputs proportional to the accumulated past errors (i.e. $K_i \int_0^t e(\tau)d\tau$). This form of control usually produces a slower response time and can destabilise the system. However, if the margin for error on the manipulated variable (system output) is small, then I control should be included in the design [39].

Derivative (D) control is a feed forward control scheme that extrapolates the rate of change in error and predicts the feature behaviour of the system. The D control uses the equation $\frac{K_d de(t)}{dt}$ to generate its control inputs. This implies that D control works against the control effort of P and I controls, slows down the system response and minimises the potential of system instability. A D controller measures only the change in error and do not know where the reference point is. Therefore it cannot actuate the system to a steady state and must be used in conjunction with P, I or PI controllers [39]. There are many types tuning methods for PID based control designs, such as trial and error and process reaction curve methods. However, the most common classical controller tuning methods are the Ziegler-Nichols and Cohen-Coon methods. These are often used when the mathematical model of the system is not available. The Ziegler-Nichols method

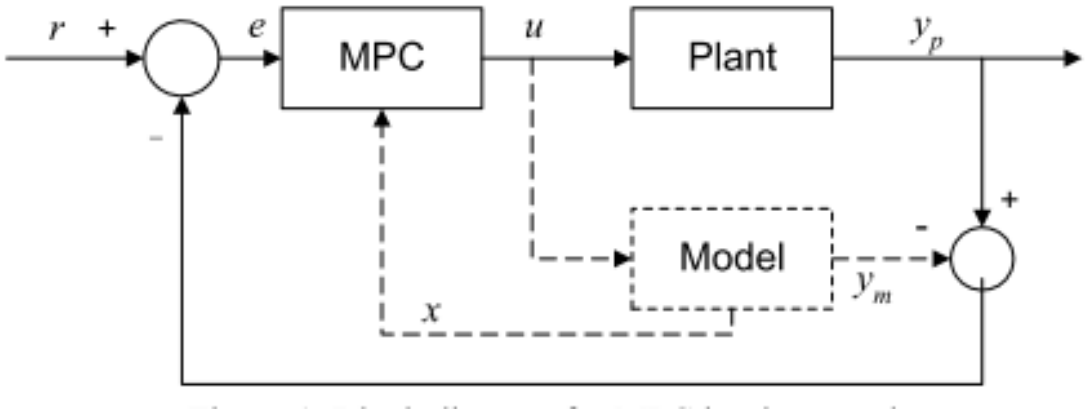

FIGURE 4: Basic Schematic of MPC [40]

works for both open and closed loop systems and the Cohen-Coon method is typically adopted to control open loop systems. For detail of the tuning method, refer to literature [41].

.4 Model Predictive Control

Traditional feedback control schemes operate by adjusting control signals in response to the change in input reference and output feedback. Model predictive control (MPC) focuses on the concept of using an explicit model of the process to predict future behaviours of the plant. Combining this with the ability to observe past and currently states, MPC can produce a set of optimal future control actions (inputs) before a change in plant state (output) has occurred. This predictive ability enables a controller to make adjustments that are smoother and closer to the optimal control values.

MPC is a subsector of optimal control. To solve an MPC is to solve an online optimisation problem at each sample instant k. The goal is to calculate a new control input vector u_k by solving said optimisation problem whilst taking into consideration of constraints.

An MPC algorithm consists of:

- A model of the plant
- Optimiser (i.e. cost function to be minimised)
- Constraints on inputs and outputs

.4.1 Receding Horizon

To understand the concept of moving horizon, a basic knowledge of what horizons represent is required.

- Prediction horizon (P): The number of samples ahead of current sampling instant, in which the process model in MPC predicts the plant output. Shorter prediction horizon

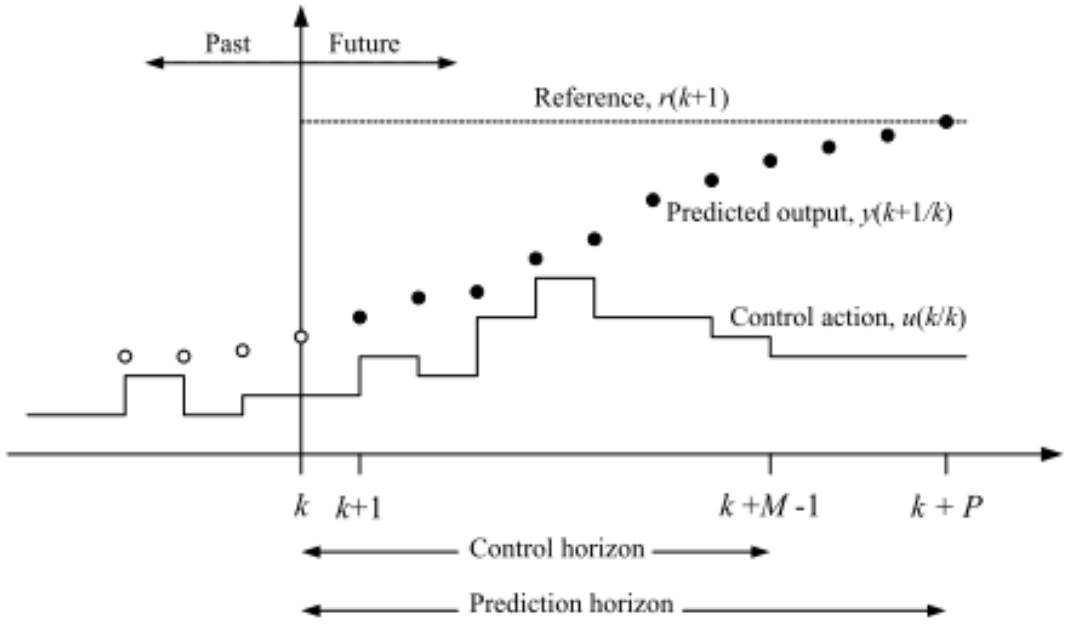

FIGURE 5: Receding horizon [42]

reduces prediction capabilities, but longer prediction horizon diminishes computational performance.

- Control horizon (M): The number of samples ahead of current sampling instant, in which the optimiser can affect the control actions. Shorter control horizon promotes smoother changes in control action. Longer control horizon promotes more aggressive changes in control action.

For the purpose of implementation, MPC is usually treated as a digital controller (discrete time domain). As shown in figure 5, at each sampling instant, an optimisation problem is solved with respect the control and prediction horizon length, the goal of said optimisation problem is to move the predicted output as close to the reference output (r_{k+1}) as possible. A set of future control action is calculated $u_k, u_(k+1) u_(k+M-1)$, the first of these control actions is then implemented into the plant and the process is repeated at the next sampling instant. As the length of control and prediction horizon tend not to change in most MPC algorithms, this cause a shift of those horizons, known as the receding horizon effect.

.4.2 Process Model

MPC relies on dynamic models of the process, which can be represented in a number of formats. MPC utilises these explicit process model to predict the future response of the plant and produce predicted future inputs.

Model Type	**Description**
Linear Dynamic Models	Most general linear state space model. Useful for approximation of simple systems.
Linear Time Invariant Models	Subgroup of Linear Dynamic Models
Input-output Models	Used when internal structure of the system is unknown. Obtained through system identification usually. Useful for suppressing state variables.
Distributed Models	Used in the case of system not being spatially uniform.
Discrete Time Models	Used for analysing systems that is sampled at discrete times.

TABLE 2: Dynamic Models

For linear systems, a simple data driven model is usually used. The most common of these linear models used by application tools such as Matlab and LabVIEW is of the form (i.e. discrete LTI):

$$X_{k+1} = AX_k + BU_k$$
$$Y_k = CX_k + DU_k$$

where

- X_k – State vector at sampling instant k.
- u_k – Input vector at sampling instant k.
- Y_k – Output vector at sampling instant k.
- A – State transition matrix
- B – Input matrix
- C – Output matrix
- D – Feedforward matrix

.4.3 Cost Function

In order to perform optimisation, MPC requires a cost function to be minimised. The cost function is usually a combination of dynamic matrices and weight matrices and the format for arranging the matrices is usually quadratic, see below:

$$J = \sum_{k=0}^{N_p} (Y_k - r)^T Q (Y_k - r) + \sum_{k=0}^{N_p} \Delta u_k^T R \Delta u_k$$

subject to

$$\Delta u' \leqslant \Delta u_k \leqslant \Delta u''$$

where

- N_p – Prediction Horizon
- r – Reference point
- Y_k – Predicted process output at sampling instant k
- Δu_k – Predicted change in control value at sampling instant k
- Q – Output error weight matrix
- R – Control input weight matrix
- $\Delta u', \Delta u''$ – constraints on inputs

The method for solving the above differential equation varies depending on the format of the cost function, the properties of the state matrix and the constraints imposed upon the systems. Tuning of the system is done by changing the values of inside matrix Q and R in correspondence to the required elements in the state or input vector. This has to be performed online, which when dealing with large X, may pose a considerable problem on computational power. Many schemes have being developed to speed up this optimisation process to enable fast online MPC designs.

.4.4 Constraints

All physical systems have constraints. This could be a limit on the length of an actuator or the flow rate of pneumatic systems. Superposed constraints to keep operation safe are also vital (e.g. pressure limit). One of MPCs advantages is that by design constraints can be added easily into the cost function when performing optimisation. Constraints are usually applied at either the input or the output or both.

Constraints play a major part in the optimisation of the system. It may cause instability, increase computational time and sometimes causes the optimisation to run into infeasible solutions. In some schematics, the constraints are excluded while performing optimisation and are later superposed on top when applying control inputs to the system. Other control schemes adopt a more adaptive approach, and introduce soft constraints [43], so that the constraints applies when system can remain stable and disappears when not.

Appendix B: Author Publication

Available online at www.sciencedirect.com

ScienceDirect

Procedia Engineering 00 (2016) 000–000

www.elsevier.com/locate/procedia

11th conference of the International Sports Engineering Association, ISEA 2016

Analysis of Performance Indices for Simulated Skeleton Descents

Chen Gong*[a], Christopher W.G. Phillips[a], Eric Rogers[b], Stephen R. Turnock[a]

[a]*Performance Sports Engineering Laboratory,*
[b]*Department of Electronics and Computer Science*
University of Southampton, University Road, Southampton, SO16 7QF, UK

Abstract

In the winter Olympic sport of Skeleton, sliders sprint and load themselves onto the sled facing head forwards. The slider uses primarily their shoulders and torso to apply control to the direction of the sled as it progressively gains speed during its descent. These small control course keeping maneuvers alongside more severe use of toe tapping onto the ice will help determine the eventual trajectory of the sled. It is therefore of interest to consider for a possible trajectory what control actions will determine the fastest descent time and in particular what metrics should be examined. In this paper a three degree-of-freedom simulation has been developed to analyse the influence of different control strategies on the descent time of a bob-skeleton. A proportional-derivative (PD) controller is used to steer the simulation down a representation of the Igls ice-track. Parametric variations of the simulation's performance were analysed and compared to identify possible correlations for controllers assist the design of an optimal controller. Analysis of the results have identified positive correlations between descent time, transverse distance travelled and energy dissipation establishing that the fastest descent time is achieved by minimising the energy lost through the descent.

Peer-review under responsibility of the organizing committee of ISEA 2016
Keywords: Skeleton;Optimisation;Race time simulation; Proportional-derivative Control; Trajectory evaluation

Nomenclature

α_c	longitudinal position of the particle representing the sled
β_c	transverse position of the particle representing the sled
F_{act}	total active forces on the particle representing the sled
r_α, $r_{\alpha\alpha}$	spatial derivative in the longitudinal direction
r_β, $r_{\beta\beta}$	spatial derivative in the transverse direction
$r_{\alpha\beta}$	spatial derivative in both longitudinal and transverse direction
m	mass of particle representing athlete and sled
g	acceleration due to gravity
h_0, h_f	initial and final height of the particle representing the sled
v_0, v_f	initial and final speed of the particle representing the sled
u(t)	control input
e(t)	error between reference position and actual position
K_p	proportional gain
K_d	derivative gain

* Corresponding author. Tel.: +442380596616; fax: +0-000-000-0000.
E-mail address: C.Gong@soton.ac.uk

Peer-review under responsibility of the organizing committee of ISEA 2016.

1. Introduction

The sport of skeleton involves the headfirst descent of an ice track performed by athletes on a sled. The goal is to achieve the fastest descent time. During a race, the sled can reach a maximum speed of around 130km/h; with the G-force reaching 5G through high banking corners and constant high levels of vibration due to uneven ice surfaces [1]. It would be of significant benefit to both coaches and athletes if an *a priori* 'optimum' trajectory could be predicted for the descent of a given track.

Through simulation, [4, 5] have shown that it is possible to find the 'optimum' descent trajectory for the Bobsleigh using optimal control algorithms. Due to the similarities between the underlying dynamics of the two sports, it is reasonable to believe a comparable approach could be used to find the 'optimum' descent trajectory for skeleton. An important element in designing any optimal control algorithm is the selection of the cost function to be minimised. In [5] it is stated that different costing strategies (i.e. minimum length path vs minimum energy dissipated path) have produced consistent difference in results, deducing that the final decent time will reduce if the energy dissipated is minimised. Though the results are promising, it cannot be trivially generalised to skeleton, since there exists discrepancies within the fundamental dynamics of the sports.

The objective of the work reported here is to identify the optimal cost function strategy for the skeleton descents by analysing the performance in simulation of a three degree-of-freedom skeleton dynamics model. Results from the simulation are used to identify feasible cost function for onward analysis.

2. Methodology

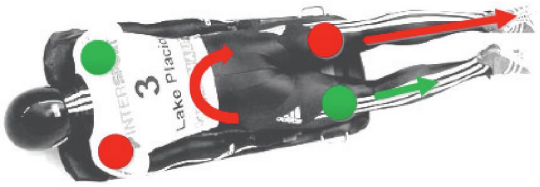

Fig. 1. The principles of steering a skeleton [1]. This figure represents a right turn. The athlete applies pressure with left shoulder and right knee. This creates a frictional imbalance between left and right runners resulting in a turning moment.

The one degree-of-freedom skeleton dynamic model built by [2] has been extended to two degrees-of-freedom following similar underlying equations of motion and surfacing mapping techniques as [3]. The model is steered by the empirical based steering model from [1], which produces yaw moments, in the same manner by which the athlete achieves a steer on the sled as shown in Figure 1. The new model is therefore extended to three degrees-of-freedom to include the influence of sled yaw relative to its track. Equation (1) relates to the transverse sled motion in the model to the actuation F_{act} generated from the empirical steering model.

$$s^2\beta_c(s) = \frac{-\left(F_{act}\cdot r_\beta + \left(\left(s^2\alpha_c(s)^2 r_{\alpha\alpha} + s^2\beta_c(s)^2 r_{\beta\beta} + s^2\alpha_c(s)\beta_c(s) r_{\alpha\beta}\right)m\ \cdot r_\beta\right)\right)\cdot r_\alpha^2}{m\left(\left(r_\alpha \cdot r_\beta\right)^2 - r_\alpha^2 r_\beta^2\right)} \qquad (1)$$

The track surface, following the convention of [3,6] and illustrated in Figure 2 uses a parametric representation of the actual modelled three dimensional surface where the position $\boldsymbol{r}$, is given as a function of a distance parameter α and transverse parameter β. In (1) the first and second derivatives of position $\boldsymbol{r}$ in directions α, β are written using the appropriate subscript. The forces acting on the sled, F_{act} (i.e. aerodynamic drag and lift are calculated using similar fundamental physical equations as [3,6], runner ice friction is forces as computed in [2]) and those due to steering control or wall collision will act to counter the gain in kinetic energy as the potential energy of the mass of the slider and sled is converted into kinetic energy. The air drag assumes a constant value of drag coefficient based on typical projected area of sled and slider. Likewise a semi-empirical value for ice friction coefficient is used.

$$\boldsymbol{r} = \begin{Bmatrix} x \\ y \\ z \end{Bmatrix} = f(\alpha, \beta) \qquad (2)$$

The track geometry, Figure 2(a), used for this simulation is a representation of the Olympic Bob track in Innsbruck, Igls, Austria. The model was built as reconstructions of track topography and a combination of straights and corners with estimated cross-section. Igls was selected as it contains a board range of corner geometries, making it suitable for testing the robustness of the dynamic model and to ensure that results obtained on this track has a fair degree of generality.

The track model was constructed by estimating the track cross-sections from physical measurements and digital images at key locations along the track. The track's centerline, Fig. 2(a) was estimated using imagery from Google Earth. 14 points were equally distributed along each cross-section (Fig. 2(b)). A cubic spline was then fitted through the respective points in each cross-section, generating 14 new splines along the length of the track. New cross-sections were interpolated using the 14 splines at 1.5m intervals along the track. This created a 3x14x890 matrix of points that could be used by the simulation as an approximation of the Igls track.

The simulation was built in the real-time Matlab-Simulink environment. A PD controller was used to steer the simulation and is designed with the objective of following a descent trajectory (β_{ref}) pre-defined by subject matter experts to be the best line of descent. The PD controller treats the dynamic model as a 'black box' and asserted control inputs $(u(t))$ in the form of nominal left and right steering forces. Said steering forces were determined by the error $(e(t))$ between current sled centre position β_c and the desired reference position β_{ref}. The magnitude and rate of these steering forces were further controlled by tuning the controller gains (i.e. proportional gain K_p and derivative gain K_d), equation (3) illustrates the basic principles of the PD controller. A 2nd order Butterworth low pass filter was implemented at the output of the PD controller to represent the steering input responses of a human athlete. The controller gains were tuned over a region ($K_p \in [0.015, 0.05]$, $K_d \in [0.04, 0.07]$) where the dynamic model were able to complete the entire simulated descent, this region of controller gains was named the 'stable region' and the corresponding steering forces were recorded. It was shown that the steering forces were directly proportional to the magnitude of the controller gains.

$$u(t) = K_p e(t) + \frac{K_d de(t)}{dt} \tag{3}$$

The intention of the simulation is that the relative proportional magnitude of ice friction and air drag forces should be tuned so that the simulated descent time agrees to a reasonable level with a typical human descent in Igls. This gives confidence to the subsequent analysis examining the course keeping actions performed by the PD controller and the impact of tuning the controller gains. Said simulations were performed over the 'stable region', the performance indices (i.e. descent time, distance travelled & energy dissipation) were recorded and their correlation were used to design the cost strategies for the optimal controller.

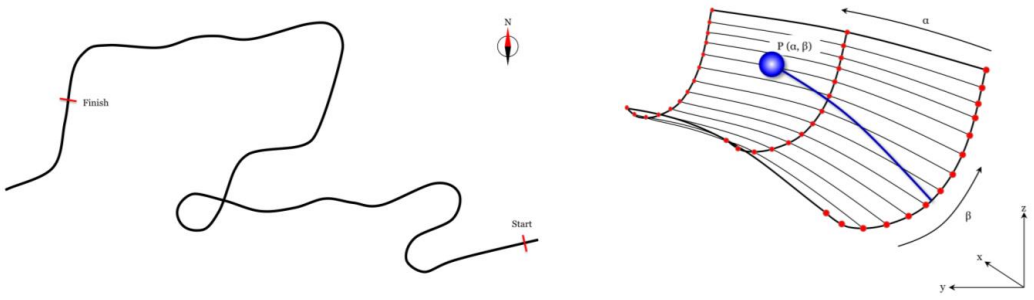

Fig. 2. (a) Overview of the Igls Bob track. (b) Schematic of track cross-section coordinates adapted from [6].

3. Simulation Results

3.1 Descent Time

Descent time is the most self-evident performance index to investigate as it ties in directly to the outcome of the race. Although the descent time is *ad hoc* to the dynamic model and track geometry, it can however adequately provide an understanding of general system behaviour and be utilised as a performance reference to gauge against other possible indices.

Fig. 3 (a) indicates that the descent time exhibits a quadratic structure initially decreasing proportionally with the value of K_d and K_p. However, once K_d is sufficiently small, the descent time increases as K_p approaches its stable boundaries. This is not truly representative of the index behaviour for the following reason:

When K_d is small, a large K_p will induce aggressive control actions and lead to instability in the system therefore leading to undesired oscillations, which causes a slower descent time. This is a defect caused by design of the controller and will skew the simulation data. In Fig. 3 (b), the x and y axes represent K_d and K_p respectively, the colour of the contour represent descent time. To avoid using data resulted from the aforementioned defect, a 'Representative Region' was put in place, indicated by the dashed box. The region cuts off at $K_p = 0.04$, which is the minimum value of K_d therefore within the region, the PD controller remains D dominant and should provide useful data. In Fig. 3 (b), the x and y axes represent K_d and K_p respectively, the colour of the

contour represent the general trend of descent time with respect to steering forces: Increments in steering force leads to increments in descent time. To keep the analysis relevant, only data from the representative region will be used for the other two performance indices.

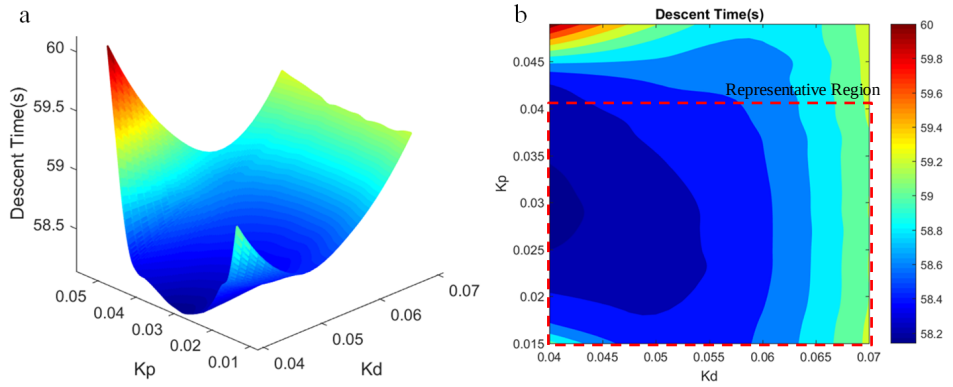

Fig. 3. (a) Surface plot of descent time vs steering force; (b) Contour plot of descent time vs steering force.

3.2 Transverse Distance Travelled

In the parametric surface representation each longitudinal spline, although varying slightly and not actually representing a viable trajectory would represent a minimal distance. The cross track error e.g. the distance away from the prescribed trajectory is referred to in this work as the transverse distance travelled and its total is calculated by integrating |β| over the duration of the simulated descent. α was not included in the calculation since all simulated descent start and end are at the same α values.

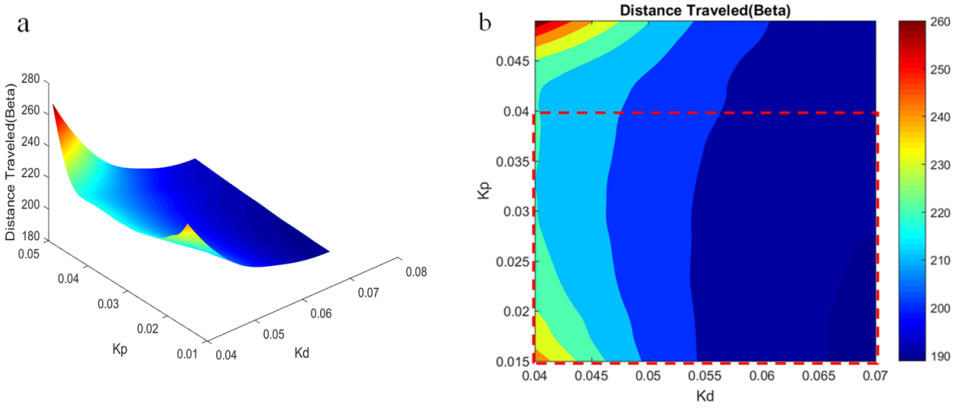

Fig. 4. (a) Surface plot of travel distance vs steering force; (b) Contour plot of travel distance vs steering force.

Fig. 4 (a) presents the simulation data in different axes orientation to provide a better view for the overall system behaviour. It is clear that distance travelled is also skewed by the controller defect. In Fig. 4 (b), the x and y axes represent K_d and K_p respectively, the colour of the contour represent the trend of distance travelled with respect to steering force; increments in steering force leads to decrements in travel distance.

3.3 Energy Dissipation

In this model, energy is lost through friction and drag. The dissipation is calculated by subtracting kinetic energy gained from the potential energy lost through the simulation. Kinetic energy gained is calculated via $\frac{1}{2}m(v-v_0)^2$ where v_0 is the initial velocity after the sprint phase and v_f is the terminal velocity, (usually at the track finish).

$$E_{lost} = m\left(g(h_f - h_0) - \frac{1}{2}(v_f^2 - v_0^2)\right) \quad (4)$$

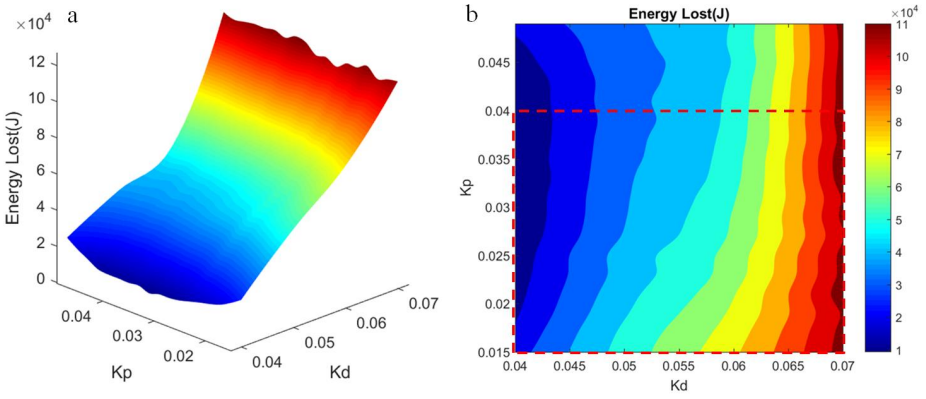

Fig. 5. (a) Surface plot of energy dissipation vs steering force; (b) Contour plot of energy dissipation vs steering force.

Fig. 5 shows that energy dissipation is affected by the controller defect to a much lesser degree. The reason for this is that energy lost is only proportional to friction caused by steering force (i.e. a simulated descent could take longer to complete but still have low energy lost). In Fig. 5, the *x* and *y* axes represent K_d and K_p respectively, the colour of the contour represents the trend of energy lost with respect to steering force; increments in steering force leads to increments in energy lost.

3.4 Correlation Analysis

To obtain suitable correlations for use in the optimal control designs, the values of each performance index were averaged across all the K_p values within the representative region. Fig. 6 presents the processed data compared against change in K_d, which can be perceived as steering forces at this point.

Characteristics identifications were carried out and the following correlations can be drawn from analysing the figures:

- Descent time exhibits a quadratically increasing characteristic with respect to the steering force.
- Transverse distance travelled exhibits a quadratically decreasing characteristic with respect to the steering force.
- Energy dissipation exhibits a quadratically increasing characterstic with respect to the steering force.

A clear correlation between performance indices can be drawn from above characteristics: Increments in energy dissipation → decrements in transverse distance travelled → Increments in descent time.

Although the simulation results demonstrated a clear correlation between the three performance indices, it however indicates that: 'By maximising the transverse distance travelled, the athlete can minimise their descent time'. Without the context of energy dissipation, this correlation seems absurd. Analysing the above statement from another angle produces a more intuitive statement: 'Instead of maximising the transverse distance travelled, athlete should not aim to reduce their travel distance in order minimise the energy lost.' Therefore the distance travelled must be used in conjunction with energy lost for defining the cost minimisation strategy.

4. Conclusion

By analysing the correlation between performance indices, a feasible cost minimisation strategy could be determined. The relationship between energy dissipation and descent time is clear and makes logical sense. However, the effect of transverse distance travelled on the descent time is more complicated and further researches with different steering strategies are required to clarify this. Currently, to achieve the best descent time, the optimal controller should aim to minimise the energy lost through the race by limiting its steering actions. This is consistent with the strategy of the best sliders who aim to steer an optimum track with a minimum of course keeping interventions.

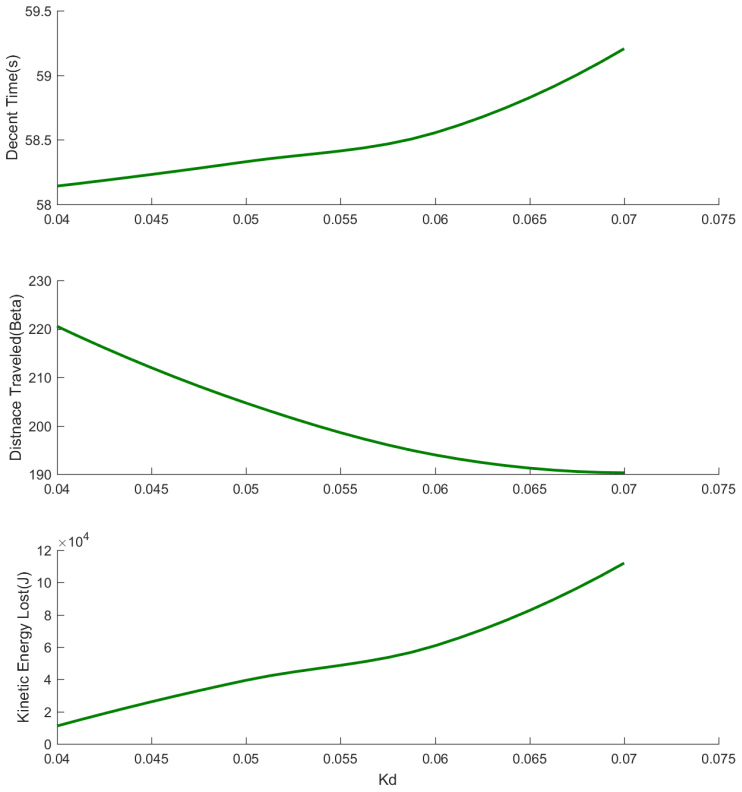

Fig. 6. Correlation graph between performance indices.

Acknowledgements

This work was conducted under the auspices of the Faculty of Engineering and the Environment at the University of Southampton and with support from the Engineering and Physical Sciences Research Council (UK) and English Institute of Sport (Research and Innovation). The authors gratefully acknowledge the support of staff and sliders at British Skeleton.

References

[1] Sawade et al, Assessment of an Empirical Bob-skeleton Steering Model, Procedia Engineering, Volume 72, 2014, Pages 447–452, The Engineering of Sport 10, 2014.
[2] Roche et al, An Analysis of the Interaction Between Slider Physique and Descent Time for the Bob Skeleton, The Engineering of Sport 7, 2008.
[3] Hubbard et al, Three-Dimensional Bobsled Turning Dynamics, International Journal of Sport Biomechanics, 1989, 5, 222-237, 1989.
[4] Y.L. Zhang, M. Hubbard, R.K. Huffman, Optimum control of bobsled steering. J. Optim.Theory Appl 85(1, 1995), pp. 1–19.
[5] F. Braghin, F. Cheli, S. Melzi, E. Sabbioni, Development of a numerical model of a bobsled driver: trajectory planning, in Proceedings of 12th Mini Conference on Vehicle System Dynamics, Identification and Anomalies, 2010, pp. 501–510.
[6] E.Sabbioni, S. Melzi, F. Cheli, & F. Braghin (2016). Bobsleigh and Skeleton. In The Engineering Approach to Winter Sports (Ch 7. pp. 183–276). Springer New York. doi:10.1007/978-1-4939-3020-3_7

Appendix C: Ethics Application

UNIVERSITY OF Southampton

ERGO application form – Ethics form

All mandatory fields are marked (M*). Applications without mandatory fields completed are likely to be rejected by reviewers. Other fields are marked "if applicable". Help text is provided, where appropriate, in italics after each question.

1. APPLICANT DETAILS

1.1 (M*) Applicant name:	Chen Gong
1.2 Supervisor (if applicable):	Prof Stephen Turnock, Prof Eric Rogers, Dr Alexander Forrester, Dr Dominic Hudson, Dr Martin Toward, Dr Christopher Phillips
1.3 Other researchers/collaborators (if applicable): *Name, address, email, telephone*	**Peter Bentley | Head of Research and Innovation, English Institute of Sport, Bisham Abbey National Sports Centre, Marlow, SL7 1RRM: 07900 651950**

2. STUDY DETAILS

2.1 (M*) Title of study:	Skeleton Simulator: Application as a driver training tool (DTT)
2.2 (M*) Type of study (*e.g. Undergraduate, Doctorate, Masters, Staff*):	Doctorate
2.3 i) (M*) Proposed start date:	15/08/2016
2.3 ii) (M*) Proposed end date:	01/04/2017

2.4 (M*) What are the aims and objectives of this study?
This is an amendment to the previous study SKELTEST003 ERGO ref: 15398, which was previously conducted and ethics approved. The aim of this study is to investigate the effectiveness of a novel Bob Skeleton driver training tool for training athletes. Bob Skeleton athletes will use the system in a variety of ways with their coach's to increase skill acquisition. The driver training tool (DTT) or simulator is designed to stimulate various perceptual systems in order to create a realistic enough experience for the athlete to respond in the same way as they would on track. This study will focus on assessing the performance of these stimuli (visual, force feedback, vibration and roll motion) and their effect on the athlete's response and decision-making.

2.5 (M*) Background to study (*a **brief** rationale for conducting the study*)**:**
A skeleton training system is required by the GB Bob Skeleton team to assist with driver training and skill acquisition. The previous study (SKELTEST001) aimed to investigate the effect on learning with various perceptual cues during a replayed run. The cues included all or a subset of; vision, audio, vibration applied to the torso and force feedback (G-cue). The results of this study showed; · Vibration levels were slightly too low according to the athletes · G-cueing increased learning rates and performance significantly

· G-cueing on the torso was too low
· Athletes wanted virtual control of the sled for more accurate responses

· Athletes wanted Roll motion for increased sense of reality Therefore, the previous amendment was designed to evaluate the effect of motion cueing with the addition of roll motion and the effect of virtual control within a virtual reality environment. The principle changes from experiment SKELTEST001 are summarised in Table 1 of the PROTOCOL document. The current study is a continuation and amendment to the existing application SKELTEST004 ERGO ref: 15398. The principle changes include:
1 – The rig will be operated in a bespoke facility at Bath University (British Skeleton Push Start House) and operated by trained University of Southampton staff/research students and or trained British Skeleton staff.
2 – The rig has being upgraded to include new pitching system located under the shoulder contact points. The pitching system adopts the same pneumatic setup as the rest of rig.
3 – A force feedback system for the participant's lower leg was installed. The system is attached to the body force feedback actuator via bungie cords and range of motion is limited via new body frames to protect the participant's knees.

2.6 (M*) Key research question (*Specify hypothesis if applicable*):

SKELETEST004 concluded that using trianing tool version 2, the inclusion of roll, vibration and force feedback stimuli increased the learning rate of the athletes whilst training in a virtual environment. It is hypothesised that the addtiona of pitching motion and force feedback on the legs will improve the imersion of said virtual environment and further improve the rate of learning.
The aim of the study is to assess the validity of said hypothesis which will involve testing a small group of selected individuals who are considered subject matter experts. Their performance as well as their given subjective feedback will be used to evaluate the effectiveness the upgrades.

2.7 (M*) Study design (*Give a **brief** outline of basic study design*)
Outline what approach is being used, why certain methods have been chosen.

The study is going to be based on assessing subjects' performance before and after implementing the pitching and leg feedback features. The subjects will be assessed on the following areas:
· Pressure awareness
Asking the subject to perform a steer, based on their awareness and perception of G-force.
· Steering timing and magnitude
Asking the subject to perform various steers with various timing and magnitude
· Speed awareness
Asking the subjects to give subjective feedback on whether they sped up or slowed down at various points of the run
· Driving line education
Showing the subjects different driving lines and how to steer those line
Each of these tasks involves the subject steering (exerting force from their shoulders and knees to the sled), which is measured by force sensors. This measured force is then analysed to determine either a late or early steer or the overall steer magnitude. By comparing sequential runs, performance can be calculated and therefore so can learning rates.

3. SAMPLE AND SETTING

3.1 (M*) How are participants to be *approached*? *Give details of what you will do if*

*recruitment is insufficient. If participants will be accessed through a third party (e.g. children accessed via a school) state if you have permission to contact them and **upload any letters of agreement to your submission in ERGO**.*
3 experienced current coaches and all ex-sliders 3 athletes ranging in skill level and experience from European Cup League to World-Class 2 Male 1 Female

3.2 (M*) Who are the proposed sample and where are they from (e.g. fellow students, club members)? *List inclusion/exclusion criteria if applicable. NB The University does not condone the use of 'blanket emails' for contacting potential participants (i.e. fellow staff and/or students).* *It is usually advised to ensure groups of students/staff have given prior permission to be contacted in this way, or to use of a third party to pass on these requests. This is because there is a potential to take advantage of the access to 'group emails' and the relationship with colleagues and subordinates; we therefore generally do not support this method of approach.* *If this is the only way to access a chosen cohort, a reasonable compromise is to obtain explicit approval from the Faculty Ethics Committee (FEC) and also from a senior member of the Faculty in case of complaint.*
3 current coaches have been selected based on their current employment with GB Skeleton as the lead coaching staff for all squads. All three coaches are also experienced ex-sliders. 1 World-cup athletes – all Olympic contenders - Advanced 2 Intercontinental or European Cup league athletes - Intermediate

3.3 (M*) Describe the relationship between researcher and sample (*Describe any relationship e.g. teacher, friend, boss, clinician, etc.*)
EIS (English Institute of Sport) is the project sponsor and collaborator with the University of Southampton. EIS also has an invested research and innovation program with GB Skeleton, and therefore has created the relationship between researcher and sample.

3.4 (M*) Describe how you will ensure that fully informed consent is being given: (*include how long participants have to decide whether to take part*)
Participants will be emailed the following documents for review and approval prior to the study: - Consent form - Participant Information Sheet - Health Screening question sheet - to ensure participants are healthy and comply with study requirements Participants will have time to read, consider and ask any questions prior to study commencement.

4. RESEARCH PROCEDURES, INTERVENTIONS AND MEASUREMENTS

4.1 (M*) Give a brief account of the procedure as experienced by the participant *(Make clear who does what, how many times and in what order. Make clear the role of all assistants and collaborators. Make clear total demands made on participants,*

including time and travel). ***Upload any copies of questionnaires and interview schedules to your submission in ERGO****.*
Each subject will be asked to attend training session on two days per week for the Skeleton Summer Training period 29th June 2016 – 1st October 2016. (Pitch Experiment will be carried out for 2 days between above training period, Pitch motion will not be implemented until ethics submission has being approved) Each training session will be limited to 5 full runs and only one session per day with at least a day between sessoins. After all safety and risks have been made clear by the operator, the subject will be fitted to the system to ensure a safe and comfortable posture is maintained during training. During this fitting, the system will be switched off at the mains power and all pressure will be released from the pneumatic lines. Fitting includes saddle adjustment, torso harness adjustment and helmet adjustment. After setup, the subject and coaches will work on improving the four areas previously identified in section 2.7. -All three coaches have already attended a 2 day testing session on the 5th and 6th of August 2013 and 16th June 2015 to evaluate the system and provide performance feedback. The sessions included detailed analysis of each sub-system of the simulator and its effectiveness for training. This was limited to 5 full runs per day, each run lasting no more than 70seconds. The coaches then agreed with the experimenter on ways to present post-run data to the subjects. All three coaches, and GB Skeleton's Sled & DTT technician and Performance Analyst have been fully trained in the saftey surrounding the system, its safe operation and trouble shooting by the principal researcher. For the first session, the principal researcher will shadow the skeleton staff to ensure safe operation. For future sessions, the princpal researcher or other University of Southampton staff may be present or will otherwise be available for contact and remote assistance. -Simulator Operator - The simulator operator will primarily be involved with participant setup prior to each set of runs. They will be required to monitor the subject's posture during the experiment. -Collaborators - All research collaborators present will not have any direct roles to play during experiments however may provide feedback and assistance where necessary. -The main individual running the session, researcher, simulator operator or technician, will be responsible for conducting the experiment. Firstly they will ensure correct participant set up and calibration. They will then run the experiment by setting the conditions for the experiment and giving the participant information just before it begins. The researcher/simulator operator/technician will stand close to the participant (within 1m) while monitoring the feedback sensors and measurement equipment on the control PC. The researcher/simulator operator/technician will have access to an emergency stop button within reach at all times.

5. STUDY MANAGEMENT

5.1 (M*) State any potential for psychological or physical discomfort and/or distress?
During this experiment the participants should experience no psychological distress. Minor physical discomfort may occur during exposure to vibration, motion and force feedback applied to the head, torso and leg.

5.2 (M*) Explain how you intend to alleviate any psychological or physical discomfort and/or distress that may arise? (if applicable)
The primary researcher or at least one trained skeleton staff member will be present during all operation of the simulator.

The system is capable of applying two kinds of motions; high frequency (3Hz – 80Hz) vibration to the sled and athlete torso, and low frequency (0 Hz – 5Hz) roll motion and vibration with much larger amplitudes. As the participant will be exposed to vibration for all runs, exposure levels must be known and ensured they do not exceed UNUSUAL levels.

Vibration Exposure: Electrodynamic Vibration (High frequency vibration)

The high frequency vibration stimulus is generated from Gaussian white noise played through the audio card on the control PC. The noise signal is modified during the run in both amplitude and frequency of the signal the noise is added to. The signal is a sinusoidal wave, which is derived from the virtual sled speed. This variation is calculated from the physics engine, which computes the physical parameters of the run. The vibration signal is band pass filtered from 3Hz to 80Hz (See SkelSimSafetyManual.doc section 5 for PSD and details of signal).

The measured VDV for high frequency vibration during a single maximum run is VDV – 6.38m/s-1.75

Vibration Exposure: Roll motion (Low frequency vibration)

Participants will experience roll motion while on the system. The Roll movement is intended to provide vestibular system stimuli for steering decision cues. Roll is applied by a pneumatic actuator to the platform which rotates on bearing housings either end of the rig.

The platform is able to roll +/-47 deg (+/-45Deg operating stroke).

The measured VDV for low frequency roll vibration during a single maximum run is VDV -5.51 ms-1.75

Please refer to SkelSimSafety Manual section 6 for Roll vibration exposure measurement values and details.

Therefore the maximum VDV for a single run is calculated from the root-mean-quad summation of the high and low frequency VDV. The Max VDV per run is; VDV – 7.12 ms-1.75

The total absolute maximum daily VDV is calculated from the root-mean-quad summation of both high and low frequency vibrational motion for all possible number of exposures per day. Therefore, Max daily VDV total = 10.65 ms-1.75

This is within the USUSAL exposure limit. Vibration will also be monitored during the experiment with an accelerometer to ensure UNUSUAL levels are not reached.

Please refer to SkelSimSafetyManual.doc section 5 for more details and failure exposure conditions.

Force Feedback:

Force is applied to the participants back and helmet. It is intended to be a representation of the G-forces experienced during on ice sliding, where the G values are calculated in real-time by the Physics engine. The force applied to the body is a reduced amplitude to not cause discomfort for the participant. As F=ma, By knowing the mass of the subjects head and torso and multiplying it by the simulated acceleration (in G), the force can be controlled in real-time. The acceleration trace has been Low Pass filtered to remove high frequency spikes to provide a smoother feeling for the subject. Simulated G-force has also been limited to a maximum of SIX G.

Please see SkelSimSafetyManual.doc section 7 for force calculations and details.

In this experiment, the proposed maximum head loading is hardware limited to 7.05kg. This equates to approx. 1.5G (i.e. 30% of the 'real' force)

NOTE: although head force limit is restricted to 7.05kg (69.2N), the subject can relax and not resist the force. In this case the mechanical end stop beneath the helmet will prevent any force being exerted on the head (see figure Safety Schematic). In other words, the subject can resist the force as much or as little as he or she likes.

In this experiment, the proposed maximum torso loading, distributed over the body, is 35 kg. This equates to approx. 1G (i.e. 33% of the 'real' force), and less for heavier athletes.

An additional force will be applied to the torso (up to 10kg) while the platform is

rolling to provide a feeling of 'gravity' is constantly applied even while rolling. This force is independent of the G force (ie holding force can be applied even if no virtual G-load is calculated at roll angles). This force is not required to keep the athletes securely on the system, however simply works with the cueing system.
45kg is the maximum possible force calculated for the heaviest athlete, however as forces are calculated based on individual athletes, lighter athletes will feel proportionally less force.
Participants are restrained on the system by a harness. The harness will hold the participants at all possible roll angles even if the system is unpowered and depressurised. Furthermore, a steel saddle is mounted to the sled keeping the athlete in position.

5.3 Explain how you will care for any participants in 'special groups' *(i.e. those in a dependent relationship, vulnerable or lacking in mental capacity)* **(if applicable)?**

Not applicable

5.4 Please give details of any payments or incentives being used to recruit participants (if applicable)?

Not applicable All GB Skeleton associated participants are being paid for their time during the required experimental sessions. All expenses (food, accommodation and travel) will be covered by GB Skeleton and EIS.

5.5 i) How will participant anonymity and/or data anonymity be maintained (if applicable)?

Two definitions of anonymity exist:
i) Unlinked anonymity - *Complete anonymity can only be promised if questionnaires or other requests for information are not targeted to, or received from, individuals using their name or address or any other identifiable characteristics. For example if questionnaires are sent out with no possible identifiers when returned, or if they are picked up by respondents in a public place, then anonymity can be claimed. Research methods using interviews cannot usually claim anonymity – unless using telephone interviews when participants dial in.*
ii) Linked anonymity - *Using this method, complete anonymity cannot be promised because participants can be identified; their data may be coded so that participants are not identified by researchers, but the information provided to participants should indicate that they could be linked to their data.*

Linked anonymity will be controlled with unique participant ID numbers. The link between participant name and ID number will be stored on a password protected file and computer. ID numbers will be randomly assigned to the participant. Participants will be made aware of anonymity on the consent form.

5.5 ii) How will participant confidentiality be maintained (if applicable)?

Confidentiality is defined as the non-disclosure of research information except to another authorised person. Confidential information can be shared with those who are already party to it, and may also be disclosed where the person providing the information provides explicit consent.

All participants have a confidentiality contract in place with GB Skeleton and EIS. The University of Southampton, researcher and all collaborators also have a non-disclosure confidentiality contract with UK Sport.

5.6 (M*) How will personal data and study results be stored securely during and after the study? *Researchers should be aware of, and compliant with, the Data Protection policy of the University. You must be able to demonstrate this in respect of*

handling, storage and retention of data.
All data acquired during the study will be stored on a password protected computer and backed up on the university network under a password protected file store.

5.7 (M*) Who will have access to these data?
All personal data acquired will only be accessible to the researcher and supervisors. Access to collaborators will be subject to individual consent by the participant. All study data acquired during experimental tests will be available to the researcher, supervisors, collaborators, coach and participant in relation to data.

N.B. – Before you upload this document to your ERGO submission remember to:

1. Complete ALL mandatory sections in this form

2. Upload any letters of agreement referred to in question 3.1 to your ERGO submission

3. Upload any interview schedules and copies of questionnaires referred to in question 4.1

Appendix D: Noise & Vibration Information

STUDIES INVOLVING EXPOSURE OF HUMAN PARTICIPANTS TO NOISE OR VIBRATION

In addition to the University Ethics Application form, please complete and submit the following if you are conducting a study in which people will be exposed to noise or vibration.

APPLICANT INFORMATION

Applicant name:	Chen Gong
Supervisor(s):	Prof Stephen Turnock, Prof Eric Roger, Dr Alexander Forrester, Dr Dominic Hudson
Other researchers / collaborators:	**EIS**

Title of study:
Skeleton Simulator: Application as a driver training tool (DTT)

EXPOSURE TO NOISE OR VIBRATION:

Describe exposure conditions in an attached document (this may be included be in your research protocol). Identify all noise and vibration and show calculations used to decide if exposures are USUAL or UNUSUAL according to ISVR Technical Report 808 (1996).

Exposure details attached?	X
Exposures are USUAL, or	X
Exposures are UNUSUAL, or	
Cannot decide.	

PARTICIPANTS:

Selection of Subjects: (Give details)

Health Questionnaire	X
Screening Tests	
Other Confidential Information	
Contra-indications	

CONTROL OF STIMULUS:

(Describe method for generating, controlling, and measuring the stimulus, including any safety features preventing over-exposure.) See next page.

All Stimulus details can be found in Protocol—v7.pdf – Section 8.1

Noise will be generated with a loudspeaker positioned underneath the subjects head (~25cm) to represent the sound of the sled on the ice. The signal source is the audio track form the on-board video camera (GoPro Hero2) with microphone which was mounted on the front of the sled during testing in Lake Placid 2012.
Peak noise level at the subject head position has been measured at 86dB(A) with an SPL meter.
The maximum exposure for 88dB(A) is 30minutes.
The cumulative duration of the noise for all the tests per day per subject is less than 20 minutes.
Furthermore, the helmet will attenuate the noise level.
The noise level at the experimenter head position has been measured at 72dB(A) allowing more than 8 hours exposure. The Experimenter will only be exposed to noise for a maximum of 2 hours per day. This shows that exposure is below the Lower Exposure Action Value of the Control of Noise at Work Regulation 2005.

The vibration stimulus will be generated by using a scaled acceleration trace recorded on the sled during track testing in Lake Placid (March 2012) as the input to an electrodynamic shaker mounted underneath the sled. The accelerometer was mounted on the top side of the sled in a central position. The accelerometers used had a range of +/-25G and was acquired at 500Hz. A 3-80Hz cut off Bandpass filter was applied to the data and then converted to a line level audio signal, making the input contain 3 -80Hz frequency content. Verification of appropriate cueing levels will be confirmed with the preliminary test athletes. These athletes were on the sled during testing when the acceleration was recorded The vibration levels were scaled down from the real recorded data.

Acceleration peaks during a skeleton run exceed +/-6G (~58.8m/s2) and exceed a VDV value of 15m/s-1.75.

The scaled signal results in the following maximum, minimum and VDV values.

The magnitude of vibration is limited by output power of the electrodynamic shaker amplifier. This maximum was used to measure the VDV for the experiment which shows USUAL exposure levels.
Vibration measurements were made with a subject (informed member of staff) on the sled while a full decent was replayed with the electrodynamic shaker. An accelerometer was used to measure the acceleration at the sled/human interface.
The output signal generated contained the following frequency weighted content;

- r.m.s value of 1.068m/s2
- Maximum value of 10.523m/s2
- Minimum value of -7.362m/s2
- Mean value of 0 m/s2

This was recorded for a duration of 30 seconds.
The VDV (Wk weighted, ISO2631 (2001)) was calculated for the replayed signal as 4.19 m/s-1.75.
Maximum total daily VDV exposure level can be calculated from the root-mean-quad summation of the all the daily exposures. Based on a maximum of 6 runs, this results in a total VDVmax value of 6.56 m/s-1.75.
This VDV value is below the UNUSUAL threshold of 15m/s-1.75, and is considered an absolute maximum as the participants will only experience vibration exposure for less than 30 seconds at a time.
Vibration will be monitored during the experiment. Both participant and experimenter will have access to a hardware emergency stop.

Is equipment within calibration and electrical safety inspection periods? Yes [X] No [ ]

OTHER POTENTIAL HAZARDS:

(e.g. devices or implements inserted into the ear, application of static pressure to the ear, caloric stimulation, use of electrodes, other attachments to subject, physical manipulation of the subject, administration of drugs or application of any compound, control of stimulation using non-proprietary software)

OTHER RELEVANT ETHICAL AND SAFETY PRECAUTIONS: Participant must complete Pre-Screening Health check form – SEE – HealthCheck.pdf

SUBJECT CONSENT FORMS:

I will return all subject consent forms to the Faculty Ethics Committee by*: 1/12/2016
**Delete if not applicable and provide an explanation.*

Appendix E: Consent Form

UNIVERSITY OF Southampton

CONSENT FORM (*v6.0*)

Study title: Skeleton Simulator: Application as a driver training tool (DTT)

Researcher name: Chen Gong
Study reference: SKELTEST004
Ethics reference: 15398

Please initial the box(es) if you agree with the statement(s):

I have read and understood the information sheet (1st June 2016, PISv7.0) and have had the opportunity to ask questions about the study.	☐
I agree to take part in this research project and agree for my data to be used for the purpose of this study	☐
I understand my participation is voluntary and I may withdraw at any time without my legal rights being affected	☐
I understand that I will be subjected to varying degrees of vibration, force, roll and pitch motion levels during the experiment. I agree to notify the researcher if I feel any form of psychological and or physical discomfort before, during and after the experiment. I enter into this study fully understanding that I may feel physical fatigue levels lower than those experienced while performing the sport of Bob Skeleton.	☐

Data Protection

I understand that information collected about me during my participation in this study will be stored on a password-protected computer and that this information will only be used for the purpose of this study. All files containing any personal data will be made anonymous.

Name of participant: (print name).....

Signature of participant:.....

Date:.....

Appendix F: Research Protocol

UNIVERSITY OF Southampton

Protocol

Study Title: Skeleton Simulator: Application as a driver training tool (DTT)

Researcher(s) Chen Gong

Funder: UK Sport, GB Skeleton, EPSRC, and University of Southampton
Sponsor (if known):

PROTOCOL DOCUMENT OVERVIEW

This document overview is intended to provide a quick reference to information relating to risk and safety issues.
The following table shows the principle risks and ethical issues considered and addressed by the experimenters.

Potential Risk	Possible Cause	Prevention Method and or Justification
Excessive vibration exposure to body	-Vibration exposure magnitude too high from electrodynamic shaker	-Measured VDV is well below UNUSUAL exposure levels of 15m/s$^{1.75}$. VDV and R.M.S has been measured at four points of body contact to the sled (shoulders, upper chest, Stomach and pelvis). Values do not exceed VDV of 6 m/s$^{1.75}$ and R.M.S of 1.5m/s^{2} *(See section 8.2 for more information)*
	-Vibration frequencies outside applicability of frequency weightings	- Vibration stimulus has been filtered between 3Hz and 80Hz to contain content within the Wk frequency weighted spectra. *(See section 8.2 for more information and PSD graphs)*
	-Vibration uncomfortable for participant	-Participant will be holding an emergency stop which when pressed will disable the vibration. Experimenter will also be holding an emergency stop to disable vibration -R.M.S and VDV levels, monitored during experiment
Excessive vibration exposure to head	-Injury from head vibration	-The head is NOT in direct contact with any part of the sled which is vibrating. Participants can rest their head on the rig which is NOT vibrating (isolated from the sled and electrodynamic shaker as shown in *Appendix B),* therefore risk of head vibration has been mitigated.
Excessive force applied to the head and/or neck	-Force exerted in various axes	-Force on the helmet is only applied in the vertical direction (DOWN ONLY). The head is free to rotate in all normal axes (Pitch, Roll and Yaw) even when force is applied in the vertical direction.
	-Excess pressure applied from actuator	-Participant can resist force as much as desired. Helmet movement is restricted in the vertical direction (down) by mechanical limits (*see Appendix B for photo*). Furthermore, before the helmet reaches this point, the actuator is

		limited by displacement extension (i.e the actuator is set to a maximum which means it is unable to provide any further force beyond this point). Pressure is limited by locked regulator to cap the maximum output pressure and resultant force to 69 N (~7 kg).
Excessive force applied to the body	-Excess pressure applied from actuator - Excess force applied to the knee joint -Discomfort caused from force applied too quickly	-Maximum force from actuator is limited by locked pressure regulator to cap the maximum output pressure and resultant force to 280 N (~29 kg). Actuator displacement limits. (*Please refer to section 8.3 for more information on mechanical failure prevention on both actuators*). -Maximum force from actuator applied at knee joint is limited by locked pressure regulator to 35N (~3.6 kg) -The system incorporates compliance in the harness and sled to prevent 'step' force inputs to the body, reducing any unexpected discomfort
Noise exposure	-Excess Noise levels applied to the participants ears	-Noise levels have been measured and set with reference to a SPL meter at the location of the participants head. The level is below the daily exposure limits for the experiment duration. Furthermore, the noise level will be attenuated by the participant wearing a helmet. (*please see section 8.1 for more noise exposure information*)
Subject informed consent	-Subject is not fully aware of all risks of involvement.	-Participant will be given a general overview of the study in the *Participant Information Sheet*. Before the participant signs the consent form, he or she will be given an explanation of the system and will see the system operating. All risk and safety issues will be explained and highlighted. (*See section 6 of the protocol for more information*)

1. Background

The sport of Bob Skeleton involves the athlete sliding down an ice track. The slider lies head first on a sled only centre metres off the track surface. The slider is able to steer the sled's direction by applying force onto the front two corners with his or her shoulders and the rear corners with his or her knees.

During the descent, the athlete can experience sustained centripetal forces of up to six G. This force, combined with the vibration makes the sport very physically demanding. Furthermore, the athlete and sled are often recorded at speeds up to 130km/h.

Training for such a sport is critical for safe and successful participation, however for GB Skeleton athletes this can be difficult as there is no ice track here in the UK. Therefore a training system capable of providing steering cues would be greatly beneficial for the athletes and coaches alike during off season sliding periods to accelerate learning and skill acquisition.

UK Sport has initiated a project with the University of Southampton to develop a Skeleton simulation system for this training purpose.

2. Study Aim

In previous studies SKELTEST001 and SKELTEST002 (ERGO ref:15398) and as presented in C. Sawade's PhD thesis, *Learning Interventions in Olympic Skeleton through the use of Physical Simulation, 2014* the simulator was used to understand if positive In-Simulator Learning is possible on a Skeleton bob simulator. Participants were asked to perform a specified steer through a corner of a skeleton ice track descent. The corner was 'replayed' to them from data obtained from track testing in Lake Placid. The data was replicated in four ways; video playback, audio playback, vibration (audio tactile transducer) from acceleration traces and force feedback on head and torso from acceleration data. By varying which of the four types of information was 'replayed' it is possible to observe the effect of varying the degrees of perceptual cueing and feedback on performance and learning. At the end of the study, it was found all perceptual cues combined to permit an effective steering input. It was also found that the skeleton training system could be used as an effective driver training tool (DTT) (*Learning Interventions in Olympic Skeleton through the use of Physical Simulation (2014), PhD Thesis, C. Sawade*). The aim of this experiment is to further assess the validity of using the simulator as DTT and evaluate the effectiveness of adding shoulder pitch motion and leg force feedback.

3. Method

The method for testing these hypotheses is to measure how quickly the participant can learn a skill based behaviour following a set of given rules. Measurement will be done by comparing steering force of the shoulders and knees against a pre-defined acceptable execution standard of the steer. The delta of both timing and percentage of magnitude will be mapped over several runs. The slope of these delta curves will define the amount of learning the participant has achieved on that corner.

New perceptual cues will be provided systematically to the participant, and the effect on the learning curves will be assessed.

The study will involve 3 EIS British Skeleton funded athletes and 3 British Skeleton coaches as participants. All athletes are of World-cup standard.

The participants will use the simulator outside of their usual training program for the specific purpose of testing the effectiveness of the upgrades. Upon completion of evaluation, the simulator will be used by a cohort of athletes as part of their summer training program as advised and supervised by their coaches.

There will be two sessions per day; one morning session (8am-12pm) and one afternoon session (1pm to 5pm). The tests will be carried out over 2 consecutive days.

Each participant will be required to complete 4 runs of the track, 2 runs per session. Three different pitching algorithms as well as a baseline null algorithm will be tested in each run.

The runs will include replayed visual, audio, vibration and force feedback information of the whole track or specific corners as decided by the coach.
The coach and support staff will monitor and assess progress during the program.

4. Materials

The experiment will be performed using a newly developed training system rig. The system consist of the following:

- A skeleton sled mounted on four spring loaded support members which are attached to the frame
- The frame is constructed of 40x40 aluminium extrusion profile
- Vibration input is created using a ButtKicker Advance (see user manual attached in appendix) and powered by a 300Watt power amplifier
- Force feedback is applied using two Festo pneumatic linear actuators (1x 32"bore x 320mm, 1x 62" Bore x 100mm). The cylinders are controlled by high speed pneumatic valves by Enfield Technologies (valves are powered and controlled by Enfield Technologies controller driver 1 x LS-V14s and 1x LS-V25s. The analogue PID electronics (2 x LS-C4.
- Two in-line load cells are mounted at the end of the pneumatic cylinders to provide feedback to the electronics of the measured force output – (1x 500N Richmond Industries load cell, 1 x 2000N Richmond industries load cell.)
- Thin film flexible force sensors are used to measure the steering force of the participant (4 x flexiforce A401 sensors), powered by custom electronics for calibration and adjustment.
- All electronic I/O will be connected to a National Instruments DAQ card (1x NI PCI 6229), which will interface all signals to and from the control software Labview.
- The participant will be strapped into place with a modified 5 point safely harness which will be attached to one of the pneumatic cylinders for force feedback.
- The participant will wear a helmet which will have a connection point to the other pneumatic cylinder for head force feedback.
- Two desktop power supplies will be used to power all sensors and electronic equipment, @ output voltages of +/-14Vdc and +24Vdc (max output current is 2A).
- A video projector will be connected to the control PC for video playback.
- Externally powered speakers will be connected to the control PC for audio playback

5. Participants

The participants currently identified are all associated with GB Skeleton as either an athlete or support coach or staff. GB Skeleton along with EIS was involved in the selection process of this participant for the study. All Participants are aged 18 or over.

3 experienced athletes (2 male, 1 female)

3 GB Skeleton employed coaches

6. Procedure

Roles and responsibilities:
Researcher-

- Ensure all test equipment is functional and working correctly
- Ensure system is calibrated

- Ensure simulator operator is sufficiently trained and experienced with the safety aspects and procedures
- Ensure simulator operator is sufficiently trained and experienced with the full operation of the system – including loading, replaying, feedback data
- Liaise with simulator operator

Simulator Operator:

- To have been trained, instructed and confident on all safety aspects and procedures by UoS researcher
- To have been trained, instructed and confident on the operation of the simulator by UoS researcher
- To have read, comprehended and understood the safety and operators manual
- Liaise with UoS researcher as when required/necessary
- To report faults to the UoS researcher
- Ensure all test equipment is functional and working correctly
- Responsible for safe participant setup
- Run experiment
  - Input all experiment conditions
  - Monitor experiment parameters
  - Provide feedback to participant and Coach
- Secure all data on password protected computer
- Liaise with athletes and organise testing schedule

Coach:

- Provide feedback of system features and performance
- The correct run data is loaded: i.e. track line and full track/specific corner
- Ensure all participants are in safe position and posture during tests.
- Provide feedback to participants on their performance

Elite Athlete's:

- Provide feedback of system features and performance
- Follow researcher, simulator operator and coaches instructions, adhering to all safety requirements at all times

Novice Participants:

- Participate in experiment where required and instructed
- Follow researcher, simulator operator and coaches instructions, adhering to all safety requirements

Each test consists of the following routine-

- Explaining to the participant what will occur during the test- including relevant perceptual cues and risks.
  - Demonstration of the system and its features with informed member of staff.
  - Explanation of operation
  - Examination of risks and consequences of involvement
- Setup participant on the system – fitting and safety checks
- Simulator operator will set the test to run
  - Pre-recorded data will be read into the system, including video and standard steer information
  - Prompt and entry of athlete initials or ID for data recording and tracking
  - Select "Start Run" – count down will begin for three seconds (this will give the participant information to begin)
  - The run will start and all steering forces will be recorded and written to a separate file with the participant ID

- Once the run is complete – there will be a chance for a break while the coach looks at the results of the run and gives any required feedback
- The process will repeat for required number of runs.

- All files will be backed up on a secure file store on the university server.

Please refer to Appendix A for experiment schedule.

7. Statistical analysis

The force of shoulder and knee steering will be recorded with the FlexiForce sensors. The participants steering output will be compared to the "standard steer" set by the coach. The difference of timing and percentage of maximum steer will be plotted across all runs. The trended slope will determine the rate of learning across the 5 runs.

8. Ethical issues

8.1 Noise Exposure:

Noise will be generated with a loudspeaker positioned underneath the subjects head (~25cm) to represent the sound of the sled on the ice. The signal source is a scaled version of the audio track form the on-board video camera (GoPro Hero2) with microphone which was mounted on the front of the sled during testing in Lake Placid 2012.

Peak noise level at the subject head position has been measured at 86dB(A) with an SPL meter. The maximum exposure for 88dB(A) is 30minutes.

The cumulative duration of the noise for all the tests per day per subject is less than 20 minutes. Furthermore, the helmet will attenuate the noise level.

The noise level at the experimenter head position has been measured at 72dB(A) allowing more than 8 hours exposure. The Experimenter will only be exposed to noise for a maximum of 2 hours per day. This shows that exposure is below the Lower Exposure Action Value of the Control of Noise at Work Regulation 2005.

8.2 Vibration Exposure:

As the participant will be exposed to vibration for 2 of the 4 corners, exposure levels must be known and ensured levels do not exceed UNUSUAL levels.

The vibration stimulus will be generated by using an acceleration trace recorded on the sled during track testing in Lake Placid (March 2012). The accelerometer was mounted on the top side of the sled in a central position. The accelerometers used had a range of +/-25G and was acquired at 500Hz. A 3Hz-80Hz bandpass filter was applied to the data and then converted to a line level audio signal, making the input contain 3-80Hz frequency content. Verification of appropriate cueing levels will be confirmed with the preliminary test athletes. These athletes were on the sled during testing when the acceleration was recorded

The vibration levels were scaled down from the real recorded data.

Acceleration peaks during a skeleton run exceed +/-6G (~58.8m/s^2) and exceed a VDV value of 15m/$s^{-1.75}$.

The scaled signal results in the following maximum, minimum and VDV values.

The magnitude of vibration is limited by output power of the electrodynamic shaker amplifier. This maximum was used to measure the VDV for the experiment which shows USUAL exposure levels.

Vibration measurements were made with a subject (informed member of staff) on the sled while a full decent was replayed with the electrodynamic shaker. An accelerometer was used to measure the acceleration at the sled/human interface.

The output signal generated contained the following frequency weighted content;

- r.m.s value of 1.4977m/s^2
- Maximum value of 10.4430m/s^2
- Minimum value of -7.362m/s^2
- Mean value of 0 m/s^2

This was recorded for duration of 30 seconds.
The VDV (Wk weighted, ISO2631 (2001)) was calculated for the replayed signal as 5.9418 m/s$^{-1.75}$.

Maximum total daily VDV exposure level can be calculated from the root-mean-quad summation of the all the daily exposures. Based on a maximum of 6 runs, this results in a total VDV_{max} value of 6.56 m/s$^{-1.75}$.

This VDV value is below the UNUSUAL threshold of 15 m/s$^{-1.75}$, and is considered an absolute maximum as the participants will only experience vibration exposure for less than 30 seconds at a time.

Furthermore, the actual level will be lower than this for equipment protection.

Vibration will also be monitored during the experiment with an accelerometer to ensure UNUSUAL levels are not reached.

8.3 Force Feedback:

Force is applied to the participants back and helmet. It is intended to be a representation of the G-forces experienced during on ice sliding; however the forces will be a scaled version of the real value of acceleration.
This will ensure that the force does not cause discomfort.

As F=ma,
By knowing the mass of the subjects head and torso and multiplying it by the recorded acceleration (in G), the force can be controlled in real-time.
The acceleration trace has been Low Pass filtered to remove high frequency spikes to provide a smoother feeling for the subject.

Calculation to determine maximum force on subject:

The maximum forces on the body during a real sled run can be calculated from the g-loads sustained during cornering. In this experiment, subjects will be exposed to scaled forces based on these g-forces. These forces will be the same for all subjects, and therefore the ratio of the scaled forces to the actual forces will be greatest for the lightest subjects.

The maximum force applied to the head of a 55kg athlete during a real sled run can be estimated from:

Subject head weight = 4.5kg

Sustained G-loads during actual run (up to 4 seconds in longer corners) = 5G (recorded with accelerometer)

Therefore sustained loads on head = 5g x 4.5kg = 18kg

In this experiment, the proposed maximum head loading is hardware limited to 7.05kg. This equates to approx. 1.5G (i.e. 30% of the 'real' force)

> NOTE: although head force limit is capped at 7.05kg (69.2N), the subject can relax and not resist the force. In this case the mechanical end stop beneath the helmet will prevent any force being exerted on the head (see figure Safety Schematic). In other words, the subject can resist the force as much or as little as he or she likes.

The forces applied to the subject's torso during a real sled run can be estimated from:

Average minimum subject torso weight = 35kg

Sustained load on torso during actual run = 5g x 35kg = 140kg

In this experiment, the proposed maximum torso loading, distributed over the body is hardware limited to 28.6 kg. This equates to approx. 0.8 G (i.e. 20% of the 'real' force).

Furthermore, limits have been set to eliminate any chance of force levels exceeding the intended levels. These limits include:

- Physical position limit of actuator - actuator will not be able to extend beyond a particular "safe" point.
- Software limits - the command signal will only be able to output force commands inside the safe force range
- Pressure limit - the pneumatic airline will be set at 1 bar to ensure maximum force generated is only; 69.2N on the helmet and 280.4N on the torso. The pressure regulator used to limit this pressure will be locked to avoid any accidental change from occurring.
- The force on the torso will be applied to the back harness, which will distribute the load across the participant's back, shoulders and lower buttocks at 6 points. The harness will also include a compliant material between the participant and the harness for comfort. By distributing the load in this manner, no point loads will exceed 46.73N on the participant's torso.
- Safety limits have been built onto the rig to provide a mechanical stop for the helmet in the unlikely event too much force is applied. The helmet will be unable to move beyond these points causing no unusual postural positions for the participant.
- Force level will be measured and monitored with load cell to ensure excess force is not applied

Please see attached schematic of CAD model as reference.

- Furthermore, the participant will be holding an emergency stop button which will disable the pneumatic valves in the event of any discomfort.

The simulator operator will also have an emergency stop button available to disable the system in the unlikely event of an error or discomfort.

9. Data protection and anonymity

Linked anonymity will be controlled with unique participant ID numbers. The link between participant name and ID number will be stored on a password protected file and computer.

ID numbers will be randomly assigned to the participant.

Participants will be made aware of anonymity on the consent form.

All data acquired during the study will be stored on a password protected computer and backed up on the university network under a password protected file store.
All personal data acquired will only be accessible to the researcher and supervisors.
Access to collaborators will be subject to individual consent by the participant.
All study data acquired during experimental tests will be available to the researcher, supervisors, collaborators, coach and participant in relation to data.

All participants have a confidentiality contract in place with GB Skeleton and EIS. The University of Southampton, researcher and all collaborators also have a non-disclosure confidentiality contract with EIS.

Appendix

A. Experiment Schedule

Three test blocks:
Block 1: 30th June & 2nd July 7th & 9th July
Block 2: 4th & 6th August 11th & 13th August
Block 3: 8th & 10th September 15th & 17th September

Schedule for athletes in groups of two or three. This schedule may run with concurrent groups in a morning or afternoon session in one of the test blocks. At least an hour shall be taken between the morning and afternoon sessions.
Two participants:

1. 2 Athletes arrive for group 1 debrief session – 15 minutes
2. Athlete 1 calibration – 15 minutes
3. Athlete 1 to complete test using all perceptual cues – 30minutes
    a. 1 run – become familiar with the sensation
    b. 5 runs –force recorded for steer execution & analysis
4. Athlete 2 calibration – 15 minutes
5. Athlete 2 to complete test using all perceptual cues – 30minutes
    a. 1 run – become familiar with the sensation
    b. 5 runs –force recorded for steer execution & analysis
6. Athlete 1 to complete test using all perceptual cues – 30minutes
    a. 1 run – become familiar with the sensation
    b. 5 runs –force recorded for steer execution & analysis
7. Athlete 2 to complete test using all perceptual cues – 30minutes
    a. 1 run – become familiar with the sensation
    b. 5 runs –force recorded for steer execution & analysis

Three participants:

1. 3 Athletes arrive for group 2 debrief session – 15 minutes
2. Athlete 3 calibration – 15 minutes
3. Athlete 3 to complete test using all perceptual cues – 30minutes
    a. 1 run – become familiar with the sensation
    b. 5 runs –force recorded for steer execution & analysis
4. Athlete 4 calibration – 15 minutes
5. Athlete 4 to complete test using all perceptual cues – 30minutes
    a. 1 run – become familiar with the sensation
    b. 5 runs –force recorded for steer execution & analysis
6. Athlete 5 calibration – 15 minutes
7. Athlete 5 to complete test using all perceptual cues – 30minutes
    a. 1 run – become familiar with the sensation
    b. 5 runs –force recorded for steer execution & analysis
8. Athlete 3 to complete test using all perceptual cues – 30minutes
    c. 1 run – become familiar with the sensation
    d. 5 runs –force recorded for steer execution & analysis
9. Athlete 4 to complete test using all perceptual cues – 30minutes
    e. 1 run – become familiar with the sensation
    f. 5 runs –force recorded for steer execution & analysis
10. Athlete 5 to complete test using all perceptual cues – 30minutes
    g. 1 run – become familiar with the sensation
    h. 5 runs –force recorded for steer execution & analysis

This schedule will run for each for each of the blocks above as detailed by the coaching staff. Athlete's performance will be assessed and monitored during each block and between to understand progression.

B. Head vibration isolation

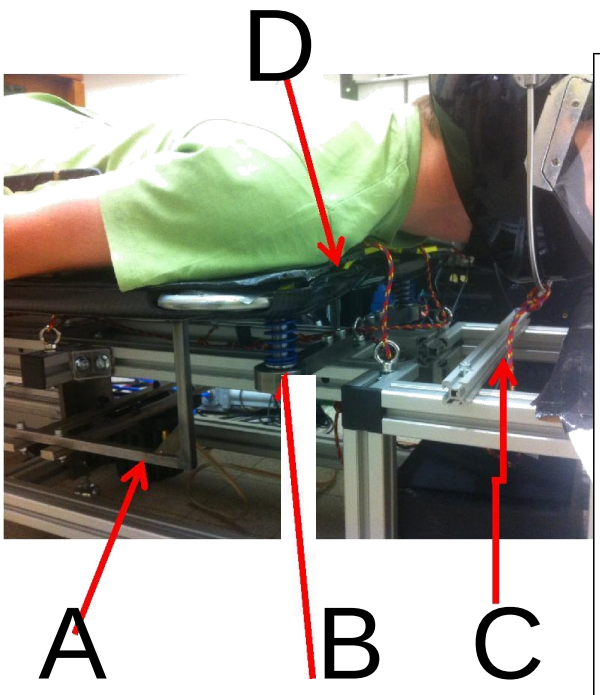

A – Electrodynamic shaker is attached to the underside of the sled frame

B- The sled is mounted on the rig with four suspension springs, to isolate it from the base of the rig.

C – Mechanical limit stop. This is on the base of the rig and therefore is not vibrating during the experiment. In the event of the subject relaxing their neck muscles, the helmet will make contact with the stop, preventing any further exposure to force.

D –Accelerometer used to measure vibration at the sled human interface. During the experiment, a whole body vibration meter (Rion) is used to monitor vibration dose value.

C. Product Information

See attached file for ButtKicker Manual (BK4-OwnersManual-Web2.pdf)

ButtKicker Amplifier-
The ButtKicker Power Amplifier BKA300-4 is a 300 watt amplifier that is also included in the wireless ButtKicker Kit (BK-Kit-4). Built with BASH® technology, this digital ButtKicker amplifier is convection cooled (no fan) and has numerous features.

Features

- Convection Cooled (no fan)
- Pre-set EQ Functions for Movies, Music and Games
- Wireless Audio Send and Receive Units
- Line Out For Daisy Chaining Multiple Amps
- 120v / 240v Convertible
- Includes Wireless Remote Conrol
- High Quality 5-way Binding Post Outputs
- 3' Male to Male RCA Cable
- Male to Female 'Y' Adapter
- Speaker Level Interface Adapter

Power Amplifier BKA300-4 Specs.

Dimensions:	*8.25" L x 9.25" W x 3.5"H*
Weight:	*4.6lbs. / 2kgs.*
Power Output:	*300 watts rms @ 4 ohms / 150 watts rms @ 2 ohms - 120V / 240V Convertible*
Frequency Response:	*10-300Hz*
Input Sensitivity:	*100mVolt*

See attached file for Enfield Technologies Data sheets (ET-LS-V15s-Datasheet.pdf, ET-LS-V25s-Datasheet.pdf, LS-C40-C41_Datasheet.pdf and LS-C41_Guide.pdf)

See attached file for Load cell data sheet (200 series in line load cell data sheet3.pdf)

See attached file for FlexiForce data sheet (A401-force-sensor.pdf)

Appendix G: Pitch Information Sheet

Pitch Actuation System

The Mark II simulator was built with limited motion cueing capabilities. After the athletes had time to practice on the Mark II, it was identified that some important steering cues were missing. One such cue is the pitching motion (that) athletes experience under their shoulders when the sled enters/exits a corner. The pitching motion is predominantly a proprioception cue, one which many elite athletes use to judge their steer timings. Therefore it is critical to produce an accurately timed motion cue.

Adding an extra motion cue onto the existing system could inadvertently affect the performance of other components on the VRS, such as the diminished response speed of the roll motion due to the distribution of flow rate. Therefore, it is important to select the appropriate components when designing the upgrades. In the VRS location, air is supplied by a Bambi VTS200 Silent Oil Free Compressor & Dryer unit, which have an average operating pressure of 8 bar during a typical simulated descent (less if consecutive simulations were performed). The existing system uses approximately 5 bars of pressure whilst in operation, in theory this implies only actuators with an operating pressure of 3 bars or less could be used. In practice, since the platform will only be actuated through corners, there exist margins of flexibility. However, to ensure performance and to comply with health and safety regulation when using the compressor, the actuator that requires the lowest operation pressure and fulfils the design specifications was used. Through physical experimentation, it was deemed that a pitching distance of at least 20mm is required for the participant to experience the motion cue.

Spring Guide Assembly

The real sled is free to move vertically from bouncing and vibrating on ice, it is also free to contort. This freedom of motion gives the feeling of the sled runner compressing and ultimately allow the athlete to perceive the texture of the ice surface. If the sled on the simulator is not permitted to move and contort, the steering motion will feel very unnatural. A spring guide system was developed to suspend the sled and athlete from the frame. Figure 1a displays an exploded view of the spring guide. The spring guide consists of a spring, a linear guide, a runner block and a spherical bearing which is housed on the custom base support shaft. The design ensures that the sled is free to pivot around its centre point to allow the athlete to feel contortion when steering. Stiffness of the spring was chosen to simulate the stiffness of the runners (2 springs equal 1 runner, each at approximately $20000 Nm^{-1}$). Due to budget constraints, Mark III VRS was designed to use as many parts from the Mark II as possible, therefore the springs and the support shaft were reused, but the linear guide and runner block had to be redesigned.

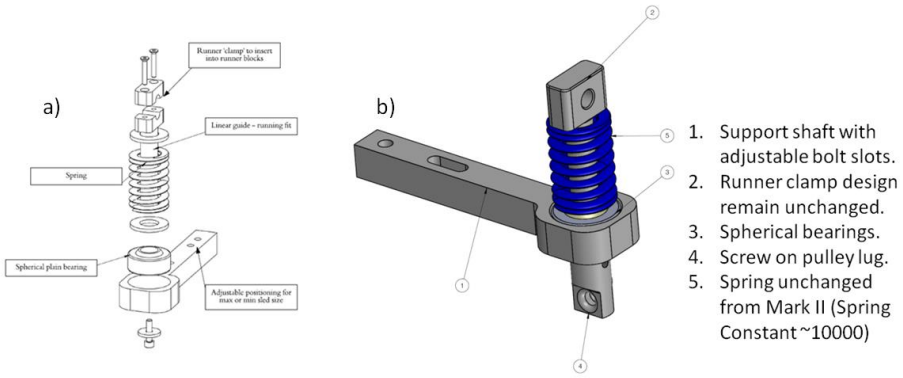

Figure 1: a) Spring guide system from Mark II, b) spring guide system from Mark III

Actuation System

Since minimum motion stroke required is 20mm and the spring stiffness is approximately 10000Nm^{-1}, an estimation of the force required from the actuator can be calculated (~200N). Athletes on the sled would also increase the frame stiffness. Therefore, even though there are flexibilities in the design, the actuators should still be selected base on the ability to generate at least 200N of force whilst operating on 3 – 4 bars of air pressure. The actuator selected for this task is the Festo standard cylinder DNCI-32 (bore 32" x 125mm total stroke) with integrated displacement encoder, which has maximum stroke length of 80mm and a piston diameter of 32mm. It has a minimum operating pressure of 0.6 bar and a theoretical force of 483N at 6 bar of air. It is coincidentally the smallest pneumatic actuation unit Festo supplies suitable for this kind of application.

Early design concepts for the hardware layout consisted of vertical actuators mounted on pivots joints directly under the spring guide system to perform actuation through the linear guide. This design was deemed unfeasible for the following reasons:

- Available space underneath the spring guide is limited, in order to install the actuator, considerable amount of additional frame works have to be installed underneath the current 'cradle'. This will weaken the structural integrity of the supporting framework and create a safety hazard. Installing additional framework also decreases the range of roll motion of the 'cradle', as the extra material will intercept with the base frame.
- In this proposed setup, the actuator has to be mounted on pivoting joint, to allow for rotation when the sled body is pitched. However this pitching motion creates a side force of up to 250N on the piston rod, which is not designed to withstand any form of perpendicular force loading. This is especially true for the model with integrated displacement encoder. Any application of side forces will damage the sensors embedded in around the rim of the piston. Piston support could be added in the form of FEN_FENG. In order to apply adequate support at stroke length of 20mm, the minimum rod diameter has to be 32mm. This implies each linear guide would weigh 1.57kg and require an unreasonable amount of frame works to be added, which is simply not practical.

Figure 2 displays the final actuation system layout. The new layout adopts a pulley based design, removing the major disadvantages from the previous iteration. The new design requires the installation of only one v-shaped aluminium crossbar underneath the spring guides to act as the attachment points for the pulleys. The aluminium crossbar was attached within the inner ‘cradle’ and will therefore not obstruct the movement range of roll. The actuators are installed on a horizontal planed, inclined at the angle that produces the least amount side forces (effectively none) on the piston rod. The placement of the actuators and the crossbar is designed for even weight distribution.

The system uses two modes of actuation. Whilst pitching upwards, the spring guides provide all necessary force and the movement and the actuators are used to control the rate of pitch. Whilst pitching downwards, the actuators produce all the forces buy pulling on the spring guides. The original spring guides were modified, the linear guides have being elongated and threaded on one end for attaching to the pulley lug (refer to figure 1 b). Actuators and spring guides are connected via tort steel cables to minimise loss of system response rate.

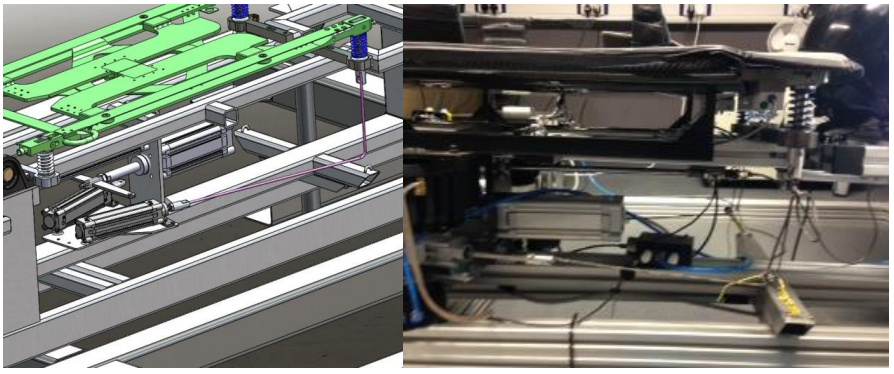

Figure 2: CAD design of should actuation system (left), Photograph of implemented actuation system (right)

Appendix H: Post Experiment Questionaire

UNIVERSITY OF Southampton

Pitch perceptual cuing test

This questionnaire is to be completed after the entire testing session has been completed.

NAME (Optional) ……

Q.1 – How effective do you think the implementation of pitch is for training steering actions from the perspective of a coach?

0 2.5 5 7.5 10
|_____|_____|_____|_____|

Q.2 – Please rate the following perceptual cues out of 10 with relation to realism. (How real and immersive did it feel?)
Pitch - /10
Leg Force Feedback - /10

Q.3 – Which pitch algorithm did you find the most useful when trying to steer?
(Please list in order of usefulness – Proportional_1, Proportional_2, Impulse_1, Impulse_2 or Impulse_3?

1……..
2……..
3……..
4……..
5……..

Q.4 – Do you think the Pitch level was too high? YES / NO

Q.5 – Do you think the Pitch level was too low? YES / NO

Q.6 – Do you think the Force Feedback level was too high on the Leg? YES / NO

Q.7 – Do you think the Force Feedback level was too low on the Leg? YES / NO

Q.8 – Did you feel safe on the system? YES / NO
If No, please state what caused this……..

Q.9 – What are your thoughts on the different pitch algorithms, what do you want to see changed to them?

……
……
……
……
……
……
……
……

UNIVERSITY OF Southampton

Q.10 – General comments on the system upgrade (Pitch and Leg Force Feedback)-
(Please feel free to provide positive and/or constructive feedback to help improve the system)

……
……
……
……
……
……
……
……
……
……
……
……

THANK YOU FOR YOUR HELP AND TIME!!